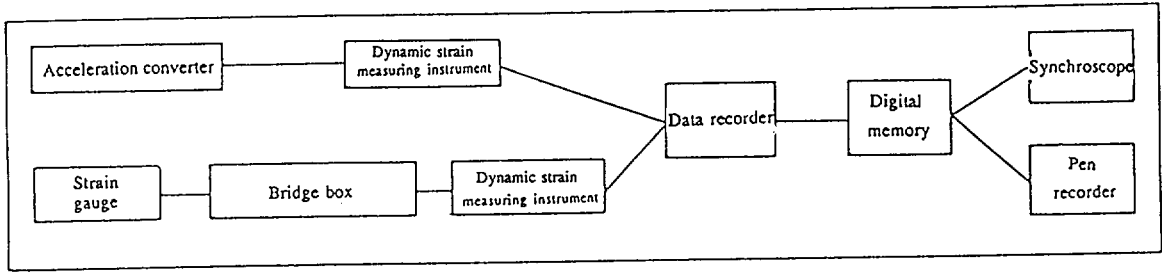


3.4 Deceleration and strain measurements

The measuring instruments used to measure the deceleration and strain during a drop impact are as follows:

Acceleration converter	: Kyowa Electronic Instruments Co., Ltd.	AS-1000TA (1000 G(max))
Strain gauge	: ditto	KFC-5-D17-16 (Orthogonal 45-degree tri-axis type)
Bridge box	: ditto	DB120K
Dynamic strain measuring instrument	: ditto	DPM-110B R270A
Data recorder	: TEAC Corporation	(The tape speed is 19 cm/sec during recording and playback.)
Digital memory	: Iwasaki Electric Co., Ltd.	DM305
Synchroscope	: ditto	SS-5215
Pen recorder	: Yokogawa Electric Corporation	TYPE-3052

Fig. (II)-A-App.9 shows the deceleration and strain measurement circuits.



**Fig. (II)-A-App.9 Block Diagram of Deceleration and Strain Measurements**

The acceleration converter is fixed with screws on a plane machined flat at positions at 0, 90, 180, and 270 degrees of the shell of this packaging body, 320 mm from both ends on the line.

The strain gauge is attached to the packaging body with a cyanoacrylate adhesive. After that, a coating agent is applied to the strain gauge to ensure water resistance.

Fig. (II)-A-App.10 shows the installation position of the acceleration converter and strain gauge.

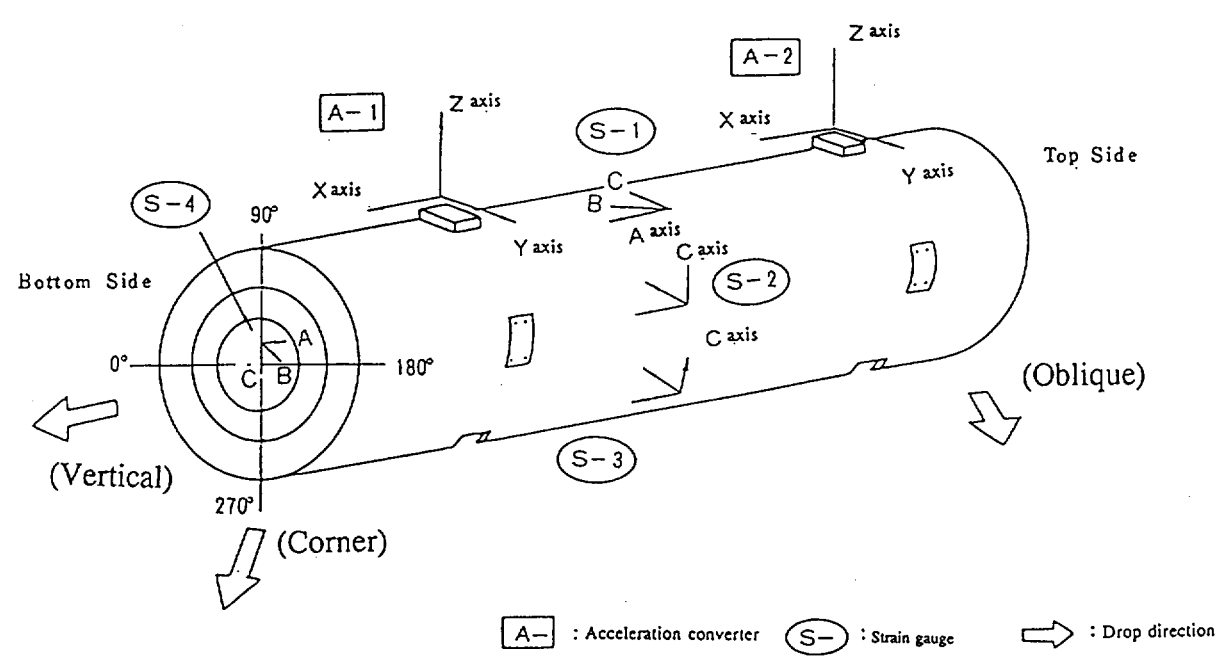


**Fig. (II)-A-App.10    Installation Positions of the Acceleration Converter and Strain Gauge**

**Deceleration and strain readings**

The phenomenal waveform recorded in the data recorder is reproduced to the synchroscope and pen recorder via the digital memory. Therefore, it is read.

The deceleration was read from the waveform whose high-frequency component was eliminated because the high frequency, due to the natural vibration of this packaging body during drop impact, is contained in the phenomenal waveform. As shown in Fig. (II)-A-App.11, the center point of each wave is connected to produce a smooth waveform. The peak value at that time represents the maximum deceleration.

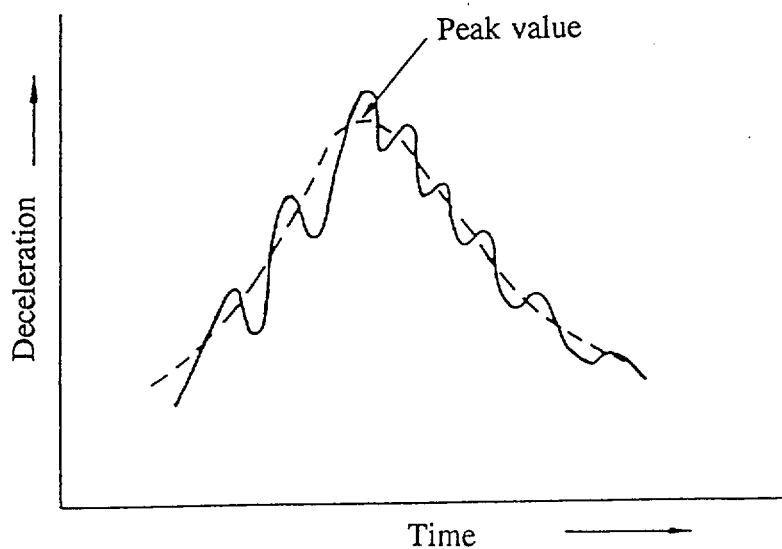


**Fig. (II)-A-App.11 Phenomenal Wave of Deceleration**

Strain is not greatly influenced by these natural vibrations. In other words, the high-frequency component of this deceleration wave does not greatly influence the strain measurement. This is shown by the simple experiment outlined below.

To examine the influence that natural vibrations exert on the acceleration converter and strain gauge, the converter and gauge are installed under the same conditions as during a drop test. Then, the shell of the cask body is struck with a hammer. After that, the vibration of the converter and gauge at that time is examined.

The results of this test indicated that no vibration waveform could be observed in the strain gauge, although an attenuation curve of 1300 to 2600 Hz (shown in Fig. (II)-A-App.12) was observed in the acceleration converter.

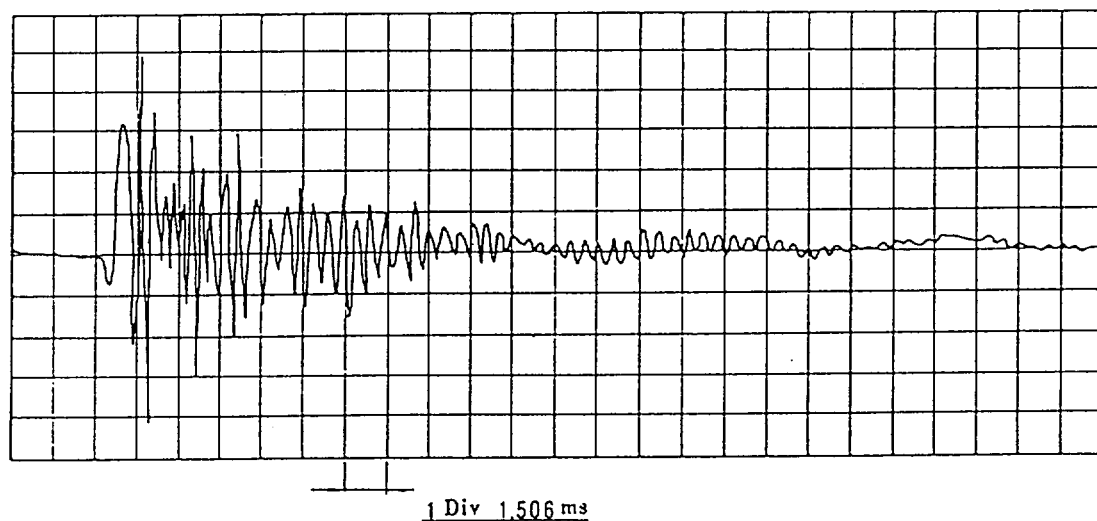


**Fig. (II)-A-App.12 Output Waveform of the Acceleration Converter Following a Hammer Stroke**

3.5 Leakage test

To check for the leakage before and after a drop test, a halogen leakage test ( $1 \times 10^{-6}$  atm·cc/sec) is conducted on the specimen body.

(a) Test summary

A halogen leakage test is conducted on the O-ring sealing part of the front lid, rotating plug lid, and penetration hole lid of a 1/2-scale model of the packaging. The halogen leakage test applies the pressure method to measure the leakage rate with a detection sensitivity of  $1 \times 10^{-6}$  atm·cc/sec. Enclosed halogen gas has a purity of more than 99.9%. Halogen gas is enclosed after the part which holds the gas is exhausted to about  $10^{\text{torr}}$ . The enclosing pressure is 4 kg/cm<sup>2</sup> abs.

(b) Test equipment

(i) Halogen leak detector

a)	Suzuki Kosakusho Co., Ltd.	SK AZ-2
	Leak detection sensitivity	$1 \times 10^{-6}$ atm·cc/sec
b)	Toshiba Corporation	HAL 6
	Leak detection sensitivity	$1 \times 10^{-6}$ atm·cc/sec

(ii) Standard leak

a)	G.E (USA)	LS-20
	Full scale	$3 \times 10^{-6}$ atm·cc/sec
		$10 \times 10^{-5}$ atm·cc/sec

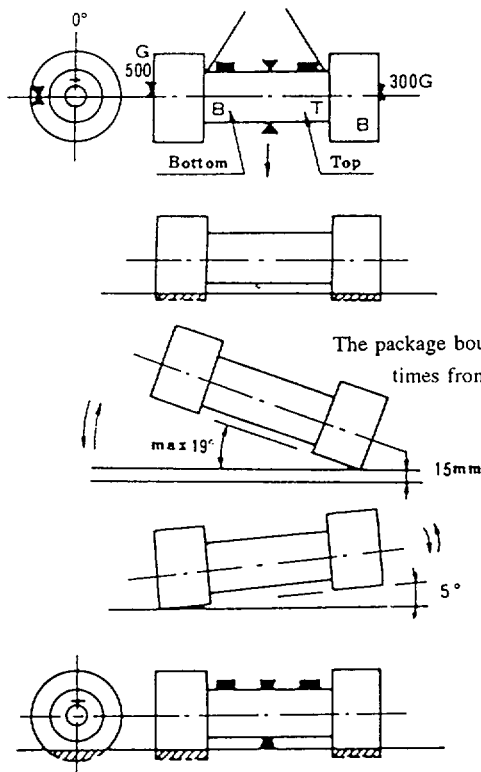
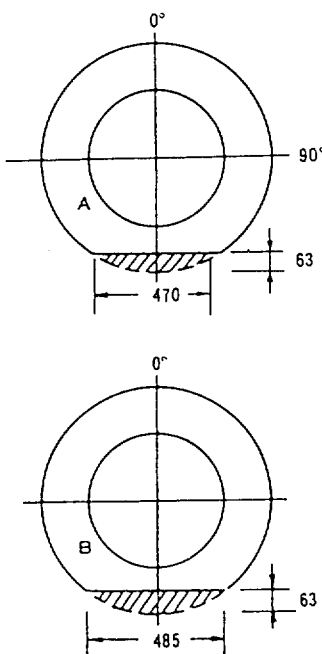
(iii) Halogen gas (Freon 12)

Asahi Flon Gas Kogyo	Purity of 99.9%
----------------------	-----------------

3.6 Test results

Table (II)-A-App.6 is a record of the test results. Fig. (II)-A-App.13 shows the acceleration waveform, while Fig. (II)-A-App.14 provides photographs taken during a drop test.

Table (II)-A-App.6 Test Conditions and Measurement Results (1)

No.									
Test No.	1	Test name	Horizontal drop 1			Drop test I ( - )		Drop height	9 m
Test date	16 : 15, March 7, 1980			Weather	Rain	Temperature	8°C	Humidity	%
Observer	Mr. Konno and Mr. Uruwashi (the Fast Breeder Reactor Development Headquarters, PNC main office)							Test order	(1)
Shock absorber	Top	B	Bottom	A	Contents	Fuel supporting can and dummy pipe A			
Measurement items									
Item	Record	Remark			Item	Record	Remark		
Acceleration (strain gauge type)	○	max A2 212G(Z)			Contents damage	○	Not damaged.		
Acceleration (spring type)	○	210G (300G), 340G (500G)			Leak (halogen leak)	○	No leaks.		
Strain distribution	○	Max S2 1404μ (A)							
Shock absorber deformation									
Packaging body damage	○	Not damaged.							
Lid unit damage	○	Not damaged.			Still photograph				
Drop attitude and status					Deformation and damage status (in mm)				
<div>■ Strain accelerometer ✕ Spring accelerometer ▼ Strain gauge ■ Projection</div> 					<div>Shock absorber deformation</div> 				
Model pipe A: STPG with one end closed, B: STPG with both ends open Acceleration (strain gauge type): Tri-axis acceleration converter AS-TA1000 Acceleration (spring type): Acceleration sensor    Strain gauge: KFC-5-D17-16									

**Table (II)-A-App.6 Test Conditions and Measurement Results (2)**

No. \_\_\_\_\_

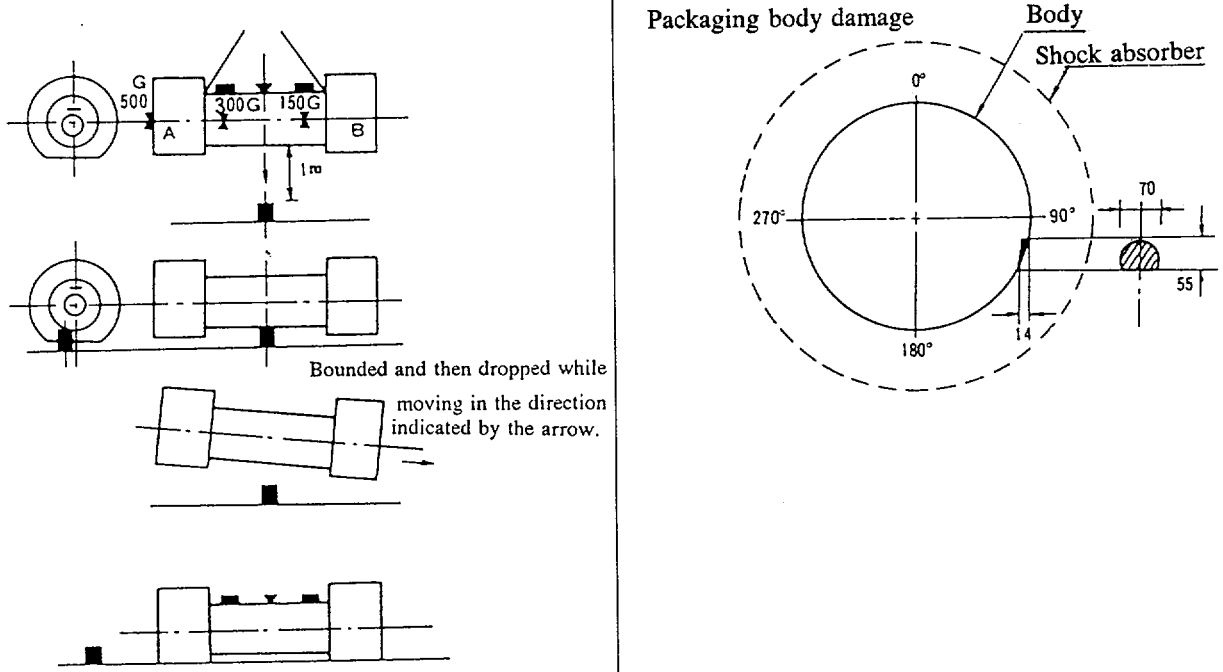
Test No.	2	Test name	Horizontal drop 1 Drop test II (center)			Drop height	1 m	
Test date	13 : 12, March 10, 1980		Weather	Fine	Temperature	16.5°C	Humidity	32 %
Observer	Mr. Konno (the Fast Breeder Reactor Development Headquarters, PNC main office) Mr. Kano and Mr. Nakamura (the Irradiation Fuel Assembly Testing Room, PNC Oarai)						Test order	(3)
Shock absorber	Top B Bottom A		Contents	Fuel supporting and dummy pipe A				
Measurement items								
Item	Record	Remark	Item	Record	Remark			
Acceleration (strain gauge type)	○	max A1 193G (z)	Contents damage	○	Not damaged.			
Acceleration (spring type)	○	55G (150G), 90G (300G) 160G (500G)	Leak (halogen leak)	○	No leaks.			
Strain distribution	○	max S1 651 μ (A) Measured at only one point.						
Shock absorber deformation								
Packaging body damage	○	Damaged.						
Lid unit damage	○	Not damaged.	Still photograph					
Drop attitude and status			Deformation and damage status (in mm)					
<div>■ Strain accelerometer</div> <div>➤ Spring accelerometer</div> <div>▼ Strain gauge</div> <div>■ Projection</div>			<div></div>					
Model pipe A: STPG with one end closed, B: STPG with both ends open Acceleration (strain gauge type): Tri-axis acceleration converter AS-TA1000 Acceleration (spring type): Acceleration sensor Strain gauge: KFC-5-D17-16								

Table (II)-A-App.6 Test Conditions and Measurement Results (3)

No.									
Test No.	3	Test name	Horizontal drop 1 Drop test II (eccentric)				Drop height		1 m
Test date	12 : 00, March 10, 1980			Weather	Fine	Temperature	16.5°C	Humidity	34 %
Observer	Mr. Konno (the Fast Breeder Reactor Development Headquarters, PNC main office) Mr. Tano, Mr. Kano, and Mr. Nakamura (the Irradiation Fuel Assembly Testing Room, PNC Oarai)							Test order	(2)
Shock absorber	Top	B	Bottom	A	Contents	Fuel supporting can and dummy pipe A			
Measurement items									
Item	Record	Remark			Item	Record	Remark		
Acceleration (strain gauge type)	○	max A1 99G(Z)			Contents damage	○	Not damaged.		
Acceleration (spring type)	○	255G (50G), > 50G (50G)			Leak (halogen leak)	-			
Strain distribution	○	max S3 245 μ (A)							
Shock absorber deformation	○								
Packaging body damage	○	Not damaged.							
Lid unit damage	○	Not damaged.			Still photograph				
Drop attitude and status					Deformation and damage status (in mm)				
<div>■ Strain accelerometer</div> <div>✕ Spring accelerometer</div> <div>▼ Strain gauge</div> <div>■ Projection</div> <div></div>					<div>Shock absorber damage</div> <div>The stainless cover is broken partially, and a hole that is 21.5 mm deep is made by the projection.</div> <div></div>				
Model pipe A: STPG with one end closed, B: STPG with both ends open									
Acceleration (strain gauge type): Tri-axis acceleration converter AS-TA1000									
Acceleration (spring type): Acceleration sensor Strain gauge: KFC-5-D17-16									

Table (II)-A-App.6 Test Conditions and Measurement Results (4)

No. \_\_\_\_\_

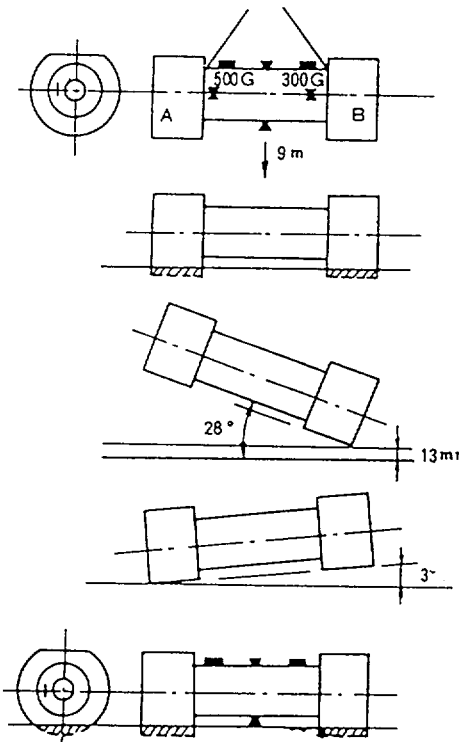
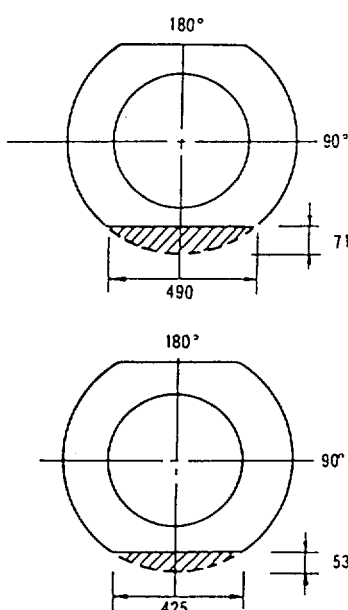
Test No.	4	Test name	Horizontal drop 2 Drop test I ( - )			Drop height	9 m	
Test date	17 : 00, March 10, 1980		Weather	Fine	Temperature	16°C	Humidity	32 %
Observer	Mr. Konno (the Fast Breeder Reactor Development Headquarters, PNC main office) Mr. Toyokawa (the Irradiation Material Testing Room, PNC Oarai)						Test order	(4)
Shock absorber	Top B	Bottom A	Contents	Fuel supporting can and dummy pipe A				
Measurement items								
Item	Record	Remark	Item	Record	Remark			
Acceleration (strain gauge type)	○	max A1 231G (Z)	Contents damage	○	Not damaged.			
Acceleration (spring type)	○	190G (300G), 320G (500G)	Leak (halogen leak)	○	No leaks.			
Strain distribution	○	max S3 1038 $\mu$ (A)						
Shock absorber deformation	○							
Packaging body damage	○	Not damaged.						
Lid unit damage	○	Not damaged.	Still photograph					
Drop attitude and status			Deformation and damage status (in mm)					
<div>■ Strain accelerometer</div> <div>▶ Spring accelerometer</div> <div>▼ Strain gauge</div> <div>■ Projection</div>			Shock absorber deformation					
<div>Shock absorber damage</div> <div></div>			<div></div>					
Model pipe A: STPG with one end closed, B: STPG with both ends open Acceleration (strain gauge type): Tri-axis acceleration converter AS-TA1000 Acceleration (spring type): Acceleration sensor Strain gauge: KFC-5-D17-16								



Table (II)-A-App.6 Test Conditions and Measurement Results (5)

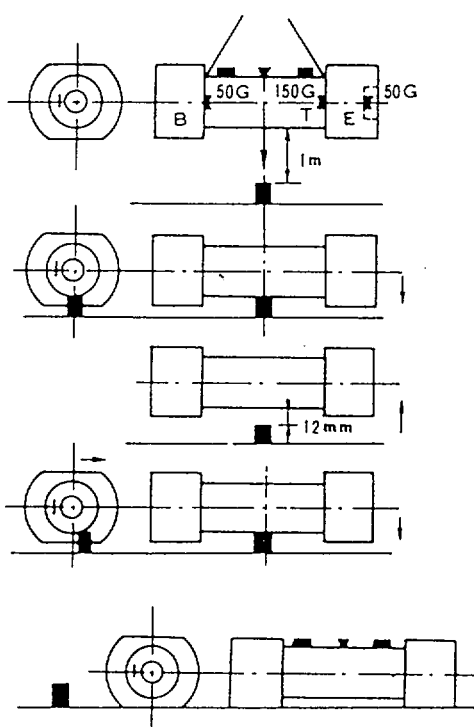
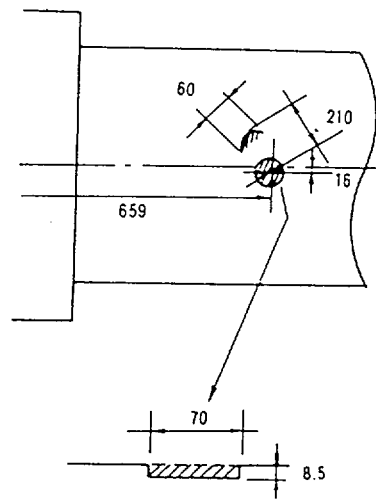
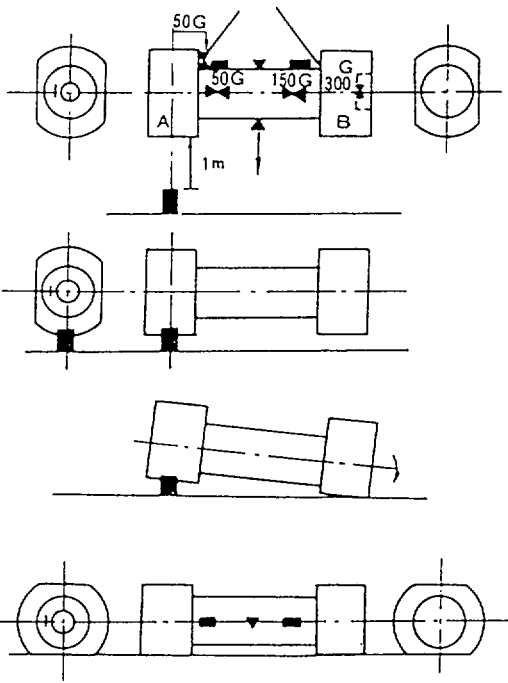
No. _____									
Test No.	5	Test name	Horizontal drop 2 Drop test II (center)				Drop height	1 m	
Test date	10 : 20, March 14, 1980		Weather	Cloudy	Temperature	8°C	Humidity	59 %	
Observer							Test order	(13)	
Shock absorber	Top	E	Bottom	B	Contents	Fuel supporting can and dummy pipe A			
Measurement items									
Item	Record	Remark			Item	Record	Remark		
Acceleration (strain gauge type)	○	max A1 124G(Z)			Contents damage		Not damaged.		
Acceleration (spring type)	○	90G (150G)			Leak (halogen leak)		No leaks.		
Strain distribution	○	max S1 789μ (A) Measured at only one point.							
Shock absorber deformation	-								
Packaging body damage	○	Damaged.							
Lid unit damage	○	Not damaged.			Still photograph				
Drop attitude and status					Deformation and damage status (in mm)				
<div>■ Strain accelerometer</div> <div>⋈ Spring accelerometer</div> <div>▼ Strain gauge</div> <div>■ Projection</div> <div></div>					<div>Body dent</div> <div></div>				
Model pipe A: STPG with one end closed, B: STPG with both ends open Acceleration (strain gauge type): Tri-axis acceleration converter AS-TA1000 Acceleration (spring type): Acceleration sensor Strain gauge: KFC-5-D17-16									

Table (II)-A-App.6 Test Conditions and Measurement Results (6)

No.									
Test No.	6	Test name	Horizontal drop 2 Drop test II (eccentric)				Drop height	1 m	
Test date	11 : 00, March 11, 1980		Weather	Fine	Temperature	10°C	Humidity	27 %	
Observer	Mr. Konno (the Fast Breeder Reactor Development Headquarters, PNC)						Test order	(1)	
Shock absorber	Top	B	Bottom	A	Contents	Dummy pipe B			
Measurement items									
Item	Record	Remark			Item	Record	Remark		
Acceleration (strain gauge type)	○	max A1 47G(Z)			Contents damage	-			
Acceleration (spring type)	○	25G (50G), 225G (50G) 60G (150G), 130G (300G)			Leak (halogen leak)	○	No leaks.		
Strain distribution	○	max S3 103μ (A)							
Shock absorber deformation	○								
Packaging body damage	○	Not damaged.							
Lid unit damage	○	Not damaged.			Still photograph				
Drop attitude and status					Deformation and damage status (in mm)				
<div>■ Strain accelerometer</div> <div>⌵ Spring accelerometer</div> <div>▼ Strain gauge</div> <div>▣ Projection</div>									
					Shock absorber damage 33-mm deep on average				
Model pipe A: STPG with one end closed, B: STPG with both ends open Acceleration (strain gauge type): Tri-axis acceleration converter AS-TA1000 Acceleration (spring type): Acceleration sensor Strain gauge: KFC-5-D17-16									

▼

■

Table (II)-A-App.6 Test Conditions and Measurement Results (7)

No.										
Test No.	7	Test name	Vertical drop Drop test I ( - )				Drop height		9 m	
Test date	17 : 00, March 11, 1980			Weather	Fine	Temperature	9°C	Humidity	24 %	
Observer	Mr. Konno (the Fast Breeder Reactor Development Headquarters, PNC main office)						Test order		(6)	
Shock absorber	Top	A	Bottom	C	Contents	Dummy pipe B				
Measurement items										
Item	Record	Remark			Item	Record	Remark			
Acceleration (strain gauge type)	○	max A1 236G(X)			Contents damage	-				
Acceleration (spring type)	○	200G (300G), 350G (500G)			Leak (halogen leak)	○	No leaks.			
Strain distribution	○	max S1 -455μ (A)								
Shock absorber deformation	○									
Packaging body damage	○	Not damaged.								
Lid unit damage	○	Not damaged.			Still photograph					
Drop attitude and status					Deformation and damage status (in mm)					
<div><div>■ Strain accelerometer</div><div>✕ Spring accelerometer</div><div>▼ Strain gauge</div><div>■ Projection</div></div> <div></div> <div>This part of the shock absorber sinks.</div> <div>All the bolt holes of the shock absorber exhibit complex buckling. The bolt holes become completely clogged.</div>					<div>Shock absorber deformation and damage</div> <div>Deformation: 47 mm on average</div> <div></div>					
Model pipe A: STPG with one end closed, B: STPG with both ends open Acceleration (strain gauge type): Tri-axis acceleration converter AS-TA1000 Acceleration (spring type): Acceleration sensor Strain gauge: KFC-5-D17-16										

**Table (II)-A-App.6 Test Conditions and Measurement Results (8)**

No.

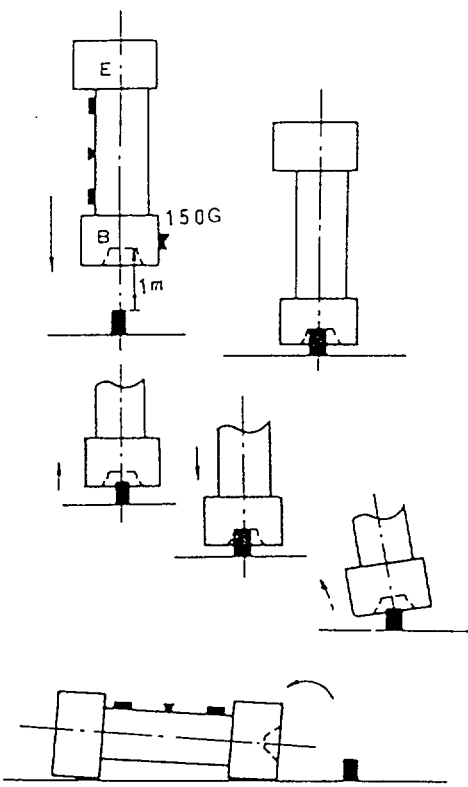
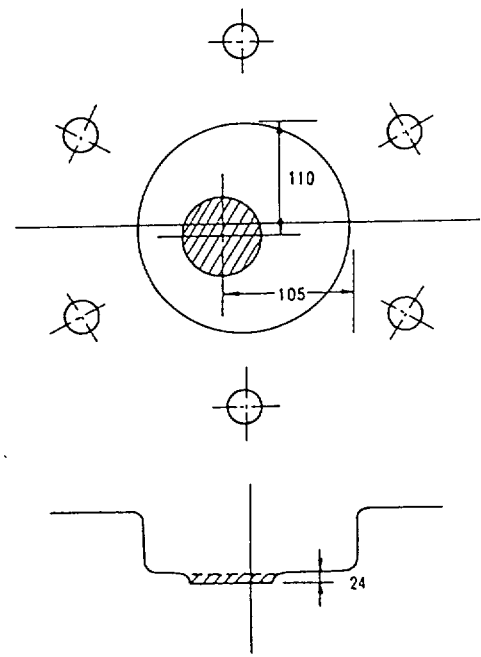
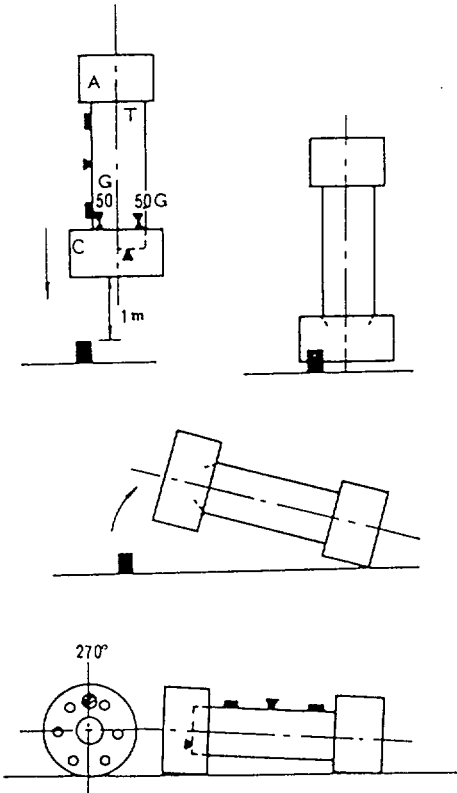
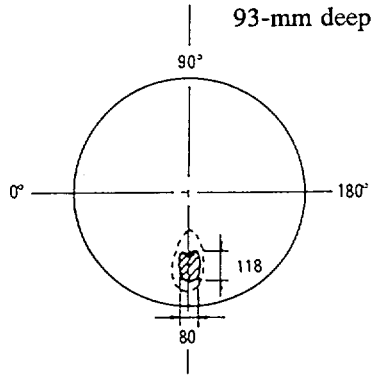
Test No.	8	Test name	Vertical drop Drop test II (center)			Drop height	1 m	
Test date	16 : 00, March 13, 1980		Weather	Fine	Temperature	13.5°C	Humidity	37 %
Observer	Mr. Konno and Mr. Uruwashi (the Fast Breeder Reactor Development Headquarters, PNC main office) Mr. Masai, Mr. Tsuzuki, and Mr. Kitano (High-Level Radioactive Material Laboratory Construction Group, PNC Tokai)					Test order	(12)	
Shock absorber	Top E	Bottom B	Contents	Fuel supporting can and dummy pipe A				
Measurement items								
Item	Record	Remark	Item	Record	Remark			
Acceleration (strain gauge type)	○	max A1 75G(X)	Contents damage	-				
Acceleration (spring type)	○	75G (150G)	Leak (halogen leak)	○	No leaks.			
Strain distribution	○	max S2 -98μ (A)						
Shock absorber deformation	○	See S-8.						
Packaging body damage	○	Not damaged.						
Lid unit damage	○	Not damaged.	Still photograph					
Drop attitude and status			Deformation and damage status (in mm)					
<div>■ Strain accelerometer</div> <div>⌘ Spring accelerometer</div> <div>▼ Strain gauge</div> <div>■ Projection</div> <div></div>			<div>Shock absorber damage</div> <div></div>					
Model pipe A: STPG with one end closed, B: STPG with both ends open Acceleration (strain gauge type): Tri-axis acceleration converter AS-TA1000 Acceleration (spring type): Acceleration sensor Strain gauge: KFC-5-D17-16								

Table (II)-A-App.6 Test Conditions and Measurement Results (9)

No.									
Test No.	9	Test name	Vertical drop Drop test II (eccentric)			Drop height		1 m	
Test date	11 : 30, March, 12, 1980		Weather	Fine	Temperature	7°C	Humidity	30 %	
Observer	Mr. Konno (the Fast Breeder Reactor Development Headquarters, PNC main office) Mr. Tsuzuki, Mr. Masai and Mr. Kitano (High-Level Radioactive Material Laboratory Construction group, PNC Tokai)						Test order	(7)	
Shock absorber	Top A	Bottom C	Contents		Fuel supporting can and dummy pipe A				
Measurement items									
Item	Record	Remark		Item	Record	Remark			
Acceleration (strain gauge type)	○	max A2 34G(X)		Contents damage	○	Not damaged.			
Acceleration (spring type)	○	15G, 17G (50G)		Leak (halogen leak)	○	No leaks.			
Strain distribution	○	max S1 -74μ (A)							
Shock absorber deformation	○								
Packaging body damage	○	Not damaged.							
Lid unit damage	○	Not damaged.		Still photograph					
Drop attitude and status				Deformation and damage status (in mm)					
<div>■ Strain accelerometer</div> <div>✕ Spring accelerometer</div> <div>▼ Strain gauge</div> <div>■ Projection</div> <div></div>				<div>Shock absorber damage</div> <div></div>					
Model pipe A: STPG with one end closed, B: STPG with both ends open Acceleration (strain gauge type): Tri-axis acceleration converter AS-TA1000 Acceleration (spring type): Acceleration sensor Strain gauge: KFC-5-D17-16									

**Table (II)-A-App.6 Test Conditions and Measurement Results (10)**

No.

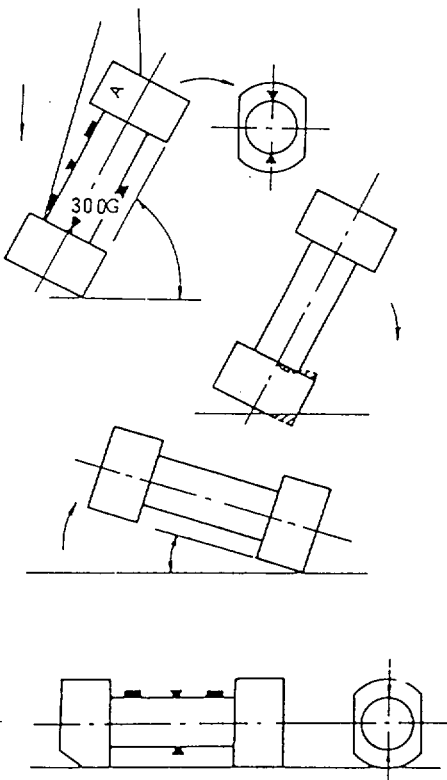
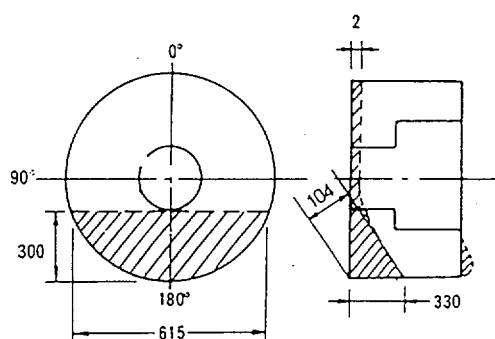
Test No.	10	Test name	Corner drop Drop test I ( - )			Drop height	9 m	
Test date	14 : 30, March 12, 1980		Weather	Fine	Temperature	9°C	Humidity	36 %
Observer	Mr. Konno (the Fast Breeder Reactor Development Headquarters, PNC main office) Mr. Tsuzuki, Mr. Masai and Mr. Kitano (High-Level Radioactive Material Laboratory Construction group, PNC Tokai)					Test order	(8)	
Shock absorber	Top A	Bottom D	Contents	Fuel supporting can and dummy pipe A				
Measurement items								
Item	Record	Remark	Item	Record	Remark			
Acceleration (strain gauge type)	○	max A2 160G(X)	Contents damage	○	Not damaged.			
Acceleration (spring type)	○	162G (300G)	Leak (halogen leak)	○	No leaks.			
Strain distribution	○	max S1 -218μ (A)						
Shock absorber deformation	○							
Packaging body damage	○	Not damaged.						
Lid unit damage	○	Not damaged.	Still photograph	○	Photo. No 10-1-10-20			
Drop attitude and status			Deformation and damage status (in mm)					
<div>■ Strain accelerometer</div> <div>⌵ Spring accelerometer</div> <div>▼ Strain gauge</div> <div>■ Projection</div> <div></div>			<div>Shock absorber deformation</div> <div></div>					
Model pipe A: STPG with one end closed, B: STPG with both ends open Acceleration (strain gauge type): Tri-axis acceleration converter AS-TA1000 Acceleration (spring type): Acceleration sensor Strain gauge: KFC-5-D17-16								

Table (II)-A-App.6 Test Conditions and Measurement Results (11)

No. \_\_\_\_\_

Test No.	11	Test name	Corner drop Drop test II ( - )				Drop height	1 m
Test date	17 : 00, March 12, 1980		Weather	Fine	Temperature	8.5°C	Humidity	33 %
Observer	Mr. Konno (the Fast Breeder Reactor Development Headquarters, PNC main office)						Test order	(9)
Shock absorber	Top A	Bottom D	Contents	Dummy pipe B				
Measurement items								
Item	Record	Remark	Item	Record	Remark			
Acceleration (strain gauge type)	<input type="radio"/>	max A1 53G(X)	Contents damage	-				
Acceleration (spring type)	<input type="radio"/>	30G, 35G (50G)	Leak (halogen leak)	<input type="radio"/>	No leaks.			
Strain distribution	<input type="radio"/>	max S1 73μ (A)						
Shock absorber deformation	<input type="radio"/>							
Packaging body damage	<input type="radio"/>	Not damaged.						
Lid unit damage	<input type="radio"/>	Not damaged.	Still photograph					
Drop attitude and status			Deformation and damage status (in mm)					
<div><div><div>■ Strain accelerometer</div><div>✕ Spring accelerometer</div><div>▼ Strain gauge</div><div>■ Projection</div></div><div></div></div>			<div>Shock absorber damage</div> <div></div>					
Model pipe A: STPG with one end closed, B: STPG with both ends open Acceleration (strain gauge type): Tri-axis acceleration converter AS-TA1000 Acceleration (spring type): Acceleration sensor Strain gauge: KFC-5-D17-16								

Table (II)-A-App.6 Test Conditions and Measurement Results (12)

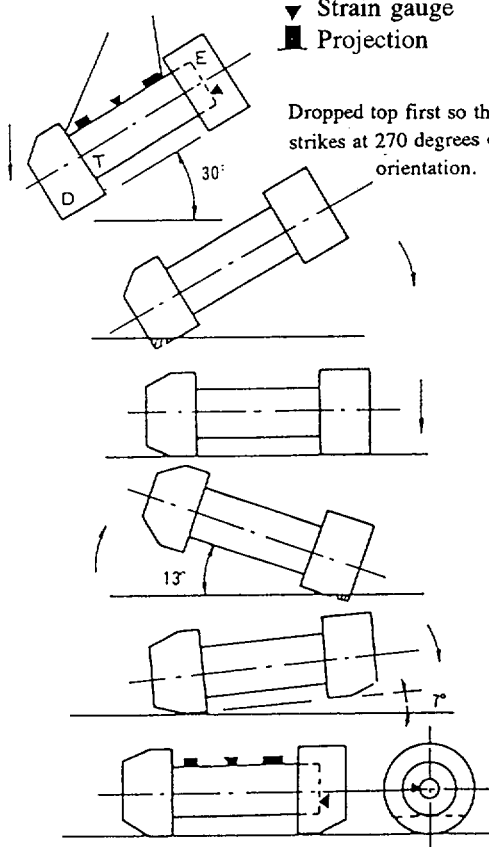
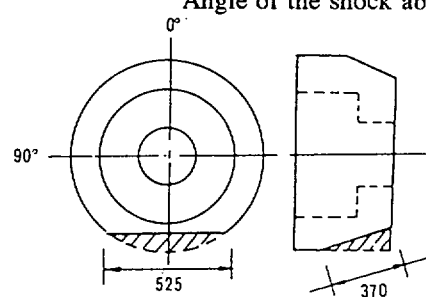
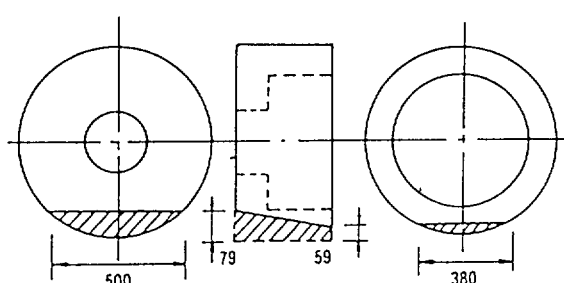
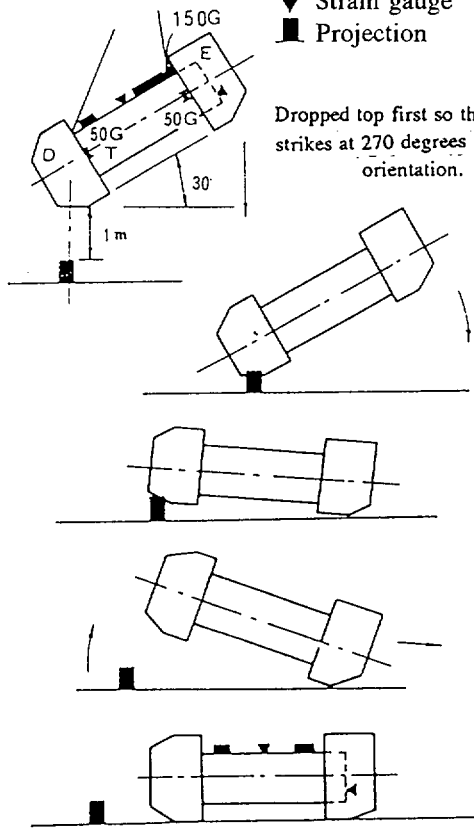
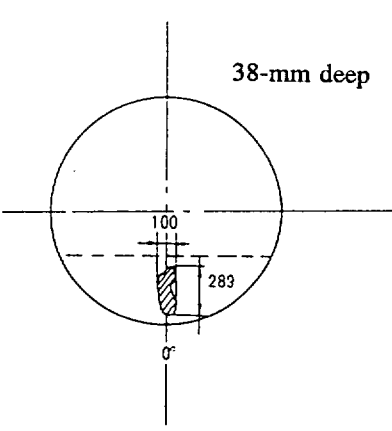
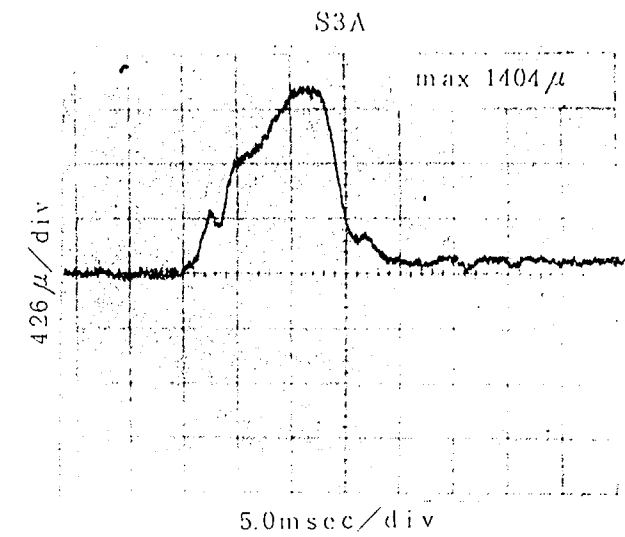
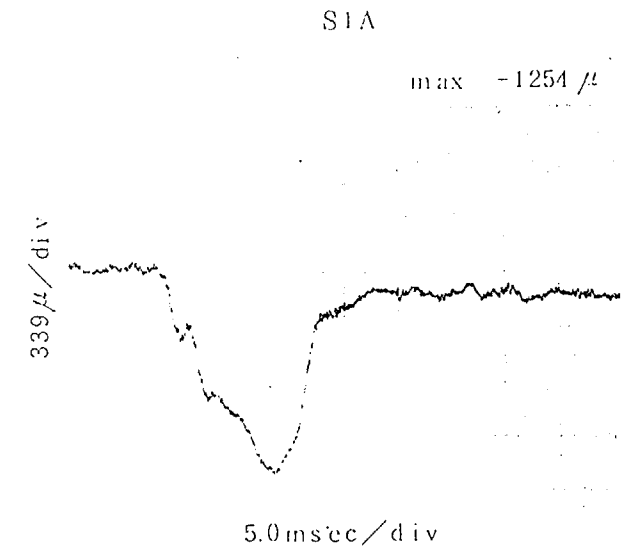
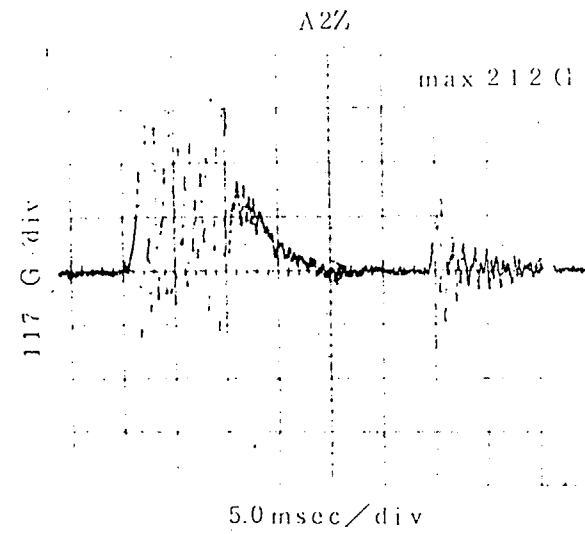
No.									
Test No.	12	Test name	Oblique test Drop test I ( - )				Drop height	9 m	
Test date	13 : 30, March 13, 1980		Weather	Fine	Temperature	13°C	Humidity	34 %	
Observer	Mr. Konno (the Fast Breeder Reactor Development Headquarters, PNC main office) Mr. Tsuzuki, Mr. Masai and Mr. Kitano (High-Level Radioactive Material Laboratory Construction group, PNC Tokai)						Test order	(10)	
Shock absorber	Top D	Bottom E	Contents	Fuel supporting can and dummy pipe A					
Measurement items and imitation pipe A									
Item	Record	Remark	Item	Record	Remark				
Acceleration (strain gauge type)	○	max A1 242G(Z)	Contents damage	○	Not damaged.				
Acceleration (spring type)	-		Leak (halogen leak)	○	No leaks.				
Strain distribution	○	max S1 -675μ (A)							
Shock absorber deformation	○								
Packaging body damage	○	Not damaged.							
Lid unit damage	○	Not damaged.	Still photograph						
Drop attitude and status			Deformation and damage status (in mm)						
<div><div>■ Strain accelerometer</div><div>▼ Spring accelerometer</div><div>▼ Strain gauge</div><div>■ Projection</div></div> <div><div>Dropped top first so that the corner strikes at 270 degrees of the specimen's orientation.</div></div>			<div>Shock absorber deformation</div> <div>Angle of the shock absorber</div> <div></div> <div></div>						
Model pipe A: STPG with one end closed, B: STPG with both ends open Acceleration (strain gauge type): Tri-axis acceleration converter AS-TA1000 Acceleration (spring type): Acceleration sensor Strain gauge: KFC-5-D17-16									



Table (II)-A-App.6 Test Conditions and Measurement Results (13)

No. _____									
Test No.	13	Test name	Oblique test Drop test II ( - )				Drop height	1 m	
Test date	15 : 10, March 13, 1980		Weather	Fine	Temperature	14°C	Humidity	37 %	
Observer	Mr. Konno and Mr. Unuwashi (the Fast Breeder Reactor Development Headquarters, PNC main office) Mr. Yagi, Mr. Matsumoto, and Mr. Kitamura (High-Level Radioactive Material Laboratory Construction Group, PNC)						Test order	(11)	
Shock absorber	Top	D	Bottom	E	Contents	Dummy pipe B			
Measurement items									
Item	Record	Remark		Item	Record	Remark			
Acceleration (strain gauge type)	○	max A2 44G(Z)		Contents damage	-				
Acceleration (spring type)	○	30G (150G), 25G, 28G (50G)		Leak (halogen leak)	○	No leaks.			
Strain distribution	○	max S2 128μ (B)							
Shock absorber deformation	○								
Packaging body damage	○	Not damaged.							
Lid unit damage	○	Not damaged.		Still photograph					
Drop attitude and status				Deformation and damage status (in mm)					
<div><div><div>■ Strain accelerometer</div><div>✕ Spring accelerometer</div><div>▼ Strain gauge</div><div>■ Projection</div></div></div>				<div>Shock absorber damage</div> 					
Model pipe A: STPG with one end closed, B: STPG with both ends open Acceleration (strain gauge type): Tri-axis acceleration converter AS-TA1000 Acceleration (spring type): Acceleration sensor Strain gauge: KFC-5-D17-16									

Test number 1 (Horizontal drop 1, drop test I)



**Fig. (II)-A-App.13(a) Phenomenal Waveforms Reproduced on a Synchroscope**

(II)-A-App-42

Test number 2 (Horizontal drop 1, drop test II (center)

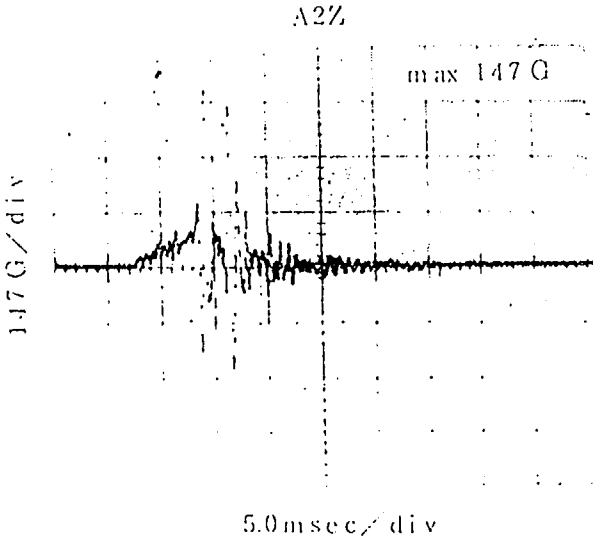
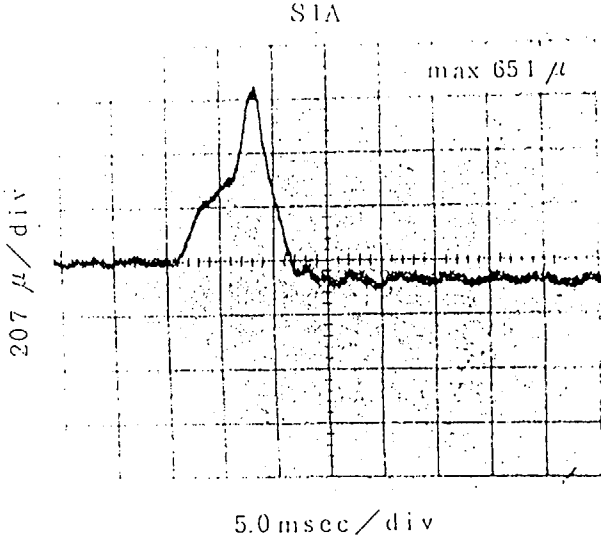
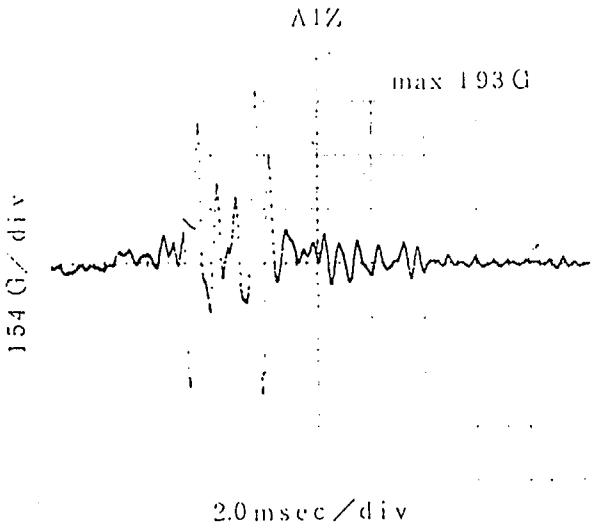


Fig. (II)-A-App.13(b) Phenomenal Waveforms Reproduced on a Synchroscope

(II)-A-App-43

Test number 3 (Horizontal drop 1, drop test II (eccentric))

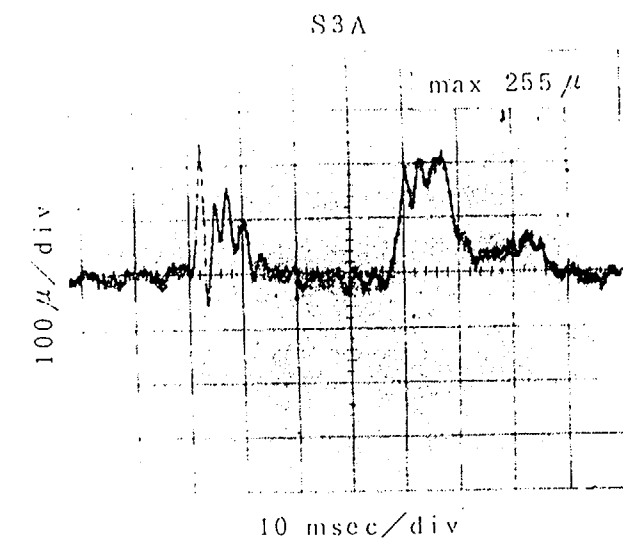
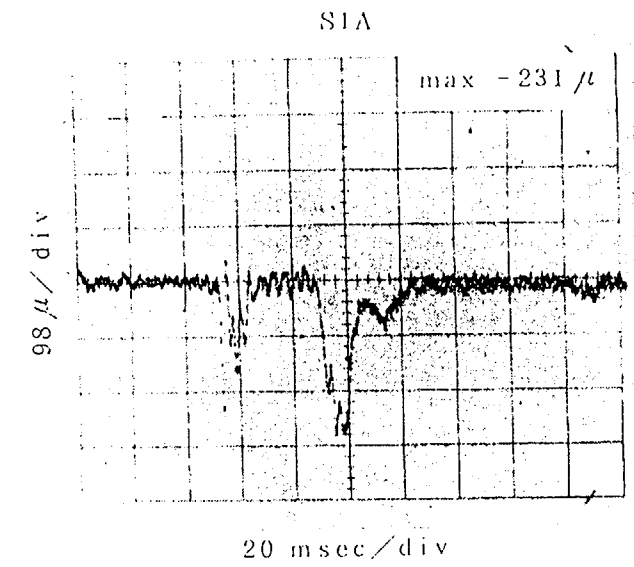
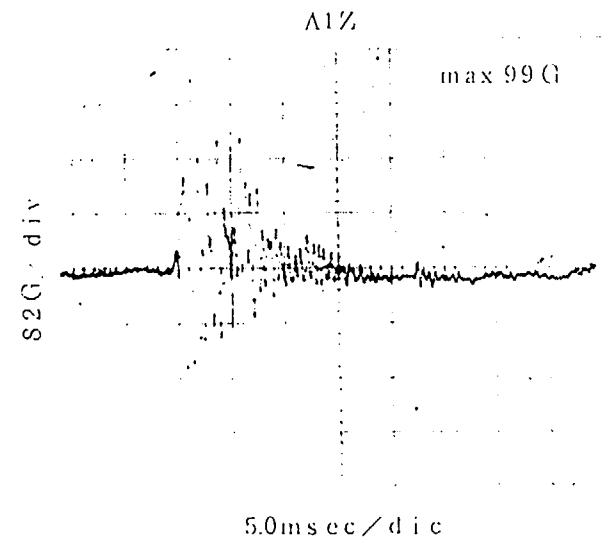
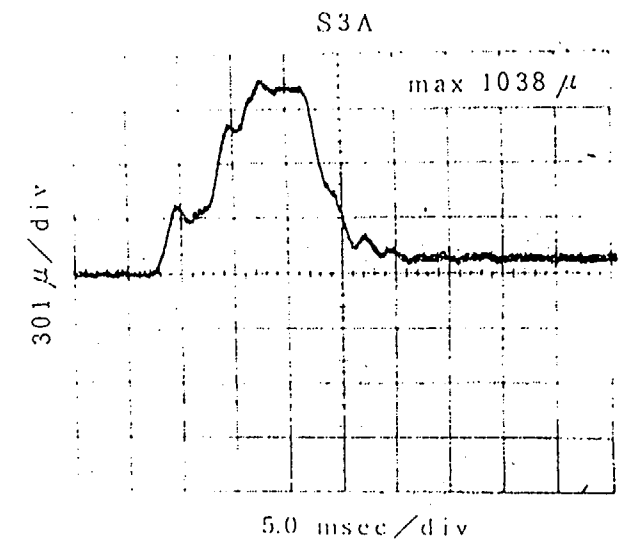
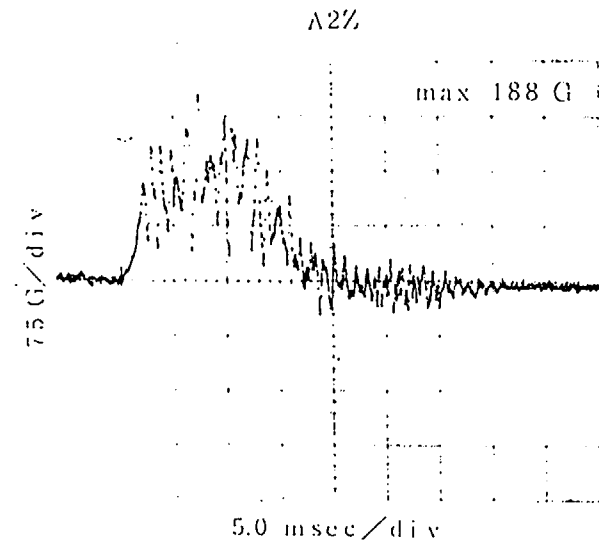
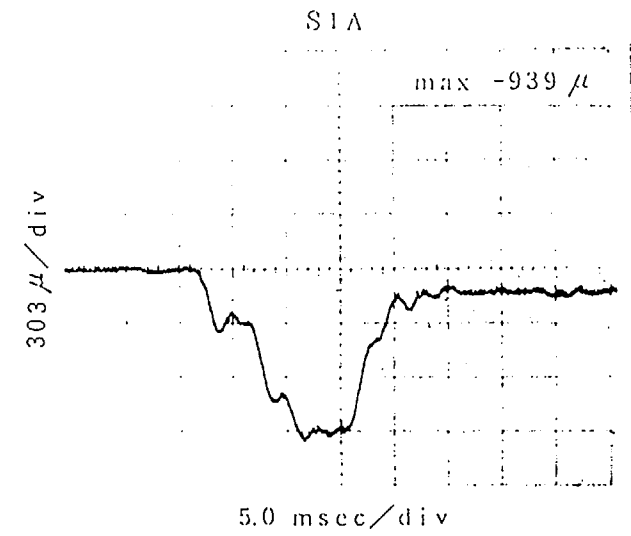
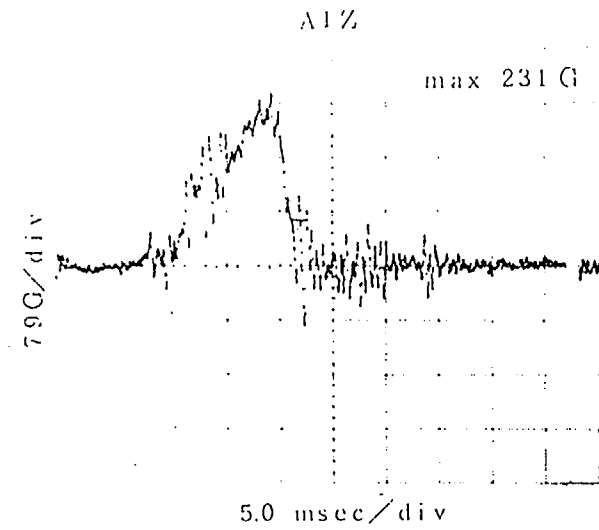


Fig. (II)-A-App.13(c) Phenomenal Waveforms Reproduced on a Synchroscope

Test number 4 (Horizontal drop 2, drop test I)



(II)-A-App-45

**Fig. (II)-A-App.13(d) Phenomenal Waveforms Reproduced on a Synchroscope**

Test number 5 (Horizontal drop 2, drop test II (center))

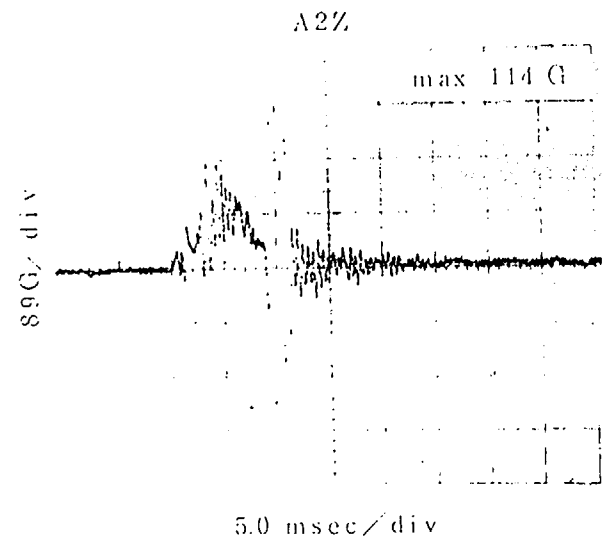
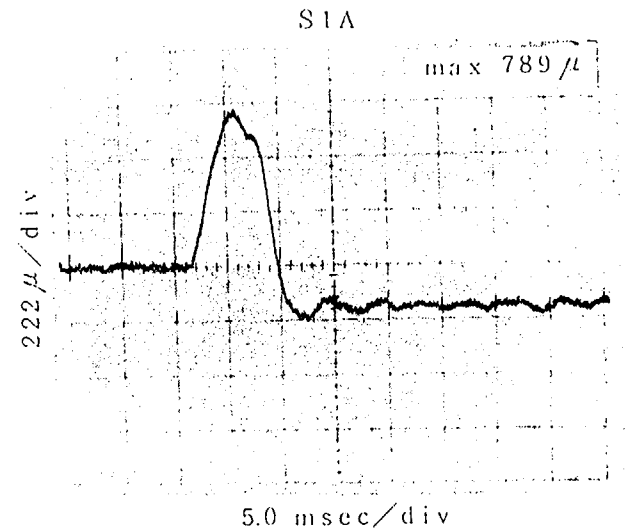
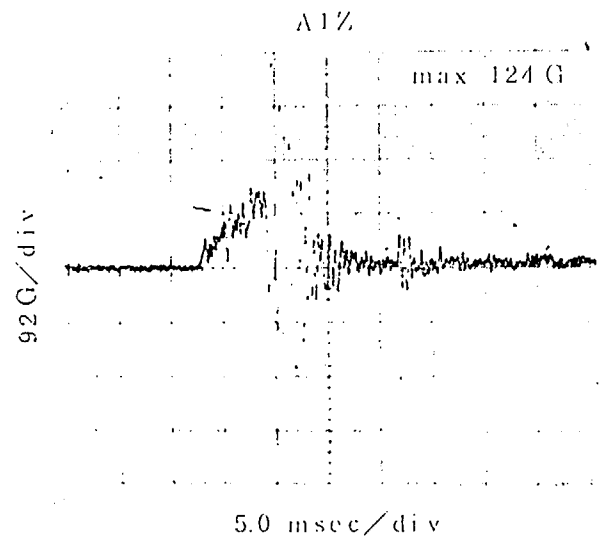
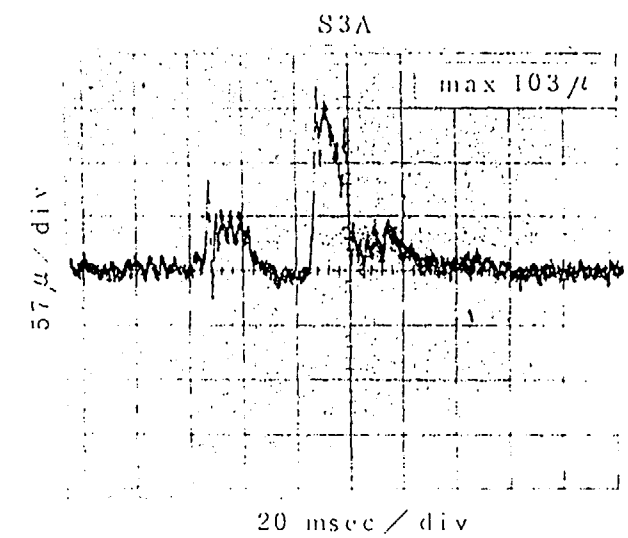
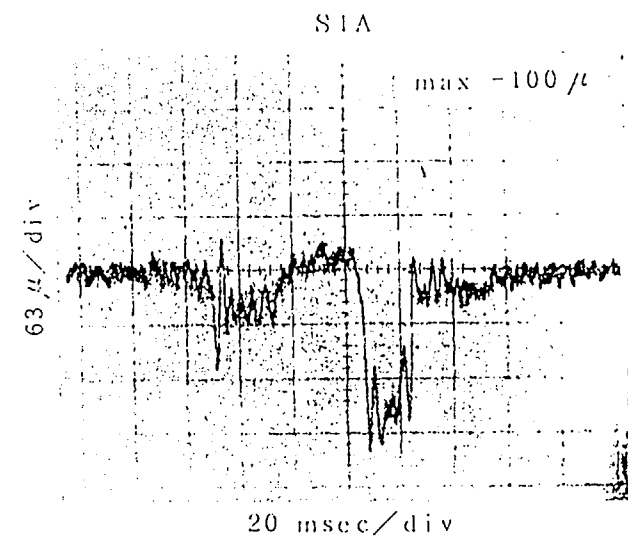
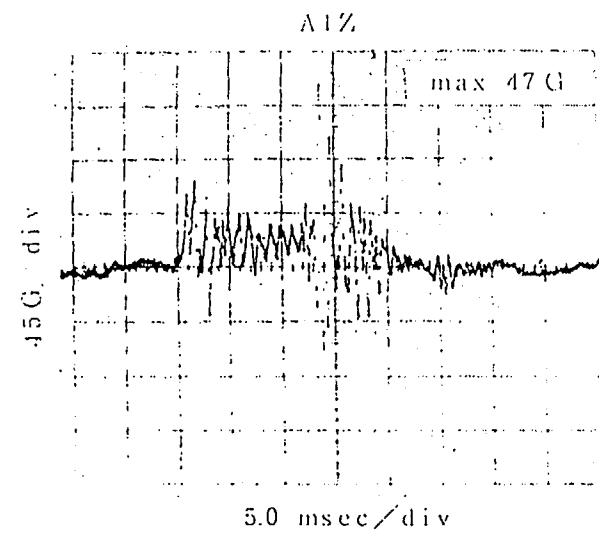


Fig. (II)-A-App.13(e) Phenomenal Waveforms Reproduced on a Synchroscope

Test number 6 (Horizontal drop 2, drop test II (eccentric)



(II)-A-App-47

Fig. (II)-A-App.13(f) Phenomenal Waveforms Reproduced on a Synchroscope

Test number 7 (Vertical drop, drop test I)

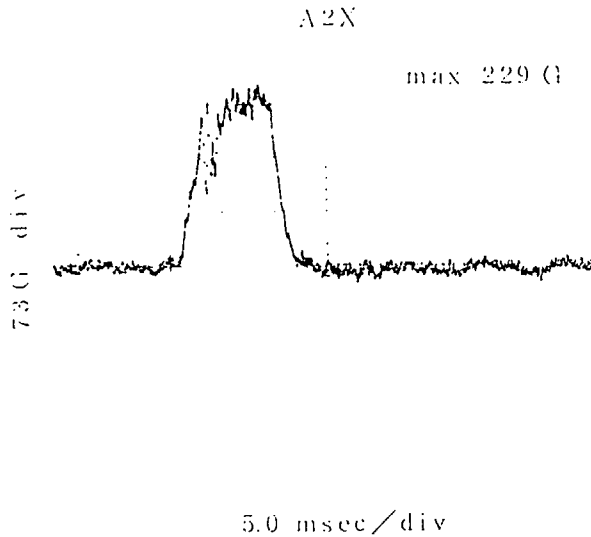
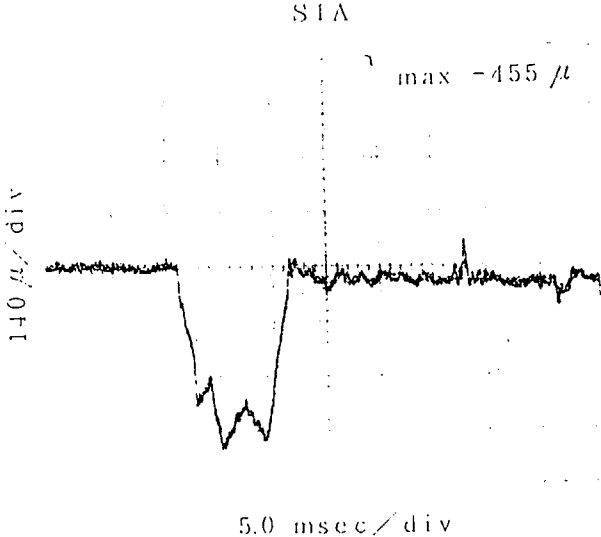
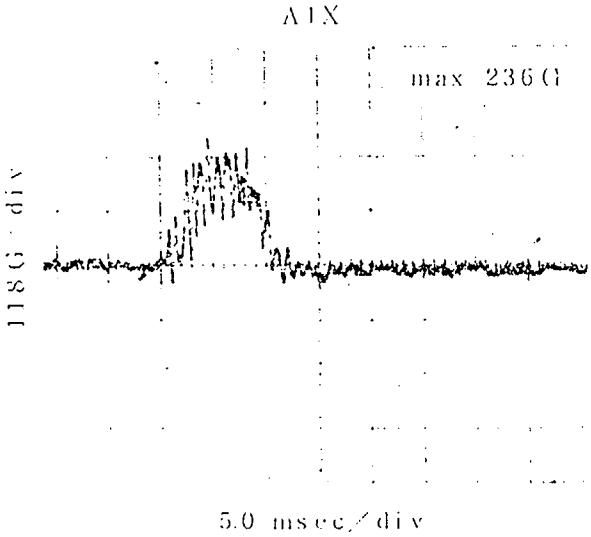
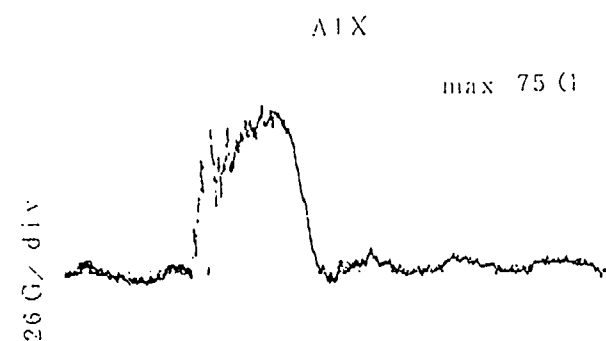


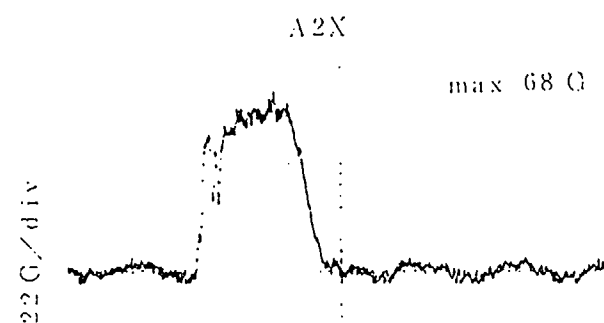
Fig. (II)-A-App.13(g) Phenomenal Waveforms Reproduced on a Synchroscope



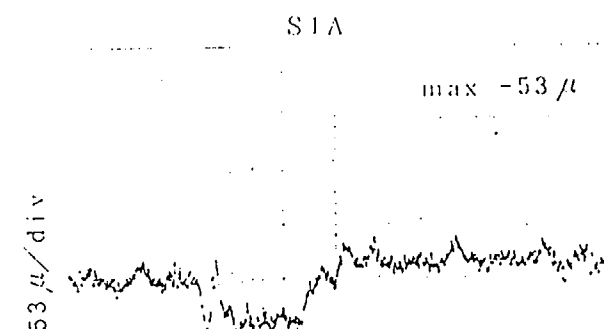
Test number 8 (Vertical drop, drop test II (center))



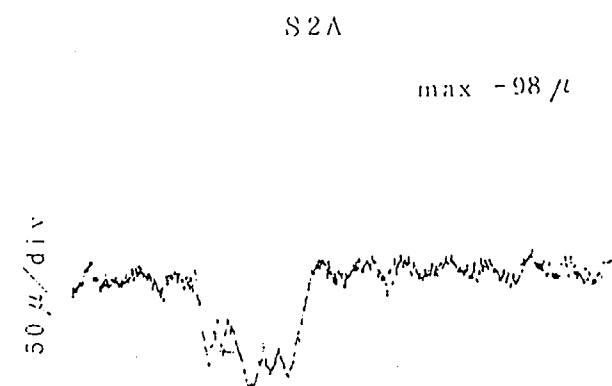
5.0 msec/div



5.0 msec/div



5.0 msec/div



5.0 msec/div

**Fig. (II)-A-App.13(h) Phenomenal Waveforms Reproduced on a Synchroscope**

Test number 9 (Vertical drop, drop test II (eccentric))

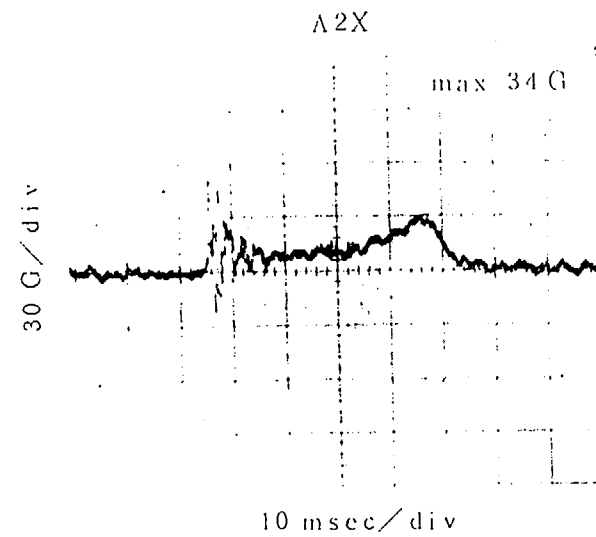
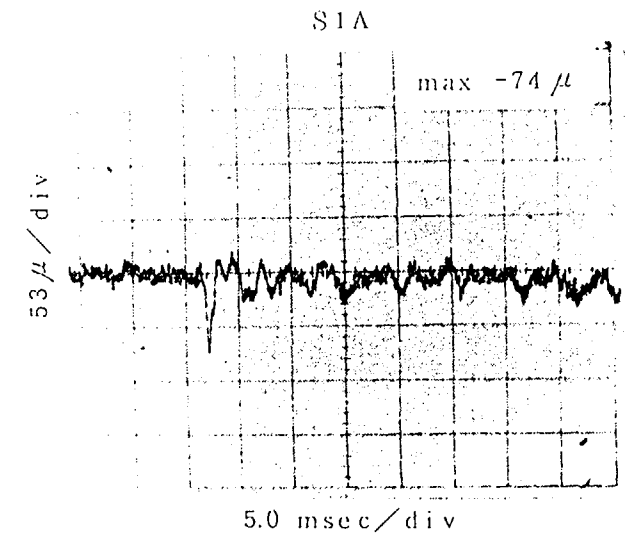
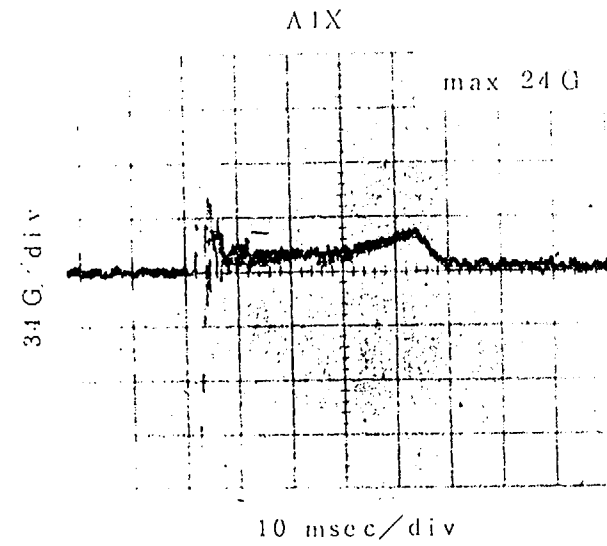


**Fig. (II)-A-App.13(i) Phenomenal Waveforms Reproduced on a Synchroscope**

Test number 10 (Corner drop, drop test I)

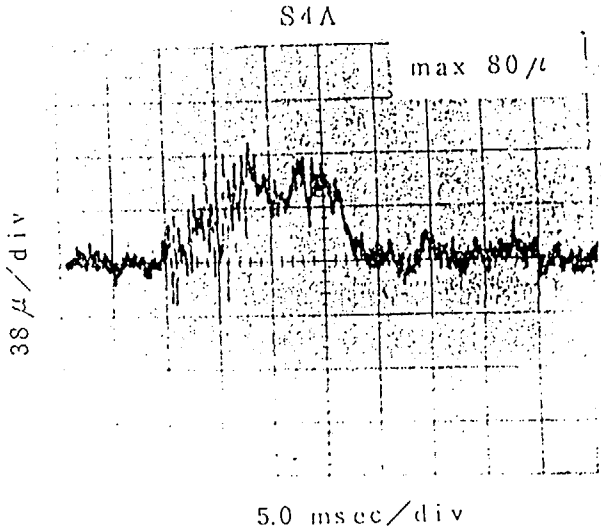
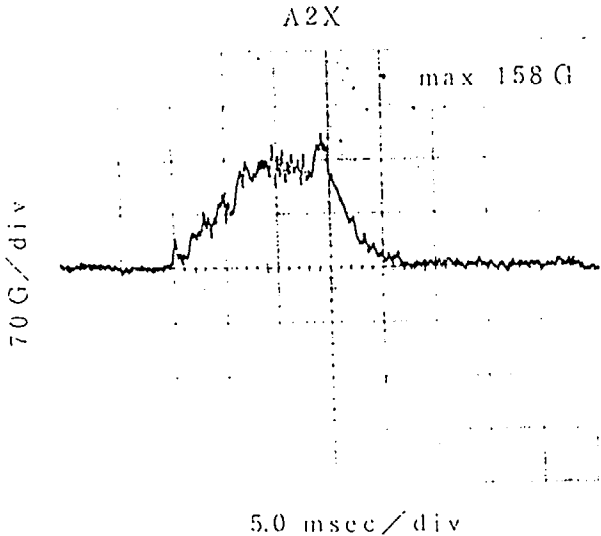
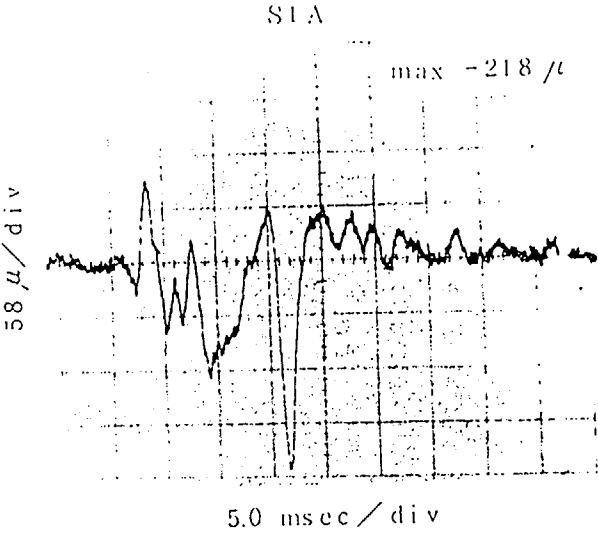
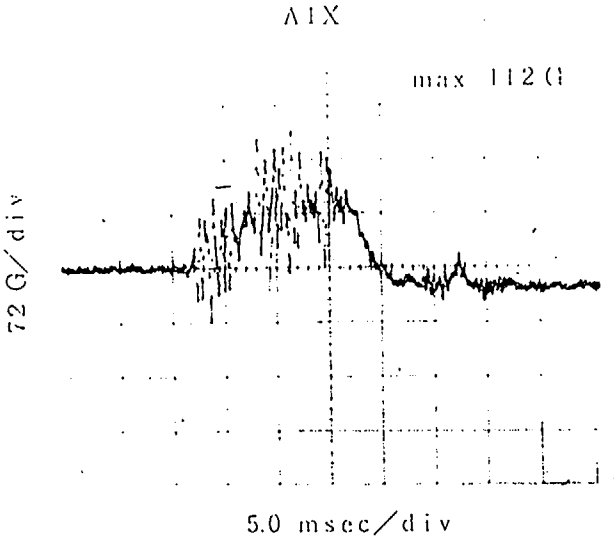
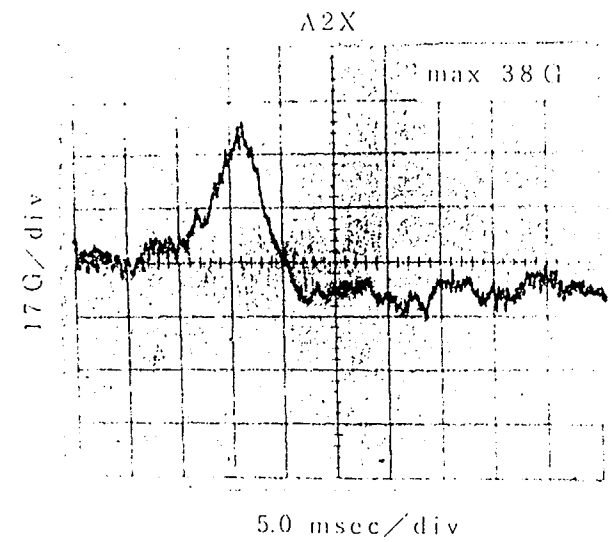
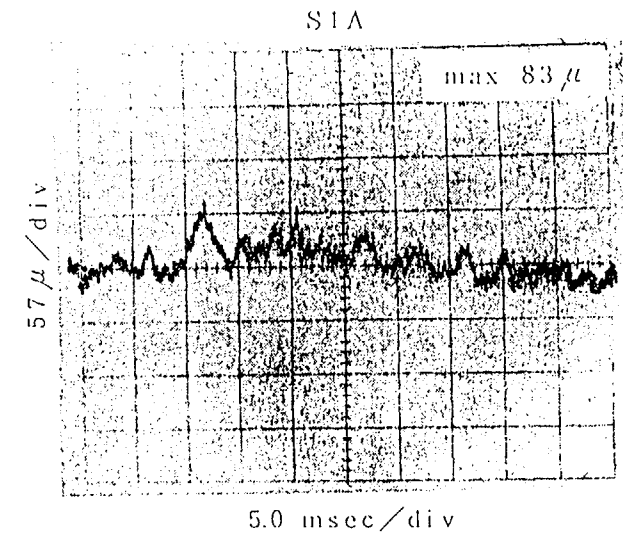
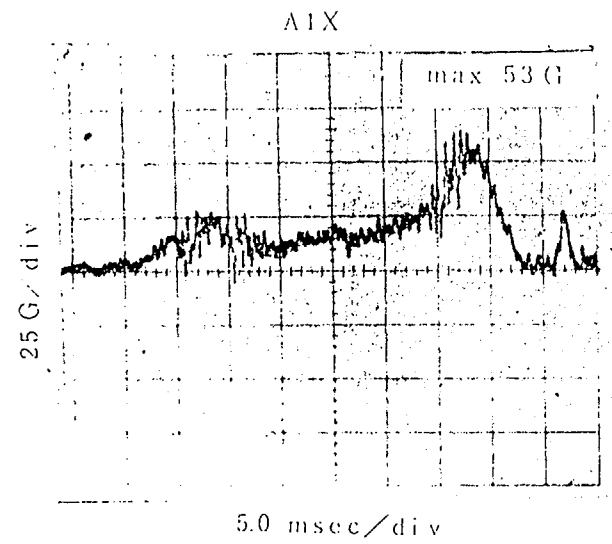


Fig. (II)-A-App.13(j) Phenomenal Waveforms Reproduced on a Synchroscope

(II)-A-App.-51

Test number 11 (Corner drop, drop test II)



**Fig. (II)-A-App.13(k) Phenomenal Waveforms Reproduced on a Synchronoscope**

(II)-A-App.-53

Test number 12 (Oblique drop, drop test I)

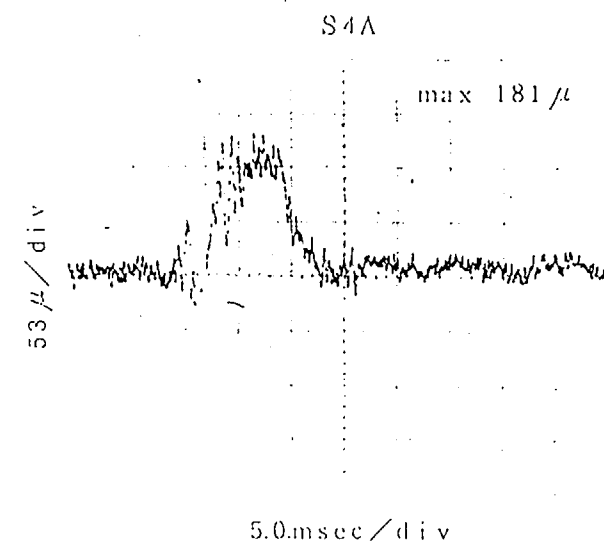
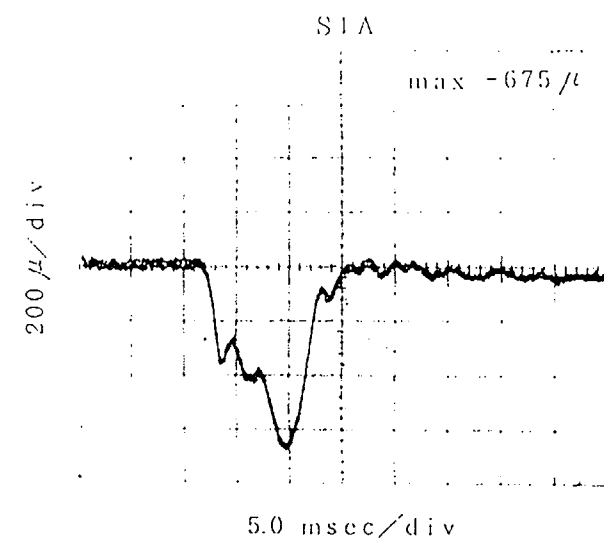
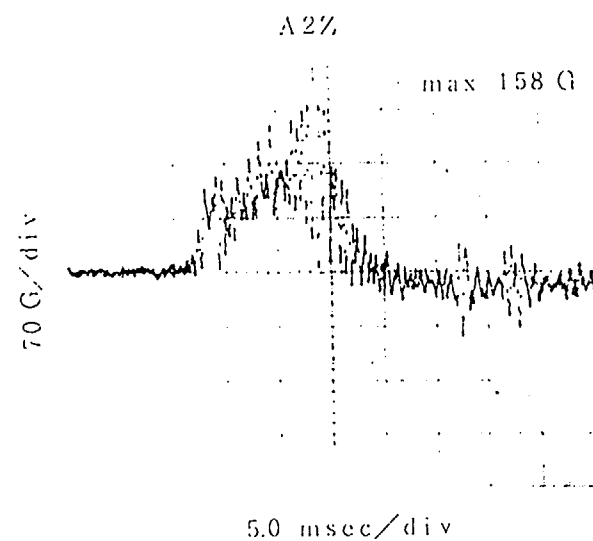
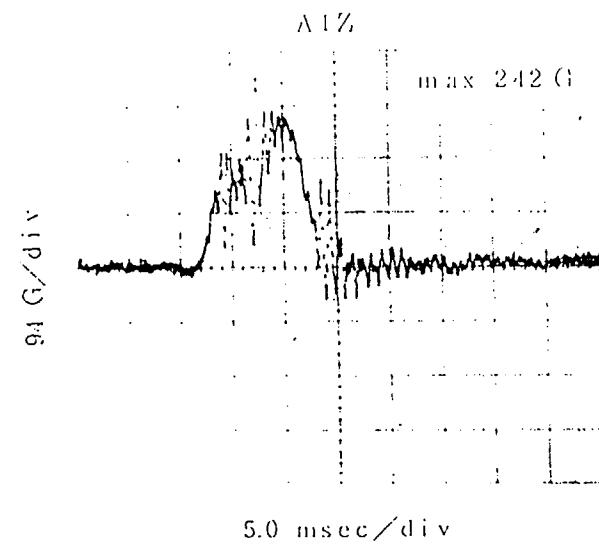
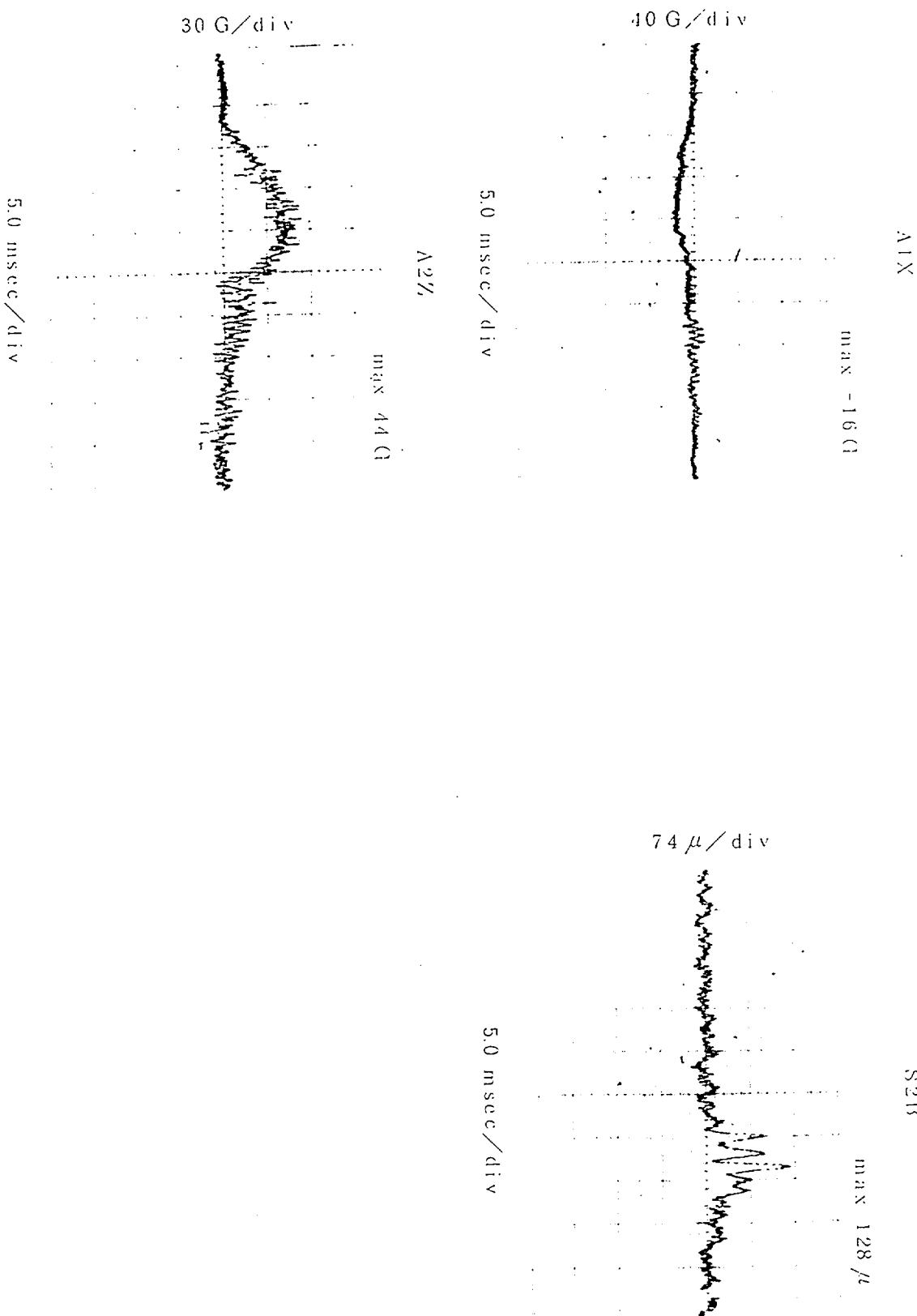


Fig. (II)-A-App.13(I) Phenomenal Waveforms Reproduced on a Synchroscope

Test number 13 (Oblique drop, drop test II)



(II)-A-App.-54

Fig. (II)-A-App.13(m) Phenomenal Waveforms Reproduced on a Synchroscope

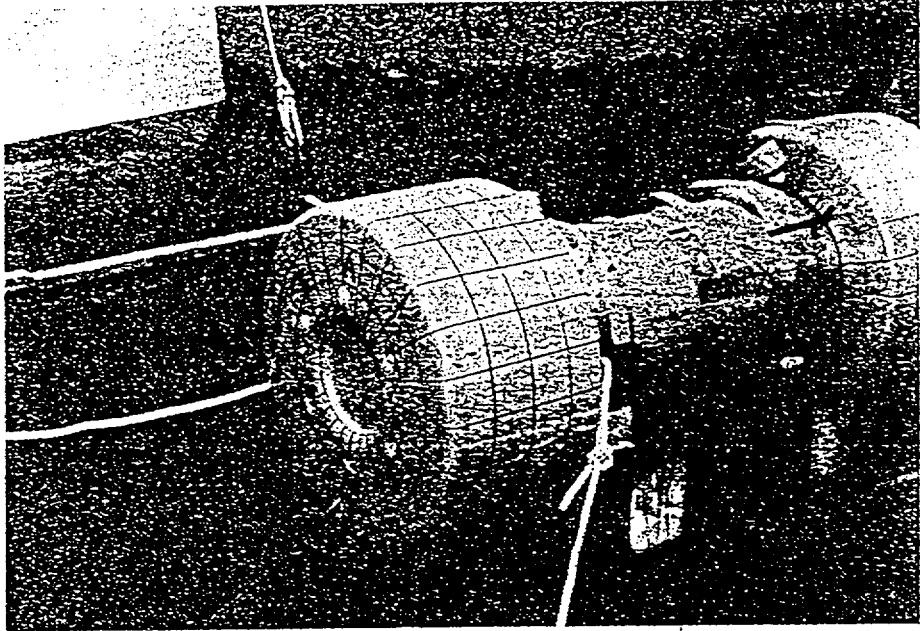


Fig. (II)-A-App.14 (a) Before a Drop Test

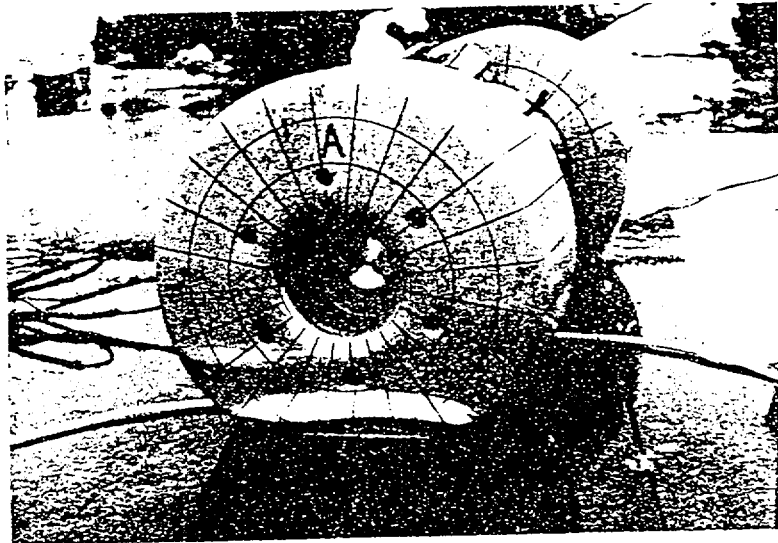


Fig. (II)-A-App.14(b) Horizontal Drop

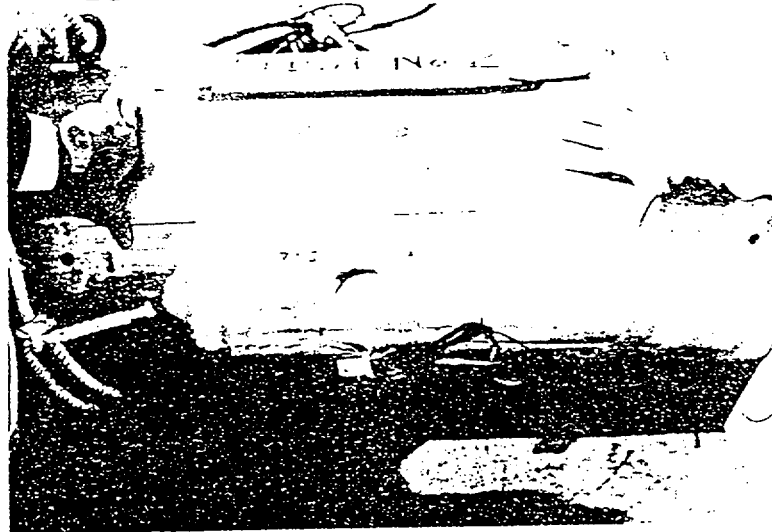


Fig. (II)-A-App.14(c) Drop Test II on the Shell



Fig. (II)-A-App.14(d) Drop Test II on Circumference of the Shock Absorber



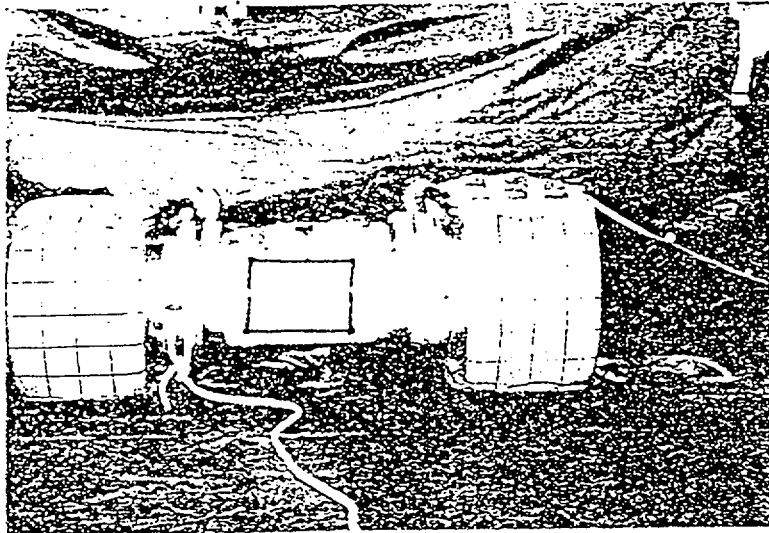


Fig. (II)-A-App.14(e) Horizontal Drop

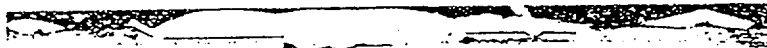


Fig. (II)-A-App.14(f) Drop Test II on the Shell

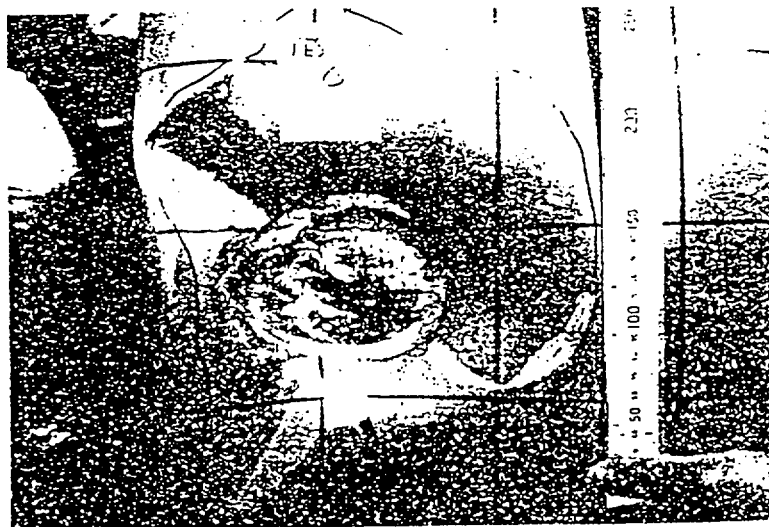


Fig. (II)-A-App.14(g) Drop Test II on Circumference of the Shock Absorber

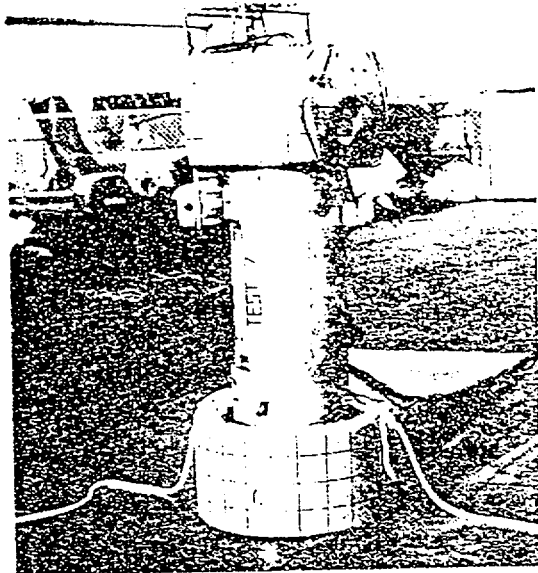


Fig. (II)-A-App.14(h) Vertical Drop

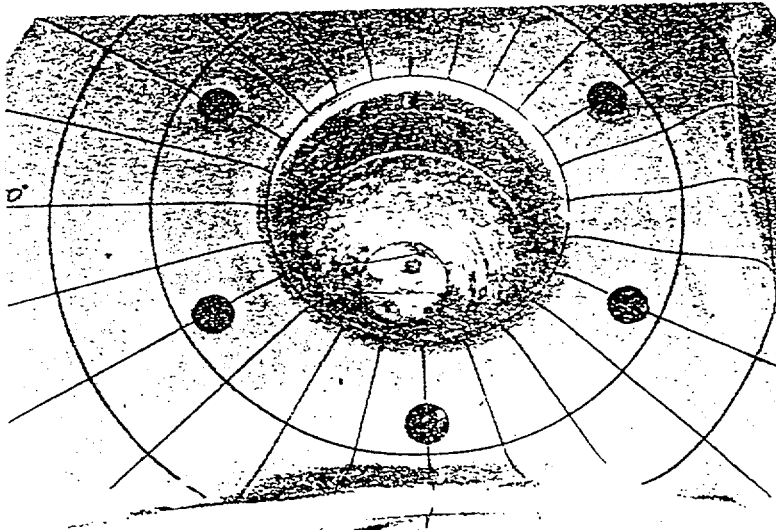


Fig. (II)-A-App.14(i) Drop Test II on the Center of the Shock Absorber

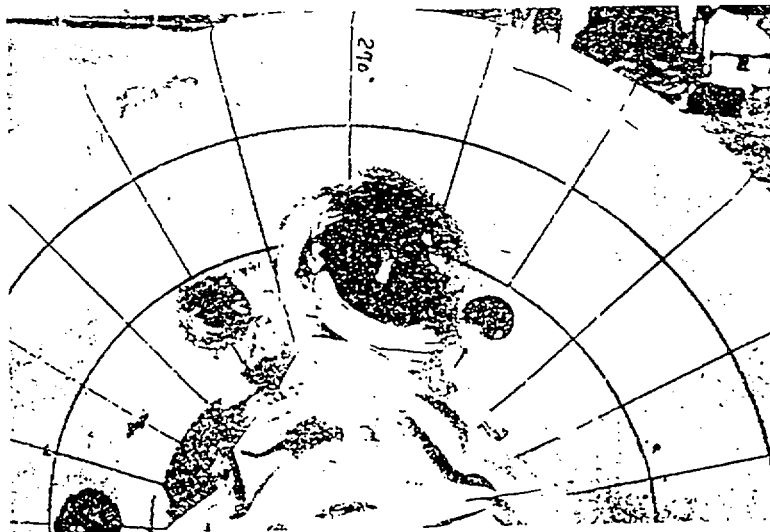


Fig. (II)-A-App.14(j) Drop Test II on the End Surface of the Shock Absorber

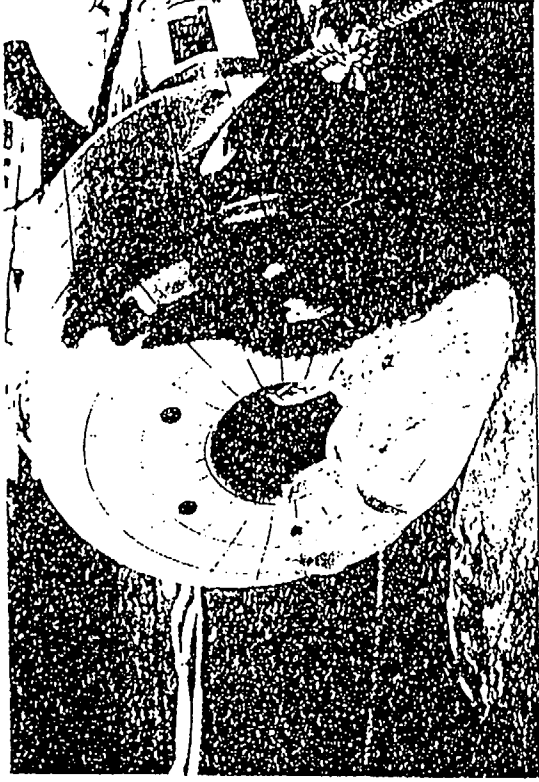


Fig. (II)-A-App.14(k) Corner Drop

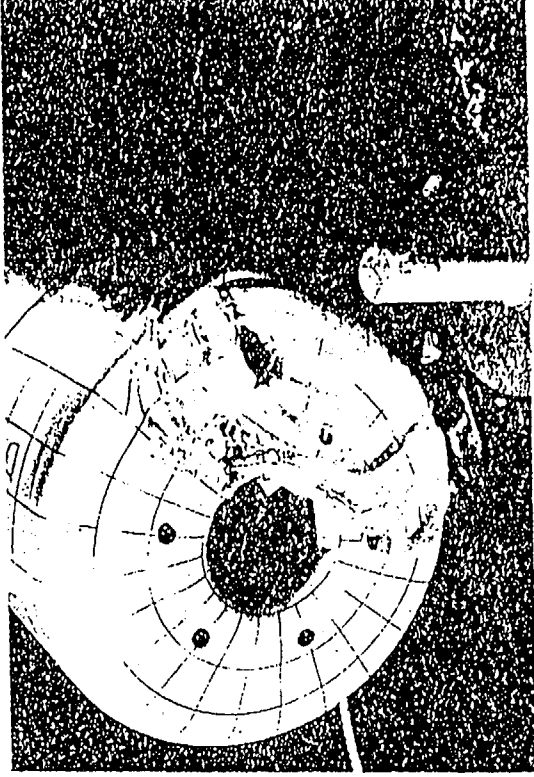


Fig. (II)-A-App.14(l) Drop Test II on the Shock Absorber

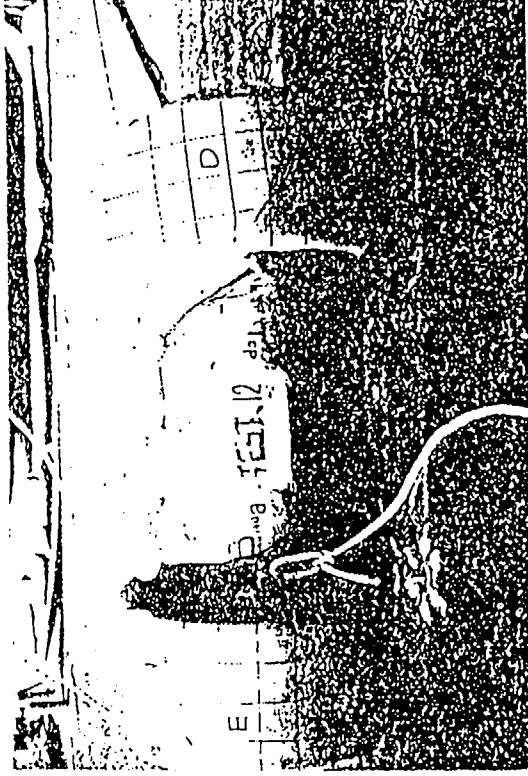


Fig. (II)-A-App.14(m) Oblique Drop



Fig. (II)-A-App.14(n) Drop Test II on the Shock Absorber

### 3.4 Comparison of the results obtained by evaluation and by a 1/2-scale model

Regarding the deformation value of the shock absorber, for every drop test, the result obtained on the 1/2-scale model by an analysis applying the same method as used to evaluate the actual packaging is compared with the result obtained by an experimental drop test as shown in Table (II)-A-App.7. All analytical results obtained by drop test I using the code, SHOCK-2, indicate a greater deformation value for the shock absorber compared with the corresponding experimental results. Therefore, analytical results that are on the safe side are obtained. It is presumed that the deformation has increased because the contribution by the deformation of the covering plate is not considered. Regarding the impact deceleration, the values shown in Table (II)-A-App.7 are obtained by adding the effect of the covering plate to the deceleration obtained by using the code, SHOCK-2, in the same manner as is done when the actual packaging is analyzed. In the case of impact deceleration, the analytical values are also higher than the experimental values. Therefore, the values used in the structural evaluation are on the safe side.

**Table (II)-A-App.7 Comparison of Results Between the 1/2-scale Model Test and Evaluation**

	1/2-model test results	1/2-model evaluation results**	Remarks
Drop test I			
(1) Vertical drop Acceleration Deformation	236 G 47 mm	285 G 54 mm	** Obtained using the same evaluation method used for an actual packaging.
(2) Horizontal drop Acceleration Deformation	231 G 63 mm	237 G 75 mm	
(3) Corner drop Acceleration Deformation	160 G 104 mm	161 G 107 mm	
Drop test II			
(1) Vertical drop Drop on the center of the shock absorber (Fir-plywood part)  Drop on the end part of the shock absorber (Balsa wood part)	24 mm  93 mm	26 mm  86 mm *	* Distance between the center of gravity and the impact point of the packaging 350 × 1/2 position
(2) Horizontal drop Deformation at the center of the outer container  Drop on the shock absorber	8.5 mm  21.5 mm +	Not penetrated.  29 mm	+ It is presumed that the value has been reduced because the target portion strikes twice during a drop.
(3) Corner drop Deformation of the shock absorber	88 mm	88 mm	

Table (II)-A-App.8 lists the experimental results and the analytical results of the shock absorber deformation when both drop test I and II are conducted. The 1/2-scale model evaluation results are higher than the experimental results. They can therefore be assumed to be on the safe side in terms of the evaluation of deformation. Table (II)-A-App.8 also lists the analytical results of the actual packaging. Therefore, the method used to calculate shock absorber deformation and the impact deceleration of the actual packaging is assumed to be proper.

**Table (II)-A-App.8 Comparison of the 1/2-Scale Model Test, 1/2-Scale Model Evaluation, and Actual Packaging Evaluation Results**

Shock absorber deformation during drop tests I + II	1/2-scale model test result	1/2-scale model evaluation results	Actual packaging evaluation results	Remarks
(1) Vertical drop	140 mm	140 mm	294 mm	* Obtained using the same evaluation method used for an actual packaging.
(2) Horizontal drop	85 mm	104 mm	236 mm	
(3) Corner drop	192 mm	195 mm	410 mm	

A leakage test is conducted before and after 1/2-scale model specimen drop test to indicate that the engineering criterion is satisfied. (See section C.4 of Chapter II.)

Moreover, the outer container, rotating plug fixing part, and penetration hole lid unit are visually inspected after the drop test is completed to confirm that the outer container is not penetrated (during drop test II), and that no deformation occurs. Therefore, the structural evaluation method used for the actual packaging is judged to be proper.

## **(II)-B THERMAL ANALYSIS**

### **B.1 Outline**

This section and its appendix describe how to calculate the temperature of every major section of this package under both normal and accident test conditions, and also determines the temperature data required to calculate the thermal stress in Chapter (II), "Structural Evaluation."

#### **B.1.1 Features of this Package**

- (1) This packaging is a dry-type packaging basically consisting of an outer container, front and rear shock absorbers, and an inner container as shown in Fig. (I)-1.
- (2) As shown in Fig. (I)-2, the outer container is made up of a double-cylindrical body shell consisting of outer and inner shells, and front and rear lid units connected to both ends of the shell part. The decay heat generated by the contents stored in the inner container is transferred through the inner container to the inner shell of the outer container, rotating plug, and shielding plug via radiation and thermal conduction, and is further transferred to the lead shield via thermal conduction. Most of the heat on the lead shield is transferred through the cement layer and heat dispersion fins to the outer shell via thermal conduction, and is finally released into the open air from the outer shell surface of the outer container via natural convection and radiation. Some of the heat from the lead shield is transferred through the front and rear lid units to the shock absorbers via thermal conduction, and is finally released into the open air through the surface cover steel plate of the shock absorbers via natural convection and radiation.
- (3) The quantity of heat generated from the contents of this package ranges between 0 and 260 W.
- (4) The pivoting trunnion and rear base plate are fixed to the transport skid as shown in Fig. (I)-3 so that this package remains in a horizontal position during transport.
- (5) In case of fire, heat will enter this package via the outer shell part of the outer container and the front and rear shock absorbers. The outer shell part of the outer container is equipped with eight fusible bismuth plugs that release gas generated from the cement layer and resin layer to prevent pressure from increasing in the outer container during a fire. Moreover, the cement layer keeps the heat from entering the outer shell to prevent any temperature increase of the internally filled lead shield.

The front and rear shock absorbers protecting the outer container lid units consist of flame-resistance treated balsa wood and fir-plywood, and are therefore insulated against heat. These shock absorbers are covered with stainless steel. The stainless steel covers are each equipped with ten fusible plugs that release gas generated from the shock absorption material to prevent pressure from excessively increasing in the shock absorbers during a fire. Furthermore, a cement layer is provided on the inside of the shock absorber that makes contact with the outer container so that the absorber can withstand the heat.

#### **B.1.2 Thermal Analysis Conditions**

Thermal analysis is performed for the package under normal and accident test conditions.



(1) Maximum decay heat

As described in Chapter (I), eight types of contents are to be stored in this package. Table (II)-B-1 lists the maximum decay heat of those contents. Contents I, and Contents IV through Contents VIII are loaded into the packaging using the same procedures. Therefore, the thermal analysis of Contents I, which have the maximum quantity of decay heat, is described below. Assuming that Contents I are placed nearest to an O-ring having a containment function, two types of Contents I will be evaluated with a maximum decay heat of 260 W. One type of Contents I has their heat generating region off the center (Contents I • eccentric) and the other type has the heat generating region in the center (Contents I • center).

The decay heat of Contents II is lower than that of Contents I. In procedures for loading the package into the fuel supporting can, Contents II differ from Contents I. The fuel pins of Contents II are stored in receiving tubes I, which are supported by a rack. Therefore, the temperature of receiving tube I is evaluated with a maximum decay heat of 64 W, that is, the maximum decay heat of Contents II. Receiving tubes I are evaluated using contents with the heat generating region in the center, since they are fixed to the center of the package by the rack.

For the structural material used for an irradiation test, the maximum decay heat (30 W) is lower than that of the other seven types of contents mentioned above. Therefore, it is apparent that the temperature of every section of the package becomes lower than that of Contents I and II. This evaluation is thus omitted.

**Table (II)-B.1 Maximum Decay Heat of the Contents**

Irradiation test fuel element							Structural material for the irradiation test
Contents I	Con- tents IV	Con- tents V	Con- tents VI	Con- tents VII	Con- tents VIII	Con- tents II	Contents III
Eccentric, Center							
260W	250W	63W	260W	3W	170W	64W	30W

(2) Environmental conditions

To evaluate the maximum temperature, the ambient temperature before and after a fire under normal and accident test conditions shall be subject to a solar heat load in open air at a temperature of 38°C. To evaluate the minimum temperature, the ambient temperature is evaluated assuming that it is in air at a temperature of -40°C, which represents the engineering criterion of a type B(U) package.

For a fire under accident test conditions the package is assumed to be left unattended for 30 minutes in a heat radiation environment at 800°C, which has a heat radiation emissivity of 0.9.

### (3) Thermal analysis model

As described in Chapter (II), "Structural Evaluation," this package becomes deformed under normal and accident test conditions. Since the thermal resistance of the package is influenced by such deformation, the deformation of the package under each test condition will be summarized as described below for the thermal analysis of the package.

During a free drop of the package under normal test conditions, the shock absorbers that cover all the opening parts of the package become deformed. However, during thermal analysis, the shock absorbers do not become deformed for the following reason. When the shock absorber becomes deformed and thinner, the heat dispersion resistance from this shock absorber is reduced, and the temperature of the package is evaluated as being low. Therefore, ignoring the deformation of the shock absorber during a free drop allows the evaluation to be on the safe side during the thermal analysis.

Under normal test conditions, the calculation is performed using a thermal analysis model with Contents I (eccentric and center) and Contents II shown in Figs. (II)-B.1 through (II)-B.3.

The deformation that allows heat to most easily enter the package is assumed in conducting the thermal analysis, since under accident test conditions, the package is left unattended for 30 minutes in a thermal environment at 800°C. The following are the conditions of the severest thermal analysis model.

- 1) The shock absorber, since it primarily consists of flame-resistance treated balsa wood, is difficult to burn and prevents heat from entering during a fire. Consequently, a deformation state, in which the thickness of the shock absorber covers the opening part of the outer container, is decreased and in which the deformation area is widened.
- 2) A deformation state in which the temperature of an O-ring (fluoro rubber: maximum allowable service temperature of 200°C) whose maximum allowable service temperature is the lowest (among the materials that constitute the boundary of containment) is increased.
- 3) A deformation state in which the temperatures of the tungsten (melting point of 3410°C) and lead shield (melting point of 327°C), which have a shielding function, increase.

Among the deformation states for each drop attitude obtained from the Structural Evaluation Results (subsections A.6.1 and A.6.2) in Chapter II, a vertical drop model is the severest thermal deformation state meeting all the conditions 1) through 3) above as described later in subsection B.5.2. The thermal analysis model shown in Figs. (II)-B.4 through B.6 is thus created for the evaluation. However, a deformation state, in which the temperature of O-rings that are used in the front and rear sampling valve lids and the penetration hole lid part increases, results from the deformation caused during horizontal drop. Therefore, the horizontal drop model shown in Fig. (II)-B.7 is also evaluated.

The thermal analysis is performed using the three-dimensional stable and unstable heat transfer calculation code, TRUMP 1), which is based on a differential method.

- 
- 1) Edwards, A.L., "TRUMP; A Computer Program for Transient and Steady state Temperature Distributions in Multidimensional Systems", Lawrence Radiation Laboratory, Livermore, Report UCRL-14754, Rev 2.

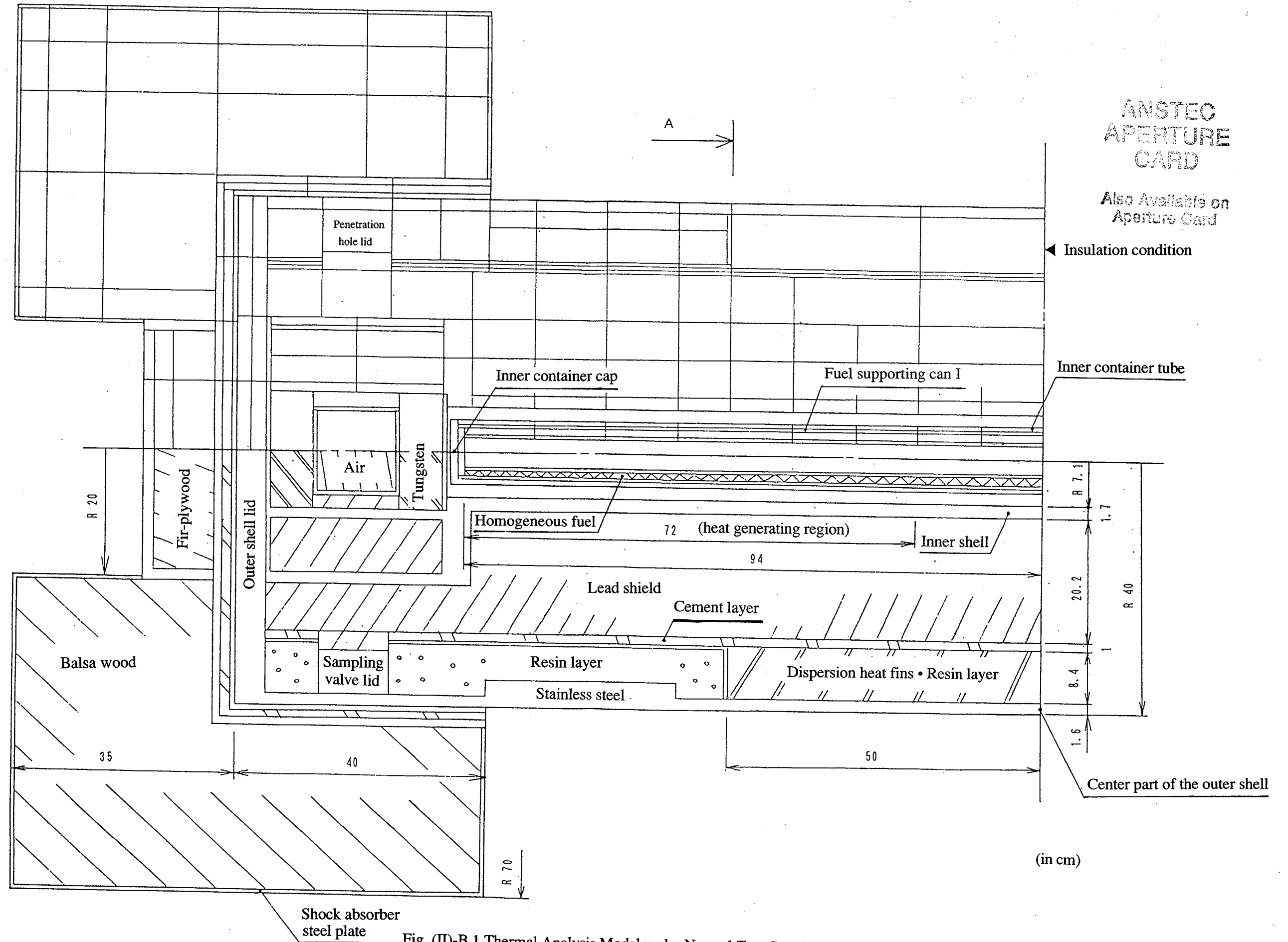
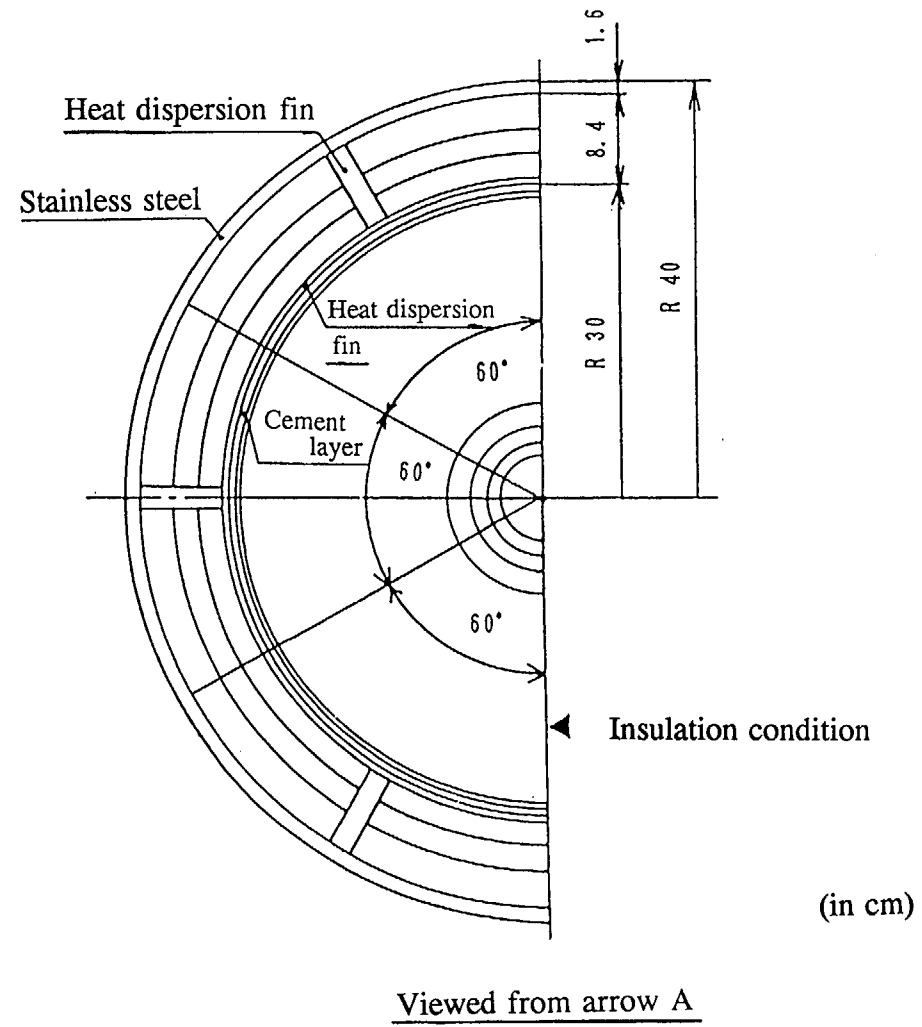


Fig. (II)-B.1 Thermal Analysis Model under Normal Test Condition (Contents I/eccentric) (1/2)

(II)-B-5



**Fig. (II)-B.1 Thermal Analysis Model under Normal Test Conditions (Contents I/eccentric)(2/2)**

# ANSTEC APERTURE CARD

Also Available on  
Aperture Card

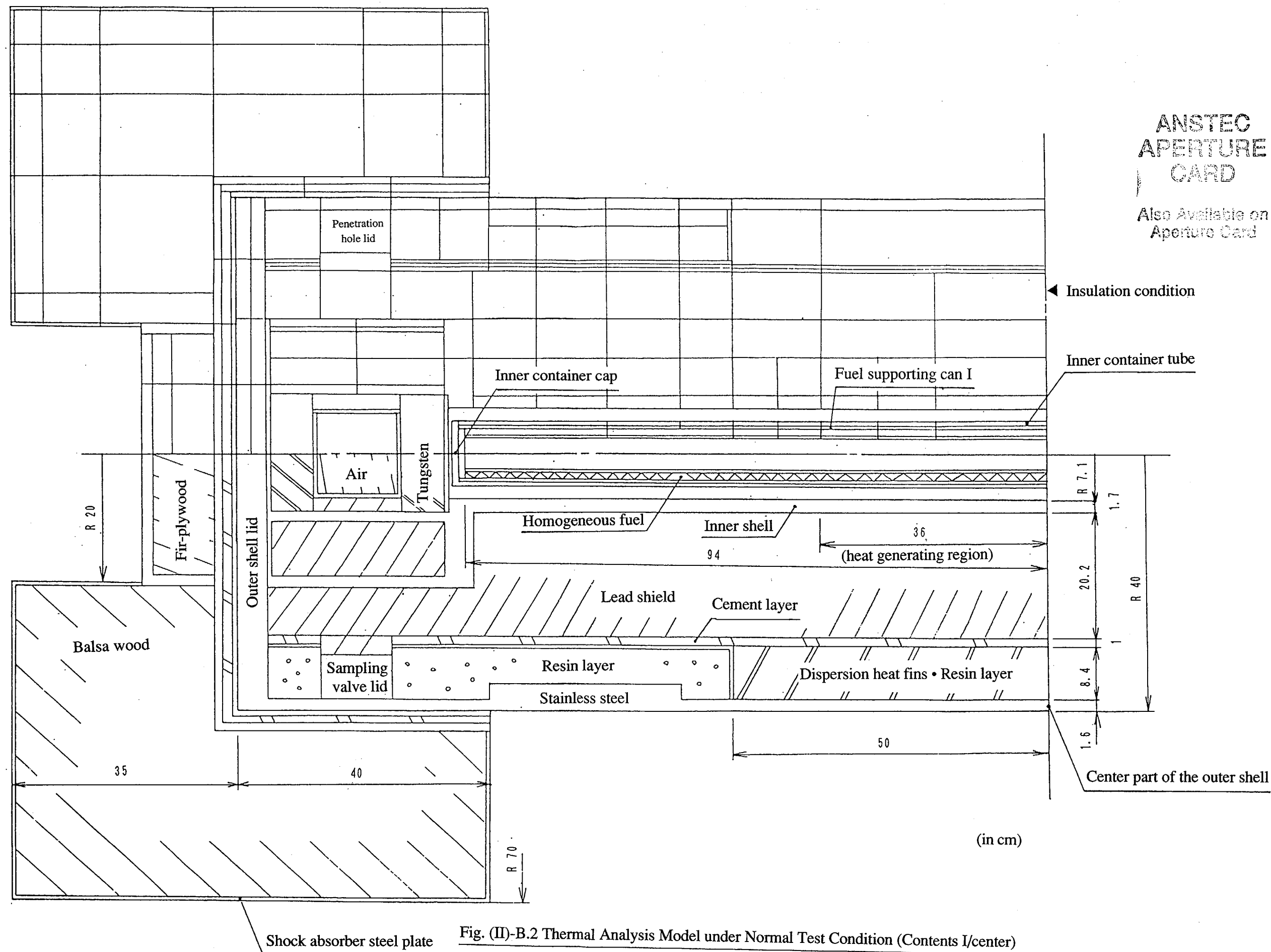


Fig. (II)-B.2 Thermal Analysis Model under Normal Test Condition (Contents I/center)

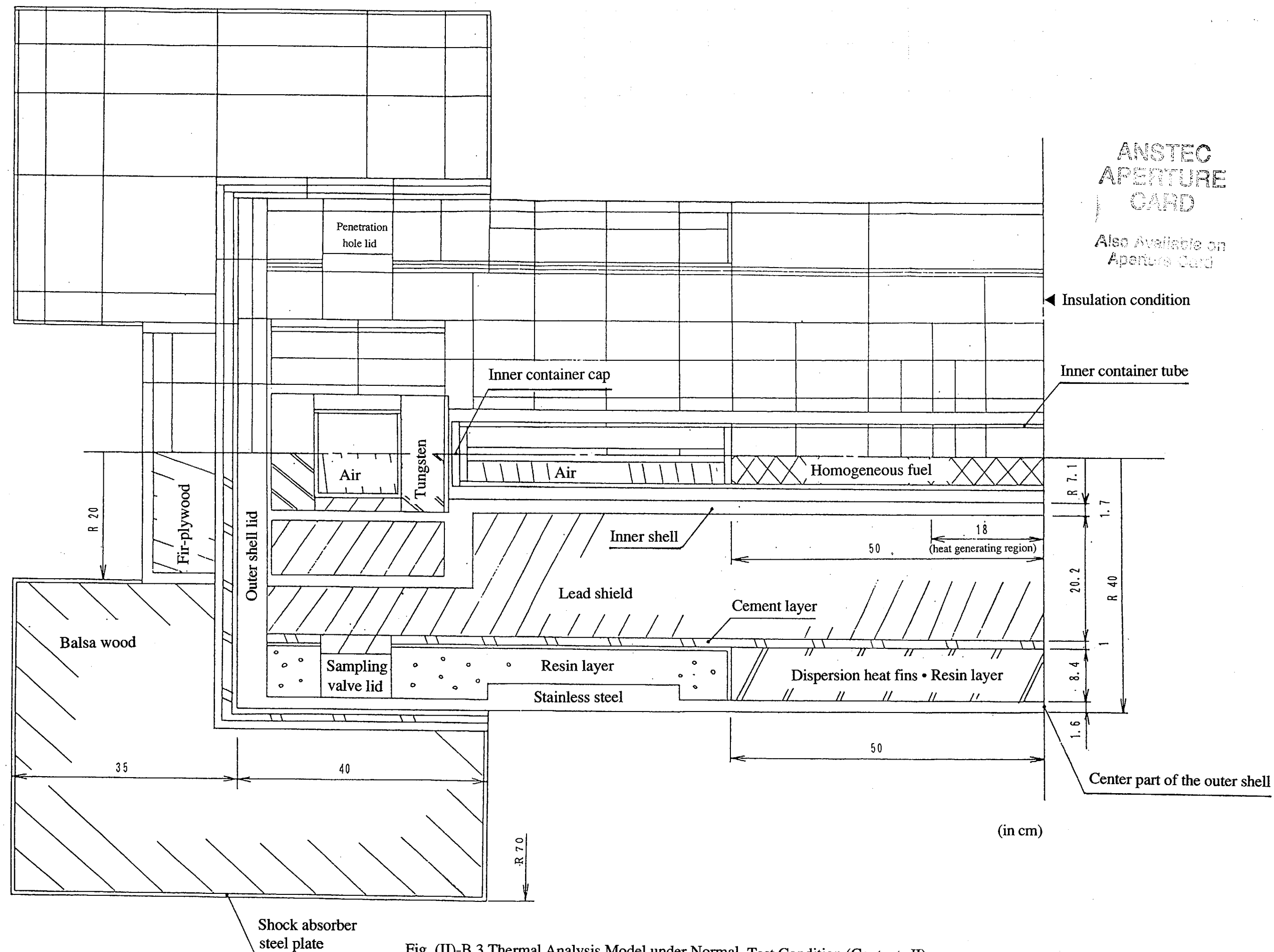


Fig. (II)-B.3 Thermal Analysis Model under Normal Test Condition (Contents II)

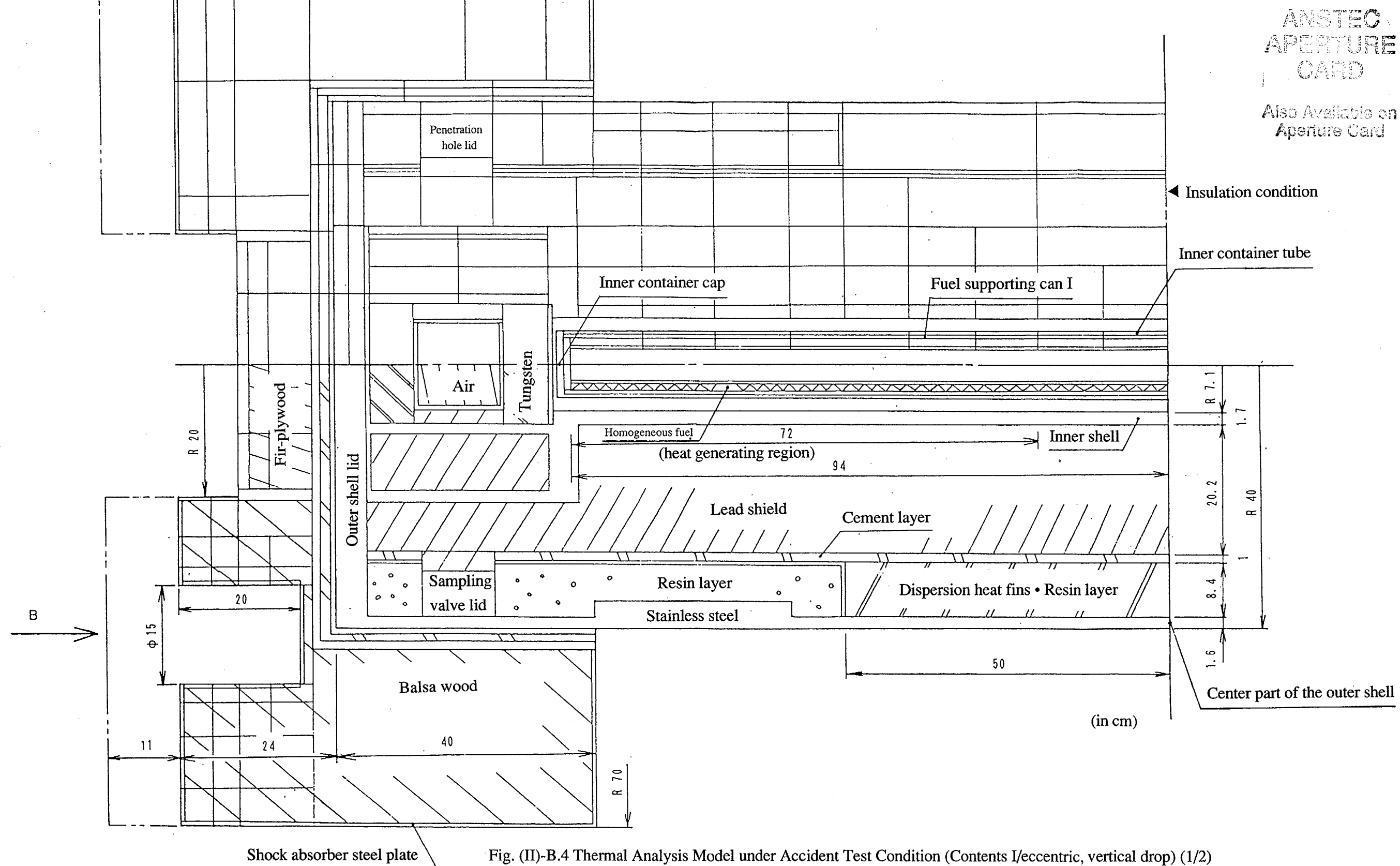
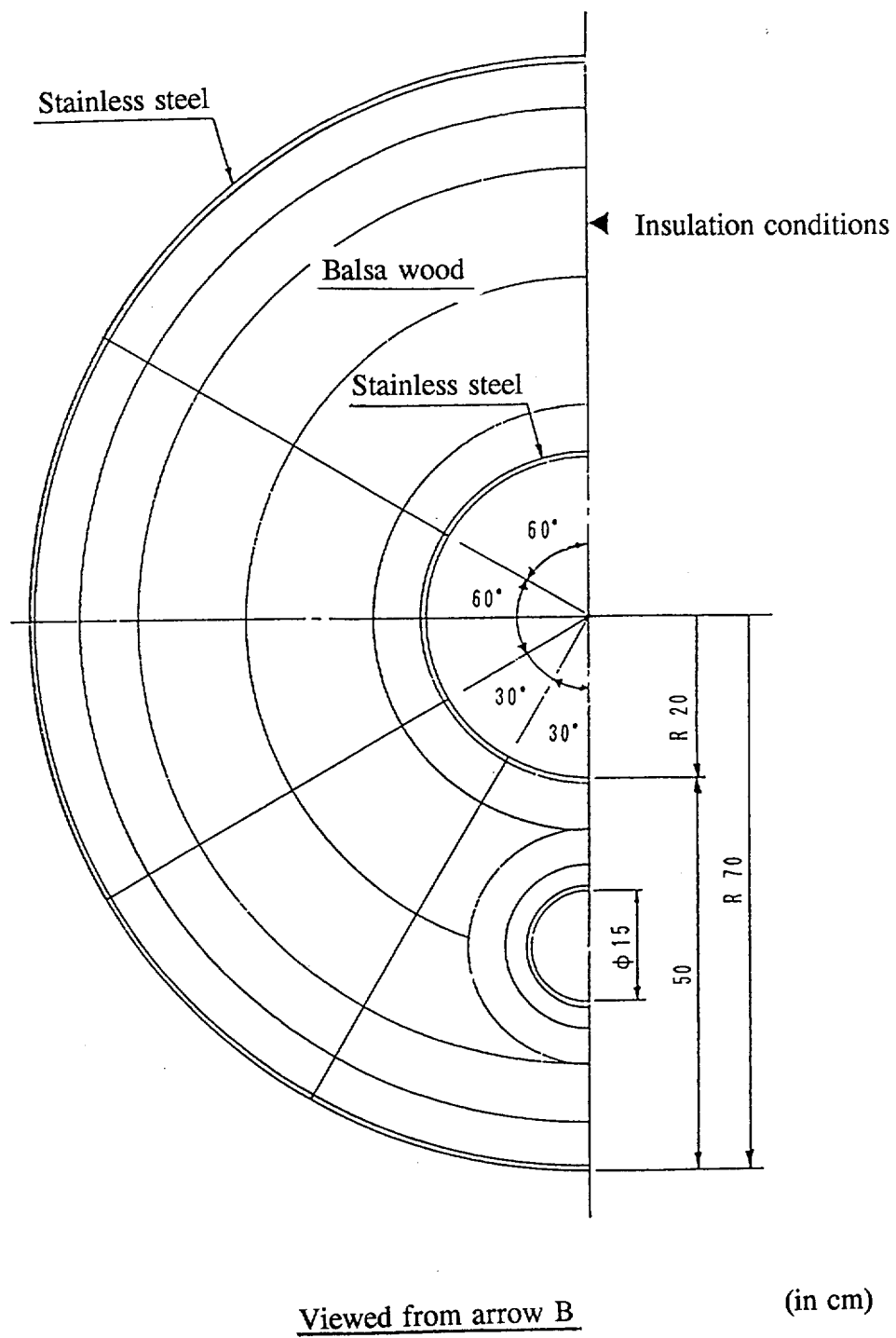


Fig. (II)-B.4 Thermal Analysis Model under Accident Test Condition (Contents I/eccentric, vertical drop) (1/2)



**Fig. (II)-B.4 Thermal Analysis Model under Accident Test Conditions**  
**(Contents I/eccentric, vertical drop) (2/2)**



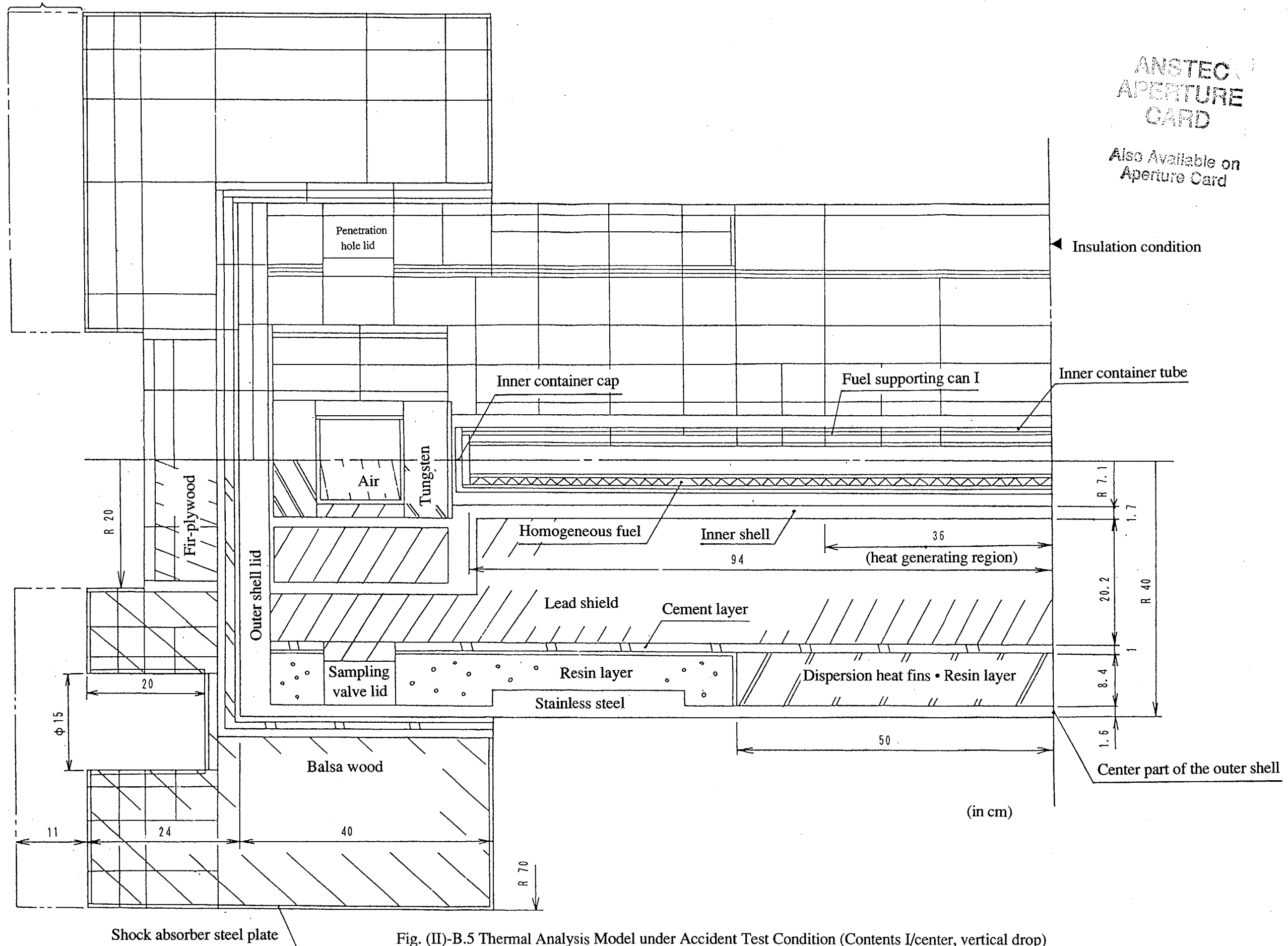


Fig. (II)-B.5 Thermal Analysis Model under Accident Test Condition (Contents I/center, vertical drop)

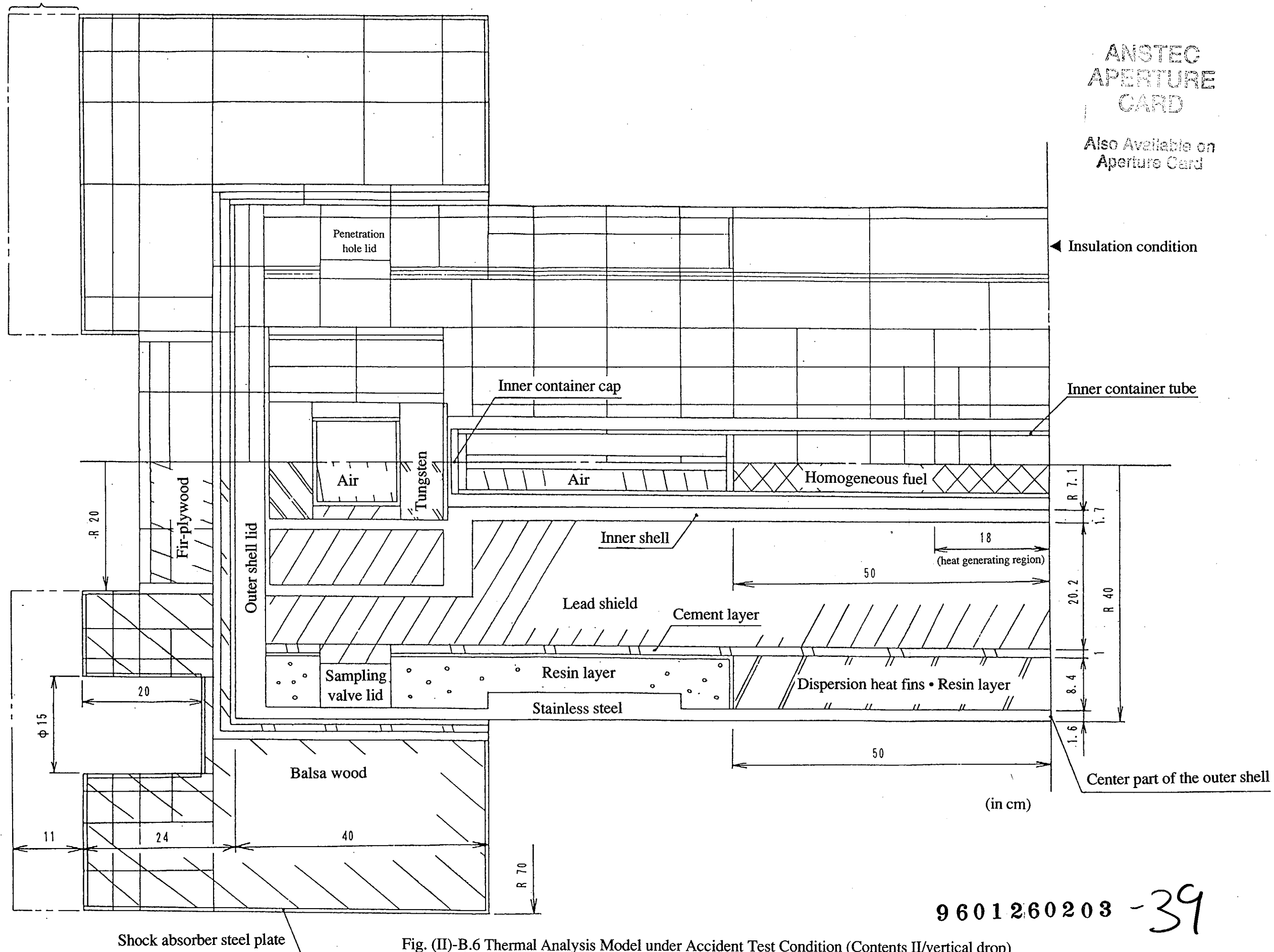
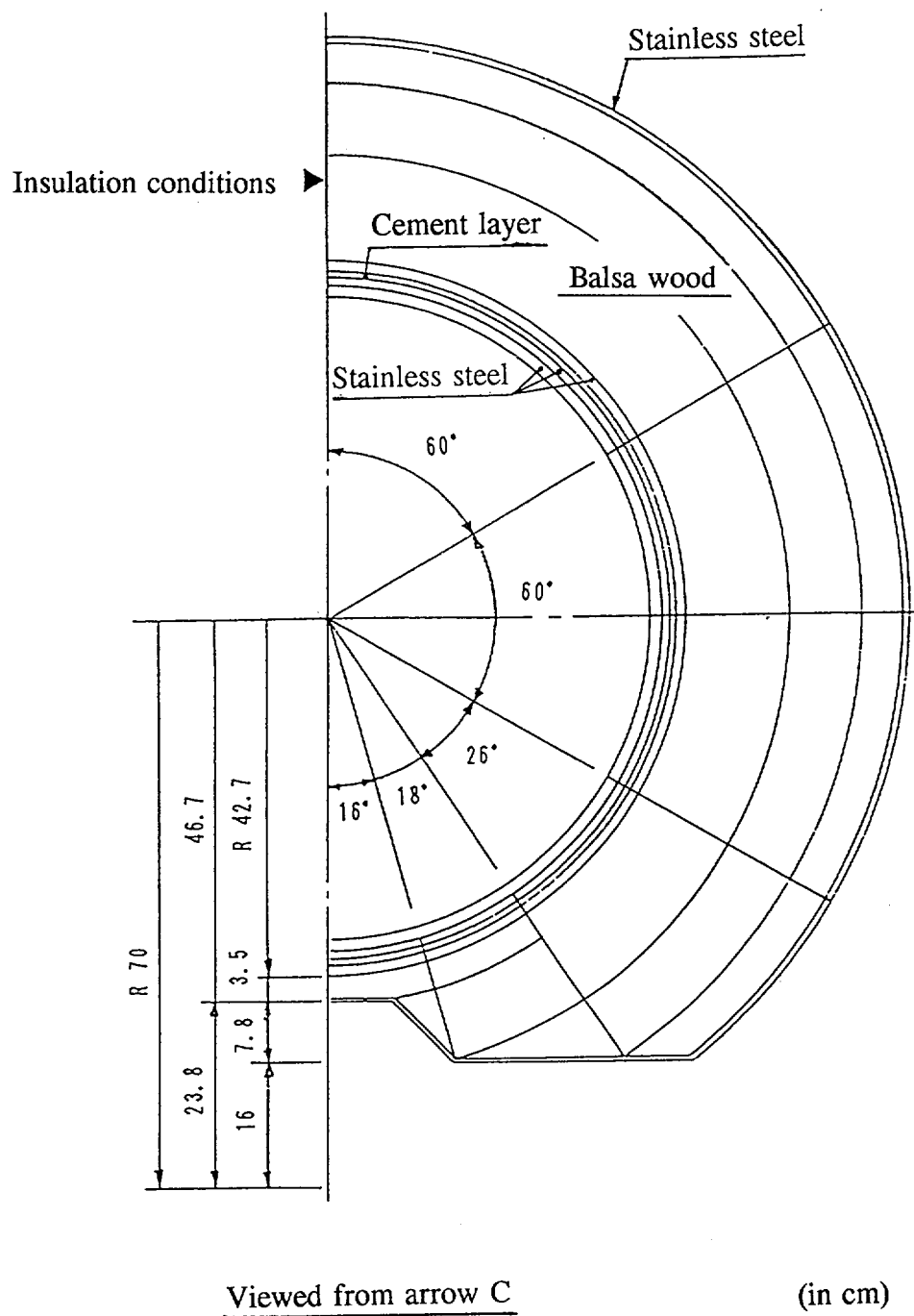


Fig. (II)-B.6 Thermal Analysis Model under Accident Test Condition (Contents II/vertical drop)

9601260203 -39





**Fig. (II)-B.7 Thermal Analysis Model under Accident Test Conditions**  
**(Contents I/eccentric, horizontal drop (2/2))**

(4) Conditions and method of the thermal analysis

According to the description provided in steps (1), (2), and (3), the thermal analysis conditions are as shown in Table (II)-B.2.

In all, there are four evaluation cases under normal test conditions ; three receiving states (Contents I • eccentric, Contents I • center, and Contents II) in which two types of contents are loaded, and one evaluation at the minimum temperature.

In all, there are four evaluation cases under accident test conditions ; the three receiving states mentioned above in the case of a package dropped vertically, and an evaluation of the package (Contents I • eccentric) during a horizontal drop to evaluate the temperature of the O-ring used in the containment boundary of a shell part penetration hole.

Table (II)-B.3 gives the thermal evaluation method.

Table (II)-B.2 Thermal Analysis Conditions

Conditions		Decay heat	Environmental conditions			Emissivity on the packaging surface	Gas	
			Ambient temperature	Solar heat load	Ambient emissivity		Inner shell	Fuel supporting can I *1 (receiving tube I)
Normal test conditions								
Contents I • eccentric		260W	Still air 38°C	Yes	1.0	0.37 <sup>*4</sup>	Air	Helium
Contents I • center								
Contents II		64W						Air
Minimum temperature		0W	Still air -40°C	No				Helium (Contents I) Air (Contents II)
Accident test conditions								
Initial conditions	Contents I • eccentric	260W	Still air 38°C	Yes	1.0	0.37 <sup>*4</sup>	Air	Helium
	Contents I • eccentric <sup>*2</sup>							
	Contents I • center							
	Contents II		64W				Air	
During a fire	Contents I • eccentric	260W	Fire 30 minutes 800°C	No	0.9 <sup>*3</sup>	0.8 <sup>*3</sup>	Air	Helium
	Contents I • eccentric <sup>*2</sup>							
	Contents I • center							
	Contents II		64W				Air	
After a fire	Contents I • eccentric	260W	Still air 38°C	Yes	1.0	0.55 <sup>*4</sup>	air	Helium
	Contents I • eccentric <sup>*2</sup>							
	Contents I • center							
	Contents II		64W				Air	

\*1 For the receiving state of Contents II, the fuel pin is loaded into receiving tube I instead of into fuel supporting can I.

\*2 This package is used as the thermal analysis model during a horizontal drop.

\*3 Safety criterion during the transport of a radioactive substance (Determined by the Atomic Energy Commission in January 21, 1975.)

\*4 See footnotes 1) and 2).

1) Goldsmith, A. etal., "Handbook of Thermophysical Properties of Solid Materials" Revised Edition, Vol. I, the MacMillan Company, New York, pp157-172, 1961.

2) "Dennetsu Kougaku Shiryo" Third Edition, The Japan Society of Mechanical Engineers, page 148

**Table (II)-B.3 Thermal Analysis Method**

Item		Contents	
		Contents I	Contents II
Maximum decay heat		260W	64W
Thermal calculation model	Package	Three-dimensional thermal analysis model	
	Contents	Homogenized and approximated	
Thermal calculation method	Calculation of the package temperature distribution	Three-dimensional heat transfer calculation code, TRUMP	
	Calculation of the fuel pin surface temperature	Radiation and heat conduction	
Maximum internal pressure		$P.V/T = \text{Constant}$	

(5) Evaluation results

1) Temperature

Tables (II)-B.4 and (II)-B.5 list the temperatures of this package under normal test conditions.

Tables (II)-B.6 and (II)-B.7 list the maximum temperatures under accident test conditions, while Figs. (II)-B.8 through (II)-B.11 show the change in temperature.

2) Pressure

Tables (II)-B.8 and (II)-B.9 list the pressures that are generated in this package under normal and accident test conditions.

The results mentioned above show that the temperature on the package surface under normal test conditions is 72°C. This temperature does not exceed the temperature (85°C) established by the law. The temperatures of the O-rings (fluoro rubber) that are installed on the rear lid, shielding plug lid, front lid, rotating plug lid (hereafter called outer shell lids), penetration hole lid, and sampling valve lids are between 75°C (maximum) and -40°C (minimum). These temperatures are within the range of the allowable service temperature (-50 to 200°C).

The pressure generated in this package does not exceed the pressure criterion used to evaluating the strength of the structure and the maximum service pressure 700 kPa(G)(7 kg/cm<sup>2</sup>G) established by the engineering criteria.

The maximum thermal stress that occurs in this package is 83.4 N/mm<sup>2</sup> (8.5 kg/mm<sup>2</sup>) in the inner shell and 6.4 N/mm<sup>2</sup> (0.7 kg/mm<sup>2</sup>) in the outer shell. Neither stress value exceeds the design criterion values (see subsection A.5.1.2) of 174 N/mm<sup>2</sup> (17.7 kg/mm<sup>2</sup>) (material quality: SUS304, temperature: 90°C) and 180 N/mm<sup>2</sup> (18.4 kg/mm<sup>2</sup>) (material quality: SUS304, temperature: 80°C), respectively.

Therefore, this package can satisfy the engineering criteria under normal test conditions without requiring a special cooling system.

The maximum temperature (see Table (II)-B.6) of the O-ring (fluoro rubber) that has a containment function under accident test conditions is 125°C. This temperature does not exceed the maximum service temperature (200°C). The maximum temperatures (see Table (II)-B.6) of the lead shield and tungsten that provide shielding are 193°C and 133°C, respectively. These temperatures do not exceed either melting point (327°C and 3410°C). Therefore, the lead shield and tungsten do not melt. This means that they maintain their shielding performance. The maximum temperature (see Table (II)-B.6) of neutron shielding material made of resin is 656°C. The composition near the outer shell may change due to carbonization. This resin is thus ignored in the shield analysis, and, to be on the safe side, is replaced by water in the criticality analysis.

The maximum internal pressure generated in this package does not exceed the design pressure.

The maximum thermal stress that occurs in the package is 340 N/mm<sup>2</sup> (34.7 kg/mm<sup>2</sup>) in the inner shell and 113 N/mm<sup>2</sup> (11.6 g/mm<sup>2</sup>) in the outer shell. Neither stress value exceeds the design criterion values (see subsection A.6.3.2) of 485 N/mm<sup>2</sup> (49.5 kg/mm<sup>2</sup>) (material quality: SUS304, temperature: 100°C) and 254 N/mm<sup>2</sup> (26.0 kg/mm<sup>2</sup>) (material quality: SUS304, temperature: 700°C), respectively.

Therefore, the safety of this package is maintained even under accident test conditions.



**Table (II)-B.4 Package Temperature under Normal Test Conditions (Contents I)**

Part	Maximum temperature		Minimum temperature *1
	Eccentric	Center	
Shock absorber steel plate	64°C	60°C	-40°C
Outer shell	72°C	66°C	-40°C
Heat dispersion fins	73°C	67°C	-40°C
Outer shell lids	73°C	64°C	-40°C
Sampling valve lids	75°C	65°C	-40°C
Penetration hole lid	75°C	65°C	-40°C
Lead shield	84°C	76°C	-40°C
Tungsten	80°C	67°C	-40°C
Resin	73°C	67°C	-40°C
Inner shell	85°C	77°C	-40°C
Gas in the inner shell	165°C	140°C	-40°C
Inner container tube	241°C	235°C	-40°C
Inner container cap	227°C	76°C	-40°C
Fuel supporting can I	300°C	295°C	-40°C
Gas in fuel supporting can I	338°C	333°C	-40°C
Fuel pins	375°C	370°C	-40°C
O-rings	75°C	65°C	-40°C

\*1 Indicates the temperature of each part when the decay heat is set to 0 W under low-temperature ambient conditions of -40°C.

**Table (II)-B.5 Package Temperature under Normal Test Conditions (Contents II)**

Part	Maximum temperature	Minimum temperature *1
Shock absorber steel plate	59°C	-40°C
Outer shell	61°C	-40°C
Heat dispersion fins	61°C	-40°C
Outer shell lids	60°C	-40°C
Sampling valve lids	61°C	-40°C
Penetration hole lid	61°C	-40°C
Lead shield	69°C	-40°C
Tungsten	60°C	-40°C
Resin	61°C	-40°C
Inner shell	70°C	-40°C
Gas in the inner shell	123°C	-40°C
Inner container tube	157°C	-40°C
Inner container cap	64°C	-40°C
Receiving tube I	245°C	-40°C
Gas in receiving tube I	305°C	-40°C
Fuel pins	365°C	-40°C
O-rings	61°C	-40°C

\*1 Indicates the temperature of each part when the decay heat is set to 0 W under low-temperature ambient conditions of -40°C.

**Table (II)-B.6 Maximum Temperature under Accident Test Conditions (Contents I)**

Part	Eccentric		Center/ver- tical drop	Time elapsed after a fire
	Vertical drop	Horizontal drop		
Shock absorber steel plate	781°C	781°C	781°C	0.5 h
Shock absorber steel plate*1	797°C	785°C	797°C	0.5 h
Outer shell	656°C	656°C	651°C	0.5 h
Heat dispersion fins	405°C	405°C	401°C	0.5 h
Outer shell lids	125°C	114°C (8.5h)	116°C	8.0 h
Sampling valve lids	120°C (3.0h)	120°C	114°C (2.5h)	2.9 h
Penetration hole lid	120°C (3.0h)	120°C	114°C (2.5h)	2.9 h
Lead shield	193°C	193°C	190°C (1.2h)	1.5 h
Tungsten	133°C	133°C	123°C	7.5 h
Resin	656°C	656°C	651°C	0.5 h
Inner shell	193°C	193°C	189°C (1.4h)	1.5 h
Gas in the inner shell	228°C	228°C	202°C (4.0h)	3.0 h
Inner container tube	278°C (4.0h)	278°C (4.0h)	284°C	3.0 h
Inner container cap	255°C	255°C	132°C	7.0 h
Fuel supporting can I	328°C (4.0h)	328°C (4.0h)	332°C	3.5 h
Gas in fuel supporting can I	363°C	363°C	366°C	3.5 h
Fuel pins	397°C (4.0h)	397°C (4.0h)	400°C	3.5 h
O-rings	125°C	120°C (8.5h)*2	116°C	8.0 h

\*1 Indicates the section damaged during a drop accident.

\*2 O-rings of the penetration hole lid part

Note: The time other than that indicated in the fifth column is indicated in parentheses.

**Table (II)-B.7 Maximum Temperature under Accident Test Conditions (Contents II)**

Part	Maximum temperature	Time elapsed after a fire
Shock absorber steel plate	781°C	0.5 h
Shock absorber steel plate*1	797°C	0.5 h
Outer shell	650°C	0.5 h
Heat dispersion fins	399°C	0.5 h
Outer shell lids	113°C	8.0 h
Sampling valve lids	109°C	3.5 h
Penetration hole lid	109°C	3.5 h
Lead shield	186°C	1.3 h
Tungsten	119°C	7.5 h
Resin	650°C	0.5 h
Inner shell	183°C	1.5 h
Gas in the inner shell	193°C	3.0 h
Inner container tube	223°C	3.0 h
Inner container cap	122°C	8.0 h
Receiving tube I	289°C	3.0 h
Gas in receiving tube I	341°C	3.0 h
Fuel pins	392°C	3.0 h
O-rings	113°C	8.0 h

\*1 Indicates the section damaged during a drop accident.

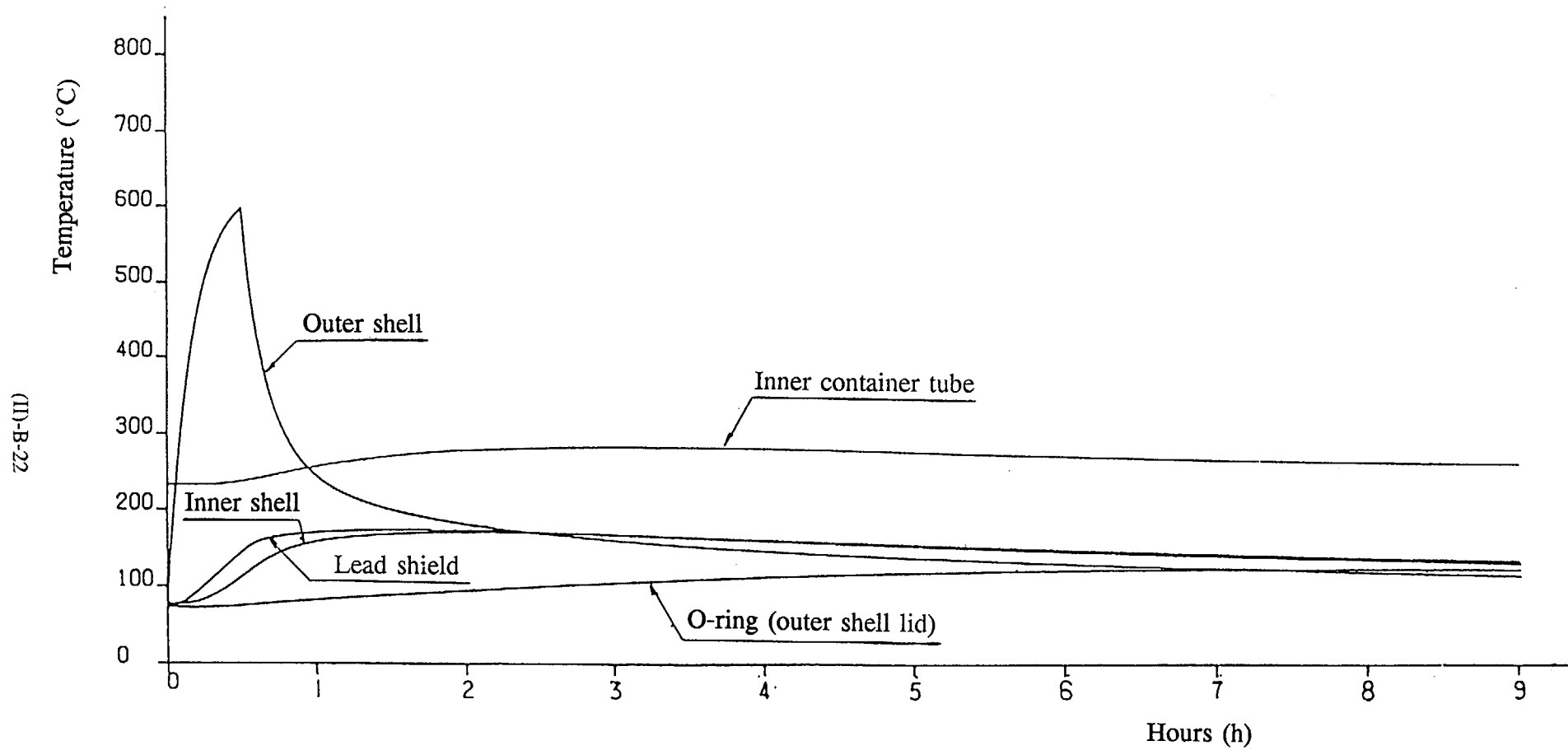


**Fig. (II)-B.8 Change in Temperature under Accident Test Conditions(Contents I/eccentric, vertical drop)**

(II)-B-23

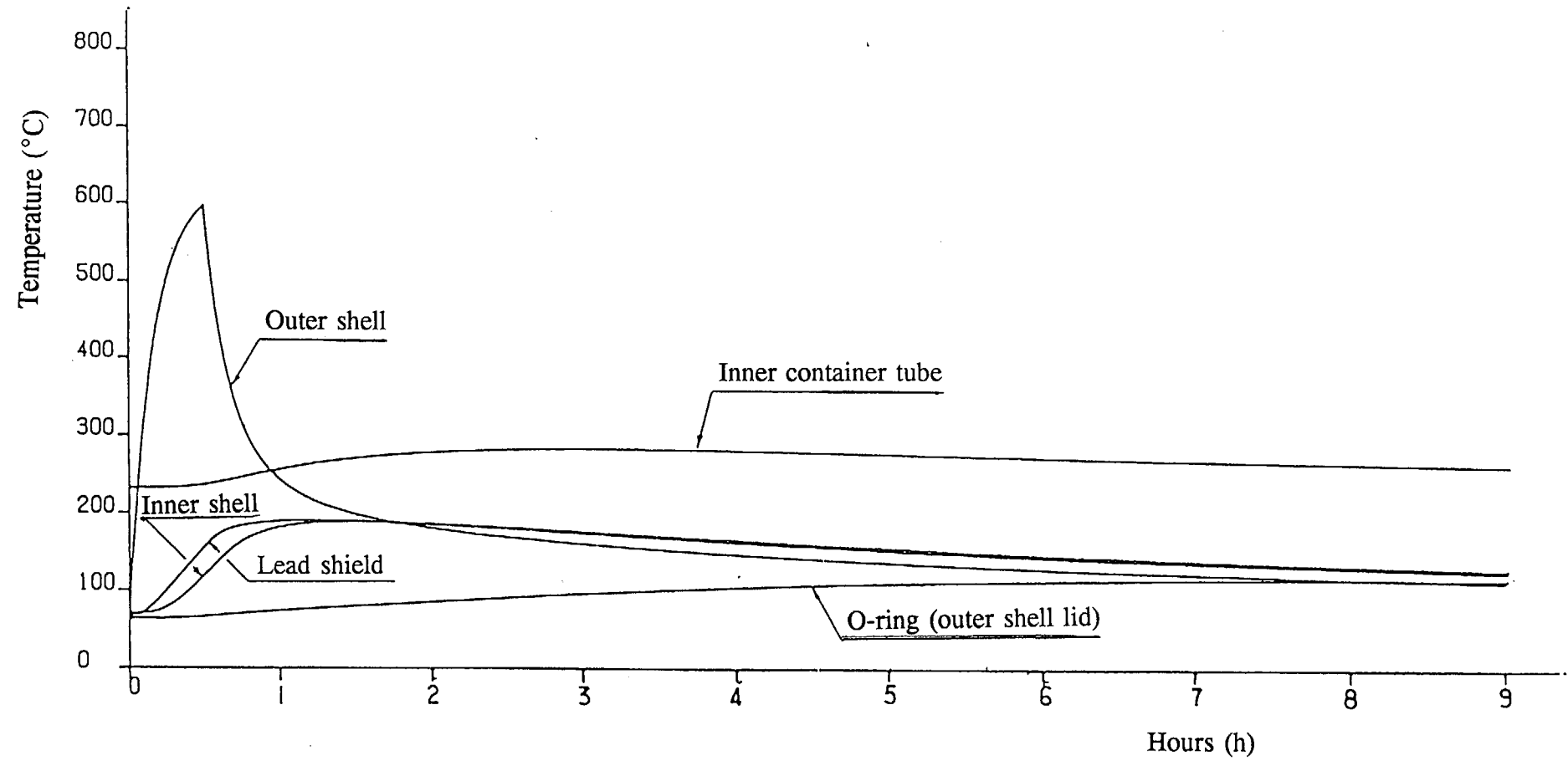


**Fig. (II)-B.9 Change in Temperature under Accident Test Conditions(Contents I/center, vertical drop)**

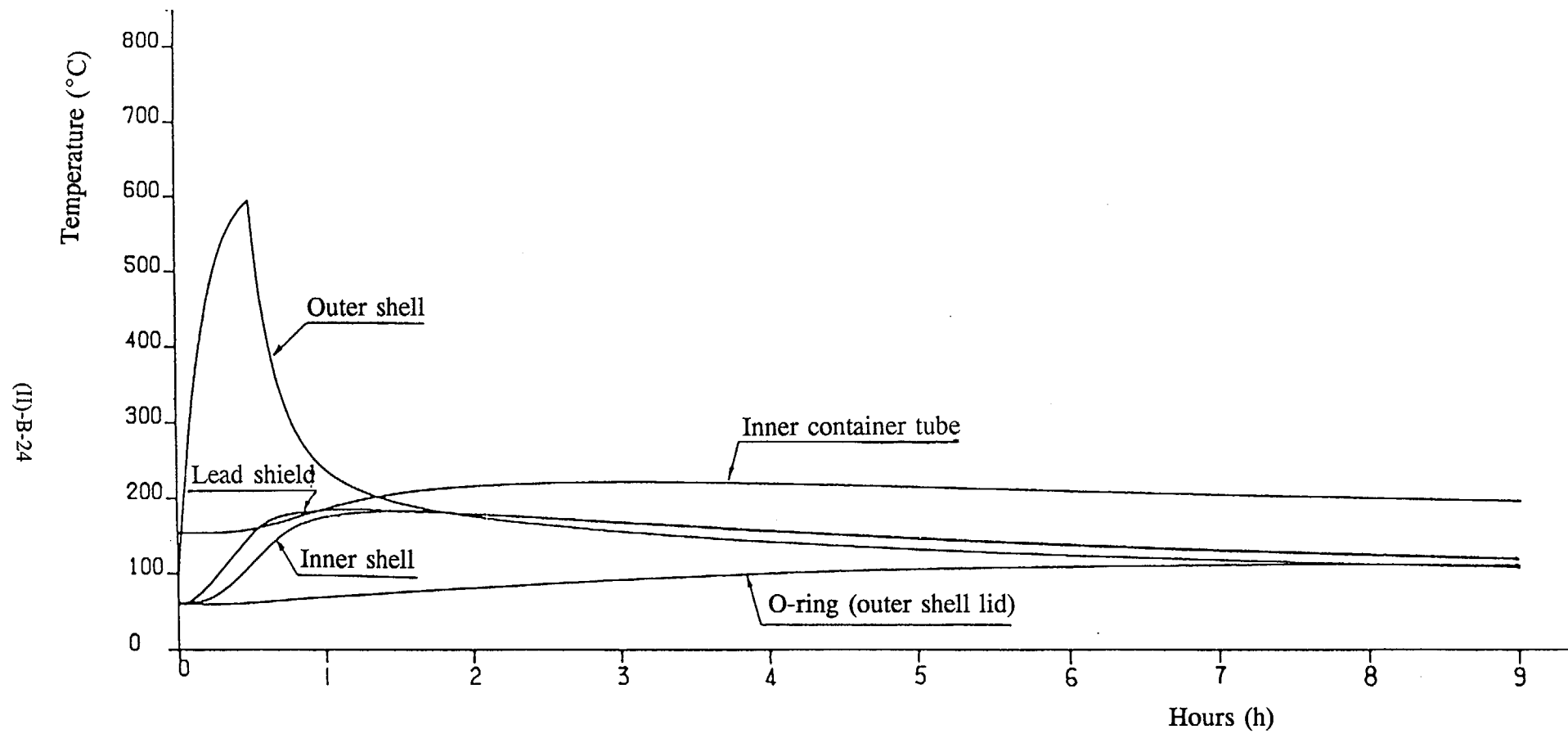


**Fig. (II)-B.10** Change in Temperature under Accident Test Conditions(Contents II, vertical drop)

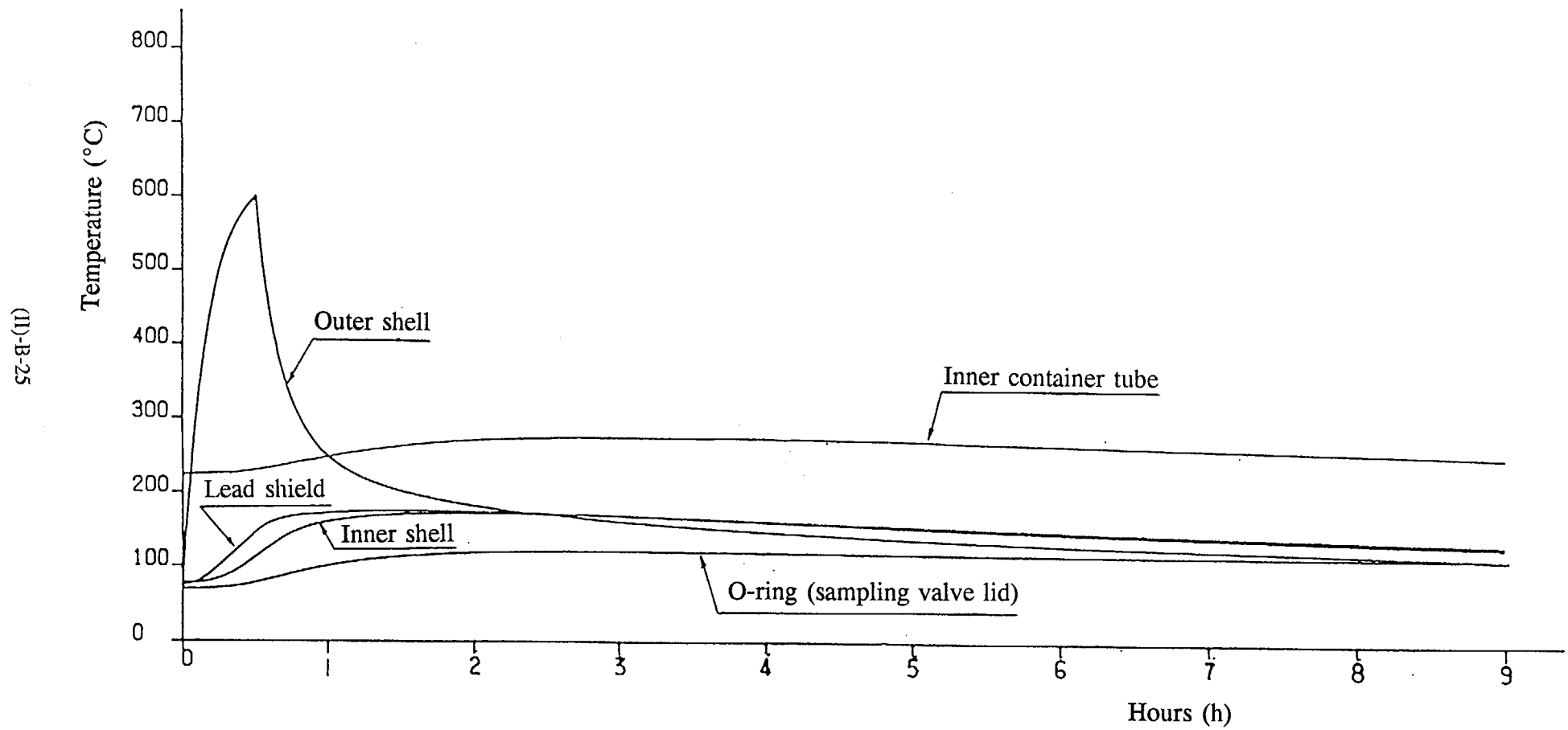


**Fig. (II)-B.11** Change in Temperature under Accident Test Conditions(Contents I/eccentric, horizontal drop)



**Table (II)-B.8 Maximum Internal Pressure under Normal Test Conditions**

Type of contents	Inner shell	Fuel supporting can I (receiving tube I <sup>*1</sup> )
Contents I • eccentric	60 kPa (0.6 kg/cm <sup>2</sup> G)	210 kPa (2.1 kg/cm <sup>2</sup> G)
Contents I • center	50 kPa (0.5 kg/cm <sup>2</sup> G)	210 kPa (2.1 kg/cm <sup>2</sup> G)
Contents II	40 kPa (0.4 kg/cm <sup>2</sup> G)	610 kPa <sup>*1</sup> (6.1 kg/cm <sup>2</sup> G)

\*1 For Contents II, indicates the maximum internal pressure of receiving tube I rather than of supporting can I.

**Table (II)-B.9 Maximum Internal Pressure under Accident Test Conditions**

Type of contents	Inner shell	Fuel supporting can I (receiving tube I <sup>*1</sup> )
Contents I • eccentric	80 kPa (0.8 kg/cm <sup>2</sup> G)	230 kPa (2.3 kg/cm <sup>2</sup> G)
Contents I • eccentric <sup>*2</sup>	80 kPa (0.8 kg/cm <sup>2</sup> G)	230 kPa (2.3 kg/cm <sup>2</sup> G)
Contents I • center	70 kPa (0.7 kg/cm <sup>2</sup> G)	230 kPa (2.3 kg/cm <sup>2</sup> G)
Contents II	70 kPa (0.7 kg/cm <sup>2</sup> G)	660 kPa <sup>*1</sup> (6.6 kg/cm <sup>2</sup> G)

\*1 For Contents II, indicates the maximum internal pressure of receiving tube I rather than of fuel supporting can I.

\*2 This package is used as the thermal analysis model during a horizontal drop.

## B.2 Thermal Properties of the Materials

The thermal properties of the principal materials are as follows:

(1) Stainless steel

Table (II)-B.10 <sup>1)2)</sup> lists the thermal properties of the stainless steel. This material is primarily used for the outer shell, inner shell, inner container, fuel supporting can, supporting can, rack, receiving tube, and shock absorber steel plate.

(2) Lead

Table (II)-B.11 <sup>3)</sup> lists the thermal properties of the lead. This material is used for the lead shield between the outer shell and inner shell. It functions as a shield against gamma rays released by the contents.

(3) Copper

Table (II)-B.12 <sup>4)</sup> lists the thermal properties of the copper. This material is used for the heat dispersion fins.

(4) Fuel

Table (II)-B.13 <sup>5)</sup> lists the thermal properties of the fuel.

(5) Balsa wood

The thermal properties of the flame-resistance treated balsa wood were analyzed. Table (II)-B.14 <sup>5)6)</sup> lists the resulting information. This material is used for the shock absorbers and protects the packaging body from external heat and shock.

(6) Cement

Table (II)-B.15 <sup>7)</sup> lists the thermal properties of the cement. This material is used for the cement layer between the lead shield and resin layer or intermediate shell, and prevents heat from entering the package during a fire. The cement layer used for the shock absorbers also prevents the combustion heat of the wood from entering the package.

- 
- 1) Goldsmith. A. et al., "Handbook of Thermophysical Properties of Solid Materials "Revised Edition, Vol. II, the MacMillan Company, New York, pp157-172, 1961.
  - 2) "Dennetsu Kougaku Shiryo" Third Edition, The Japan Society of Mechanical Engineers, page 148
  - 3) "Lead Handbook" Japanese Lead Zinc Demand Society, pages 59-65, 1975
  - 4) E.R.G. Eckert, "Introduction to the Transfer of Heat and Mass" First Edition, McGraw-Hill Book Company, New York, p268, 1950.
  - 5) U.S.A.E.C. "Reactor Handbook" Second Edition, Vol. I. Interscience Publishers, Inc., New York, p293, p1097, 1960.
  - 6) "PNC-SJ299 80-16", Power Reactor and Nuclear Fuel Development Corporation, 1980.
  - 7) "TN Report 9493"

(7) Air

Table (II)-B.16 <sup>1)</sup> lists the thermal properties of the air. Air is present inside the inner shell, inner container, and receiving tube.

(8) Fir-plywood

The thermal properties of the fir-plywood were analyzed. Table (II)-B.17 <sup>2)3)</sup> lists the resulting information. This material is used for a part of the shock absorbers.

(9) Resin

Table (II)-B.18 <sup>3)</sup> lists the thermal properties of the resin. This material is used for the resin later between the outer shell and cement layer or intermediate shell. It functions as a shield against neutrons released by the contents.

(10) Tungsten

Table (II)-B.19 <sup>4)</sup> lists the thermal properties of the tungsten. This material is used for the rotating plugs and shielding plugs. It functions as a shield against gamma rays released by the contents.

(11) Helium

Table (II)-B.20 <sup>5)</sup> lists the thermal properties of the helium. The fuel supporting can is filled with helium.

- 
- 1) "Dennetsu Kougaku Shiryo" Third Edition, The Japan Society of Mechanical Engineers, page 300
  - 2) E.R.G. Eckert, "Introduction to the Transfer of Heat and Mass" First Edition, McGraw-Hill Book Company, New York, p270, 1950.
  - 3) "PNC-SJ299 80-16", Power Reactor and Nuclear Fuel Development Corporation, 1980
  - 4) U.S.A.E.C. "Reactor Handbook" Second Edition, Vol. I. Interscience Publishers, Inc., New York, p672, 1960.
  - 5) "The Thermodynamic and Transport Properties of Helium and Nitrogen" WANL-TME-1753.

**Table (II)-B.10 Thermal Properties of the Stainless Steel**

Specific gravity $\text{kg/m}^3$		7898
		( $\text{g/cm}^3$ )
Emissivity	(a) (Note)	0.37
	(b) (Note)	0.55
Temperature ( $^{\circ}\text{C}$ )	Specific heat $\text{kJ/kg} \cdot \text{K}$ ( $\text{cal/g} \cdot ^{\circ}\text{C}$ )	Thermal conductivity $\text{W/m} \cdot \text{K}$ ( $\text{cal/s} \cdot \text{cm} \cdot ^{\circ}\text{C}$ )
60	0.482 (0.115)	15.5 (0.0370)
171	0.523 (0.125)	17.5 (0.0417)
282	0.557 (0.133)	19.2 (0.0459)
393	0.574 (0.137)	20.8 (0.0496)
893	0.653 (0.156)	27.0 (0.0645)

Notes:

- (a) Surface not exposed to a fire.  
(b) Surface exposed to a fire.

**Table (II)-B.11 Thermal Properties of the Lead**

Specific gravity $\text{kg/cm}^3$ ( $\text{g/cm}^3$ )		11330 (11.33)	Melting point $^{\circ}\text{C}$	327.3
Temperature	Specific heat $\text{kJ/kg} \cdot \text{K}$ ( $\text{cal/g} \cdot ^{\circ}\text{C}$ )	Thermal conductivity $\text{W/m} \cdot \text{K}$ ( $\text{cal/s} \cdot \text{cm} \cdot ^{\circ}\text{C}$ )		
0	0.126 (0.0302)	35.4 (0.0846)		
100	0.131 (0.0314)	33.2 (0.0794)		
200	0.136 (0.0325)	31.9 (0.0763)		
300	0.141 (0.0336)	30.9 (0.0738)		

**Table (II)-B.12 Thermal Properties of the Copper**

Specific gravity	kg/m <sup>3</sup> (g/cm <sup>3</sup> )	8955 (8.955)
Melting point	°C	1083
Specific heat	kJ/kg · K (cal/c · °C)	0.383 (0.0915)
Temperature	°C	Thermal conductivity W/m · K (cal/s · cm · °C)
0		386 (0.922)
100		379 (0.905)
200		374 (0.893)
400		363 (0.868)
600		353 (0.843)

**Table (II)-B.13 Thermal Properties of the Fuel**

Specific gravity	kg/m <sup>3</sup> (g/cm <sup>3</sup> )	10800 (10.8)
Temperature °C	Specific heat kJ/kg · K (cal/g · °C)	Thermal conductivity W/m · K (cal/s · cm · °C)
100	0.263 (0.0628)	10.5 (0.0250)
200	0.282 (0.0674)	8.16 (0.0195)
300	0.293 (0.0700)	6.78 (0.0162)
400	0.301 (0.0719)	5.78 (0.0138)

**Table (II)-B.14 Thermal Properties of the Balsa Wood (Flame resistance treated)**

Specific gravity	$\text{kg/m}^3$ ( $\text{g/cm}^3$ )	240	(0.24)
Temperature	$^{\circ}\text{C}$	Specific heat	$\text{kJ/kg} \cdot \text{K}$ ( $\text{cal/g} \cdot ^{\circ}\text{C}$ )
Under 285		2.30	(0.55)
285 or more		1.05	(0.25)
Temperature	$^{\circ}\text{C}$	Thermal conductivity	$\text{W/m} \cdot \text{K}$ ( $\text{cal/s} \cdot \text{cm} \cdot ^{\circ}\text{C}$ )
27		0.286	( $6.84 \times 10^{-4}$ )
100		0.342	( $8.17 \times 10^{-4}$ )
150		0.322	( $7.70 \times 10^{-4}$ )
200		0.320	( $7.65 \times 10^{-4}$ )
200 or more		0.320	(Constant) ( $7.65 \times 10^{-4}$ )

**Table (II)-B.15 Thermal Properties of the Cement**

Specific gravity	$\text{kg/m}^3$ ( $\text{g/cm}^3$ )	2300	(2.30)
Specific heat	$\text{kJ/kg} \cdot \text{K}$ ( $\text{cal/g} \cdot ^{\circ}\text{C}$ )	0.879	(0.210)
Thermal conductivity	$\text{W/m} \cdot \text{K}$ ( $\text{cal/s} \cdot \text{cm} \cdot ^{\circ}\text{C}$ )	1.60	( $3.82 \times 10^{-3}$ )

Table (II)-B.16 Thermal Properties of Air

Tem- pera- ture	Specific gravity kg/m <sup>3</sup> (g/cm <sup>3</sup> )	Specific heat kJ/kg • K (cal/g • °C)	Thermal conductivity W/m • K (cal/s • cm • °C)	Coefficient of the kinematic viscosity m <sup>2</sup> /s (cm <sup>2</sup> /s)	Expansion ratio 1/°C	Prandtl number -
0	1.251 (1.251 × 10 <sup>-3</sup> )	1.00 (0.240)	0.0241 (5.75 × 10 <sup>-5</sup> )	1.38 × 10 <sup>-5</sup> (0.138)	3.66 × 10 <sup>-3</sup>	0.72
40	1.091 (1.091 × 10 <sup>-3</sup> )	1.01 (0.241)	0.0272 (6.50 × 10 <sup>-5</sup> )	1.75 × 10 <sup>-5</sup> (0.175)	3.19 × 10 <sup>-3</sup>	0.71
100	0.916 (0.916 × 10 <sup>-3</sup> )	1.01 (0.242)	0.0316 (7.56 × 10 <sup>-5</sup> )	2.39 × 10 <sup>-5</sup> (0.239)	2.68 × 10 <sup>-3</sup>	0.70
200	0.722 (0.722 × 10 <sup>-3</sup> )	1.03 (0.245)	0.0386 (9.22 × 10 <sup>-5</sup> )	3.58 × 10 <sup>-5</sup> (0.358)	2.11 × 10 <sup>-3</sup>	0.69
400	0.508 (0.508 × 10 <sup>-3</sup> )	1.07 (0.255)	0.0507 (1.21 × 10 <sup>-4</sup> )	6.45 × 10 <sup>-5</sup> (0.645)	1.49 × 10 <sup>-3</sup>	0.69
600	0.391 (0.391 × 10 <sup>-3</sup> )	1.12 (0.267)	0.0611 (1.46 × 10 <sup>-4</sup> )	9.89 × 10 <sup>-5</sup> (0.989)	1.15 × 10 <sup>-3</sup>	0.70
800	0.319 (0.319 × 10 <sup>-3</sup> )	1.16 (0.276)	0.0708 (1.69 × 10 <sup>-4</sup> )	1.37 × 10 <sup>-4</sup> (1.37)	9.32 × 10 <sup>-4</sup>	0.71

Table (II)-B.17 Thermal Properties of the Fir-Plywood

Specific gravity	kg/m <sup>3</sup> (g/cm <sup>3</sup> )	560 (0.56)
Temperature	°C	Specific heat kJ/kg • K (cal/g • °C)
Under 285		2.72 (0.65)
285 or more		1.05 (0.25)
Temperature	°C	Thermal conductivity W/m • K (cal/s • cm • °C)
20		0.17 (4.06 × 10 <sup>-4</sup> )
100		0.19 (4.54 × 10 <sup>-4</sup> )
200		0.13 (3.10 × 10 <sup>-4</sup> )
355		0.12 (2.87 × 10 <sup>-4</sup> )
355 or more		0.12 (Constant) (2.87 × 10 <sup>-4</sup> )

**Table (II)-B.18 Thermal Properties of the Resin**

Specific gravity		kg/m <sup>3</sup> (g/cm <sup>3</sup> )	1100 (1.10)
Temperature °C	Specific heat	kJ/kg · K (cal/g · °C)	Thermal conductivity W/m · K (cal/s · cm · °C)
50	1.44 (0.343)	0.256 (6.12 × 10 <sup>-4</sup> )	
100	1.73 (0.412)	0.270 (6.44 × 10 <sup>-4</sup> )	
200	2.38 (0.569)	0.325 (7.76 × 10 <sup>-4</sup> )	
300	3.26 (0.779)	0.380 (9.08 × 10 <sup>-4</sup> )	

**Table (II)-B.19 Thermal Properties of the Tungsten**

Specific gravity kg/m <sup>3</sup> (g/cm <sup>3</sup> )		18000 (18.0)	Melting point °C	3410
Temperature °C	Specific heat kJ/kg · K (cal/g · °C)	Temperature °C	Thermal conductivity W/m · K (cal/s · cm · °C)	
20	0.137 (0.0328)	-78	172 (0.41)	
1000	0.151 (0.0361)	0	167 (0.40)	
-	-----	1225	117 (0.28)	



**Table (II)-B.20 Thermal Properties of the Helium**

Specific gravity		kg/m <sup>3</sup> (g/cm <sup>3</sup> )	12 (0.012)
Temperature °C	Specific heat	Kj/kg · K (cal/g · °C)	Thermal conductivity W/m · K (cal/s · cm · °C)
100	5.19	(1.24)	0.175 (4.19 × 10 <sup>-4</sup> )
200	5.19	(1.24)	0.207 (4.94 × 10 <sup>-4</sup> )
300	5.19	(1.24)	0.236 (5.64 × 10 <sup>-4</sup> )
400	5.19	(1.24)	0.262 (6.28 × 10 <sup>-4</sup> )

**B.3 Specifications of the Components**

The thermal specifications of the parts important for thermal resistance, which are used in this packaging are described below.

(1) O-ring (fluoro rubber)

Table (II)-B.21 <sup>1)</sup> lists the thermal specifications of the O-rings (fluoro rubber).

**Table (II)-B.21 Thermal Specifications of the Fluoro Rubber**

Maximum allowable service temperature	Minimum service temperature
200°C (normal use)	-50°C

(2) Fusible plug (bismuth)

Table (II)-B.22 <sup>2)</sup> lists the thermal specifications of the fusible plug.

**Table (II)-B.22 Thermal Specifications of the Fusible Plug**

Melting point	271°C
---------------	-------

---

1) "Sealing Technology" Edited by Jun Akaoka, 1972  
2) "Dennetsu Kougaku Shiryo" Third Edition, The Japan Society of Mechanical Engineers, page 293

## B.4 Normal Test Conditions

### B.4.1 Thermal Analysis Model

For the thermal analysis of the package, the packaging, which is holding an irradiated test fuel element, is evaluated using a three-dimensional stable and unstable temperature distribution calculation code, TRUMP, which is based on the differential method. The thermal analysis model that uses the TRUMP code is explained below.

#### B.4.1.1 Analysis model

This subsection describes the model shape and evaluation conditions.

##### (1) Model shape

As described in subsection B.1(2), it is assumed that this package is not deformed under normal test conditions. Only the shock absorber becomes deformed under normal test conditions. The deformation in this case is partial. Since the shock absorber is constructed using a substance with low thermal conductivity and the heat transfer length is shortened by the deformation, the amount of heat removal increases proportionally to degree of the deformation and the temperature of the package is evaluated as being low. Therefore, the assumption mentioned above provides an evaluation, which is on the safe side.

There are three thermal analysis cases under normal test conditions : Contents I • eccentric, Contents I • center, and Contents II as described in section B.1(3).

The thermal analysis model of Contents I • eccentric is described first. This thermal analysis model is a three-dimensional model recreating the actual packaging, excluding heat dispersion fins. Because the package is symmetrical about the axis, a model of only one half of the package is used.

As described in subsection B.6.2, although the model of the heat dispersion fin part (see Fig. (II)-B.1(2/2) has 6 heat dispersion fins instead of 60 in the actual packaging, the difference does not influence the heat transfer of the dispersion heat fin part.

Below, the thermal analysis model of Contents I • center shown in Fig. (II)-B.2 is explained. This thermal analysis model is structured on the basis of the same concept as in the case of the thermal analysis model described previously. In this case, only the element division differs due to the difference in the heat generating region of the contents.

The thermal analysis model of the package, which holds Contents II shown in Fig. (II)-B.3, is also structured on the basis of the same concept as in the case of Contents I, which was described previously, except for the element division due to the difference in the heat generating region of the contents.

The fuel pin is replaced during modeling by the homogeneous substance (hereafter called a homogeneous fuel) that has a heat capacity equivalent to that of the actual pin as described below. As shown in Fig. (II)-B.12, the Contents I model assumes that there is homogeneous fuel inside the fuel supporting can. The mean specific gravity and specific heat of the homogeneous fuel are represented by the values calculated using the expression below.

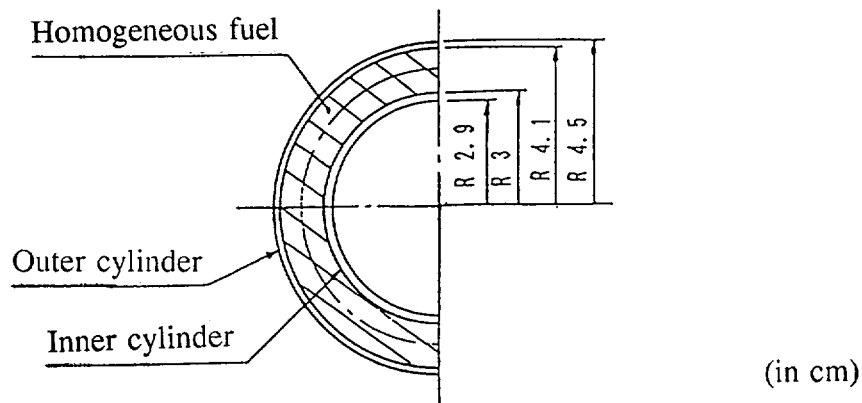


**Fig. (II)-B.12 Homogeneous Model of Contents I**

$$\rho_{av} = \frac{\sum W_i}{V}$$

$$Cp_{av} = \frac{\sum W_i \cdot Cp_i}{\sum W_i}$$

where

$\rho_{av}$	: Mean specific gravity	kg/m <sup>3</sup>
$W_i$	: Weight of each component material	kg
$V$	: Volume of the homogenized area	m <sup>3</sup>
$CP_{av}$	: Mean specific heat	kJ/kg.K
$CP_i$	: Specific heat of each component material	kJ/kg.K

Table (II)-B.23 gives the volume of the homogenized area and the weight of the component materials. Table (II)-B.24 lists the mean specific gravity and specific heat of the homogeneous fuel. Since the thermal capacity of helium is much smaller than that of other component materials, its analysis is omitted.

**Table (II)-B.23 Volume of the Homogenized Fuel Area and Weight of the Component Materials**

Item		Contents I	Contents II
Total volume	m <sup>3</sup>	0.00468	0.00694
Component material weight kg	Fuel	3.150	0.756
	Stainless steel	2.700	9.310
Total weight	kg	5.850	10.066

**Table (II)-B.24 Physical Properties of the Homogeneous Fuel**

Item		Contents I	Contents II
Specific gravity	kg/m <sup>3</sup> (g/cm <sup>3</sup> )	1250 (1.25)	1450 (1.45)
Specific heat kJ/kg · K (cal/g · °C)	100°C	0.371 (0.0886)	0.482 (0.115)
	200°C	0.398 (0.0950)	0.515 (0.123)
	300°C	0.416 (0.0994)	0.540 (0.129)
	400°C	0.427 (0.1021)	0.557 (0.133)
Thermal conductivity W/m · K (cal/s · cm · °C)	100°C	0.105 (2.51 × 10 <sup>-4</sup> )	0.0291 (6.96 × 10 <sup>-5</sup> )
	200°C	0.137 (3.28 × 10 <sup>-4</sup> )	0.0561 (1.34 × 10 <sup>-4</sup> )
	300°C	0.170 (4.07 × 10 <sup>-4</sup> )	0.0858 (2.05 × 10 <sup>-4</sup> )
	400°C	0.206 (4.92 × 10 <sup>-4</sup> )	0.125 (2.98 × 10 <sup>-4</sup> )

For Contents II, the area (center of the inner container) into which the fuel pin is loaded in the inner container is replaced in the model by a homogeneous substance as shown in Fig. (II)-B.13. The mean specific gravity and specific heat of the homogeneous fuel are calculated by the same expression used in the case of Contents I. Table (II)-B.23 lists the volume of the homogenized area and the weight of the component materials, while Table (II)-B.24 lists the mean specific gravity and specific heat of the homogeneous fuel. Since the thermal capacity of air is much smaller than that of other component materials, its analysis is omitted.

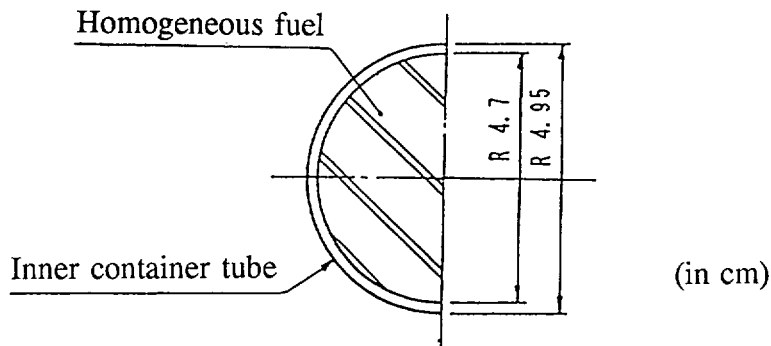


**Fig. (II)-B.13 Homogeneous Model of Contents II**

Since the fuel pin is homogenized in the thermal analysis model, the temperature of the fuel pin is evaluated as described below according to the TRUMP code calculation results obtained for the thermal analysis model.

- Contents I ... The temperature of the fuel pin using the heat transfer expression of thermal conduction and radiation is determined.
- Contents II ... A model of the contents in the inner container is created to determine the temperature of receiving tube I using the TRUMP code. Then the temperature of the fuel pin by the thermal conduction and radiation heat transfer expression is determined.

For the heat transfer coefficient between elements in the thermal analysis model, see Appendix B.6.1.

(2) Evaluation conditions

Table (II)-B.25 lists the thermal conditions used for the evaluation.

The decay heat of the contents is 260 W (maximum) for Contents I, and 64 W (maximum) for Contents II. The temperature conditions of the environment are 38°C or -40°C in still air. The emissivity on the packaging surface at that time is 0.37 (the circumferential emissivity is 1.0). Only air is to be found inside of the inner shell and a fuel supporting can, except for the helium, which is in the Contents I fuel supporting can. Given the presence of solar heat radiation, Table (II)-B.26<sup>1)</sup> lists the heat transfer value of the solar heat radiation. Using the value (200 W/m<sup>2</sup>) for the plane surfaces which do not remain horizontal during transport and the value (400 W/m<sup>2</sup>) for the curved surfaces, the heat transfer value (12 hours a day) of the solar heat radiation shown in Table (II)-B.26 is calculated until a stable state is reached.

---

1) Notification of the Science and Technology Agency, as stated in No. 5

**Table (II)-B.25 Thermal Conditions under Normal Test Conditions**

Item		Maximum temperature			Minimum temperature
		Contents I • eccentric	Contents I • center	Contents II	
Decay heat		260W		64W	0W
Environmental conditions	Ambient temperature	Still air 38°C			Still air -40°C
	Solar heat radiation	Yes			No
	Ambient emissivity	1.0			1.0
Emissivity on the packaging surface		0.37			0.37
Gas	Inside of the inner shell	Air			Air
	Fuel supporting can I (receiving tube I)*1	Helium		Air	Helium (Contents I) Air (Contents II)

\*1 In the case of Contents II, the fuel pin is loaded into receiving tube I instead of fuel supporting can I.

**Table (II)-B.26 Heat Transfer Value of the Solar Heat Radiation**

Form and location of surface	Insolation for 12 hours a day (W/m <sup>2</sup> )
Flat surfaces transported horizontally (a) Base (b) Other surfaces	0 800
Flat surfaces not transported horizontally	200
Curved surface	400

B.4.1.2 Test model

The analysis model is used instead of the test model.

## B.4.2 Maximum Temperature

Based on the analysis model and the conditions described in subsection B.4.1, the temperature distribution of the package under each condition is obtained by the TRUMP code. The maximum temperature of the fuel pin of each content is calculated based on this temperature distribution.

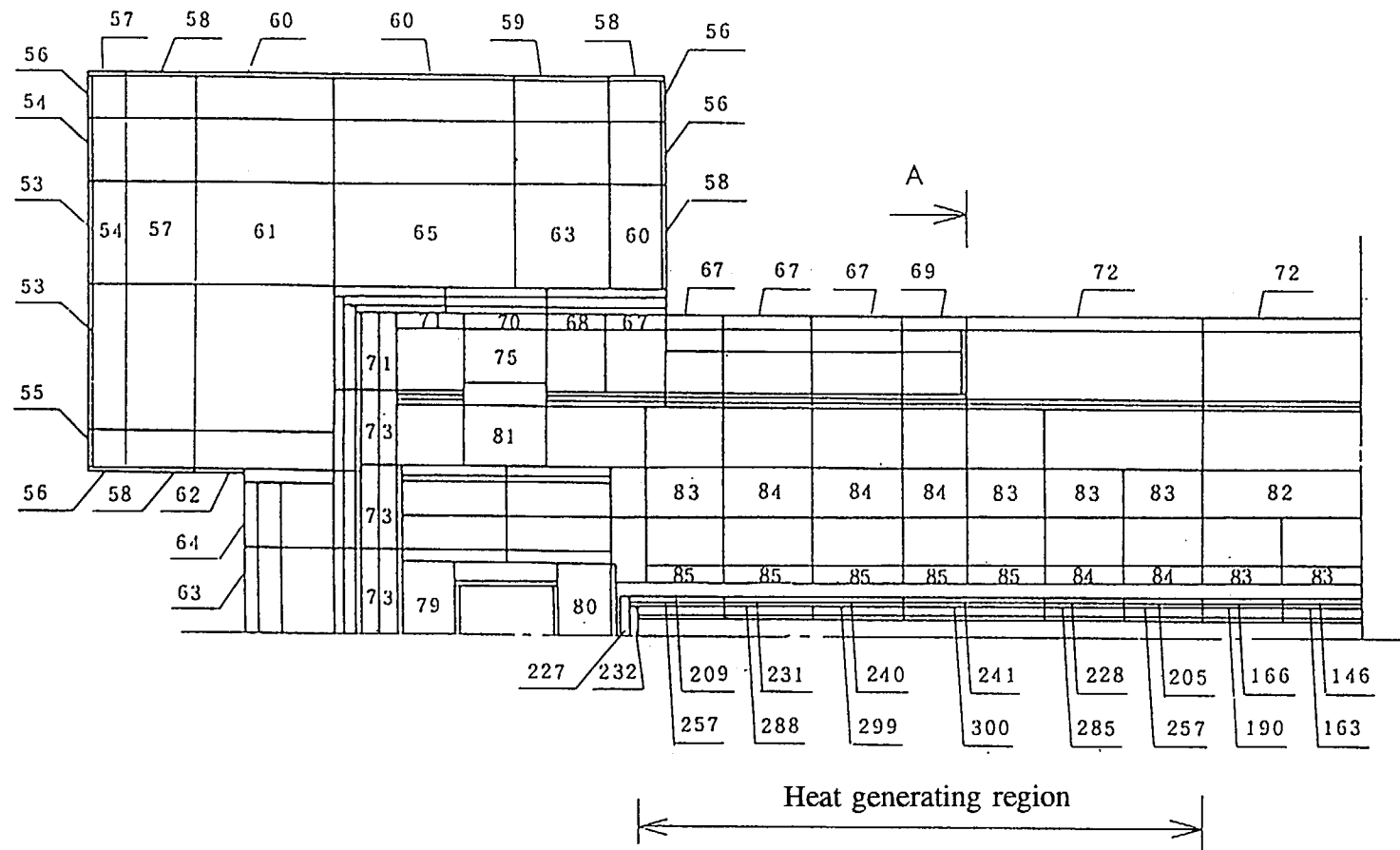
### (1) Contents I

Contents I • eccentric in which the heat generating region is located at the end, and Contents I • center in which the heat generating region is located at the center make up Contents I. Figs. (II)-B.14 and (II)-B.15 list the temperature distribution data obtained by evaluating the contents using the TRUMP code. As described in subsection B.4.1.1(1), thermal analysis model of only one half of the package is used because the package is symmetrical about the axis. In other words, the center of the package is treated as the heat insulation surface. For contents I • eccentric, the temperature of the package is evaluated as being higher than that of the actual packaging.

For Contents I, the maximum temperature of a fuel pin is calculated using fuel supporting can I and the heat transfer model shown in Fig. (II)-B.16. Assuming, to be on the safe side, that the heat flow in the axial direction is ignored and the heat flows only in the radial direction, the temperature of the fuel pin is evaluated by the heat transfer expression of the radiation and gas thermal conduction. This model assumes the case in which the heat transfer length (L) increases the most so that the highest temperature for the fuel pin will be obtained.



(II)-B-42

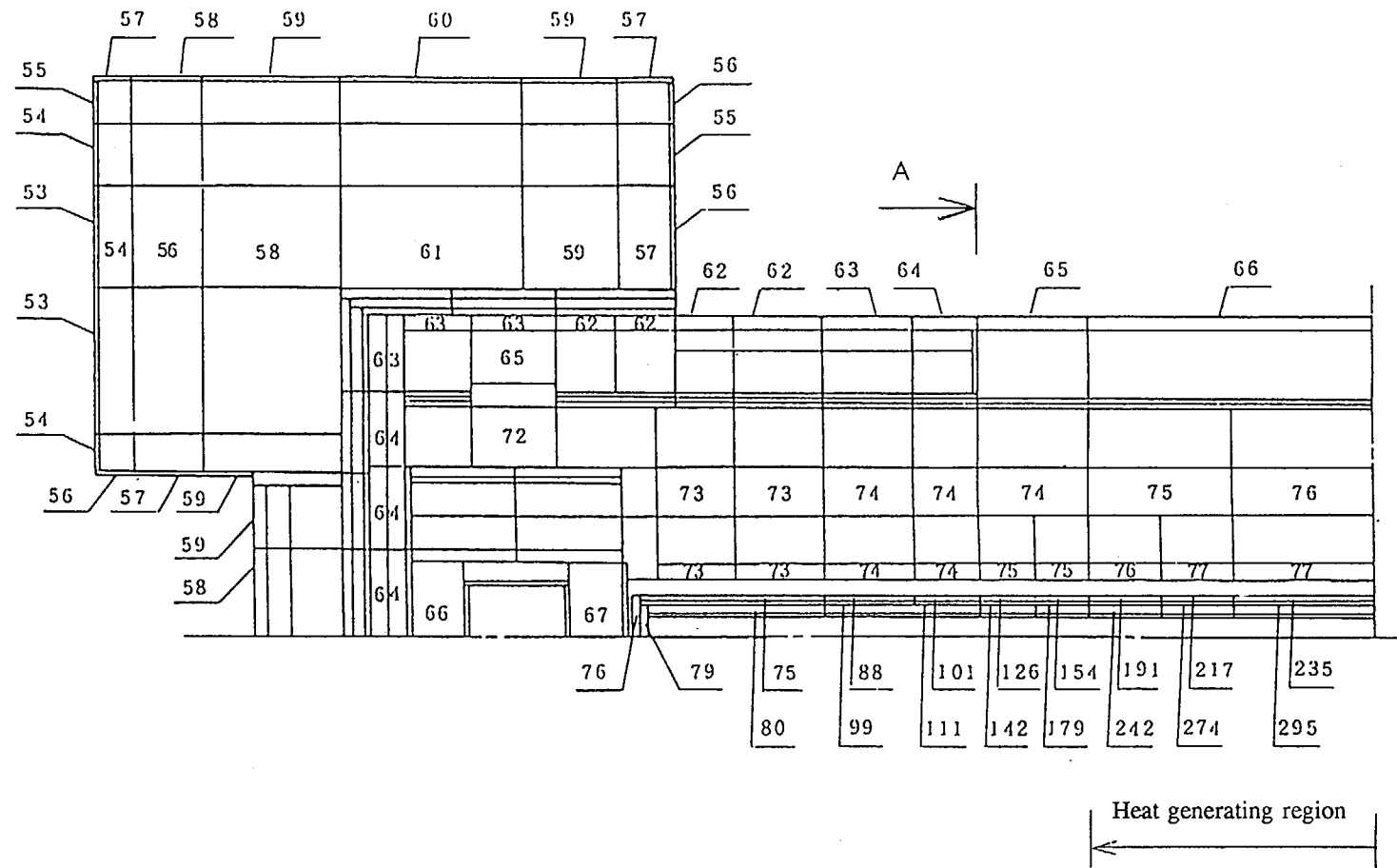


(in °C)

**Fig. (II)-B.14 Temperature of Package under Normal Test Conditions(Contents I/eccentric) (1/2)**



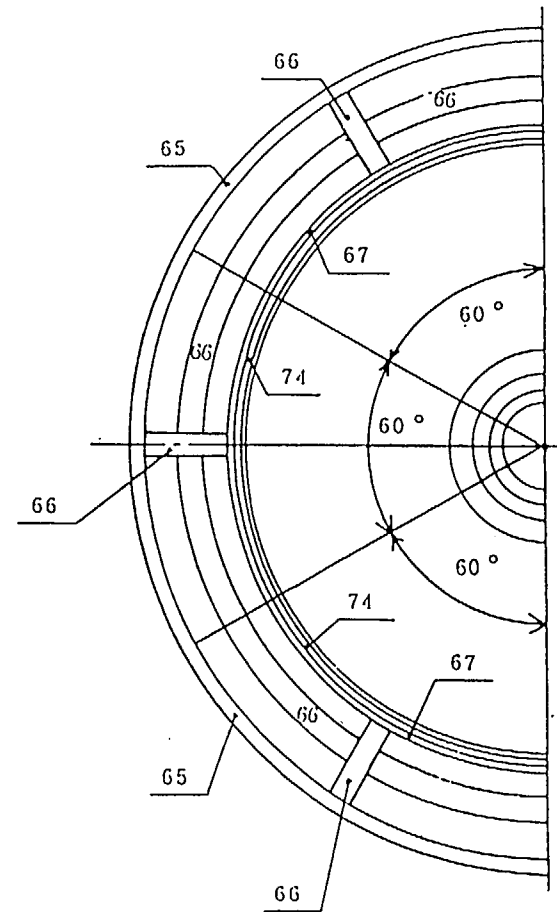
(II)-B-44



(in °C)

**Fig. (II)-B.15 Temperature of Package under Normal Test Conditions (Contents I/center) (1/2)**

(II)-B-45



(in °C)

**Fig. (II)-B.15 Temperature of Package under Normal Test Conditions(Contents I/center) (2/2)**

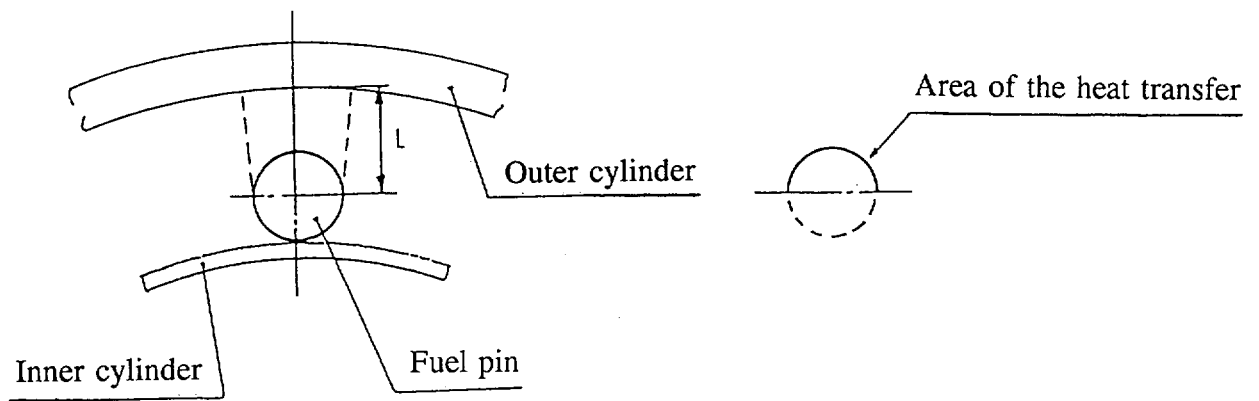


**Fig. (II)-B.16 Heat Transfer Model in Fuel Supporting Can I**

The temperature of the fuel pin for Contents I • eccentric and Contents I • center is given by the expression below.

$$\frac{Q}{A} = \frac{k}{L} (t_1 - t_2) + \sigma F \{ (t_1 + 273)^4 - (t_2 + 273)^4 \}$$

where

Q : Decay heat of each fuel pin

$$Q = \frac{260}{N} \quad W = 17.3 \quad W = 15.0 \text{ kcal/h}$$

N : Number of fuel pins = 15

A : Heat transfer area of the fuel pin

$$A = \frac{1}{2} \times \pi \times D \times L_1 = 6.22 \times 10^{-3} \text{ m}^2$$

D : Diameter of the fuel pin = 0.0055 m

L<sub>1</sub> : Heat generating length of the fuel pin = 0.72 m

L : Heat transfer length = 0.00855 m

k : Thermal conductivity of the helium = 0.200 kcal/h • m • °C  
= 0.233 W/m • K

(Interpolated value at 330°C shown in Table (II)-B.20)

$\sigma$  : Stefan-Boltzmann's constant =  $4.88 \times 10^{-8} \text{ kcal/h} \cdot \text{m}^2 \cdot \text{K}^4$   
 $F$  : Total form factor

$$F = \left( \frac{1}{\epsilon_1} + \frac{1}{\epsilon_2} - 1 \right)^{-1} = 0.23$$

$\epsilon_1$  : Emissivity of the fuel pin (stainless steel) = 0.37  
 $\epsilon_2$  : Emissivity of the outer cylinder (stainless steel) = 0.37

$t_2$  : Temperature of the outer cylinder

Contents I • eccentric =  $300^\circ\text{C}$   
 Contents I • center =  $295^\circ\text{C}$

$t_1$  : Temperature of the fuel pin

Therefore, the left side of the above equation is given by

$$\frac{Q}{A} = 2412 \text{ kcal/h} \cdot \text{m}^2$$

Each constant is assigned to the right side to obtain a value for  $t_1$  that satisfies the expression below.

$$\begin{aligned}
 \frac{Q}{A} &= \frac{0.200}{0.00855} \times (t_1 - 300) + 4.88 \times 10^{-8} \times 0.23 \times \{(t_1 + 273)^4 - 573^4\} \\
 &= 2412 \text{ kcal/h} \cdot \text{m}^2
 \end{aligned}$$

$\therefore t_1 = 375^\circ\text{C}$  ..... Contents I • eccentric

$$\begin{aligned}
 \frac{Q}{A} &= \frac{0.200}{0.00855} \times (t_1 - 295) + 4.88 \times 10^{-8} \times 0.23 \times \{(t_1 + 273)^4 - 568^4\} \\
 &= 2412 \text{ kcal/h} \cdot \text{m}^2
 \end{aligned}$$

$\therefore t_1 = 370^\circ\text{C}$  ..... Contents I • center

## (2) Contents II

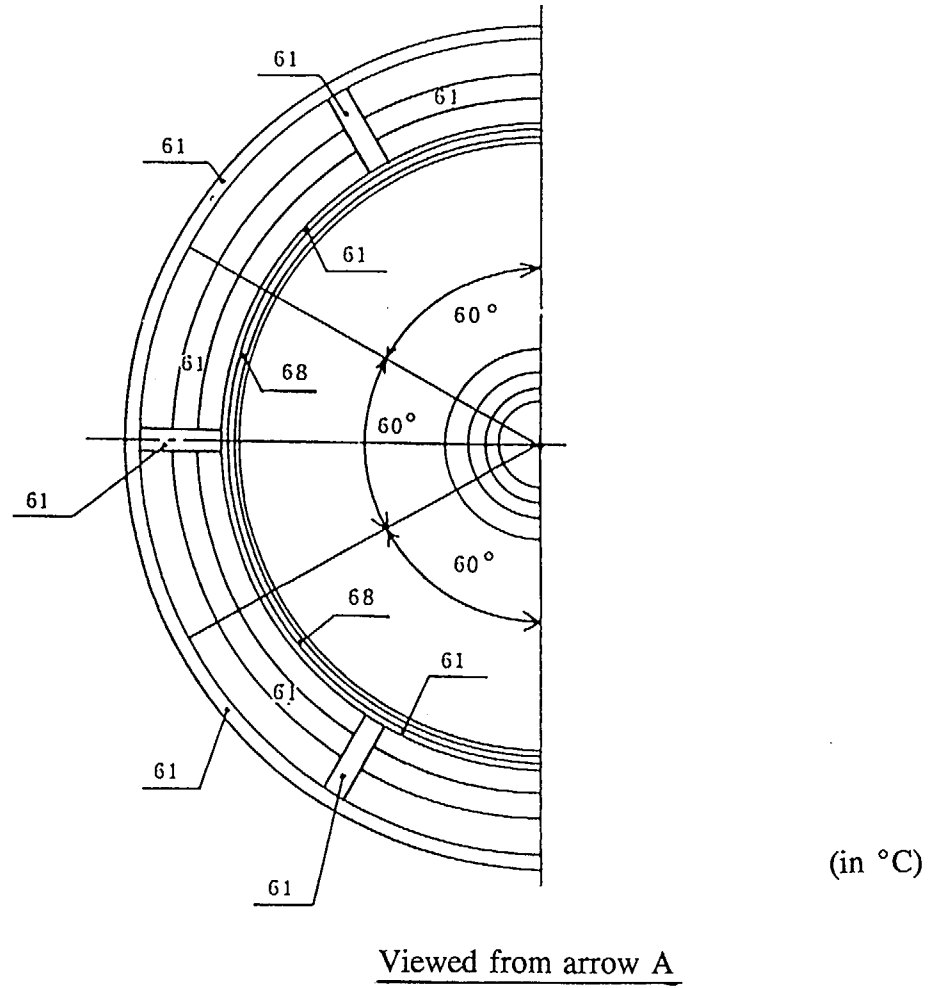
Fig. (II)-B.17 lists the temperature distribution of the package obtained when Contents II are evaluated. For Contents II, the temperature of receiving tube I is obtained by the TRUMP code using the heat transfer model shown in Fig. (II)-B.18 according to the maximum temperature of the inner container tube. Next, based on the temperature obtained for receiving tube I, the maximum temperature of the fuel pin is calculated by the heat transfer expression of the radiation and gas thermal conduction using the heat transfer model shown in Fig. (II)-B.19.

Fig. (II)-B.18 is first explained below. Six receiving tubes I are symmetrically stored in the inner container. The heat transfer of the inner container tube and receiving tubes I is evaluated as radiation and gas thermal conduction, and the heat transfer via natural convection is ignored, to be on the safe side. For calculation conditions, the temperature of the inner container tube obtained above is used as the boundary temperature. The temperature of receiving tubes I is obtained on the basis of the thermal conductivity of air (Table (II)-B.16) and the total form factor (see subsection B.6.1.2(3)) between receiving tubes I and the inner container tube. Fig. (II)-B.20 shows the obtained data.

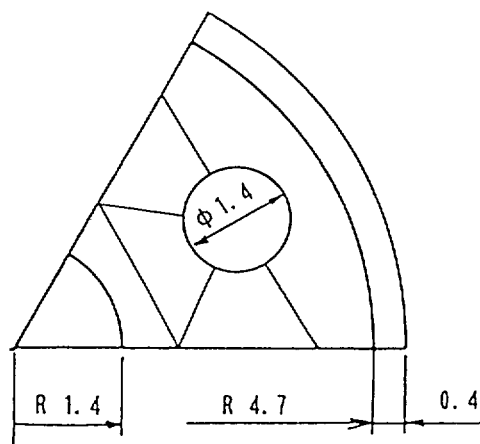
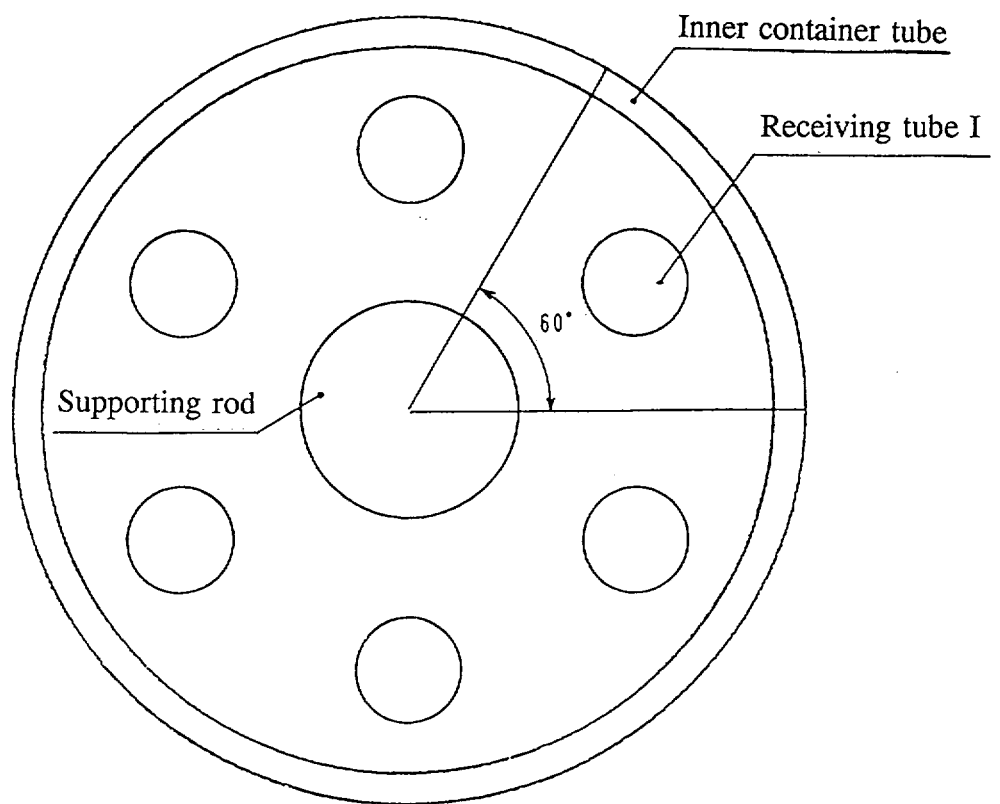
**Fig. (II)-D.17 Temperature of Package under Normal Test Conditions**  
**(Contents II) (1/2)**



(II)-B-50



**Fig. (II)-B.17 Temperature of Package under Normal Test Conditions(Contents II) (2/2)**



(in cm)

**Fig. (II)-B.18 Heat Transfer Model of Inner Container Holding Receiving Tube I**

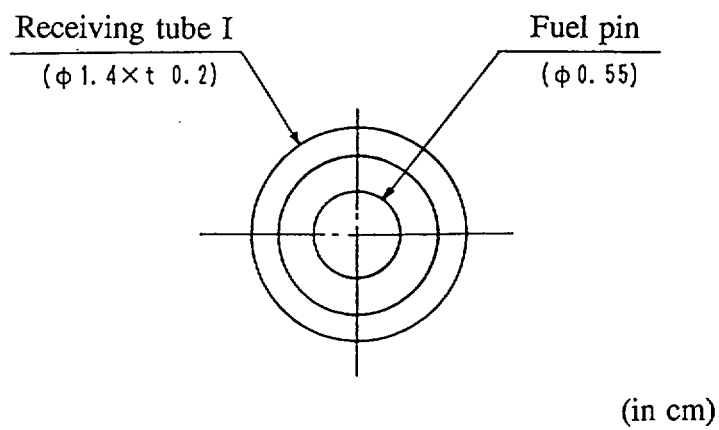


**Fig. (II)-B.19 Heat Transfer Model of Receiving Tube I**

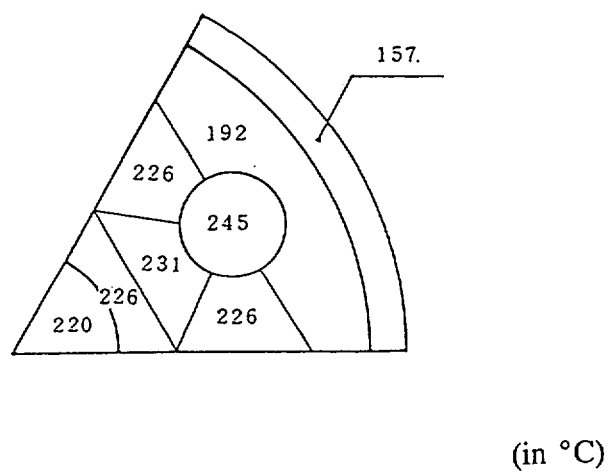


**Fig. (II)-B.20 Temperature Distribution in Inner Container Holding Receiving Tube I**

Next, based on the temperature of receiving tubes I, the maximum temperature of the fuel pin is calculated by the heat transfer expression of the radiation and gas thermal conduction.

The temperature of the fuel pin for Contents II is given by the expression below.

$$\frac{Q}{A} = \frac{k}{L} (t_1 - t_2) + \sigma F \{ (t_1 + 273)^4 - (t_2 + 273)^4 \}$$

where

Q : Decay heat of each fuel pin

$$Q = \frac{64}{N} \quad W = 10.7 \quad W = 9.2 \text{ kcal/h}$$

N : Number of fuel pins = 6

A : Heat transfer area of the fuel pin

$$A = \pi \times D \times L_1 = 3.11 \times 10^{-3} \text{ m}^2$$

D : Diameter of the fuel pin = 0.0055 m

L<sub>1</sub> : Heat generating length of the fuel pin = 0.36 m

L : Thickness of the air layer = 0.0025 m

k : Thermal conductivity of the air = 0.0386 kcal/h·m·°C  
= 0.0449 W/m·K

(Interpolated value at 300°C shown in Table (II)-B.16)

σ : Stefan-Boltzmann's constant = 4.88 × 10<sup>-8</sup> kcal/h·m<sup>2</sup>·K<sup>4</sup>

F : Total form factor

$$F = \left\{ \frac{1}{\varepsilon_1} + \frac{a_1}{a_2} \left( \frac{1}{\varepsilon_2} - 1 \right) \right\}^{-1} = 0.28$$

ε<sub>1</sub> : Emissivity of the fuel pin (stainless steel) = 0.37

ε<sub>2</sub> : Emissivity of receiving tube I (stainless steel) = 0.37

a<sub>1</sub> : Outer surface area of the fuel pin

$$a_1 = 0.0055 \times \pi \times 0.36 = 6.22 \times 10^{-3} \text{ m}^2$$

a<sub>2</sub> : Inner surface area of receiving tube I

$$a_2 = 0.0105 \times \pi \times 0.36 = 1.19 \times 10^{-2} \text{ m}^2$$

t<sub>2</sub> : Temperature of receiving tube I = 245°C

t<sub>1</sub> : Temperature of the fuel pin

Therefore, the left side of the equation is given by

$$\frac{Q}{A} = 2960 \text{ kcal/h}\cdot\text{m}^2$$

Each constant is assigned to the right side to obtain a value for  $t_1$  that satisfies the expression below.

$$\begin{aligned}\frac{Q}{A} &= \frac{0.0386}{0.0025} \times (t_1 - 245) + 4.88 \times 10^{-8} \times 0.28 \times \{(t_1 + 273)^4 - 518^4\} \\ &= 2960 \text{ kcal/h}\cdot\text{m}^2 \\ \therefore t_1 &= 365^\circ\text{C}\end{aligned}$$

Tables (II)-B.27 and (II)-B.28 list the obtained data.

**Table (II)-B.27 Maximum Temperature under Normal Test Conditions (Contents I)**

Part	Maximum temperature	
	Eccentric	Center
Shock absorber steel plate	64°C	60°C
Outer shell	72°C	66°C
Heat dispersion fins	73°C	67°C
Outer shell lids	73°C	64°C
Sampling valve lids	75°C	65°C
Penetration hole lid	75°C	65°C
Lead shield	84°C	76°C
Tungsten	80°C	67°C
Resin	73°C	67°C
Inner shell	85°C	77°C
Gas in inner shell	165°C	140°C
Inner container tube	241°C	235°C
Inner container cap	227°C	76°C
Fuel supporting can I	300°C	295°C
Gas in fuel supporting can I	338°C	333°C
Fuel pins	375°C	370°C
O-rings	75°C	65°C

**Table (II)-B.28 Maximum Temperature under Normal Test Conditions (Contents II)**

Place	Maximum temperature
Shock absorber steel plate	59°C
Outer shell	61°C
Heat dispersion fins	61°C
Outer shell lids	60°C
Sampling valve lids	61°C
Penetration hole lid	61°C
Lead shield	69°C
Tungsten	60°C
Resin	61°C
Inner shell	70°C
Gas in inner shell	123°C
Inner container tube	157°C
Inner container cap	64°C
Receiving tube I	245°C
Gas in receiving tube I	305°C
Fuel pins	365°C
O-rings	61°C

**B.4.3 Minimum Temperature**

The evaluation conditions for the minimum temperature of this package assume the case in which there is no solar heat load and no decay heat of the contents. The temperature of every section on the package at that time enters a state of equilibrium with the outside temperature. Therefore, it becomes -40°C as per the notification of science and technology agency.

Consequently, the temperature of the O-rings (used in the sampling valve lids, penetration hole lid, and front and rear lid units) that is severest, in terms of minimum service temperature, is -40°C. However, the minimum allowable service temperature for the O-rings is -50°C. Therefore, the O-rings maintain sufficient resistance.

#### B.4.4 Maximum Internal Pressure

This subsection describes how to evaluate the maximum internal pressure generated in the inner shell part of the outer container that forms the boundary of containment. Fuel supporting can I, fuel supporting can II and receiving tube II that store Contents I and IV through VII, and receiving tube I that stores Contents II form the secondary boundary of containment, so that the maximum internal pressure generated in each can is also evaluated.

Other than the fuel pin, gas (helium or air) is also to be found in the fuel supporting cans and receiving tubes. At the temperature (maximum temperature: 375°C) of the fuel pin indicated in subsection B.4.2, "Maximum Temperature", no phase change or chemical decomposition occurs.

Therefore, to be on the safe side, the internal pressure generated in the fuel supporting cans or receiving tubes is evaluated on the assumption that the internal pressure is caused by leakage of the FP gas of the fuel pin in the cans or by gas expansion due to a temperature rise in the cans.

The result of this structural evaluation shows that the fuel supporting cans and receiving tubes under normal test conditions maintain sufficient strength. Therefore, the pressure generated in the inner shell of the outer container is the result of the thermal expansion of gas (air) caused by an increase in temperature in the inner shell. Each part of the packaging is evaluated below.

(1) Internal pressure of the fuel supporting can

Contents I, IV, and V are loaded into fuel supporting can I. The burnup (5,200 MWD/MTM) of Contents V is lower than that of Contents I or IV. Contents V thus generate only a little FP gas. The burnup of Contents IV is the same (90,000 MWD/MTM) as that of Contents I. However, the weight of the fissile part that forms the majority of FP gas generation in Contents IV is less than in Contents I. Of the contents that are loaded into fuel supporting can I, Contents I have a maximum FP gas generation value and heating value.

Contents VII are loaded into fuel supporting can II. Contents VII have a lower burnup than Contents I, which means that Contents VII have fewer FP gas generation values. Contents VII also have a lower heating value than Contents I, so the temperature of the former is lower than that of the latter.

Fuel supporting can I in which Contents I are stored is evaluated below.

The FP gas generated in the fuel pin of Contents I is 4404 cc at a constant temperature (20°C) and at one atmospheric pressure, as shown in Table (II)-B.29. The pressure in fuel supporting can I when this FP gas fills the fuel supporting can I can be obtained as described below.

The gas receiving volume in fuel supporting can I is represented by value  $V_c$  obtained when the volume of both the fuel portion of the fuel pin and the stainless steel portion of the inner cylinder in fuel supporting can I is subtracted from the volume of fuel supporting can I.



Table (II)-B.29 FP Gas Generation of Contents I

Element	Number of moles* <sup>1</sup> (mol)	Volume (cc)* <sup>2</sup>	Remarks
H	$1.82 \times 10^{-4}$	4	*1 The receiving value of the fission product gas can be obtained by the ORIGEN code. *2 Volume at 20°C and at a pressure of one atmosphere
He	$3.42 \times 10^{-3}$	77	
Kr	$1.65 \times 10^{-2}$	370	
I	$1.25 \times 10^{-2}$	280	
Xe	$1.64 \times 10^{-1}$	3673	
Rn	$8.09 \times 10^{-18}$	--	

(A total of 4404 cc)

$$V_c = V_T - V_{IC} - V_F$$

- $V_T$  : Volume of fuel supporting can I

$V_{IC}$  : Volume of the inner cylinder of fuel supporting can I

$V_F$  : Volume of the fuel and end plug portions of the fuel pin
- cc

cc

cc

$$V_T = \frac{\pi \times d_i^2}{4} \times L_c \times \frac{1}{1000}$$

- $d_i$  : Inner diameter of fuel supporting can I = 83 mm

$L_c$  : Effective length of fuel supporting can I = 1890 mm

$$\begin{aligned} V_T &= \frac{\pi \times 83^2}{4} \times 1890 \times \frac{1}{1000} \\ &= 10226 \text{ cc} \end{aligned}$$

$$V_{IC} = \left\{ \frac{\pi}{4} \times (d_{oIC}^2 - d_{iIC}^2) + 5 \times \left( \frac{d_i - d_{oIC}}{2} \right) \times t \right\} \times L_c \times \frac{1}{1000}$$

- $d_{oIC}$  : Outer diameter of the inner cylinder of fuel supporting can I = 60.5 mm

$d_{iIC}$  : Inner diameter of the inner cylinder of fuel supporting can I = 57.2 mm

$t$  : Thickness of the inner cylinder's partition plate of fuel supporting can I = 2 mm

$L_c$  : Effective length of fuel supporting can I = 1890 mm

$$\begin{aligned} V_{IC} &= \left\{ \frac{\pi}{4} \times (60.5^2 - 57.2^2) + 5 \times \left( \frac{83 - 60.5}{2} \right) \times 2 \right\} \times 1890 \times \frac{1}{1000} \\ &= 789 \text{ cc} \end{aligned}$$

$$V_F = \frac{\pi \times d_{OF}^2}{4} \times n \times L_F \times \frac{1}{1000}$$

$d_{OF}$  : Outer diameter of the fuel pin cladding tube = 6.5 mm  
 $n$  : Number of fuel pins = 15  
 $L_F$  : Length of the fuel portion and end plug portion = 1200 mm

$$\begin{aligned}
 V_F &= \frac{\pi \times 6.5^2}{4} \times 15 \times 1200 \times \frac{1}{1000} \\
 &= 597 \text{ cc}
 \end{aligned}$$

and thus

$$\begin{aligned}
 V_c &= V_T - V_{Ic} - V_F \\
 &= 10226 - 789 - 597 \\
 &= 8840 \text{ cc}
 \end{aligned}$$

The pressure in fuel supporting can I when the FP gas of the fuel pin leaks into fuel supporting can I is given by the expression below.

$$P_A = P_O \times \frac{(V_c + V_{FP})}{V_c} \times \frac{T_A}{T_O}$$

$P_A$  : Maximum internal pressure = kPa  
 $P_O$  : Initial pressure = 1.0 kg/cm<sup>2</sup> abs. = 100 kpa  
 $T_A$  : Final temperature of the gas (See Table (II)-B.31.) = K  
 $T_O$  : Initial temperature of the gas = 20°C = 293 K  
 $V_{FP}$  : Volume of the FP gas = 4404 cc

$$\begin{aligned}
 P_A &= 1.0 \times \frac{(8840 + 4404)}{8840} \times \frac{T_A}{T_O} \\
 &= 1.50 \times \frac{T_A}{T_O}
 \end{aligned}$$

Based on the results given above, the maximum internal pressure  $P_A$  in fuel supporting can I in which Contents I are stored is obtained. Table (II)-B.31 lists the obtained maximum internal pressure.

## (2) Internal pressure of the receiving tube

The volume of the receiving tubes, the FP gas generation value, and the gas temperature in receiving tubes are the main factors determining the internal pressure of the receiving tubes. These factors indicate that receiving tube I has the maximum internal pressure. Therefore, receiving tube I is evaluated below.

As in step (1), the internal pressure of receiving tube I is obtained based on the assumption that the FP gas generated in the fuel pin fills receiving tube I thereby increasing the pressure in this receiving tube.

The total volume of the FP gas generated in the six fuel pins holding Contents II is 1147 cc as shown in Table (II)-B.30. Since the fuel pins are stored in receiving tube I on a one-on-one basis, the amount of FP gas vFP that leaks into receiving tube I is 191 cc.

**Table (II)-B.30 FP Gas Generation of Contents II**

Element	Number of moles* <sup>1</sup> (mol)	Volume (cc)* <sup>2</sup>	Remarks
H	$4.70 \times 10^{-5}$	1	*1 The receiving value of the fission product gas can be obtained by the ORIGEN code. *2 Volume at 20°C and at a pressure of one atmosphere
He	$8.27 \times 10^{-4}$	19	
Kr	$4.39 \times 10^{-3}$	98	
I	$3.14 \times 10^{-3}$	70	
Xe	$4.28 \times 10^{-2}$	959	
Rn	$6.31 \times 10^{-18}$	--	

(A total of 1147 cc)

The gas receiving volume in receiving tube I is represented by volume  $V_{TG}$ , which is obtained when the volume of the fuel portion and end plug portion of the fuel pin are subtracted from the volume of receiving tube I.

$$V_{TG} = V_T - V_F$$

$V_T$  : Volume of receiving tube I cc  
 $V_F$  : Volume of the fuel and end plug portions of the receiving fuel pin in receiving tube I cc

$$V_T = \frac{\pi \times d_{iT}^2}{4} \times L_T \times \frac{1}{1000}$$

$d_{iT}$  : Inner diameter of receiving tube I = 10.5 mm  
 $L_T$  : Effective length of receiving tube I = 1020 mm

$$\begin{aligned}
 V_T &= \frac{\pi \times 10.5^2}{4} \times 1020 \times \frac{1}{1000} \\
 &= 88 \text{ cc}
 \end{aligned}$$

$$V_F = \frac{\pi \times d_{oF}^2}{4} \times L_F \times \frac{1}{1000}$$

$d_{oF}$  : Outer diameter of the fuel pin = 6.5 mm  
 $L_F$  : Effective length of the fuel portion and end plug material = 460 mm

$$V_F = \frac{\pi \times 6.5^2}{4} \times 460 \times \frac{1}{1000}$$

$$= 15 \text{ cc}$$

and thus

$$V_{TG} = V_T - V_F$$

$$= 88 - 15$$

$$= 73 \text{ cc}$$

Therefore, the pressure in receiving tube I when the FP gas of the fuel pin leaks into receiving tube I is given by the expression below in the same manner as in step (1).

$$P_A = P_O \times \frac{(V_{TG} + V_{FP})}{V_{TG}} \times \frac{T_A}{T_O}$$

$$P_A = 1.0 \times \frac{(73 + 191)}{73} \times \frac{T_A}{T_O}$$

$$= 3.62 \times \frac{T_A}{T_O}$$

Based on the results provided above, the maximum internal pressure  $P_A$  in receiving tube I in which Contents II are stored is obtained. Table (II)-B.31 gives the obtained maximum internal pressure.

(3) Internal pressure of the outer container's inner shell

As described in the structural evaluation, fuel supporting cans and receiving tubes maintain sufficient strength under normal test conditions. They are not damaged in this case. Therefore, the pressure generated in the inner shell only results from the thermal expansion of gas. If, to be on the safe side, the volume expansion caused by the increase in temperature in the inner shell is ignored, the expression below will be given.

$$P_A = P_O \times \frac{T_A}{T_O}$$

$P_A$	: Maximum internal pressure	kPa
$P_O$	: Initial pressure = 1.0 kg/cm <sup>2</sup> abs.	= 100 kPa
$T_A$	: Final temperature of the gas (See Table (II)-B.31.)	K
$T_O$	: Initial temperature of the gas = 20°C	= 293 K

Based on the results given above, the maximum internal pressure  $P_A$  is obtained. Table (II)-B.31 provides the obtained maximum internal pressure.

As shown in Table (II)-B.31, the maximum internal pressure under normal test conditions does not exceed the design pressure. Therefore, these receiving containers remain sound. The maximum internal pressure also does not exceed the maximum normal operating pressure of 700 kPa (7.0 kg/cm<sup>2</sup>G), which is prescribed by the technical standard and satisfies engineering criteria.

**Table (II)-B.31 Maximum Internal Pressure under Normal Test Conditions<sup>\*2</sup>**

Contents	Inner shell		Fuel supporting can I (receiving tube <sup>*1</sup> )	
	Maximum internal pressure	Gas temperature	Maximum internal pressure	Gas temperature
Contents I • eccentric	60 kPa (0.6 kg/cm <sup>2</sup> G)	165°C	210 kPa (2.1 kg/cm <sup>2</sup> G)	338°C
Contents I • center	50 kPa (0.5 kg/cm <sup>2</sup> G)	140°C	210 kPa (2.1 kg/cm <sup>2</sup> G)	333°C
Contents II	40 kPa (0.4 kg/cm <sup>2</sup> G)	123°C	610 kPa <sup>*1</sup> (6.1 kg/cm <sup>2</sup> G)	305°C <sup>*1</sup>

<sup>\*1</sup> In the case of Contents II, the maximum internal pressure and gas temperature of receiving tube I rather than those of fuel supporting can I are indicated.

<sup>\*2</sup> Design pressure and material evaluation temperature used in the structural evaluation

Item	Design pressure	Evaluation temperature	Temperature evaluation result
Inner shell	200 kPa (2 kg/cm <sup>2</sup> G)	200°C	85°C
Fuel supporting can I	300 kPa (3 kg/cm <sup>2</sup> G)	400°C	300°C
Receiving tube I	700 kPa (7 kg/cm <sup>2</sup> G)	350°C	245°C

#### **B.4.5 Maximum Thermal Stress**

The maximum thermal stress that is generated in this packaging under normal test conditions is  $83.4 \text{ N/mm}^2$  ( $8.5 \text{ kg/mm}^2$ ) for the inner shell and  $6.4 \text{ N/mm}^2$  ( $0.7 \text{ kg/mm}^2$ ) for the outer shell, as indicated in subsection A.5.1.2 of Chapter (II). These values do not exceed the design criteria values of  $174 \text{ N/mm}^2$  ( $17.7 \text{ kg/mm}^2$ ) (material: SUS304, temperature:  $90^\circ\text{C}$ ) and  $180 \text{ N/mm}^2$  ( $18.4 \text{ kg/mm}^2$ ) (material: SUS304, temperature:  $80^\circ\text{C}$ ), respectively. Therefore, the packaging is not damaged by the thermal stress and remains sound.

#### **B.4.6 Summary and Evaluation of Results**

A package that is subject to the maximum decay heat of its contents (260 W for Contents I, 64 W for Contents II, 40 W for Contents III, 250 W for Contents IV, 63 W for Contents V, 260 W for Contents VI, 3 W for Contents VII, and 170 W for Contents VIII), has a surface temperature of  $72^\circ\text{C}$  (maximum). This temperature does not exceed the temperature ( $85^\circ\text{C}$ ) established by the law and satisfies the engineering criteria. O-rings that fulfill a containment function are used for the outer shell lids, sampling valve lids, and penetration hole lid. Their maximum temperature is  $75^\circ\text{C}$  and they range within the allowable service temperatures for an O-ring. O-rings can thus sufficiently withstand such use. The temperatures of the lead, tungsten and resin shielding materials also do not exceed their melting points so that these temperatures exert no adverse influence on the shielding performance.

As shown in Table (II)-B.31, the maximum internal pressure does not exceed the maximum service pressure  $700 \text{ kPa}$  ( $7 \text{ kg/cm}^2\text{G}$ ) prescribed by the design pressure and technical standard and satisfies the relevant engineering criteria.

The maximum thermal stress generated in this packaging is  $83.4 \text{ N/mm}^2$  ( $8.5 \text{ kg/mm}^2$ ) for the inner shell and  $6.4 \text{ N/mm}^2$  ( $0.7 \text{ kg/mm}^2$ ) for the outer shell. These values do not exceed the design criteria values of  $174 \text{ N/mm}^2$  ( $17.7 \text{ kg/mm}^2$ ) (material: SUS304, temperature:  $90^\circ\text{C}$ ) and  $180 \text{ N/mm}^2$  ( $18.4 \text{ kg/mm}^2$ ) (material: SUS304, temperature:  $80^\circ\text{C}$ ), respectively. Therefore, the packaging is not damaged by pressure or thermal stress.

Even if the package is subject to a service temperature of  $-40^\circ\text{C}$ , the performance of each material that makes up the packaging is not damaged, and the packaging remains sound.

Judging from the above results, this package can withstand the change in temperature under normal test conditions and maintains sufficient strength. The package thus remains sound.

## **B.5 Accident Test Conditions**

### **B.5.1 Thermal Analysis Model**

A thermal evaluation of the package is performed by the three-dimensional stable and unstable temperature distribution calculation code, TRUMP, which is based on a differential method.

To obtain the structural evaluation results given in subsection A.6.2.1 of Chapter (II), an evaluation was performed on the assumption that a hole is made in the shock absorber during drop test II (vertical drop). To obtain an evaluation that is on the safe side during the thermal analysis, a hole of 20 cm deep is assumed instead of the 18.4 cm-deep hole that actually resulted during the structural evaluation. In this case, the shock absorber (wood) is in direct contact with air and may burn should a fire break out. Therefore, a flame resistance treatment was applied to the shock absorber (wood) of this packaging.

Moreover, before this evaluation, a thermal test under accident test conditions was conducted using a model of the shock absorber to confirm the effects of this flame resistance treatment. For the results of this thermal test, see subsection B.6.4

The results of the thermal test mentioned above are calculated under the same conditions (the shape of the shock absorber model and the ambient temperature) as in the thermal test using the calculation code, TRUMP. The validity of the conditions under which the physical properties of wood and the burnup values are calculated is confirmed in subsection B.6.3.

The physical properties and burnup values used in the above calculation are employed for the package, and the evaluation under accident test conditions is performed by the calculation code, TRUMP.

As described in subsection C.2.1 of Chapter (I), a cement layer and fusible plug are provided in this packaging to prevent heat from getting inside the package as a result of the vaporization of moisture in the cement during a fire accident. However, when the heat entering the package is analyzed, to be on the safe side, this thermal analysis ignores the latent heat resulting from vaporization.

The thermal analysis model using the TRUMP code is explained next.

#### **B.5.1.1 Analysis model**

The model shape and evaluation conditions are described below.

##### **(1) Model shape**

As described in section B.1(2), the following three conditions should be selected in determining a thermal analysis model, which will receive the maximum thermal damage as a result of packaging deformation generated during a drop test.

- 1) As indicated by the results of the shock absorber model test, the shock absorber exhibits an excellent thermal shielding function and suppresses heat input during a fire. A deformation state is one in which the shock absorber that covers all the opening parts of the packaging becomes thinner, and in which the area becomes wider.

- 2) A deformation state is one in which the temperature of the O-ring (fluoro rubber) (among the materials constituting the boundary of containment) that has a maximum allowable service temperature of 200°C becomes higher.
- 3) A deformation state is one in which the temperatures of the tungsten and lead shields that have a shielding function become higher.

The deformation states for each drop attitude obtained from the structural evaluation are examined under the conditions mentioned above.

As described during the structural evaluation, the outer shell is not penetrated when the outer shell part of the outer container directly collides with a mild steel bar in a horizontal drop attitude during drop test II. Consequently, the cement layer that functions as a heat insulator is not damaged, and the maximum damage does not occur during a fire. When the fir-plywood part directly collides with a mild steel bar during vertical drop test II on the shock absorber, the facing plate (plate thickness of 16 mm) that covers the fir-plywood is not penetrated. The remaining thickness of the fir-plywood is 42 mm (see subsection A.6.2). This does not create the conditions for maximum damage during a fire. The cover steel plate (plate thickness of 3 mm) of the shock absorber is penetrated when the balsa wood part shown in Table (II)-B.32 directly collides with a mild steel bar. The damage sustained in this case is examined next. Among the materials that constitute the boundary of containment, the O-ring is used in the front and rear lid units, the penetration hole lid, and the front and rear sampling valve lids on the outer container's shell part. For this reason, the vertical and horizontal drops on one of these parts by which the deformation is accumulated during drop tests I and II increase the heat input to the portion in which the O-ring is used during a subsequent thermal test. This creates the conditions necessary for generating the maximum damage. The above result thus satisfies conditions 1), 2), and 3) described previously.

Fig. (II)-B.4 shows the modeled package mentioned above during a vertical drop. According to the structural evaluation results shown in subsections A.6.1.1 and A.6.2, the shock absorber become deformed by 110 mm and 184 mm during drop tests I and II, respectively. The minimum remaining thickness of the deformed shock absorber is 26 mm.

**Table (II)-B.32    Deformation of the Shock Absorber (Balsa Wood) during Drop Tests I and II**

Drop attitude	Shock absorber thickness (mm)	Total deformation during drop tests I and II (mm)	Remaining thickness of the deformed shock absorbers (mm)
Vertical drop	320	294 (110 + 184)	26
Horizontal drop	273	236 (160 + 76)	37
Corner drop	520	410 (210 + 200)	110



As shown in Fig. (II)-B.21 (see subsection B.5.2), during the thermal analysis, the shock absorber steel plate is assumed to be damaged during drop test II and a hole with a depth of 200 mm is created in this case, to be on the safe side.

As a result, the minimum thickness of the deformed shock absorbers is assumed to be 10 mm (circular form of 150 mm in diameter), to which condition 1) applies. Since the deformation occurring during drop test II is located nearest to the O-ring installed in the outer shell lid, condition 2) applies to this case, which provides the severest thermal state. Since this deformation is located nearer to the lead shield and tungsten found inside the outer shell lid than any other deformation occurring during other drop tests, condition 3) also applies to this case.

Fig. (II)-B.7 shows the modeled deformation state during a horizontal drop (Fig. (II)-A.47) on the sampling valve lid (O-ring mounting part) that constitutes the boundary of containment. During modeling, it is assumed that the remaining thickness of the balsa wood, is 35 mm, and the hole is given a conical shape, to be on the safe side. Using this model, the temperatures of the sampling valve lid and penetration hole lid parts are evaluated.

The modeling inside this packaging is based on the same concept as is the thermal analysis model under normal test conditions.

(2) Evaluation conditions

Table (II)-B.33 lists the thermal conditions used for the evaluation.

The thermal analysis under accident test conditions is performed on the assumption that the package has been subjected to mechanical tests. Therefore, the temperature distribution of the package during a fire is evaluated under normal test conditions. The decay heat of the contents is 260 W (maximum) for Contents I, and 64 W for Contents II.

With respect to thermal conditions during a fire, the ambient temperature is 800°C, the fire duration time is 30 minutes, the emissivity of the fire is 0.9, and the absorptivity on the packaging surface is 0.8, assuming that the thermal conditions are not subject to solar heat radiation. Radiation and natural convection are assumed for the heat transfer of the fire to the packaging.

With respect to the thermal conditions after a fire, the ambient temperature is 38°C in still air, assuming that the thermal conditions are subject to solar heat radiation. Table (II)-B.26 described in subsection B.4.1 lists the heat transfer values from the solar heat radiation. Natural convection and radiation are assumed for the thermal radiation from the packaging surface. Given the oxidation on the stainless steel surface, the emissivity of the packaging surface at that time is 0.55 and the ambient emissivity is 1.0.

Table (II)-B.33 Thermal Conditions under Accident Test Conditions

Conditions		Decay heat	Environmental conditions			Emissivity of the packaging surface	Gas	
			Ambient temperature	Solar heat load	Ambient emissivity		Inner shell	Fuel supporting can I *1 (receiving tube I)
Initial conditions	Contents I • eccentric	260W	Still air 38°C	Yes	1.0	0.37*4	Air	Helium
	Contents I • eccentric*2							
	Contents I • center							
	Contents II	64W						Air
During a fire	Contents I • eccentric	260W	Fire 30 minutes 800°C	No	0.9*3	0.8*3	Air	Helium
	Contents I • eccentric*2							
	Contents I • center							
	Contents II	64W						Air
After a fire	Contents I • eccentric	260W	Still air 38°C	Yes	1.0	0.55*4	air	Helium
	Contents I • eccentric*2							
	Contents I • center							
	Contents II	64W						Air

\*1 For Contents II, the fuel pin is loaded into receiving tube I rather than into fuel supporting can I.

\*2 This package indicates the thermal evaluation model during a horizontal drop.

\*3 Safety standard governing the transport of radioactive material (Determined by the Atomic Energy Commission. January 21, 1975)

\*4 See footnotes 1) and 2)

B.5.1.2 Test model

The analysis model, rather than the test model, is used.

1) Goldsmith, A. etal., "Handbook of Thermophysical Properties of Solid Materials" Revised Edition, Vol. I, the MacMillan Company, New York, pp157-172, 1961

2) "Dennetsu Kougaku Shiryo" Third Edition, The Japan Society of Mechanical Engineers, page 148

### **B.5.2 Evaluation Conditions of the Package**

The thermal analysis under accident test conditions is performed assuming that the thermal test is conducted after a mechanical test. The deformation value of this packaging is determined based on the results given in subsections A.6.1 and A.6.2 of Chapter (II) so that the deformed shape provides the severest thermal conditions.

As described in subsection B.5.1.1(1), those conditions are as follows:

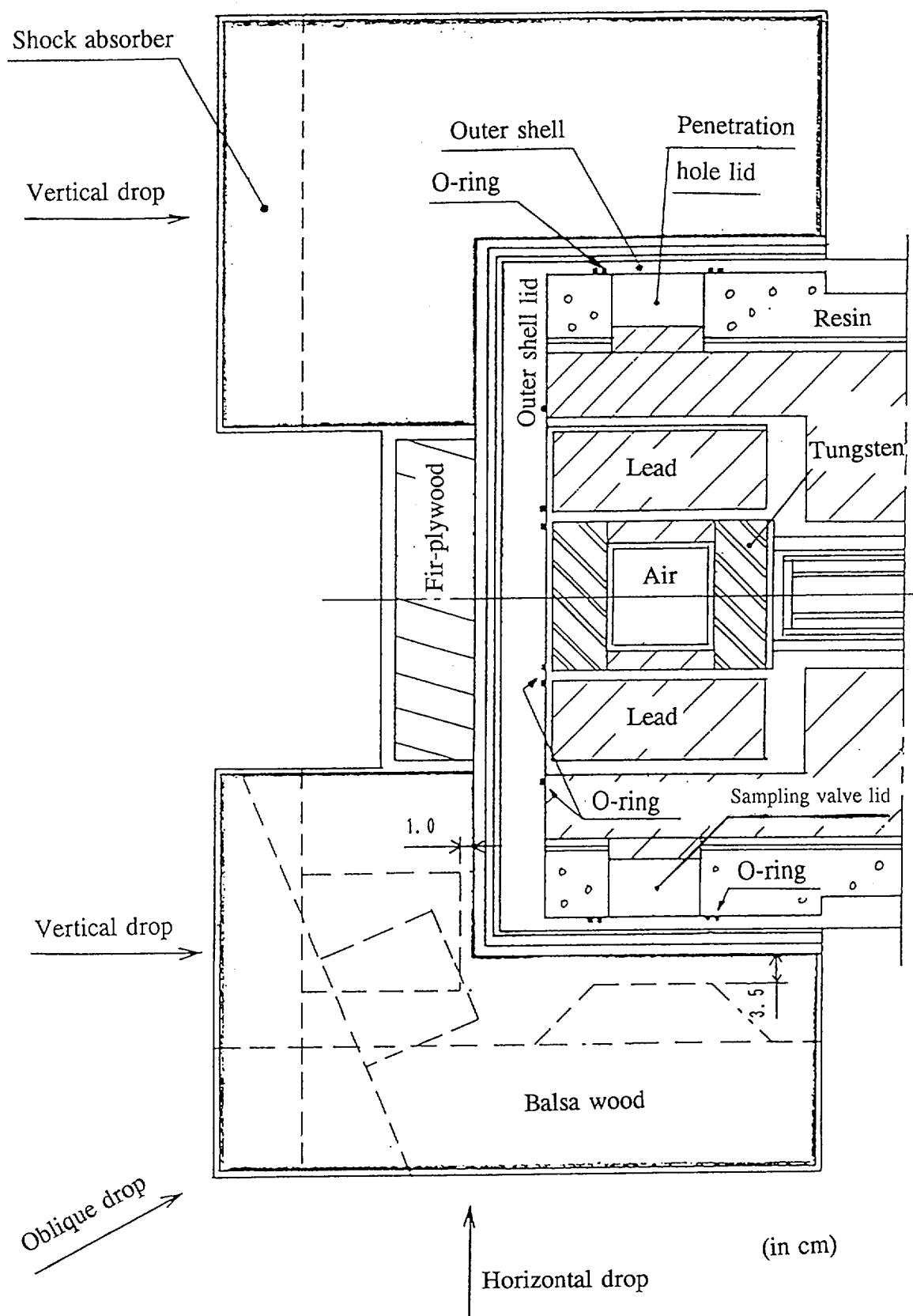
- 1) The shock absorber has an excellent thermal shielding function, which suppresses the internal heat input during a fire. The deformation state is one in which the thickness of the shock absorber that covers all the opening parts of the packaging is made thinner and allows heat to enter easily.
- 2) The deformation state is one in which the temperature of the O-ring (fluoro rubber) (among the materials constituting the boundary of containment) that has a maximum allowable service temperature of 200°C becomes higher.
- 3) The deformation state is one in which the temperatures of the tungsten and lead shields that have a shielding function become higher.

As described in condition 1), the shock absorber has an excellent shielding function, and covers the parts in which the O-ring constituting the boundary of containment is used. If both drop tests I and II are conducted, the resulting shock absorber deformation will satisfy conditions 1), 2), and 3). As shown in Fig. (II)-B.21, the O-ring is used in the outer shell lids, outer container shell part, sampling valve lids, and penetration hole lid.

The results of the structural evaluation indicate that the remaining thickness of the balsa wood during a vertical drop is small (26 mm) as shown in Table (II)-B.32. Moreover, during drop test II, a hole is made in the shock absorber near the outer shell lids where the O-ring is used. If both drop tests I and II are conducted at a horizontal drop attitude, a hole will result in the shock absorber near the sampling valve lid. The resulting residual thickness will be 37 mm.

If this package is exposed to a fire after dropping at each attitude, the temperature of the portion where the O-ring is used rises, and the temperatures of the shields described in condition 3) also increase.

To be on the safe side, this evaluation assumes that the remaining thickness of the shock absorber is 10 mm for a thermal test after a vertical drop and 35 mm for a thermal test after a horizontal drop, as shown in Fig. (II)-B.21.



----- : Indicates shapes of the shock absorber after drop tests have been conducted.

**Fig. (II)-B.21 Remaining Thickness of Shock Absorber after Drop Tests I and II**

**B.5.3 Temperature of the Package**

Based on the analysis model and the conditions described in subsections B.5.1 and B.5.2, the temperature distribution of each package part was obtained using the TRUMP code. The change in temperature for every part of the package is as shown in Figs. (II)-B.8 through (II)-B.11. The temperature of the outer shell rapidly rises after a fire starts, reaches 300°C within a few minutes, and eventually reaches 656°C 30 minutes after a fire starts. Therefore, the fusible bismuth plugs (melting point of 271°C) installed on the outer shell melt a few minutes after a fire starts. Tables (II)-B.34 and (II)-B.35 list the maximum temperature for every section of the package and the time required for each part to reach its maximum temperature after a fire starts.

Based on this temperature distribution, the maximum temperature of the fuel pins in each receiving state is calculated below.

**Table (II)-B.34 Maximum Temperature under Accident Test Conditions (Contents I)**

Part	Eccentric		Center ver- tical drop	Time elapsed after a fire
	Vertical drop	Horizontal drop		
Shock absorber steel plate	781°C	781°C	781°C	0.5 h
Shock absorber steel plate*1	797°C	785°C	797°C	0.5 h
Outer shell	656°C	656°C	651°C	0.5 h
Heat dispersion fins	405°C	405°C	401°C	0.5 h
Outer shell lids	125°C	114°C (8.5h)	116°C	8.0 h
Sampling valve lids	120°C (3.0h)	120°C	114°C (2.5h)	2.9 h
Penetration hole lid	120°C (3.0h)	120°C	114°C (2.5h)	2.9 h
Lead shield	193°C	193°C	190°C (1.2h)	1.5 h
Tungsten	133°C	133°C	123°C	7.5 h
Resin	656°C	656°C	651°C	0.5 h
Inner shell	193°C	193°C	189°C (1.4h)	1.5 h
Gas in the inner shell	228°C	228°C	202°C (4.0h)	3.0 h
Inner container tube	278°C (4.0h)	278°C (4.0h)	284°C	3.0 h
Inner container cap	255°C	255°C	132°C	7.0 h
Fuel supporting can I	328°C (4.0h)	328°C (4.0h)	332°C	3.5 h
Gas in fuel supporting can I	363°C	363°C	366°C	3.5 h
Fuel pins	397°C (4.0h)	397°C (4.0h)	400°C	3.5 h
O-rings	125°C	120°C (8.5h)*2	116°C	8.0 h

\*1 Indicates the portion damaged during a drop accident.

\*2 O-ring of the penetration hole lid part

Note: Times different from the one shown in the fifth column are indicated in parentheses.

**Table (II)-B.35 Maximum Temperature under Accident Test Conditions (Contents II)**

Part	Maximum temperature	Time elapsed after a fire
Shock absorber steel plate	781°C	0.5 h
Shock absorber steel plate*1	797°C	0.5 h
Outer shell	650°C	0.5 h
Heat dispersion fins	399°C	0.5 h
Outer shell lids	113°C	8.0 h
Sampling valve lids	109°C	3.5 h
Penetration hole lid	109°C	3.5 h
Lead shield	186°C	1.3 h
Tungsten	119°C	7.5 h
Resin	650°C	0.5 h
Inner shell	183°C	1.5 h
Gas in the inner shell	193°C	3.0 h
Inner container cylinder	223°C	3.0 h
Inner container cap	122°C	8.0 h
Fuel supporting can I	289°C	3.0 h
Gas in fuel supporting can I	341°C	3.0 h
Fuel pins	392°C	3.0 h
O-rings	113°C	8.0 h

\*1 Indicates the section damaged during a drop accident.

(1) Contents I

Contents I • eccentric which have the heat generating region located at the end, and Contents I • center which have this region located in the center are available as Contents I. The package holding Contents I • eccentric is evaluated both for vertical and horizontal drops.

The maximum temperature of the fuel pin is obtained according to the maximum temperature of fuel supporting can I (Table (II)-B.34) using the heat transfer model shown in Fig. (II)-B.22. To be on the safe side, the evaluation ignores the heat flow in the axial direction. Assuming that the heat flow exists only in the radial direction, the temperature of the fuel pin is evaluated by the heat transfer expression of the radiation and gas thermal conduction. In this model, the case in which the heat transfer length (L) is greatest is assumed so that the temperature of the fuel pin will be higher.

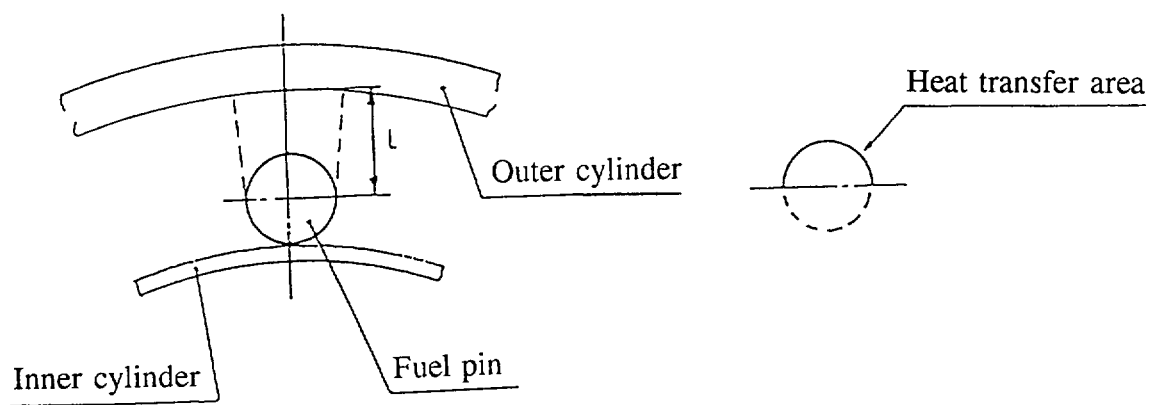


**Fig. (II)-B.22 Heat Transfer Model in Fuel Supporting Can I**

The temperature of the fuel pin for Contents I • eccentric and Contents I • center is given by the expression below.

$$\frac{Q}{A} = \frac{k}{L} (t_1 - t_2) + \sigma F \{ (t_1 + 273)^4 - (t_2 + 273)^4 \}$$

where

Q : Decay heat of each fuel pin

$$Q = \frac{260}{N} \quad W = 17.3 \quad W = 15.0 \text{ kcal/h}$$

N : Number of fuel pins = 15

A : Heat transfer area of the fuel pin

$$A = \frac{1}{2} \times \pi \times D \times L_1 = 6.22 \times 10^{-3} m^2$$

D : Diameter of the fuel pin = 0.0055 m

L<sub>1</sub> : Heat generating length of the fuel pin = 0.72 m

L : Heat transfer length = 0.00855 m

k : Thermal conductivity of the helium = 0.216 kcal/h·m·°C  
= 0.251 W/m·K

(Interpolated value at 360°C shown in Table (II)-B.20)

σ : Stefan-Boltzmann's constant = 4.88 × 10<sup>-8</sup> kcal/h·m<sup>2</sup>·K<sup>4</sup>

F : Total form factor

$$F = \left( \frac{1}{\varepsilon_1} + \frac{1}{\varepsilon_2} - 1 \right)^{-1} = 0.23$$

ε<sub>1</sub> : Emissivity of the fuel pin (stainless steel) = 0.37

ε<sub>2</sub> : Emissivity of the outer cylinder (stainless steel) = 0.37

t<sub>2</sub> : Temperature of the outer cylinder

Contents I · eccentric = 328°C

Contents I · center = 332°C

t<sub>1</sub> : Temperature of the fuel pin

Therefore, the left side of the above equation is given by

$$\frac{Q}{A} = 2412 \text{ kcal/h} \cdot m^2$$

Each constant is assigned to the right side to obtain a value of "t<sub>1</sub>" that satisfies the expression below.

$$\begin{aligned} \frac{Q}{A} &= \frac{0.216}{0.00855} \times (t_1 - 328) + 4.88 \times 10^{-8} \times 0.23 \times \{(t_1 + 273)^4 - 601^4\} \\ &= 2412 \text{ kcal/h} \cdot m^2 \end{aligned}$$

∴ t<sub>1</sub> = 397°C ..... Contents I · eccentric



$$\begin{aligned}\frac{Q}{A} &= \frac{0.216}{0.00855} \times (t_1 - 332) + 4.88 \times 10^{-8} \times 0.23 \times \{(t_1 + 273)^4 - 605^4\} \\ &= 2412 \text{ kcal/h}\cdot\text{m}^2\end{aligned}$$

$\therefore t_1 = 400^\circ\text{C}$  ..... Contents I • center

## (2) Contents II

For Contents II, the temperature of receiving tube I is obtained by the TRUMP code using the heat transfer model shown in Fig. (II)-B.23, according to the maximum temperature of the inner container cylinder. Next, based on the temperature obtained for receiving tube I, the maximum temperature of the fuel pin is calculated by the heat transfer expression of radiation and gas thermal conduction using the heat transfer model shown in Fig. (II)-B.24.

Fig. (II)-B.23 is explained first. Six receiving tubes I are symmetrically stored in the inner container. To be on the safe side, the evaluation assumes that the heat transfer between the inner container tube and receiving tube I results from radiation and gas thermal conduction, while heat transfer due to natural convection is ignored. The temperature of the inner container cylinder obtained above is used as the environmental temperature of the calculation conditions. The temperature of receiving tube I is obtained using the thermal conductivity value (Table (II)-B.16) of air and the overall form coefficient (subsection B.6.1.2(4)) of receiving tube I and the inner container cylinder. Fig. (II)-B.25 shows the resulting information.

Based on the temperature of receiving tube I, the maximum temperature of the fuel pin is calculated by the heat transfer expression of the radiation and gas thermal conduction.

The temperature of the fuel pin for Contents II is given by the expression below.

$$\frac{Q}{A} = \frac{k}{L} (t_1 - t_2) + \sigma F \{ (t_1 + 273)^4 - (t_2 + 273)^4 \}$$

where

Q : Decay heat of each fuel pin

$$Q = \frac{64}{N} \quad W = 10.7 \quad W = 9.2 \text{ kcal/h}$$

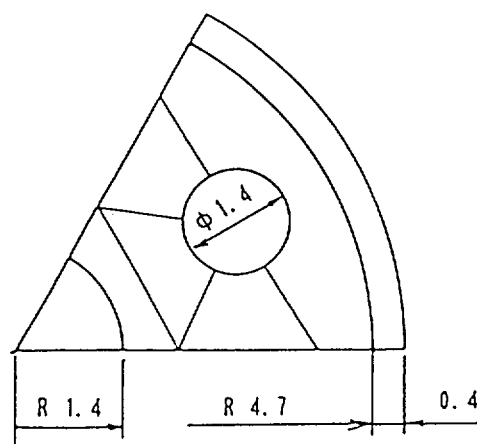
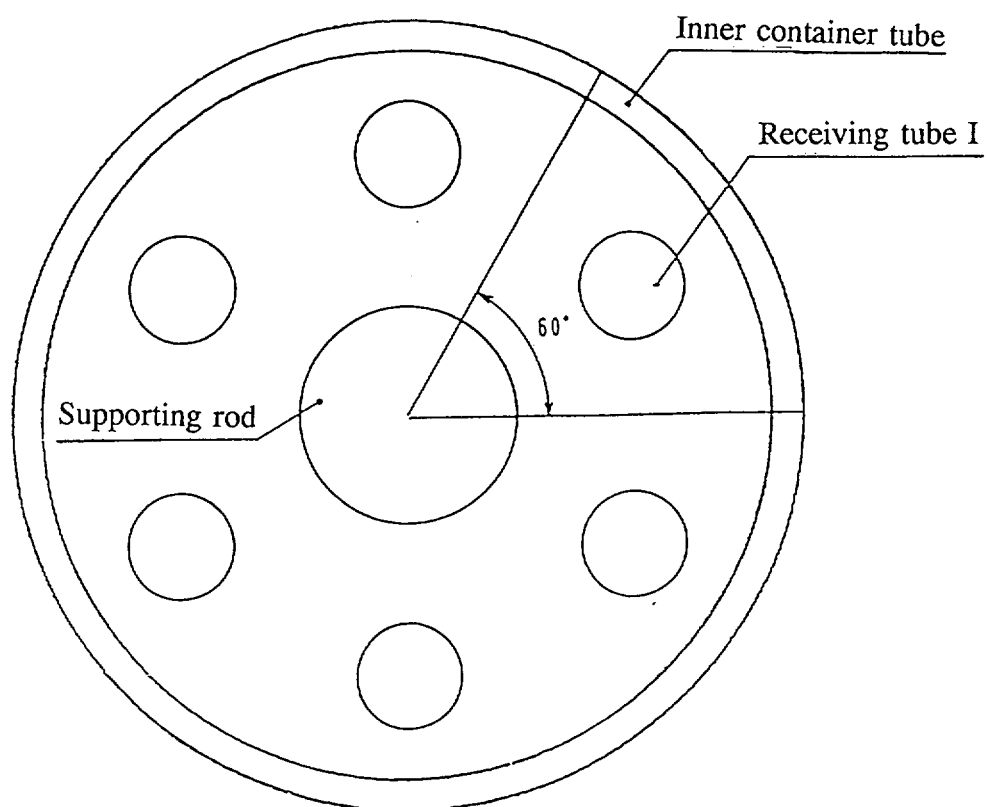
N : Number of fuel pins = 6

A : Heat transfer area of the fuel pin

$$A = \pi \times D \times L_1 = 3.11 \times 10^{-3} \text{ m}^2$$

D : Diameter of the fuel pin = 0.0055 m

L<sub>1</sub> : Heating length of the fuel pin = 0.36 m



(in cm)

**Fig. (II)-B.23 Heat Transfer Model of Inner Container Holding Receiving Tube I**

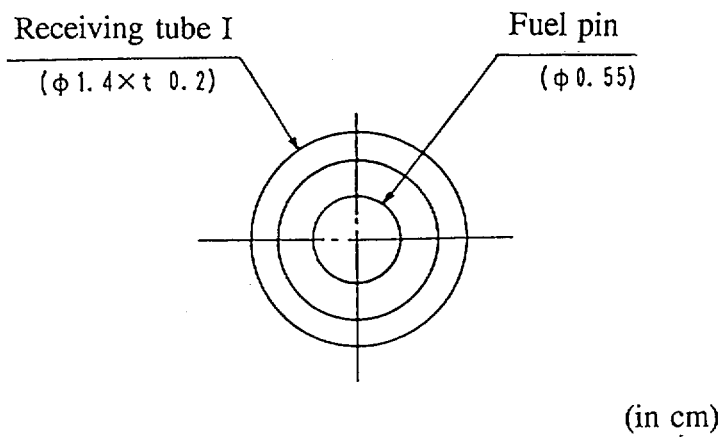


**Fig. (II)-B.24 Heat Transfer Model of Receiving Tube I**

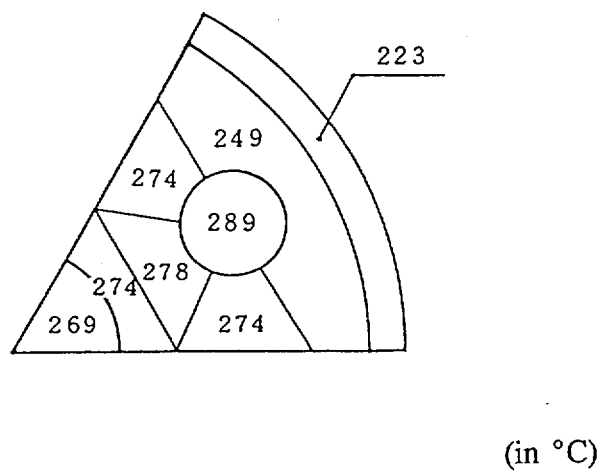


**Fig. (II)-B.25 Temperature Distribution in Inner Container Holding Receiving Tube I**

- L : Thickness of the air layer = 0.0025 m  
 k : Thermal conductivity of the air = 0.0406 kcal/h·m·°C  
       = 0.0472 W/m·K  
       (Inner insertion value at 340°C shown in Table (II)-B.16)  
 σ : Stefan-Boltzmann's constant = 4.88 × 10<sup>-8</sup> kcal/h·m<sup>2</sup>·K<sup>4</sup>  
 F : Overall form coefficient

$$F = \left\{ \frac{1}{\varepsilon_1} + \frac{a_1}{a_2} \left( \frac{1}{\varepsilon_2} - 1 \right) \right\}^{-1} = 0.28$$

- ε<sub>1</sub> : Emissivity of the fuel pin (stainless steel) = 0.37  
 ε<sub>2</sub> : Emissivity of receiving tube I (stainless steel) = 0.37  
 a<sub>1</sub> : Outer surface area of the fuel pin  
       a<sub>1</sub> = 0.0055 × π × 0.36 = 6.22 × 10<sup>-3</sup> m<sup>2</sup>  
 a<sub>2</sub> : Inner surface area of receiving tube I  
       a<sub>2</sub> = 0.0105 × π × 0.36 = 1.19 × 10<sup>-2</sup> m<sup>2</sup>

- t<sub>2</sub> : Temperature of receiving tube I = 289°C  
 t<sub>1</sub> : Temperature of the fuel pin

Therefore, the left side is given by

$$\frac{Q}{A} = 2960 \text{ kcal/h}\cdot\text{m}^2$$

Each constant is assigned to the right side to obtain "t<sub>1</sub>" that satisfies the expression below.

$$\begin{aligned}
 \frac{Q}{A} &= \frac{0.0406}{0.0025} \times (t_1 - 289) + 4.88 \times 10^{-8} \times 0.28 \times \{(t_1 + 273)^4 - 562^4\} \\
 &= 2960 \text{ kcal/h}\cdot\text{m}^2 \\
 \therefore t_1 &= 392^\circ\text{C}
 \end{aligned}$$

Table (II)-B.35 summarizes the above results.

### B.5.4 Maximum Internal Pressure

As in the case of the maximum internal pressure evaluated under normal test conditions, this subsection describes how to evaluate the internal pressure generated in the inner shell part of the outer container which constitutes the boundary of containment. Since the fuel supporting can and receiving tube also constitute the secondary boundary of containment, the maximum internal pressure generated at each part of the packaging is also evaluated.

As in subsection B.4.4, the internal pressure generated in the fuel supporting can or receiving tube is supposed to be generated by the expansion of gas resulting from the leakage of FP gas from the gas plenum part of the fuel pin and the ensuing rise of the temperature in the can.

The results of the structural evaluation indicate that fuel supporting cans I and II, and receiving tubes I and II maintain sufficient strength even under accident test conditions. Therefore, the internal pressure generated in the inner shell of the outer container is only the result of the expansion of gas due to the rise in the temperature of the inner shell. Each material is evaluated below.

(1) Internal pressure of the fuel supporting can

As in subsection B.4.4(1), if it is assumed that the FP gas stored in the gas plenum part of the 15 fuel pins is released to fuel supporting can I, the pressure of fuel supporting can I is given by the expression below.

$$P_A = P_O \times \frac{(V_c + V_{FP})}{V_c} \times \frac{T_A}{T_O}$$

$P_A$	: Maximum internal pressure	kPa
$P_O$	: Initial pressure = 1.0 kg/cm <sup>2</sup> abs.	= 100 kPa
$V_c$	: Gas receiving volume in fuel supporting can I	= 8840 cc
$V_{FP}$	: Volume of the FP gas	= 4404 cc
$T_A$	: Final temperature of the gas [See Table (II)-B.36.]	k
$T_O$	: Initial temperature of the gas = 20°C	= 293 K

$$\begin{aligned} P_A &= 1.0 \times \frac{(8840 + 4404)}{8840} \times \frac{T_A}{T_O} \\ &= 1.50 \times \frac{T_A}{T_O} \end{aligned}$$

The maximum internal pressure  $P_A$  in fuel supporting can I, in which Contents I are stored, is obtained based on the results mentioned above. Table (II)-B.36 lists the resulting information.

Table (II)-B.36 Maximum Internal Pressure under Accident Test Conditions<sup>\*3</sup>

Contents	Inner shell		Fuel supporting can I (receiving tube <sup>*1</sup> )	
	Maximum internal pressure	Gas temperature	Maximum internal pressure	Gas temperature
Contents I • eccentric	80 kPa (0.8 kg/cm <sup>2</sup> G)	228°C	230 kPa (2.3 kg/cm <sup>2</sup> G)	363°C
Contents I • eccentric <sup>*2</sup>	80 kPa (0.8 kg/cm <sup>2</sup> G)	228°C	230 kPa (2.3 kg/cm <sup>2</sup> G)	363°C
Contents I • center	70 kPa (0.7 kg/cm <sup>2</sup> G)	202°C	230 kPa (2.3 kg/cm <sup>2</sup> G)	366°C
Contents II	70 kPa (0.7 kg/cm <sup>2</sup> G)	193°C	660 kPa <sup>*1</sup> (6.6 kg/cm <sup>2</sup> G)	341°C <sup>*1</sup>

- \*1 For Contents II, the maximum internal pressure and gas temperature of receiving tube I rather than those of fuel supporting can I are indicated.
- \*2 This package indicates the thermal evaluation model used during a horizontal drop.
- \*3 Design pressure and material evaluation temperature used in the structural evaluation

Item	Design pressure	Evaluation temperature	Temperature evaluation result
Inner shell	200 kPa (2 kg/cm <sup>2</sup> G)	200°C	193°C
Fuel supporting can I	300 kPa (3 kg/cm <sup>2</sup> G)	400°C	332°C
Receiving tube I	700 kPa (7 kg/cm <sup>2</sup> G)	350°C	289°C

(2) Internal pressure of the receiving tube

As in subsection B.4.4(2), if it is assumed that the FP gas stored in the gas plenum part of the fuel pin is released to receiving tube I, the pressure in receiving tube I is given by the expression below in the same manner as in step (1).

$$P_A = P_O \times \frac{(V_{TG} + V_{FP})}{V_{TG}} \times \frac{T_A}{T_O}$$

$V_{TG}$	: Gas volume in receiving tube I	= 73 cc
$V_{FP}$	: FP gas volume under a pressure of one atmosphere	= 191 cc
$T_A$	: Final temperature of the gas [See Table (II)-B.36.]	K
$T_O$	: Initial temperature of the gas = 20°C	= 293 K

$$\begin{aligned} P_A &= 1.0 \times \frac{(73 + 191)}{73} \times \frac{T_A}{T_O} \\ &= 3.62 \times \frac{T_A}{T_O} \end{aligned}$$

The maximum internal pressure  $P_A$  in receiving tube I, in which Contents II are stored, is obtained based on the results mentioned above. Table (II)-B.36 lists the resulting information.

(3) Internal pressure of the outer container's inner shell

As described in the section dealing with the structural evaluation, the fuel supporting can and receiving tube maintain sufficient strength under accident test conditions and are not damaged. Therefore, the pressure generated in the inner shell is only the result of the thermal expansion of the air in the inner shell. The pressure in the inner shell is thus given by the expression below.

$$P_A = P_O \times \frac{T_A}{T_O}$$

$P_A$	: Maximum internal pressure	kPa
$P_O$	: Initial pressure = 1.0 kg/cm <sup>2</sup> abs.	= 100 kPa
$T_A$	: Final temperature of the gas [See Table (II)-B.36.]	K
$T_O$	: Initial temperature of the gas = 20°C	= 293 K

The maximum internal pressure  $P_A$  is obtained based on the results mentioned above. Table (II)-B.36 lists the resulting information.

As shown in Table (II)-B.36, no maximum internal pressure under accident test conditions exceeds the design pressure. The receiving tube, fuel supporting can, and inner shell remain sound. The maximum internal pressure of the packaging's inner shell is less than 700 kPa(7 kg/cm<sup>2</sup>G), which satisfies the applicable engineering criteria.

### B.5.5 Maximum Thermal Stress

Under accident test conditions, the outer shell of this packaging reaches a high temperature. Nevertheless in this case, the expansion of the resin layer and lead does not generate sufficient force to constrain the outer shell. However, the thermal stress caused by the temperature difference between the inner and outer shells may be a problem.

As evaluated in subsection A.6.3.2 of Chapter (II), the maximum thermal stress generated in this packaging results from the temperature difference between the inner and outer shells. When the elasticity and plasticity were evaluated by the calculation code, ANSYS, the maximum thermal stress on the inner shell was  $340 \text{ N/mm}^2$  ( $34.7 \text{ kg/mm}^2$ ), while the maximum thermal stress on the outer shell was  $113 \text{ N/mm}^2$  ( $11.6 \text{ kg/mm}^2$ ). These values did not exceed the relevant design criteria values of  $485 \text{ N/mm}^2$  ( $49.5 \text{ kg/mm}^2$ ) (material quality: SUS304, temperature:  $100^\circ\text{C}$ ) and  $254 \text{ N/mm}^2$  ( $26.0 \text{ kg/mm}^2$ ) (material quality: SUS304, temperature:  $700^\circ\text{C}$ ). Therefore, this packaging is not damaged by the resulting thermal stress, and remains sound.

### B.5.6 Summary and Evaluation of Results

The shock absorber is subject to cumulative deformation during drop tests I and II. This evaluation was performed on the assumption that the steel plate covering the balsa wood is penetrated by the impact on a mild steel bar during drop test II. However, such deformation is limited to the shock absorber and does not reach the outer container body. The evaluation results of the thermal test conducted immediately after the drop test are as follows:

The temperature change in every section of this package is as shown in Figs. (II)-B.8 through (II)-B.11. Tables (II)-B.6 and (II)-B.7 list the maximum temperatures for every section of the package, and the time required to reach this maximum after a fire starts.

Assume that Contents I are eccentrically stored in the packaging and that the shock absorber has become deformed as a result of a vertical drop. In this example, all the evaluation portions indicate the maximum temperature as compared with the other three cases.

As shown in Fig. (II)-B.8, the outer shell reaches the maximum temperature ( $656^\circ\text{C}$ ) 30 minutes after a fire starts. Therefore, the eight bismuth fusible plugs (which have a melting point of  $271^\circ\text{C}$ ) installed in the outer shell part of the outer container melt. The gas generated from the cement and resin layers is then released so that an excessive amount of gas does not accumulate in the outer shell part of the outer container.

Most of the heat entering from the outer shell is transferred through the heat dispersion fins (made of copper) to the cement layer, and is also transferred to the inside lead shield. The maximum temperature of the lead shield reaches  $193^\circ\text{C}$  after 1.5 hours. The maximum temperature of the lead shield is lower than the melting point ( $327^\circ\text{C}$ ) of lead. Therefore, the shielding performance does not deteriorate. The maximum temperature of the neutron shielding material resin reaches  $656^\circ\text{C}$  near the outer shell after 30 minutes. Therefore, the resin near the outer shell is partially carbonized (see subsection B.6.4 of the attached Appendix). In the shielding evaluation, the resin is thus ignored, while in the criticality analysis, to be on the safe side, the resin is replaced with water. The O-rings installed in the front and rear lid units rise slowly from the maximum temperature ( $75^\circ\text{C}$ ) under normal test conditions, and eventually reach a maximum temperature of  $125^\circ\text{C}$  eight hours after a fire starts. Since the maximum allowable service temperature of the O-rings does not exceed  $200^\circ\text{C}$ , the containment



performance is maintained.

The shock absorber steel plate that covers both ends of the package reaches 781°C 30 minutes after a fire starts. As in the outer shell of the outer container, ten bismuth fusible plugs are installed in each of the shock absorber steel plates (front and rear). The gas generated in the balsa wood is released by melting (melting point of 271°C), thereby preventing excessive pressure from being accumulated.

During a fire the balsa wood in the portion that was penetrated during drop test II burns. The temperature at that time is 797°C. However, as shown by the model test results described in subsection B.6.3, the fire is brought under natural control immediately after it starts because flame-resistance treated balsa wood is used. The temperature of the balsa wood then decreases gradually.

As shown in Table (II)-B.36, the maximum pressure inside the packaging is 80 kPa (0.8 kg/cm<sup>2</sup>G) for the inner shell part of the outer container. The FP gas of the fuel pin is evaluated, assuming that it leaks in the fuel supporting can or receiving tube. The maximum internal pressure of the fuel supporting can and receiving tube is 230 kPa (2.3 kg/cm<sup>2</sup>G) and 660 kPa (6.6 kg/cm<sup>2</sup>G), respectively. These maximum internal pressures do not exceed the design criteria pressure values of 300 kPa (3.0 kg/cm<sup>2</sup>G) and 700 kPa (7.0 kg/cm<sup>2</sup>G). They also do not exceed the maximum normal operating pressure value (700 kPa) (7.0 kg/cm<sup>2</sup>G) of the BU package.

The maximum thermal stress that occurs in the packaging is caused by the temperature difference between the inner and outer shells. This maximum thermal stress is 340 N/mm<sup>2</sup> (34.7 kg/mm<sup>2</sup>) for the inner shell, and 113 N/mm<sup>2</sup> (11.6 kg/mm<sup>2</sup>) for the outer shell. These values do not exceed the design criteria values of 485 N/mm<sup>2</sup> (49.5 kg/mm<sup>2</sup>) (material quality: SUS304, temperature: 100°C) and 254 N/mm<sup>2</sup> (26.0 kg/mm<sup>2</sup>) (material quality: SUS304, temperature: 700°C).

Therefore, the packaging is not damaged by such pressure and thermal stress.

The above-mentioned results therefore indicate that this packaging can withstand the high temperatures that may occur under accident test conditions, while, at the same time, retain has sufficient mechanical strength. The soundness of the packaging is thus maintained.

## B.6 Appendix

### B.6.1 TRUMP Input Data

This subsection describes each area's heat transfer coefficient from the inside to the outside of this package when Contents I and II are loaded.

#### B.6.1.1 Package holding Contents I

##### (1) Heat transfer between the fuel supporting can and inner container

This heat transfer is the result of the thermal conduction and radiation of air. For the thermal conduction, the thermal conductivity of air is used. For the radiation, the total form factor given by the expression below is used.

$$F = \left( \frac{1}{\epsilon_1} + \frac{1}{\epsilon_2} - 1 \right)^{-1}$$

where

F	:	Total form factor	
$\epsilon_1$	:	Emissivity of the fuel supporting can	= 0.37
$\epsilon_2$	:	Emissivity of the inner container	= 0.37

and thus

$$F = \left( \frac{1}{0.37} + \frac{1}{0.37} - 1 \right)^{-1} = 0.23$$

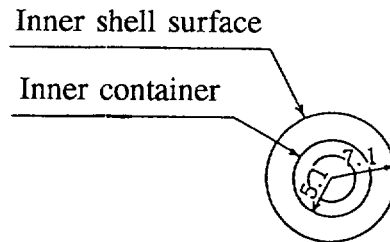
##### (2) Heat transfer between the inner container and inner shell

This heat transfer is the result of the thermal conduction and radiation of air. For the thermal conduction, the thermal conductivity of air is used. For the radiation, the total form factor given by the expression below is used.

$$F = \left\{ \frac{1}{\epsilon_I} + \frac{A_I}{A_o} \left( \frac{1}{\epsilon_o} - 1 \right) \right\}^{-1}$$

where

F	:	Total form factor	
$\epsilon_I$	:	Emissivity of the inner container	= 0.37
$\epsilon_o$	:	Emissivity of the inner shell	= 0.37
$A_I$	:	Heat transfer area of the inner container	= $2\pi \times 5.1 \times 1 \text{ cm}^2$
$A_o$	:	Heat transfer area of the inner shell	= $2\pi \times 7.1 \times 1 \text{ cm}^2$



and thus

$$F = \left\{ \frac{1}{0.37} + \frac{5.1}{7.1} \left( \frac{1}{0.37} - 1 \right) \right\}^{-1} = 0.25$$

(3) Heat transfer between the inner shell and lead shield

The lead contracts when it solidifies after casting and clamps the inner shell. There should be no gap between the inner shell and the lead, so it is assumed that there is no thermal resistance on the surface where the inner shell and lead contact each other.

(4) Heat transfer between the lead shield and cement layer

1) Under normal test conditions

To conduct an evaluation when the internal temperature is high and obtain evaluation results that are on the safe side, a gap (2 mm) is assumed to exist between the lead shield and cement layer. Therefore, the thermal conductivity of air is used.

2) Under accident test conditions

To be on the safe side, the temperature of the package during a fire is evaluated on the assumption that there is no thermal resistance between the lead shield and cement layer, since that provides severer conditions.

(5) Heat transfer between cement layer and heat dispersion fins

1) Under normal test conditions

It is assumed that there is no thermal resistance on the contact surface. As shown in Fig. (II)-B-App.1 (figure on the right), however, the heat transfer area on the contact surface per heat dispersion fin is assumed to be low when it is evaluated to be on the safe side. In other words, the area of the radial contact surface between the cement layer and heat dispersion fins is represented only by the plate thickness ( $L_2$ ) of the heat dispersion fins, while the other surface ( $L_1 - L_2$ ) is represented by the heat insulation surface. The heat transfer between the cement layer and heat dispersion fins is therefore assumed to take place in the above heat transfer area (plate thickness of the heat dispersion fins  $\times$  axial length  $\times$  number of fins).

2) Under accident test conditions

The evaluation under normal test conditions assumed the plate thickness ( $L_2$ ) of the heat dispersion fin to be the heat transfer area on the contact surface between the cement layer and the fins. Under accident test conditions, the whole length ( $L_1$ ) of the heat dispersion fin represents the heat transfer area, spreads as shown in Fig. (II)-B-App.1 (figure on the left). If the whole length ( $L_1$ ) transfers heat, the temperature of the package becomes high, and thus the evaluation results that are on the safe side will be obtained. This is also assumed in the calculations in subsection B.6.2.

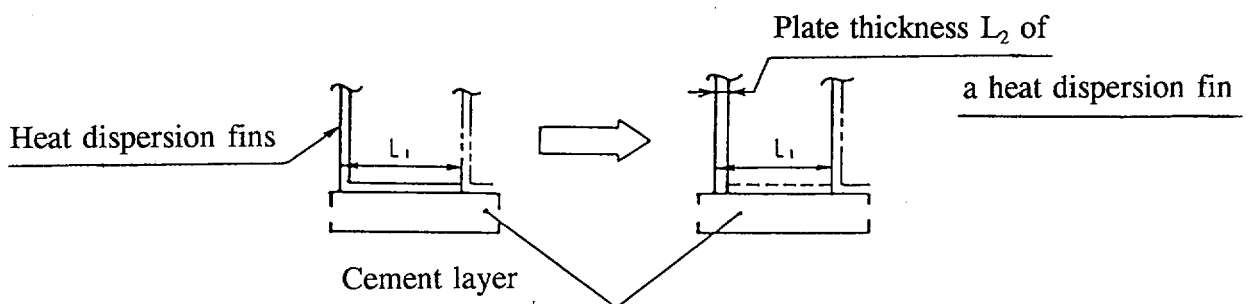


**Fig. (II)-B-App.1 Heat Transfer Model of the Cement Layer and Heat Dispersion Fins**

(6) Heat transfer between the heat dispersion fins and the resin layer

1) Under normal test conditions

The thermal conductivity of the heat dispersion fins (made of copper) is much higher than that of the resin. Almost all heat flows to the outer shell via the heat dispersion fins, whether or not there is the thermal resistance between the heat dispersion fins and resin layer. Therefore, it is assumed that there is no thermal resistance between these two sections.

2) Under accident test conditions

The resin layer of the outer shell is carbonized and a gap appears. If there is not such gap, the internal temperature of the packaging will rise. Therefore, it is assumed that there is no thermal resistance between the heat dispersion fins and resin layer.

(7) Heat transfer between the heat dispersion fins and the outer shell

The heat dispersion fins and the outer shell are welded together. Therefore, for the evaluations it is assumed that there is no thermal resistance between the heat dispersion fins and the outer shell.

(8) Cement layer and intermediate shell

1) Under normal test conditions

To assume a high internal temperature and obtain evaluation results that are on the safe side, a gap (2 mm) is assumed to exist between the cement layer and the intermediate shell. The heat transfer between these two parts takes place via the thermal conduction of air; therefore, the thermal conductivity value of air is used in the calculation.

2) Under accident test conditions

If there is no thermal resistance between the cement layer and the intermediate shell, the internal temperature of the packaging rises. Therefore, it is assumed that there is no thermal resistance between these parts.

(9) Heat transfer between the intermediate shell and the resin

For the same reason given in step (6)-1), it is assumed that there is no thermal resistance between the intermediate shell and the resin.

(10) Heat transfer between the lead shield and the tungsten

The tungsten is buried in the lead shield and is located along the axial direction of the packaging. In this package, a shock absorber, which has low thermal conduction in the axial direction, is installed. Therefore, there is hardly any heat flow in the axial direction. As a result, the presence of thermal resistance between the lead shield and the tungsten does not influence the temperature distribution of the packaging, and it is therefore assumed that such thermal resistance does not exist.

(11) Heat transfer by the air layer in the rotating plug

This portion is a closed layer, exhibiting only a slight temperature difference between the fluid and its ambient solid. Therefore, there is no convection. Heat transfer within the rotating plug can be represented by the thermal conduction of air, so the thermal conduction value of air is used in the calculation.

(12) Heat transfer between the outer shell and the surrounding environment

Heat transfer between the outer shell and the surrounding environment takes place through natural convection and radiation.

1) Heat transfer coefficient between the outer shell and the surrounding environment

This heat transfer coefficient is given as follows using the heat transfer expression<sup>1)</sup> of a horizontal cylinder transferred via natural convection:

$$H = 0.52 \times \frac{k}{L} \cdot \left( \frac{g \cdot \beta \cdot L^3 \cdot Pr \cdot \Delta t}{\nu^2} \right)^{1/4} \quad 10^4 \leq Gr \times Pr < 10^8$$

$$H = 0.126 \times k \cdot \left( \frac{g \cdot \beta \cdot Pr \cdot \Delta t}{\nu^2} \right)^{1/3} \quad 10^8 \leq Gr \times Pr$$

where

H	:	Heat transfer coefficient	kcal/h · m <sup>2</sup> · °C
k	:	Thermal conductivity	kcal/h · m · °C
g	:	Gravity acceleration	9.807 m/s <sup>2</sup>
β	:	Expansion ratio	1/°C
Δt	:	Temperature difference	°C
L	:	Diameter	0.8 m
ν	:	Coefficient of kinematic viscosity	m <sup>2</sup> /s
Pr	:	Prandtl number	-
Gr	:	Grashof number	-

If it is assumed that the air temperature is 0°C, the expression below will result.

$$\begin{aligned} k &= 5.75 \times 10^5 \text{ cal/s} \cdot \text{cm} \cdot ^\circ\text{C} = 2.07 \times 10^{-2} \text{ kcal/h} \cdot \text{m} \cdot ^\circ\text{C} \\ \beta &= 3.66 \times 10^{-3} \text{ } 1/^\circ\text{C} \\ Pr &= 0.72 \\ \nu &= 0.138 \text{ cm}^2/\text{s} = 0.138 \times 10^{-4} \text{ m}^2/\text{s} \\ g &= 9.807 \text{ m/s}^2 \\ L &= 0.8 \text{ m} \end{aligned}$$

Therefore, the heat transfer coefficient in  $10^4 \leq Gr \times Pr < 10^8$  is as follows:

$$\begin{aligned} H &= 1.228 \times \Delta t^{1/4} && \text{kcal/h} \cdot \text{m}^2 \cdot ^\circ\text{C} \\ &= 3.41 \times 10^{-5} \times \Delta t^{1/4} && \text{cal/s} \cdot \text{cm}^2 \cdot ^\circ\text{C} \\ &= 1.43 \times \Delta t^{1/4} && \text{W/m}^2 \cdot \text{K} \end{aligned}$$

---

1) Jacob, M., "Heat Transfer" Vol. I, John Wiley & Sons, Inc., New York, p525.

Table (II)-B-App.1 lists the heat transfer coefficients obtained at other temperatures besides 0°C. The heat transfer coefficients in  $10^8 \leq Gr \times Pr$  are also obtained in the same manner as mentioned above. Table (II)-B-App.1 lists the obtained heat transfer coefficients.

**Table (II)-B-App.1    Heat Transfer Coefficient between the Outer Shell and Surrounding Environment**

Temperature °C	Heat transfer coefficient    W/m <sup>2</sup> ·K (cal/s·cm <sup>2</sup> ·°C)	
	$10^8 \leq Gr \times Pr$	$10^4 \leq Gr \times Pr < 10^8$ *1
0	$1.56 \times \Delta t^{1/3}$ ( $3.72 \times 10^{-5} \times \Delta t^{1/3}$ )	$1.43 \times \Delta t^{1/4}$ ( $3.41 \times 10^{-5} \times \Delta t^{1/4}$ )
40	$1.43 \times \Delta t^{1/3}$ ( $3.42 \times 10^{-5} \times \Delta t^{1/3}$ )	$1.38 \times \Delta t^{1/4}$ ( $3.30 \times 10^{-5} \times \Delta t^{1/4}$ )
100	$1.27 \times \Delta t^{1/3}$ ( $3.03 \times 10^{-5} \times \Delta t^{1/3}$ )	$1.31 \times \Delta t^{1/4}$ ( $3.13 \times 10^{-5} \times \Delta t^{1/4}$ )
200	$1.09 \times \Delta t^{1/3}$ ( $2.60 \times 10^{-5} \times \Delta t^{1/3}$ )	$1.23 \times \Delta t^{1/4}$ ( $2.93 \times 10^{-5} \times \Delta t^{1/4}$ )
400	$0.86 \times \Delta t^{1/3}$ ( $2.05 \times 10^{-5} \times \Delta t^{1/3}$ )	$1.10 \times \Delta t^{1/4}$ ( $2.62 \times 10^{-5} \times \Delta t^{1/4}$ )
600	$0.72 \times \Delta t^{1/3}$ ( $1.71 \times 10^{-5} \times \Delta t^{1/3}$ )	$1.01 \times \Delta t^{1/4}$ ( $2.41 \times 10^{-5} \times \Delta t^{1/4}$ )
800	$0.63 \times \Delta t^{1/3}$ ( $1.50 \times 10^{-5} \times \Delta t^{1/3}$ )	$0.94 \times \Delta t^{1/4}$ ( $2.25 \times 10^{-5} \times \Delta t^{1/4}$ )

\*1    Used for evaluations during a fire.

- 2) Radiation  
The total form factor between the outer shell and the surrounding environment is given by the expression below.

$$F = \left( \frac{1}{\varepsilon_1} + \frac{1}{\varepsilon_2} - 1 \right)^{-1}$$

where

- F       :     Total form factor
- $\varepsilon_1$    :     Emissivity of the outer shell
- $\varepsilon_2$    :     Emissivity of the surrounding environment

In the expression mentioned above,  $\varepsilon_1$  and  $\varepsilon_2$  vary depending on existing conditions. Table (II)-B-App.2 lists each emissivity value, and the results calculated by the above expression.

**Table (II)-B-App.2    Total Form Factor between the Outer Shell and the surrounding Environment**

Item	During a fire	After a fire	Others
Emissivity of the outer shell ( $\varepsilon_1$ )	0.8	0.55	0.37
Emissivity of the ambient environment ( $\varepsilon_2$ )	0.9	1.0	1.0
Total form factor (F)	0.73	0.55	0.37

(13) Heat transfer between the shock absorber’s vertical plane and the surrounding environment

The heat transfer between the shock absorber’s vertical plane and the surrounding environment takes place via natural convection and radiation.

1) Heat transfer coefficient between the shock absorber’s vertical plane and the surrounding environment

This heat transfer coefficient is derived from the heat transfer expression<sup>1)</sup> for a vertical plane in which heat is transferred via natural convection:

$$H = 0.59 \times \frac{k}{L} \cdot \left( \frac{g \cdot \beta \cdot L^3 \cdot Pr \cdot \Delta t}{\nu^2} \right)^{1/4} \qquad 10^4 < Gr \times Pr < 10^9$$

where

H	:	Heat transfer coefficient	kcal/h · m <sup>2</sup> · °C
k	:	Thermal conductivity	kcal/h · m · °C
g	:	Gravity acceleration	9.807 m/s <sup>2</sup>
β	:	Expansion ratio	1/°C
Δt	:	Temperature difference	°C
L	:	Height of the vertical plane	0.4 m
ν	:	Coefficient of kinematic viscosity	m <sup>2</sup> /s
Pr	:	Prandtl number	-
Gr	:	Grashof number	-

In the expression mentioned above, k, β, ν, and Pr are the physical property values of air, and they vary depending on the temperatures involved. Using the values shown in Table (II)-B.16, the heat transfer coefficient at each temperature can be calculated. Table (II)-B-App.3 lists the calculated results.

1) W. H. McAdams, "Heat Transmission" Third Edition, McGraw Hill Book Company, Inc., New York, p172, 1954.

**Table (II)-B-App.3    Heat Transfer Coefficient between the Shock Absorber's Vertical Plane and the Surrounding Environment**

Temperature °C	Heat transfer coefficient    W/m <sup>2</sup> ·K (cal/s·cm <sup>2</sup> ·°C)
0	$1.67 \times \Delta t^{1/4}$ $(4.00 \times 10^{-5} \times \Delta t^{1/4})$
40	$1.62 \times \Delta t^{1/4}$ $(3.88 \times 10^{-5} \times \Delta t^{1/4})$
100	$1.54 \times \Delta t^{1/4}$ $(3.67 \times 10^{-5} \times \Delta t^{1/4})$
200	$1.44 \times \Delta t^{1/4}$ $(3.44 \times 10^{-5} \times \Delta t^{1/4})$
400	$1.29 \times \Delta t^{1/4}$ $(3.07 \times 10^{-5} \times \Delta t^{1/4})$
600	$1.18 \times \Delta t^{1/4}$ $(2.83 \times 10^{-5} \times \Delta t^{1/4})$
800	$1.11 \times \Delta t^{1/4}$ $(2.64 \times 10^{-5} \times \Delta t^{1/4})$

2) Radiation

The total form factor between the shock absorber's vertical plane and the surrounding environment is given by the expression below.

$$F = \left( \frac{1}{\varepsilon_1} + \frac{1}{\varepsilon_2} - 1 \right)^{-1}$$

where

- F       :     Total form factor
- $\varepsilon_1$    :     Emissivity of the shock absorber's vertical plane
- $\varepsilon_2$    :     Emissivity of the surrounding environment

In the expression mentioned above,  $\varepsilon_1$  and  $\varepsilon_2$  vary depending on the conditions. With these values, the total form factor (F) can be calculated by using the above expression. Since values  $\varepsilon_1$  and  $\varepsilon_2$  in the above expression are the same as in (12), "Heat Transfer between the Outer Shell and the Surrounding Environment", the total form factors shown in Table (II)-B-App.2 can be used.



- (14) Heat transfer between the shock absorber's horizontal plane and the surrounding environment

Heat is transferred between the shock absorber's horizontal plane and the surrounding environment via natural convection and radiation.

- 1) Heat transfer coefficient between the shock absorber's horizontal plane and the surrounding environment

This heat transfer coefficient is derived from the heat transfer expression<sup>1)</sup> for a horizontal cylinder in which heat is transferred via natural convection:

$$H = 0.52 \times \frac{k}{L} \cdot \left( \frac{g \cdot \beta \cdot L^3 \cdot Pr \cdot \Delta t}{\nu^2} \right)^{1/4} \quad 10^4 \leq Gr \times Pr < 10^8$$

$$H = 0.126 \times k \cdot \left( \frac{g \cdot \beta \cdot Pr \cdot \Delta t}{\nu^2} \right)^{1/3} \quad 10^8 \leq Gr \times Pr$$

where

H	:	Heat transfer coefficient	kcal/h · m <sup>2</sup> · °C
k	:	Thermal conductivity	kcal/h · m · °C
g	:	Gravity acceleration	9.807 m/s <sup>2</sup>
β	:	Expansion ratio	1/°C
Δt	:	Temperature difference	°C
L	:	Diameter	1.4 m
ν	:	Coefficient of kinematic viscosity	m <sup>2</sup> /s
Pr	:	Prandtl number	-
Gr	:	Grashof number	-

In the expression mentioned above, k, β, ν, and Pr are the physical property values of air, and they vary depending on the temperature. Using the values shown in Table (II)-B.16, the heat transfer coefficient at each temperature can be calculated. Table (II)-B-App.4 lists the calculated results.

---

1) Jakob, M., "Heat Transfer" Vol. I, John Wiley & Sons, Inc., New York, p525

**Table (II)-B-App.4    Heat Transfer Coefficient between the Shock Absorber’s Horizontal Plane and the Surrounding Environment**

Temperature °C	Heat transfer coefficient    W/m <sup>2</sup> ·K (cal/s·cm <sup>2</sup> ·°C)	
	10 <sup>8</sup> ≤ Gr × Pr	10 <sup>4</sup> ≤ Gr × Pr < 10 <sup>8</sup> *1
0	1.56 × Δt <sup>1/3</sup> (3.72 × 10 <sup>-5</sup> × Δt <sup>1/3</sup> )	1.24 × Δt <sup>1/4</sup> (2.96 × 10 <sup>-5</sup> × Δt <sup>1/4</sup> )
40	1.43 × Δt <sup>1/3</sup> (3.42 × 10 <sup>-5</sup> × Δt <sup>1/3</sup> )	1.20 × Δt <sup>1/4</sup> (2.87 × 10 <sup>-5</sup> × Δt <sup>1/4</sup> )
100	1.27 × Δt <sup>1/3</sup> (3.03 × 10 <sup>-5</sup> × Δt <sup>1/3</sup> )	1.14 × Δt <sup>1/4</sup> (2.72 × 10 <sup>-5</sup> × Δt <sup>1/4</sup> )
200	1.09 × Δt <sup>1/3</sup> (2.60 × 10 <sup>-5</sup> × Δt <sup>1/3</sup> )	1.07 × Δt <sup>1/4</sup> (2.55 × 10 <sup>-5</sup> × Δt <sup>1/4</sup> )
400	0.86 × Δt <sup>1/3</sup> (2.05 × 10 <sup>-5</sup> × Δt <sup>1/3</sup> )	0.95 × Δt <sup>1/4</sup> (2.28 × 10 <sup>-5</sup> × Δt <sup>1/4</sup> )
600	0.72 × Δt <sup>1/3</sup> (1.71 × 10 <sup>-5</sup> × Δt <sup>1/3</sup> )	0.88 × Δt <sup>1/4</sup> (2.10 × 10 <sup>-5</sup> × Δt <sup>1/4</sup> )
800	0.63 × Δt <sup>1/3</sup> (1.50 × 10 <sup>-5</sup> × Δt <sup>1/3</sup> )	0.82 × Δt <sup>1/4</sup> (1.96 × 10 <sup>-5</sup> × Δt <sup>1/4</sup> )

\*1 Used for evaluations during a fire.

2) Radiation

The total form factor between the shock absorber’s horizontal plane and the surrounding environment is given by the expression below.

$$F = \left( \frac{1}{\varepsilon_1} + \frac{1}{\varepsilon_2} - 1 \right)^{-1}$$

where

- F       :     Total form factor
- ε<sub>1</sub>     :     Emissivity of the shock absorber’s horizontal plane
- ε<sub>2</sub>     :     Emissivity of the ambient environment

In the expression mentioned above, ε<sub>1</sub> and ε<sub>2</sub> vary depending on existing conditions. With these values, the total form factor (F) can be calculated by using the above expression. Since values ε<sub>1</sub> and ε<sub>2</sub> in the above expression are the same as in (12), "Heat Transfer between the Outer Shell and the Surrounding Environment," the total form factors shown in Table (II)-B-App.2 are used.

(15) Heat transfer between the part (hole) of the shock absorber damaged during drop test II (vertical drop) and the surrounding environment

The damaged part discussed here is assumed to be located in the position indicated in Fig.(II)-B-App.2 and heat is transferred via the thermal conduction and radiation of air. In this case, the thermal conductivity value of air and the total form factor are used.

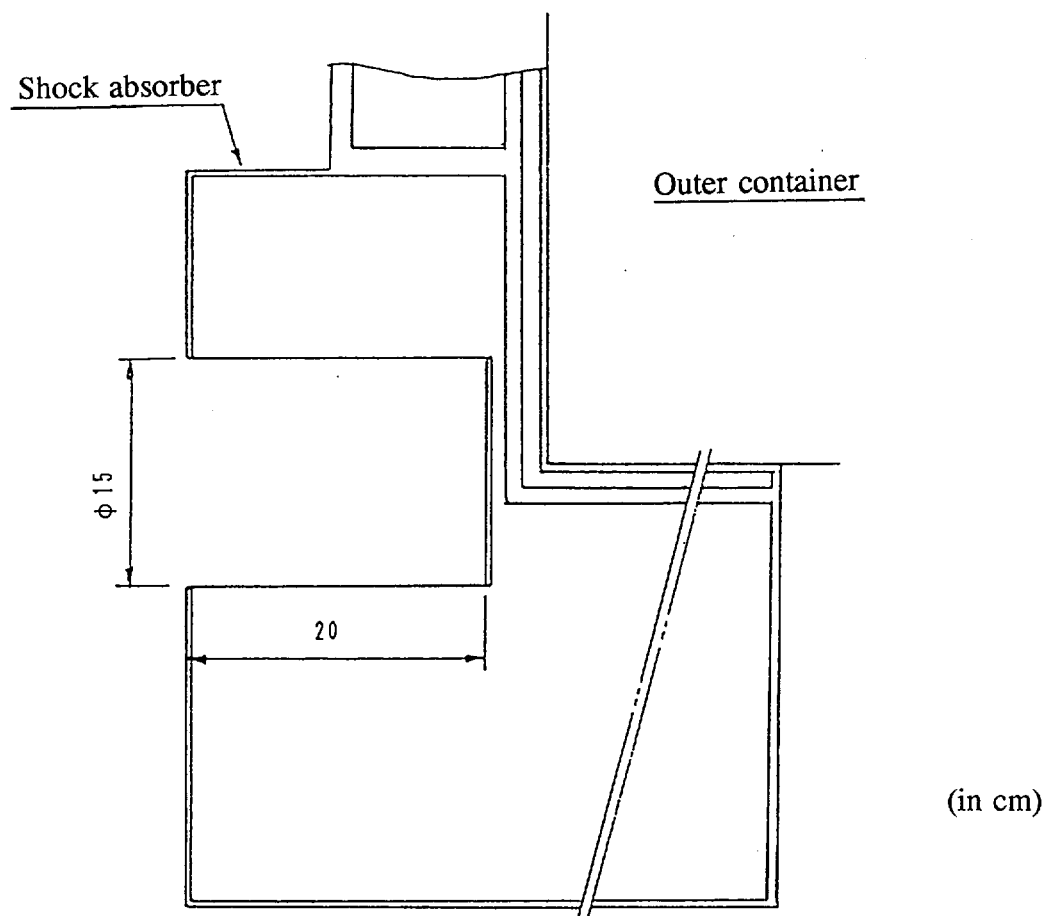


**Fig. (II)-B-App.2 Shape of the Shock Absorber Damaged during Drop Test II**

The radiation that passes between the damaged part of the shock absorber and the surrounding environment is assumed to be as shown in Fig. (II)-B-App.3. The form factors in each case are first obtained, and thereafter each total form factor is calculated.

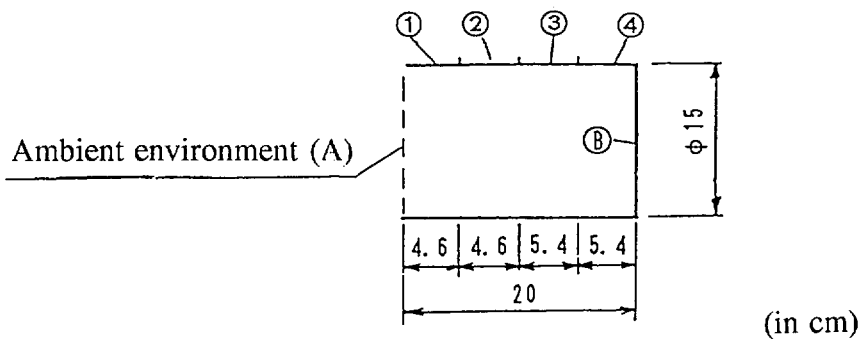


**Fig. (II)-B-App.3 Form Factor Model**

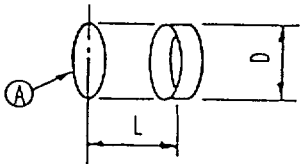
The form factor is calculated by using the expression<sup>1)</sup> below.

$$f_{iA} = \frac{X^2 + \frac{1}{2}}{\sqrt{X^2 + 1}} - X \qquad , \qquad X = \frac{L}{D}$$

where

- $f_{iA}$  : Form factors ( $f_{1A}$ ,  $f_{2A}$ ,  $f_{3A}$ , and  $f_{4A}$ )
- $D$  : Diameter = 15 cm
- $L$  : Length

- $L_{1A} = 2.3$  cm
- $L_{2A} = 6.9$  cm
- $L_{3A} = 11.9$  cm
- $L_{4A} = 17.3$  cm



1) R. Siegel. etal., "Thermal Radiation Heat Transfer", McGraw-Hill Book Company, Inc., New York.

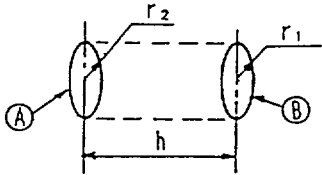
If each constant is assigned to the above expression and calculations are carried out, the values given below will be obtained.

$$\begin{aligned} f_{1A} &= 0.3641 \\ f_{2A} &= 0.1865 \\ f_{3A} &= 0.0914 \\ f_{4A} &= 0.0456 \end{aligned}$$

The remaining form factors are calculated by the expression<sup>1)</sup> below.

$$f_{BA} = \frac{1}{2} \left\{ Y - \sqrt{Y^2 - 4 \left( \frac{R_1}{R_2} \right)^2} \right\}$$

$$Y = 1 + \frac{1 + R_2^2}{R_1^2}, \quad R_1 = \frac{r_1}{h}, \quad R_2 = \frac{r_2}{h}$$



where

$f_{BA}$	:	Form factor	
$h$	:	Inter-surface distance	= 20 cm
$r_1$	:	Radius	= 7.5 cm
$r_2$	:	Radius	= 7.5 cm

If each constant is assigned to the above expression and calculations are carried out, the value below will be obtained.

$$f_{BA} = 0.1111$$

Using the form factors given above, each total form factor can be obtained by the expression below.

$$F = \left( \frac{1}{\epsilon_1} + \frac{1}{\epsilon_2} - 1 \right)^{-1} \times f_{NM}$$

where

$F$	:	Total form factors ( $F_{1A}$ , $F_{2A}$ , $F_{3A}$ , $F_{4A}$ , and $F_{BA}$ )
$f_{NM}$	:	Form factors ( $f_{1A}$ , $f_{2A}$ , $f_{3A}$ , $f_{4A}$ , and $f_{BA}$ )
$\epsilon_1$	:	Emissivity on the shock absorber surface
$\epsilon_2$	:	Emissivity of the ambient environment

---

1) R. Siegel. etal., "Thermal Radiation Heat Transfer", McGraw-Hill Book Company, Inc., New York

Item	During a fire	After a fire
Steel plate ( $\varepsilon_1$ )	0.8	0.79
Balsa wood ( $\varepsilon_1$ )	0.8	0.95 <sup>1)</sup>
Ambient environment ( $\varepsilon_2$ )	0.9	1.0

Each constant is assigned to the above expression. Table (II)-B-App.5 lists the obtained values.

**Table (II)-B-App.5    Total Form Factor between the Damaged Part Surface and the Surrounding Environment**

Position	During a fire	After a fire
$F_{1A}$	0.268	0.346
$F_{2A}$	0.137	0.177
$F_{3A}$	0.067	0.087
$F_{4A}$	0.034	0.043
$F_{BA}$	0.082	0.061

---

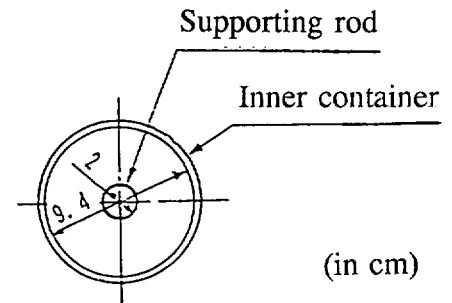
1) W.H. McAdams, "Heat Transmission" Third Edition, McGraw-Hill Book Company, Inc., New York, p477, 1954

### B.6.1.2 Package into which Contents II are loaded

#### (1) Heat transfer between the supporting rod and the inner container

Heat is transferred between the supporting rod and the inner container via the thermal conduction and radiation of air. To calculate the thermal conduction, the thermal conductivity of air is used. To calculate the radiation, the total form factor given by the expression below is used.

$$F = \left\{ \frac{1}{\varepsilon_I} + \frac{A_I}{A_o} \left( \frac{1}{\varepsilon_o} - 1 \right) \right\}^{-1}$$



where

F : Total form factor

$\varepsilon_I$  : Emissivity of the supporting rod = 0.37

$\varepsilon_o$  : Emissivity of the inner container = 0.37

$A_I$  : Heat transfer area of the supporting rod =  $\pi \times 2.0 \times 1 \text{ cm}^2$

$A_o$  : Heat transfer area of the inner container =  $\pi \times 9.4 \times 1 \text{ cm}^2$

and thus

$$F = \left\{ \frac{1}{0.37} + \frac{2.0}{9.4} \left( \frac{1}{0.37} - 1 \right) \right\}^{-1} = 0.32$$

#### (2) Heat transfer between the parts outside the inner container

The heat transfer in this case is the same as for the package into which Contents I are loaded. Since each value is given in subsections B.6.1.1(2) through B.6.1.1(15), further discussion is omitted here.

#### (3) Total form factor in the inner container

The total form factor between the nodes shown in Fig. (II)-B-App.4 is given by the expression<sup>1)</sup> below.

$$F_{i-j} = \left\{ \frac{1}{f_{i-j}} + \left( \frac{1}{\varepsilon_i} - 1 \right) + \frac{A_i}{A_j} \left( \frac{1}{\varepsilon_j} - 1 \right) \right\}^{-1}$$

where

$F_{i-j}$  : Total form factor

$\varepsilon_i, \varepsilon_j$  : Emissivity of nodes i and j (both stainless steel) = 0.37

1) W.H. McAdams, "Heat Transmission" Third Edition, McGraw Hill Book Company, Inc., New York, p76, 1954.

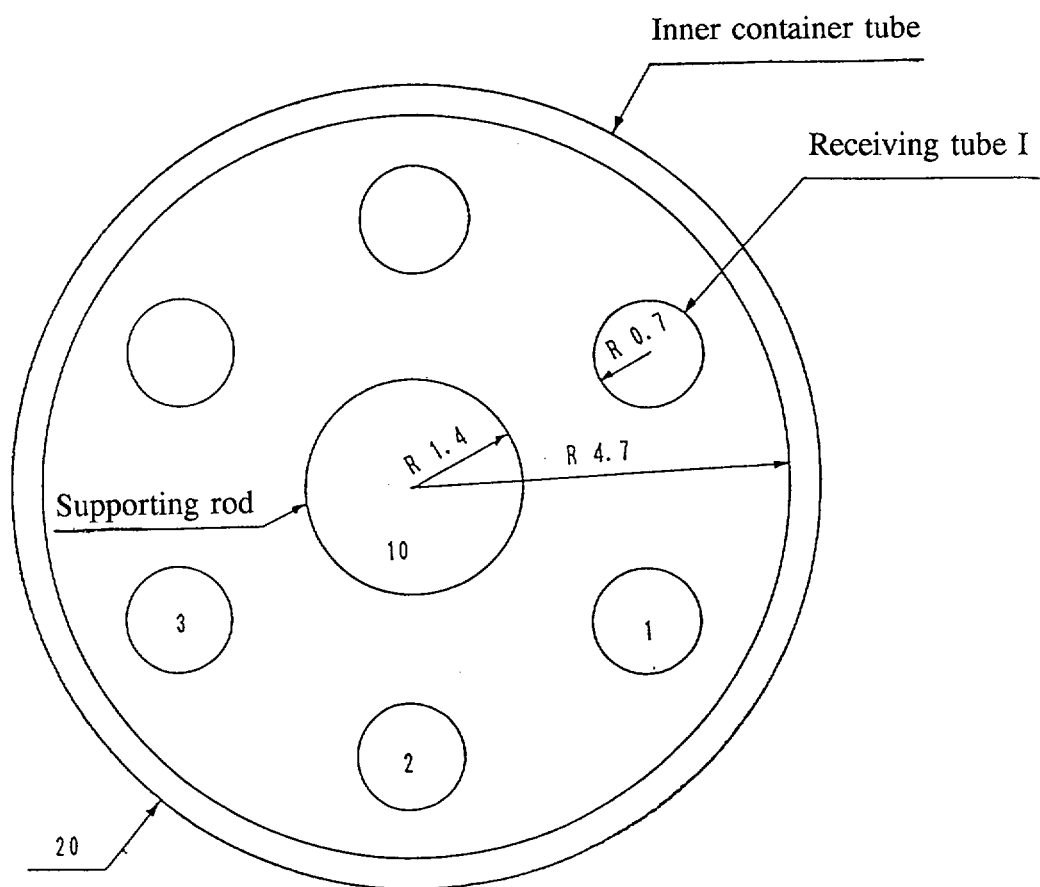


**Fig. (II)-B-App.4 Cross-sectional View of the Inner Container Holding Contents II**



$A_i, A_j$ : Surface area of node i and surface area of node j  
 $A_1 = A_2 = A_3 = 2\pi \times 0.7 \times 1 \text{ cm}^2$   
 $A_{10} = 2\pi \times 1.4 \times 1 \text{ cm}^2$   
 $A_{20} = 2\pi \times 4.7 \times 1 \text{ cm}^2$   
 $f_{i-j}$  : Form factor

Assigning the nodes shown in Fig. (II)-B-App.4 to the form factor ( $f_{i-j}$ ) gives the following five types of form factors ( $f_{1-2}$ ,  $f_{1-3}$ ,  $f_{1-10}$ ,  $f_{1-20}$ , and  $f_{10-20}$ ) by using the expression<sup>1)</sup> below. Fig. (II)-B-App.5 shows the relations between the nodes shown in Fig. (II)-B-App.4.

$$f_{1-2} = \frac{1}{2 \times 2\pi \cdot r_1} \int_{-\phi^1}^{\phi^1} (2r_1 - d \cdot \sin\phi) d\phi$$

$$\begin{aligned}
 f_{1-3} = \frac{1}{2 \times 2\pi \cdot r_1} & \left[ \int_{\phi^2}^{\phi^3} \left\{ 2r_1 + d \cdot \sin\phi - d \cdot \cos\left(\frac{\pi}{6} + \phi\right) \right\} d\phi \right. \\
 & + \int_{\phi^3}^{\pi/6} (r_1 + d \cdot \sin\phi - r_2) d\phi \\
 & + \int_{\pi/6}^{\phi^4} \left\{ r_1 + d \cdot \sin\left(\frac{\pi}{3} - \phi\right) - r_2 \right\} d\phi \\
 & \left. + \int_{\phi^4}^{\phi^5} \left\{ 2r_1 + d \cdot \cos\left(\frac{\pi}{6} + \phi\right) - d \cdot \sin\phi - r_2 \right\} d\phi \right]
 \end{aligned}$$

$$f_{1-10} = \frac{1}{2 \times 2\pi \cdot r_1} \int_{-\phi^6}^{\phi^6} (r_1 + r_2 - d \cdot \sin\phi) d\phi$$

where

$r_1$  : Radius of receiving tube I = 0.7 cm  
 $r_2$  : Radius of the supporting rod = 1.4 cm  
 $d$  : Center pitch between receiving tube I and the supporting bar = 3.5 cm

---

1) Kiyoharu Abe, "Application of Orthography to the Angle Factor Calculation in Radiation Problems", JAERI-M5486, 1973

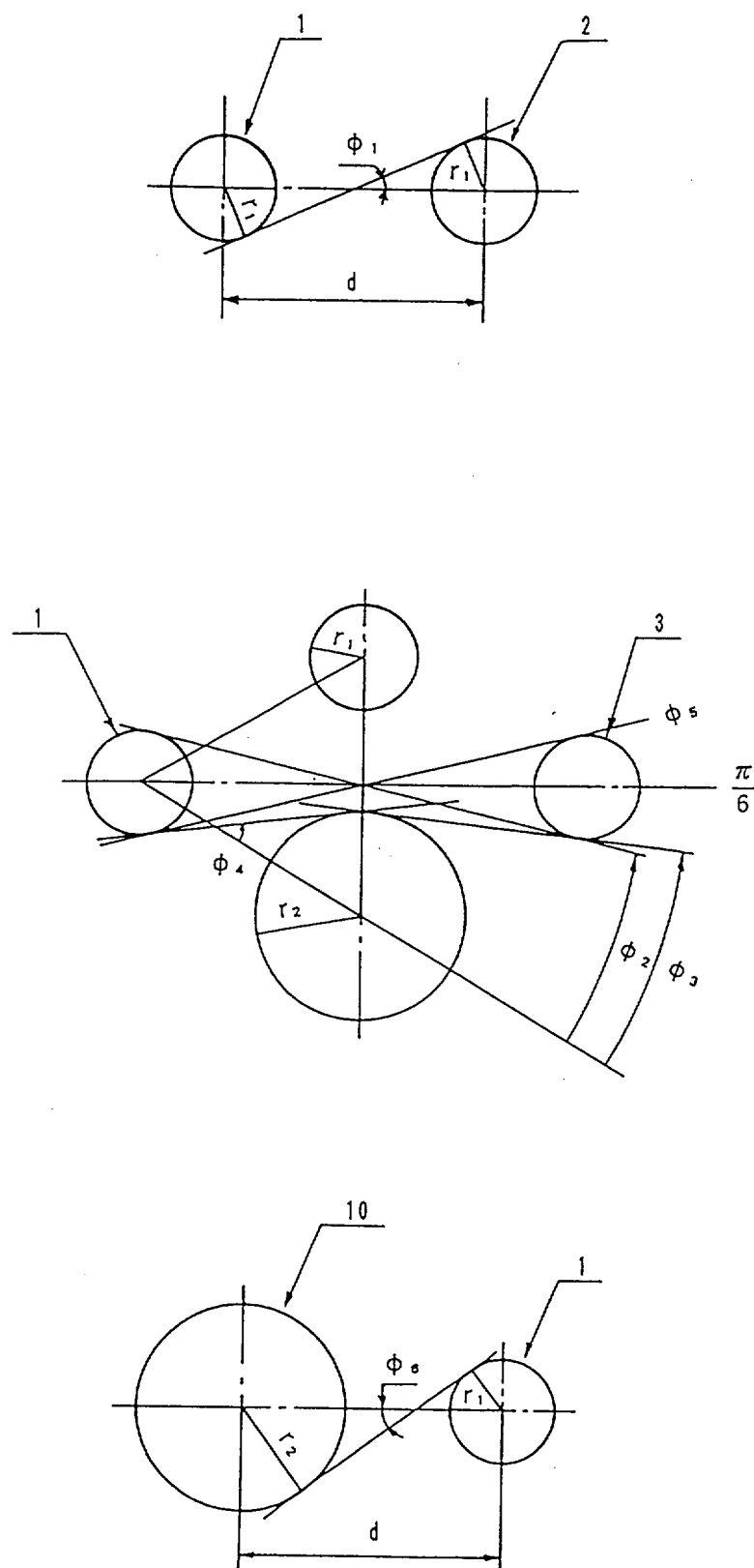


**Fig. (II)-B-App.5 Correlation between Receiving Tube I and Supporting Rod**

$\phi$  : Angle of the integration range, Radian

$$\phi_1 = \sin^{-1} \left( \frac{2r_1}{d} \right) = 0.4115$$

$$\phi_2 = \frac{\pi}{6} - \sin^{-1} \left( \frac{2r_1}{\sqrt{3} \cdot d} \right) = 0.2906$$

$$\phi_3 = \frac{\pi}{3} - \sin^{-1} \left( \frac{r_1 + r_2}{d} \right) = 0.4037$$

$$\phi_4 = \sin^{-1} \left( \frac{r_1 + r_2}{d} \right) = 0.6435$$

$$\phi_5 = \frac{\pi}{6} + \sin^{-1} \left( \frac{2r_1}{\sqrt{3} \cdot d} \right) = 0.7566$$

$$\phi_6 = \sin^{-1} \left( \frac{r_1 + r_2}{d} \right) = 0.6435$$

If each constant is assigned to the above expression, the values below are obtained.

$f_{1-2} = 0.06455$   
 $f_{1-3} = 0.03222$   
 $f_{1-10} = 0.14809$

Based on the correlation ( $A_i \cdot f_{i,j} = A_j \cdot f_{j,i}$ ) of the form factors, the expression below results.

$$f_{10-1} = \frac{A_1}{A_{10}} \times f_{1-10} = \frac{0.7}{1.4} \times 0.14809 = 0.07405$$

Given the definition  $\sum_{j=1}^n f_{i,j} = 1$  of the form factor, the expression below results.

$f_{1-20} = 1 - (2 \cdot f_{1-2} + 2 \cdot f_{1-3} + f_{1-10}) = 0.65837$   
 $f_{10-20} = 1 - 6 \cdot f_{10-1} = 0.55573$

These values are assigned to the expression that gives the total form factor mentioned above. Table (II)-B-App.6 lists the obtained results.

**Table (II)-B-App.6 Total Form Factor of the Inner Container**

$F_{1-2}$	0.0529
$F_{1-3}$	0.0290
$F_{1-10}$	0.1074
$F_{1-20}$	0.2877
$F_{10-20}$	0.2494

## B.6.2 Modeling of the Heat Dispersion Fins

### B.6.2.1 Outline

It is difficult to recreate all sixty heat dispersion fins in the circumferential direction because the number of meshes to be divided is limited. Therefore, the model obtained when a heat dispersion fin is recreated and the model resulting when several heat dispersion fins are combined into one are calculated under the same conditions, and the temperature in the corresponding position of each model is compared to confirm that such an evaluation can be performed using the models obtained when several heat dispersion fins are combined. The modeling of the heat dispersion fins is used to evaluate the actual packaging.

### B.6.2.2 Analysis model and calculation conditions

#### (1) Analysis model

Sixty heat dispersion fins are installed in the center of the packaging in the circumferential direction. A resin with a low thermal conductivity is filled around the heat dispersion fins. Therefore, most of the heat in the heat dispersion fin part flows in the radial direction. A cross-section model (two-dimensional model) at the center of this packaging, which exhibits a heat transfer state in the radial direction is used for the calculation. Based on the above results, the model ( $\theta = 6^\circ$ ) obtained when a heat dispersion fin is imitated and the model ( $\theta = 60^\circ$ ) obtained when ten heat dispersion fins combined into one were used. As shown in Fig. (II)-B-App.6, these models are two-dimensional and have a width of 10 cm in the axial direction of the packaging.

#### (2) Analysis conditions

As described in the above item, (1) "Analysis model," this analysis model is a cross-section model of this packaging, so the thermal properties of component materials use the values in Tables (II)-B.10 through (II)-B.18 described in section B.2. The heat transfer between the outer shell and the surrounding environment uses the values in Tables (II)-B-App.1 and (II)-B-App.2 described in subsection B.6.1 because such transfer takes place via natural convection and radiation. Moreover, to obtain the heat flow in the heat dispersion fin part during a fire, the thermal conditions under accident test conditions (Table (II)-B.33) are used as the thermal conditions for the calculation.

### B.6.2.3 Results

Fig. (II)-B-App.7 shows the results that were calculated by the analysis model under the calculation conditions mentioned above. As shown in Fig. (II)-B-App.7, the temperature at each part of the model obtained when several heat dispersion fins are combined into one has proved to be almost the same as each temperature in the corresponding parts (the outer shell, dispersion heat fins, and cement layer) of the model when a heat dispersion fin is recreated. This justifies the models of the heat dispersion fins.

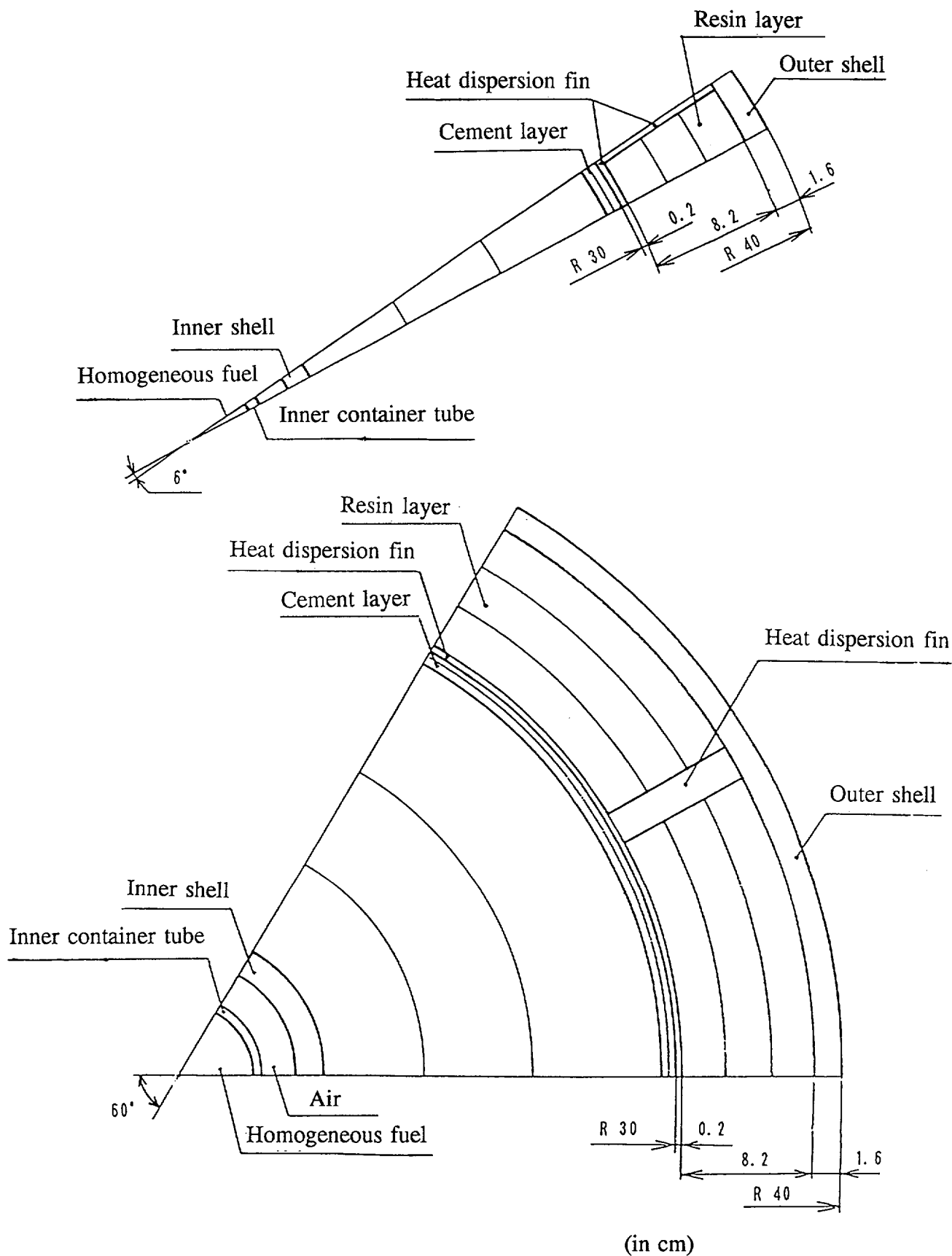


**Fig. (II)-B-App.6 Heat Transfer Model of Heat Dispersion Fin**

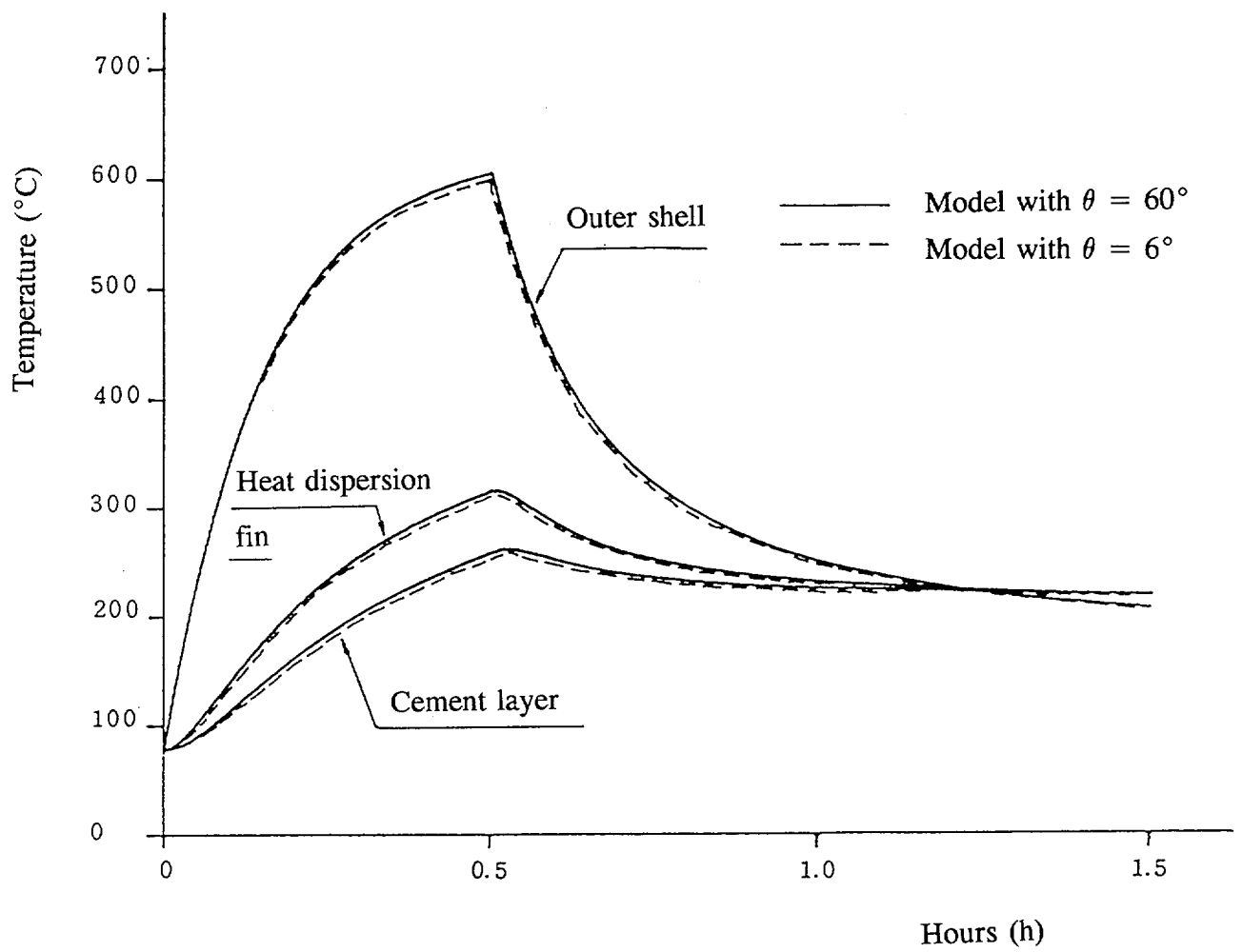


**Fig. (II)-B-App.7 Change in Temperature under Accident Test Conditions  
(Heat dispersion fin)**

## B.6.3 Thermal Test and Evaluation of the Shock Absorber Model

### B.6.3.1 Outline

This evaluation is performed under the same thermal conditions (shock absorber model shape, surrounding temperature etc.) as those for the thermal test of the shock absorber model, using the TRUMP code. The results of the test and the evaluation are then compared to justify the application of the physical properties of the wood used for the analysis of the actual packaging and to confirm the validity of the conditions used for its calculation.

### B.6.3.2 Shock absorber model

The test model used for the thermal test is a circumscribed rectangular solid measuring  $60 \times 60 \times 100$  cm, whose outer surface is covered by a carbon steel plate. Two holes (15 in diameter  $\times$  20 cm in depth) such as the one that appears during drop test II are made in the test model, and a damaged steel plate is fixed to the bottom of these holes. Asbestos measuring about 5 cm is attached to the center of the test model to prevent the temperature from affecting the balsa wood. A thermocouple is then installed along the center line (passing through the center of the two holes) of the test model so that the temperature of each section can be measured.

### B.6.3.3 Analysis model and calculation conditions

#### (1) Analysis model

The cross section of a test model is a square of  $60 \times 60$  cm. As shown in Fig. (II)-B-App.8, however, the analysis model is a column of 34 cm in radius whose surface area (heat transfer area between the surrounding environment and the shock absorber model) and cubic volume are equivalent. The damaged hole is 15 in diameter  $\times$  20 cm in depth, and is divided into nodes as shown in Fig. (II)-B-App.8.

#### (2) Calculation conditions

##### 1) Environmental conditions

For comparison with the results of a thermal test, a calculation is performed under the same conditions as those of the thermal test. Tables (II)-B-App.7 and (II)-B-App.8 list the conditions in this case. Since the thermal test was conducted using an indoor annealing furnace, the influence of solar heat is not considered. For parts other than the damaged parts, the heat transfer between the test model and surrounding environment uses the values shown in Tables (II)-B-App.2 through (II)-B-App.4. In the case of the damaged parts the heat transfer between the test model and the surrounding environment uses the values shown in Table (II)-B-App.5.

##### 2) Physical properties

Thermal conductivity differs depending on whether it is going with or against the grain of the wood. Thermal conductivity in the direction of the grain of the wood is higher than that in the direction against the grain of the wood. In this case, the value of the thermal conductivity in the direction of the grain is used so that the maximum amount of heat that may enter during a fire can be evaluated. Specific heat does not change so much before carbonization, so it is set as a constant (0.55). Specific heat is set as  $0.25^{1)2)}$  after carbonization is completed.

- 
- 1) "Dennetsu Kougaku Shiryo" Third Edition, The Japan Society of Mechanical Engineers, page 297
  - 2) E.R.G. Eckert, "Introduction to the Transfer of Heat and Mass "First Edition, McGraw-Hill Book Company, New York, p270, 1950

(II)-B-App-23

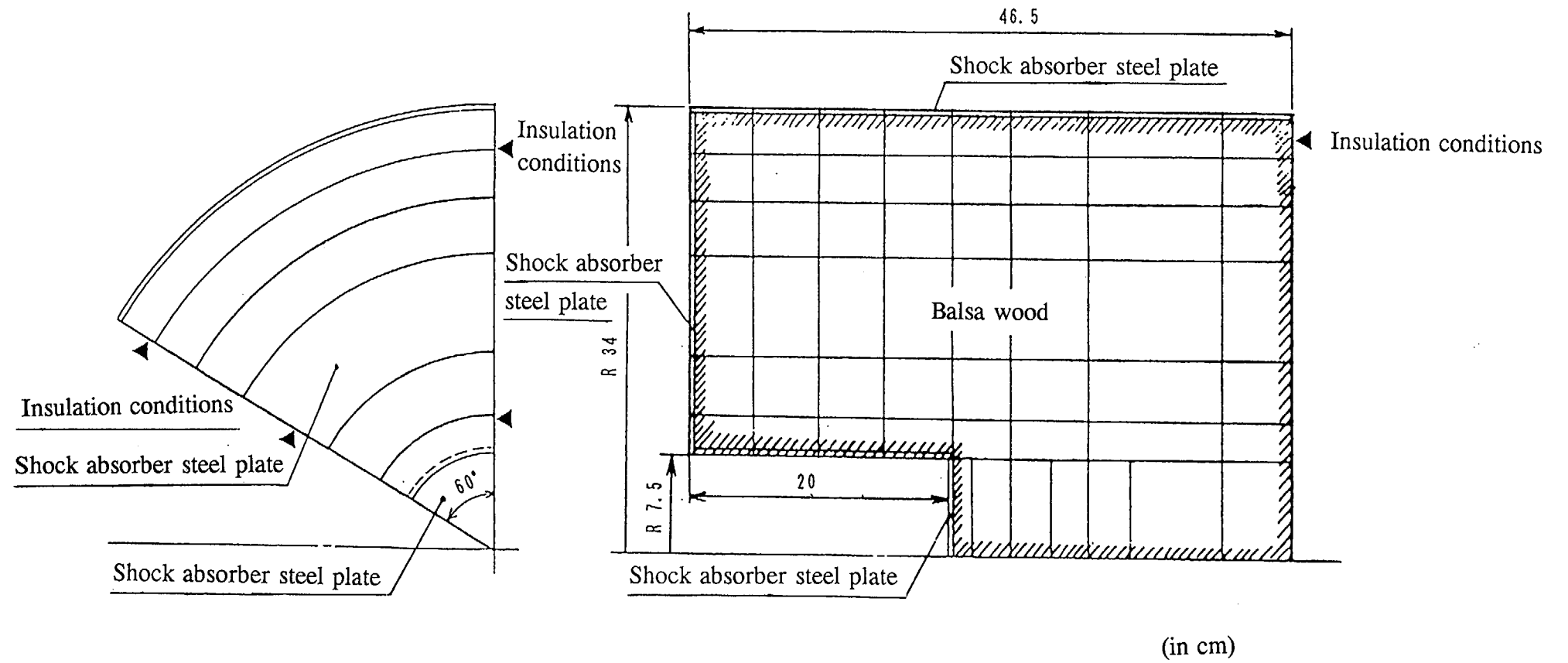


**Fig. (II)-B-App.8 Thermal Test Analysis Model**



In this case, the carbonizing temperature is set as 285°C<sup>1)2)</sup>. In other words, the values shown in Table (II)-B-App.14 are used.

For carbon steel, the values shown in Table (II)-B-App.9 are used.

**Table (II)-B-App.7 Thermal Conditions Used for the Calculation**

Item		During a fire	After a fire
Absorptivity of the shock absorber surface		0.8	0.79 <sup>*1</sup>
Environmental conditions	Ambient emissivity	0.9	1.0
	Solar heat load	--	No
	Ambient temperature	29°C ~ 850°C <sup>*2</sup>	

\*1 Emissivity of the carbon steel  
 \*2 Uses the test data. (See Table (II)-B-App.8.)

**Table (II)-B-App.8 Ambient Temperature**

Time (minute)	Ambient temperature (°C)
0	850
30	850
31	835
38	325
45	180
65	80
90	70
210	40
330	29
450	29

1) J.A. Anderson, "Design of an Extreme Crash Resistant Package", SAND 78-1129C  
 2) Kakuichi Kitahara, Wood Physics, Morikita Shuppan

**Table (II)-B.14 Thermal Properties of Balsa Wood (Flame Resistance Treatment) <sup>1)2)</sup>**

Specific gravity	kg/m <sup>3</sup> (g/cm <sup>3</sup> )	240	(0.24)
Temperature	°C	Specific heat	KJ/kg · K (cal/g · °C)
Under 285		2.30	(0.55)
285 or more		1.05	(0.25)
Temperature	°C	Thermal conductivity	W/m · K (cal/s · cm · °C)
27		0.286	(6.84 × 10 <sup>-4</sup> )
100		0.342	(8.17 × 10 <sup>-4</sup> )
150		0.322	(7.70 × 10 <sup>-4</sup> )
200		0.320	(7.65 × 10 <sup>-4</sup> )
200 or more		0.320 (Constant)	(7.65 × 10 <sup>-4</sup> )

**Table (II)-B-App.9 Thermal Properties of Carbon Steel <sup>3)</sup>**

Specific gravity	kg/m <sup>3</sup> (g/cm <sup>3</sup> )	7830	(7.83)
Specific heat	KJ/kg · K (cal/g · °C)	0.46	(0.11)
Temperature	°C	Thermal conductivity	W/m · K (cal/s · cm · °C)
0		55.4	(0.1323)
100		51.9	(0.124)
200		48.5	(0.1158)
300		45.0	(0.1075)
400		41.5	(0.0992)
600		34.6	(0.0827)
800		31.2	(0.0744)

- 1) U.S.A.E.C. "Reactor Handbook" Second Edition, Vol. I, Interscience Publishers, Inc., New York, p1097, 1960  
2) "PNC-SJ299 80-16," Power Reactor and Nuclear Fuel Development Corporation, 1980  
3) E.R.G. Eckert, "Introduction to the Transfer of Heat and Mass "First Edition, McGraw-Hill Book Company, New York, p266, 1950

As shown in Figs. (II)-B-App.9 and (II)-B-App.10, the combustion heat of balsa wood is assumed to be as described below. The total heating value of the combustion is derived from the resulting numeric values of the thermal tests so that the combustion of the shock absorber damaged part can be evaluated. Fig. (II)-B-App.9 shows an expanded view of the damaged part which was flame resistance-treated as shown in Fig. (II)-B-App.17 in subsection B.6.4.

The volumes of the complete combustion area ( $V_1$ ) and incomplete combustion area ( $V_2$ ) shown in Fig. (II)-B-App.9 are first given by

$$V_1 = \frac{\pi}{4} \times (16^2 - 15^2) \times 20 = 487cm^3$$

$$V_2 = \frac{\pi}{4} \times (21^2 - 16^2) \times 20 + \frac{\pi}{4} \times 15^2 \times 3 = 3437cm^3$$

Next, the heating values of these areas are calculated by Dulong's equation<sup>1)</sup>, shown below. This equation indicates the calories used when each element is burned independently. However, the decomposition heat resulting from element decomposition, the formation heat of the new compound, and the decomposition heat of the flame resistance agent are required during combustion because in actuality each element exists in a compound state. The decomposition heat and formation heat must be subtracted from the results of this equation to obtain the actual calories. In this case, however, they are ignored to be on the safe side. By the flame resistance treatment, most of the incomplete combustion area becomes charcoal but is not reduced to ashes. However, in this case, the combustion heat is obtained on the assumption that half of this area is completely burned.

$$Q_B = 8100 \cdot C + 34200 \times \left( H - \frac{O}{8} \right) + 2500 \cdot S$$

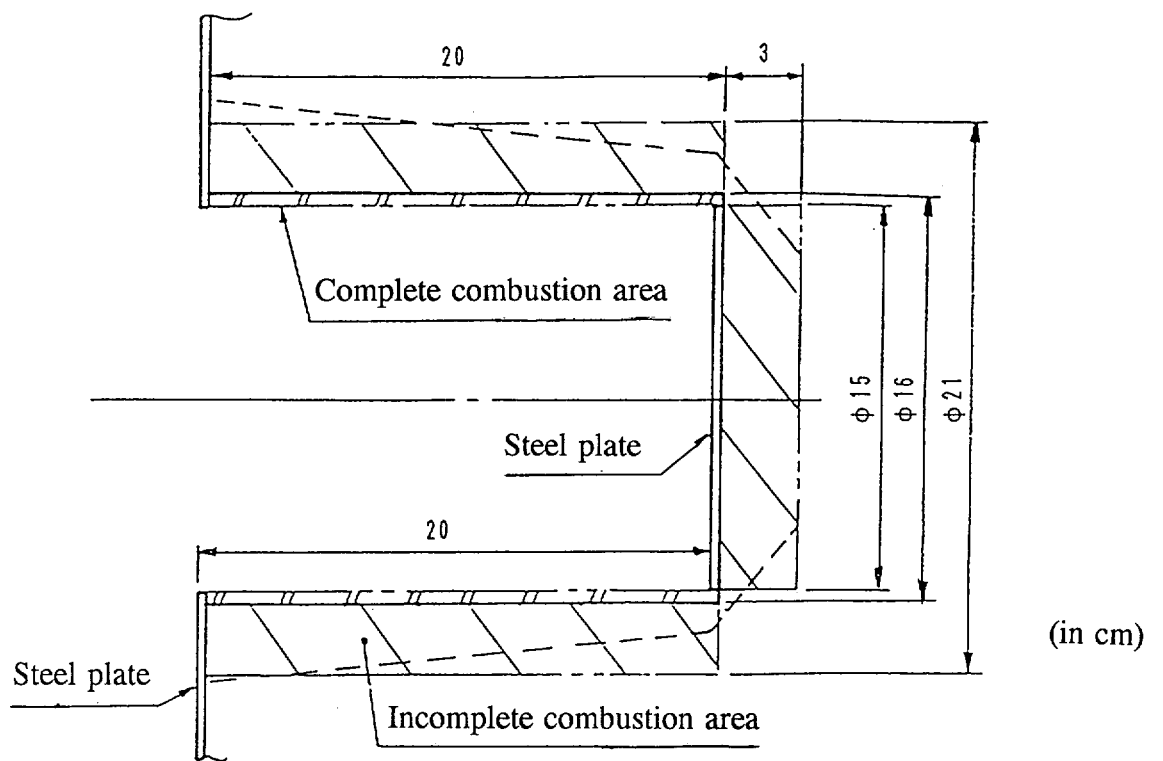
where

$Q_B$	:	Combustion heat	kcal/kg
$C$	:	Carbon value contained in the burned solid	kg
$H$	:	Hydrogen value contained in the burned solid	kg
$O$	:	Oxygen value contained in the burned solid	kg
$S$	:	Sulfur value contained in the burned solid	kg

The values below are assigned to the above expression to obtain the combustion heat ( $Q_B$ ) generated when 1 kilogram of wood completely burns. In the case of complete combustion, the whole kilogram of wood burns. Each constant is thus given as follows according to the elements composing the wood<sup>2)</sup>:

---

1) Edited by Takatoshi Yoshida, "Combustion Engineering", Kyoritsu Shuppan  
 2) "Kagaku Daijiten 9", Edited by Editorial Committee of Chemistry Dictionary, Kyoritsu Shuppan, page 269



Note: The broken line indicates the boundary of the carbonization range.

**Fig. (II)-B-App.9 Combustion Area**

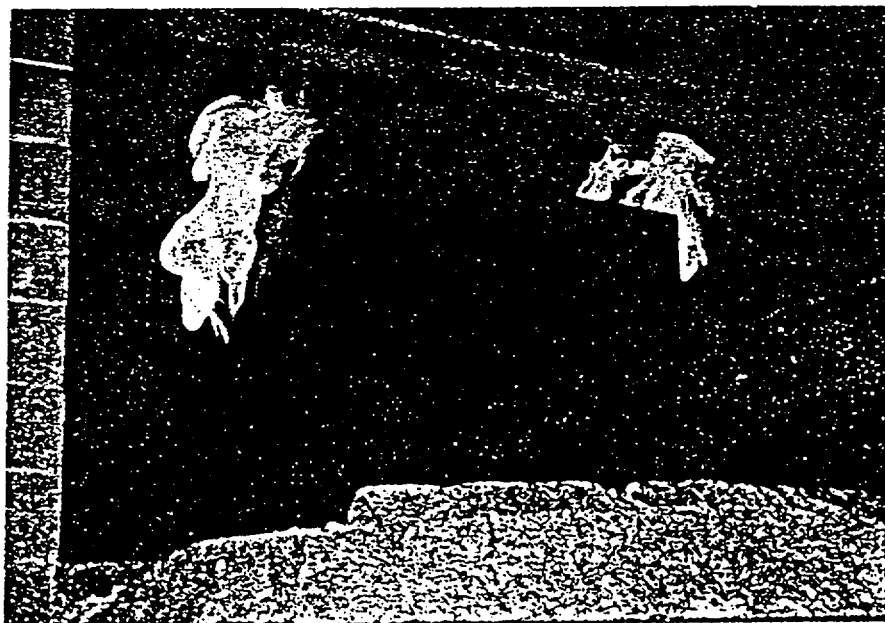


**Fig. (II)-B-App.10 Furnace Test**

$$\begin{aligned}C &= 0.50 \text{ kg} \\H &= 0.06 \text{ kg} \\O &= 0.43 \text{ kg} \\S &= 0.01 \text{ kg}\end{aligned}$$

If each constant is assigned to the above expression, the combustion heat ( $Q_B$ ) is given by

$$Q_B = 4289 \text{ kcal/kg}$$

The weight ( $W_1$ ) of the completely burned area of the wood and the weight ( $W_2$ ) of the incompletely burned area of the wood are derived from the specific gravity of wood ( $0.24 \text{ g/cm}^3$ ) and the volume of the areas. To obtain the weight of the incomplete combustion area, since half of this area is assumed to have burned completely, the volume obtained when the incomplete combustion area is divided by two is used in the calculation.

$$\begin{aligned}W_1 &= V_1 \times 0.24 = 487 \times 0.24 = 117 \text{ g} \\W_2 &= V_2 \times 0.24 = \frac{3437}{2} \times 0.24 = 413 \text{ g}\end{aligned}$$

Consequently, the combustion heat ( $Q_1$ ) in the complete combustion area and the combustion heat ( $Q_2$ ) in the incomplete combustion area are given by the expression below.

$$\begin{aligned}Q_1 &= Q_B \times 0.117 = 502 \text{ kcal} \\Q_2 &= Q_B \times 0.413 = 1772 \text{ kcal}\end{aligned}$$

The total heating value ( $Q$ ) is given by

$$Q = Q_1 + Q_2 = 2274 \text{ kcal}$$

If the shock absorber is heated during a thermal test, the wood is decomposed by the heat and inflammable gas is generated. This inflammable gas then burns, and although the wood itself also burns, most of the combustion results from the burning of the gas. As shown in Fig. (II)-B-App.10, the flame that is generated by the combustion of the inflammable gas shoots out from the hole. In this case, only half of combustion heat is assumed to be found in the hole while the other half is to be found outside the hole. Also, the wood is assumed to have been burning thirty minutes in this case, although it burned thirty-odd minutes during the thermal test. The heating value ( $q$ ) per unit time is thus given by

$$q = \frac{Q}{2} \times \frac{1}{T}$$

where

$q$	:	Heating value per unit time	kcal/h
$Q$	:	Total heating value	= 2274 kcal
$T$	:	Combustion time	= 0.5 h

and thus

$$q = 2274 \text{ kcal/h}$$

This value is used as the heating value resulting from the combustion heat. This combustion heat was used as one of the input conditions during an actual packaging fire, and as the input conditions for the evaluation conducted in this model test.

#### B.6.3.4 Results

Fig. (II)-B-App.11 shows the results calculated using the TRUMP code. This figure indicates the maximum temperature in the specified positions for temperature measurement of the balsa wood the time required. The numbers in the figure correspond to the time (minute). In this figure, the temperatures at five different measurement points are all evaluated slightly high. Therefore, the physical properties of balsa wood used and the conditions applied during the calculation are on the safe side.

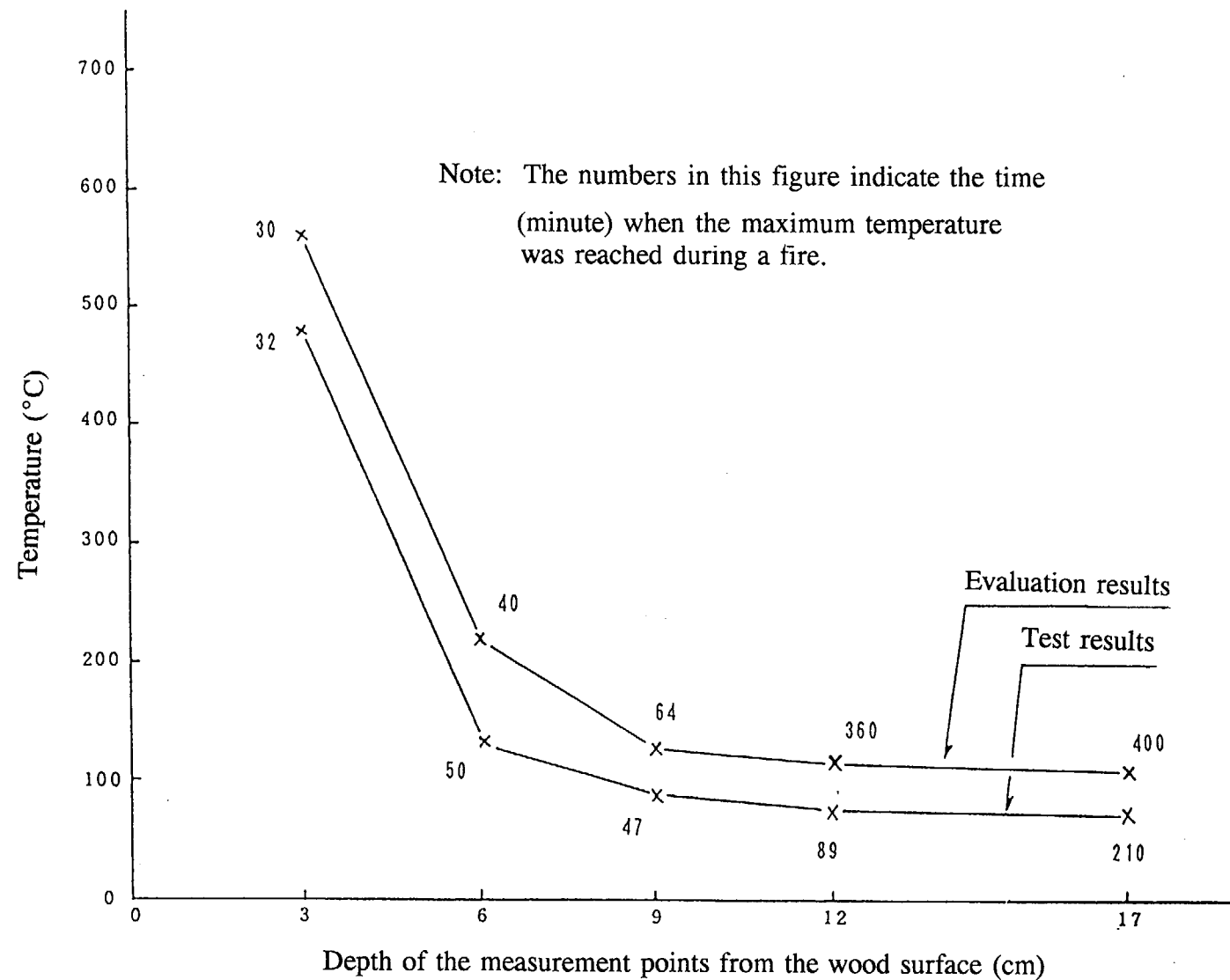


**Fig. (II)-B-App.11 Maximum Temperature and Time When It Was Reached by the Measurement Position**

## **B.6.4 Thermal Test of the Shock Absorber Model**

### **B.6.4.1 Outline**

The shock absorber used in this package is made of wood such as balsa wood. Structural evaluation results obtained for this package showed that a hole develops in the shock absorber steel plate subjected to drop test II (vertical drop). It is known that the shock absorber may also burn during a fire, therefore, a flame resistance treatment was applied to this balsa wood. To check the effect of this treatment, a test model (test model A) of the shock absorber's damaged part (hole measuring 15 in diameter  $\times$  20 cm in depth) was manufactured. To ensure that the treatment would have the desired effect, the shock absorber was symmetrically filled with both flame-resistance-treated balsa wood and nontreated balsa wood. The thermal test has shown that the flame-resistance-treated balsa wood goes out as soon as it is taken out of the furnace, into which it is placed to simulate the conditions of a fire. On the other hand, the nontreated balsa wood does not go out even four hours after it is taken out of the furnace. The balsa wood had to be put into a water tank to completely extinguish the fire. The test model (test model B whose fusible plug hole is included in the model) used to examine the carbonization of the resin was also subjected to a thermal test at the same time.

### **B.6.4.2 Test method**

This test applies the furnace test method. For this test, an annealing furnace (250 (width)  $\times$  370 (length)  $\times$  160 (height) cm) was used. Fig. (II)-B-App.12 shows the dimensions of the annealing furnace. A test model was put into this furnace after being placed on truck frame. Fig. (II)-B-App.13 shows the dimensions of test model A, while Fig. (II)-B-App.14 shows the dimensions of test model B.

The temperature in this test was increased as described below. The temperature in the furnace was first gradually increased to about 800°C. Next, the truck frame carrying the test model was carried into the furnace. After the temperature in the furnace reached 800°C with the door closed, it was maintained for 30 minutes and a thermal test was carried out. A C.A sheath thermocouple (material quality: SUS304, outer diameter: 1.6 mm and 3.2 mm) was used to measure the temperature inside the test model, on the test model surface, and around the test model.



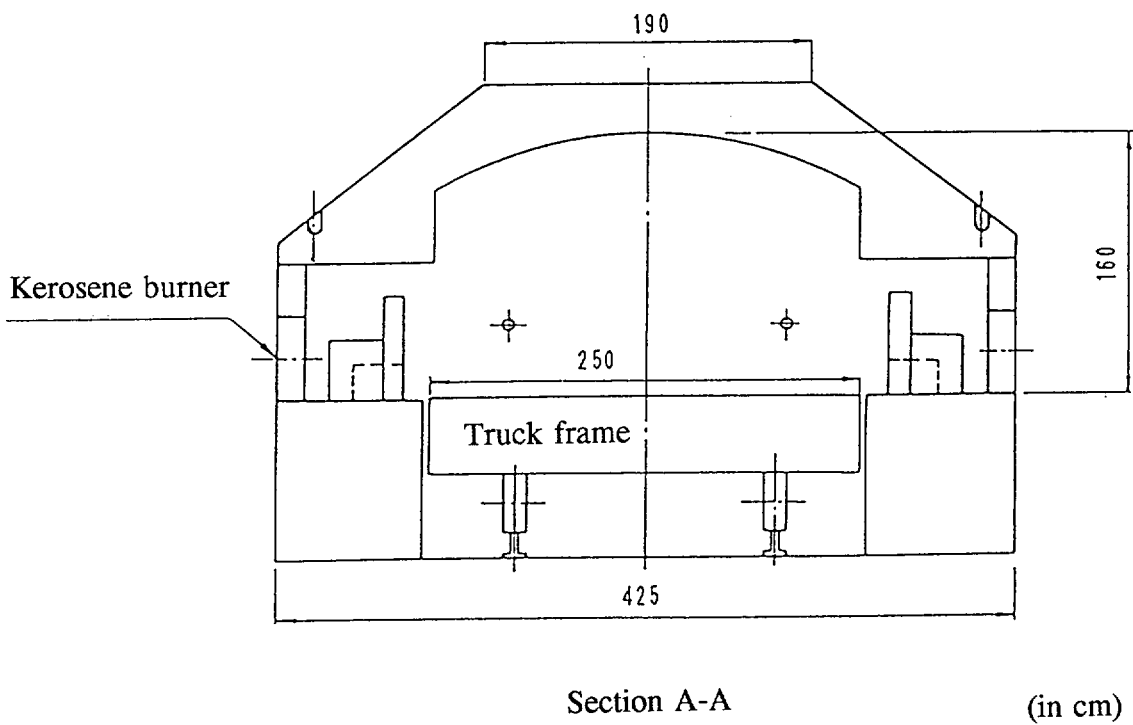
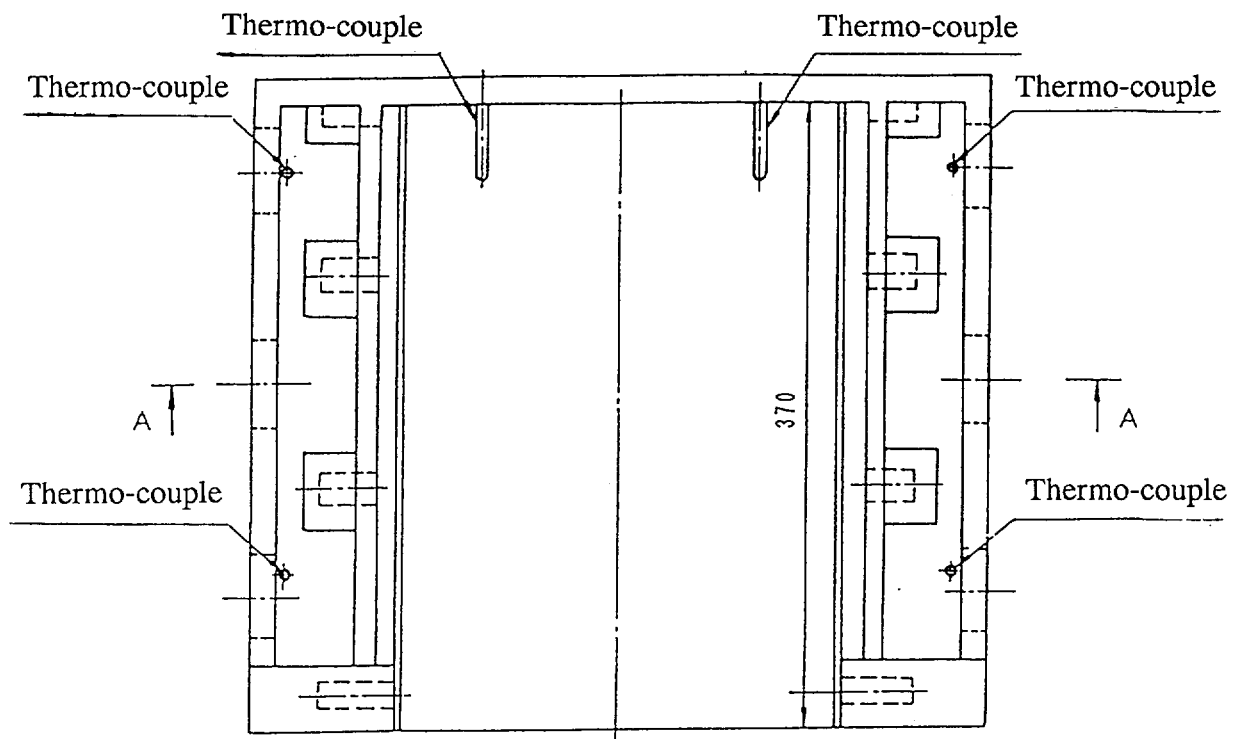
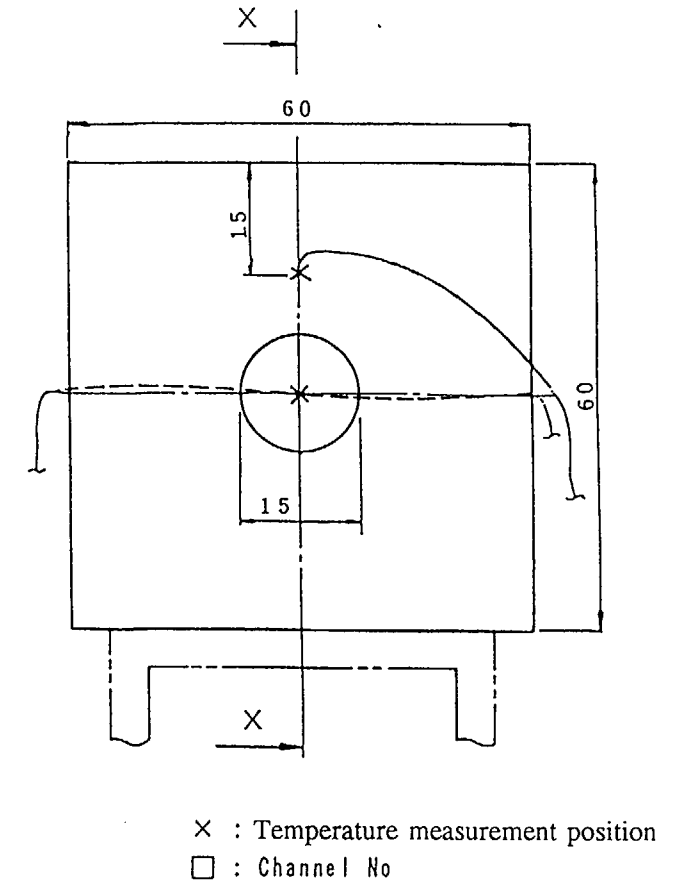
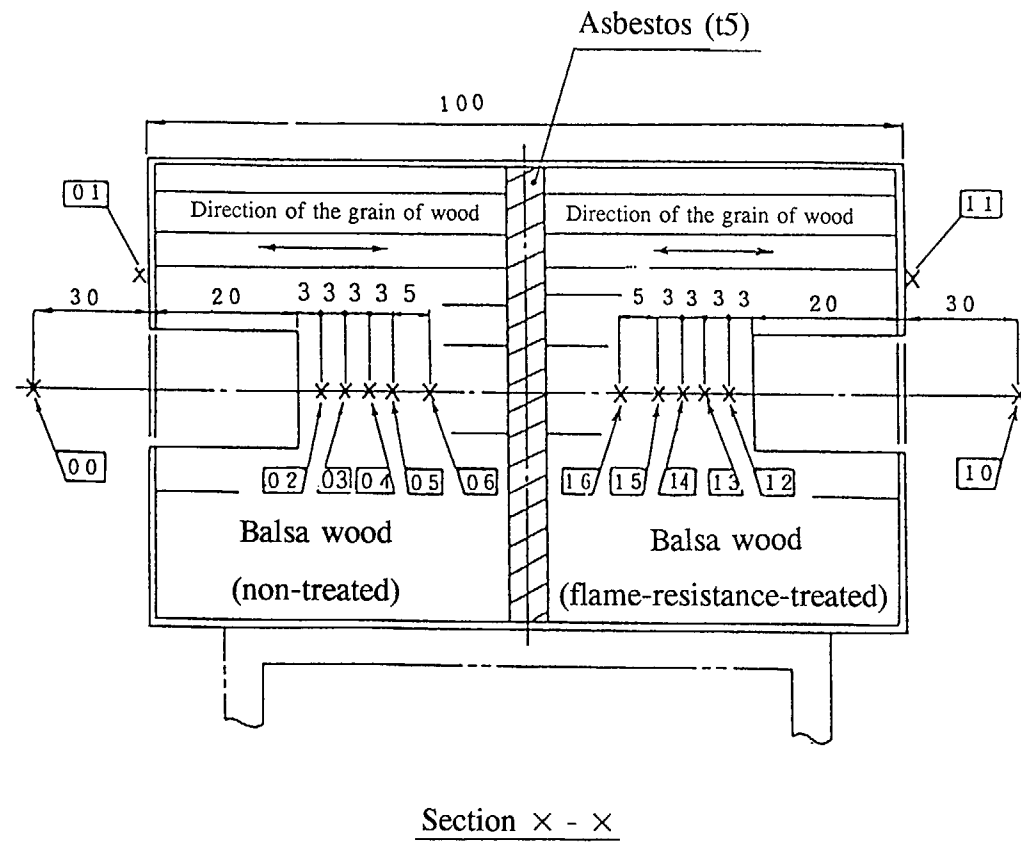


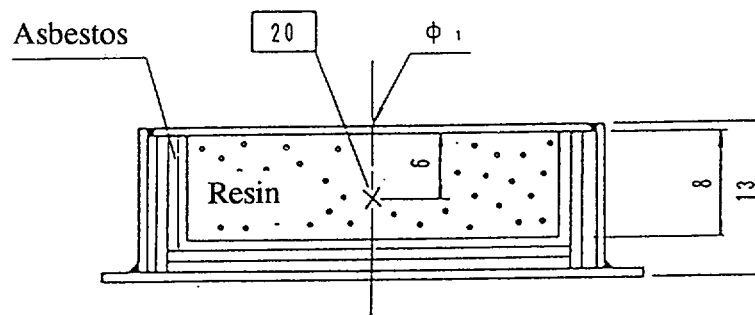
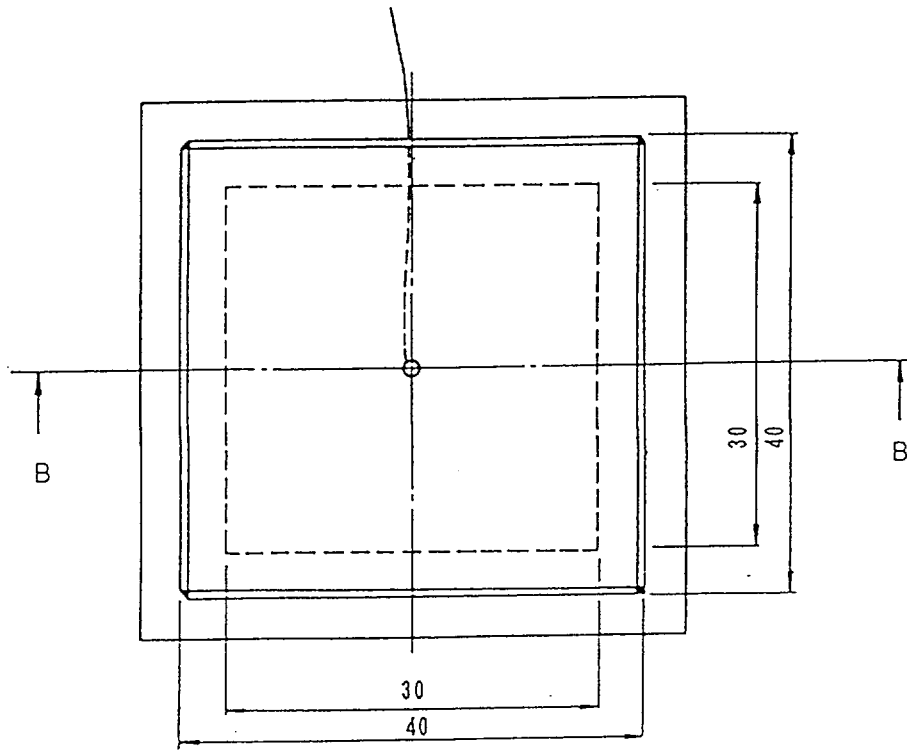
**Fig. (II-B-App.12 Annealing Furnace**

(II)-B-App-33



(in cm)

**Fig. (II)-B-App.13 Test Model A**



Section B-B

× : Temperature measurement position

□ : Channel No

(in cm)

**Fig. (II)-B-App.14 Test Model B**

### B.6.4.3 Test results

#### (1) Test model A

Fig. (II)-B-App.15 (on the side made of treated balsa wood) and Fig. (II)-B-App.16 (on the side made of the nontreated balsa wood) show the changes over time at each temperature measurement point in test model A. The ambient temperature (00, 10) and surface temperature (01, 11) during a fire were maintained between 800 and 820°C, and between 840 and 860°C, respectively. When the flame-resistance-treated balsa wood was taken out of the furnace after a fire, combustion stopped and the flames went out. This indicates that the balsa wood was not in a natural ignition state, but rather in a flameless ignition state. This test confirmed that the temperature on the test model surface and inside the test model decreases by natural cooling after the balsa wood is taken out of the furnace. Moreover, this temperature does not increase again.

Nontreated balsa wood continued burning even four hours after it was taken out of the furnace following a fire. The balsa wood had to be put in a water tank to completely extinguish the fire. This test also confirmed that the internal temperature of the test model slowly increases by natural cooling even after the balsa wood is taken out of the furnace.

Fig. (II)-B-App.17 shows the carbonization of the balsa wood (both nontreated and treated). The damaged part of the flame-resistance-treated balsa wood is carbonized without being reduced to ashes, and the shape of the damaged part (hole) is maintained. On the other hand, the nontreated balsa wood completely falls apart and is reduced to ashes. Then the hole is enlarged towards the inside. The dimensions of the carbonization shown in Fig. (II)-B-App.17 are the values obtained the flame was extinguished about four hours after a fire after the temperature of the treated balsa wood started decreasing after a fire and the effect of flame-resistance treatment was ensured, which was the purpose of this test.

#### (2) Test model B

Fig. (II)-B-App.18 shows the changes over time at each temperature measurement point in test model B. The maximum temperature of resin at a depth of 6 cm is approximately 130°C. In test model B, gas shoots out of the hole of a fusible plug when the balsa wood is taken out of a furnace following a thermal test. No flames appear in this case. As shown in Fig. (II)-B-App.19, the state during disassembly is not influenced by the hole (fusible plug), and the balsa wood is uniformly carbonized over an area of about 1 cm.

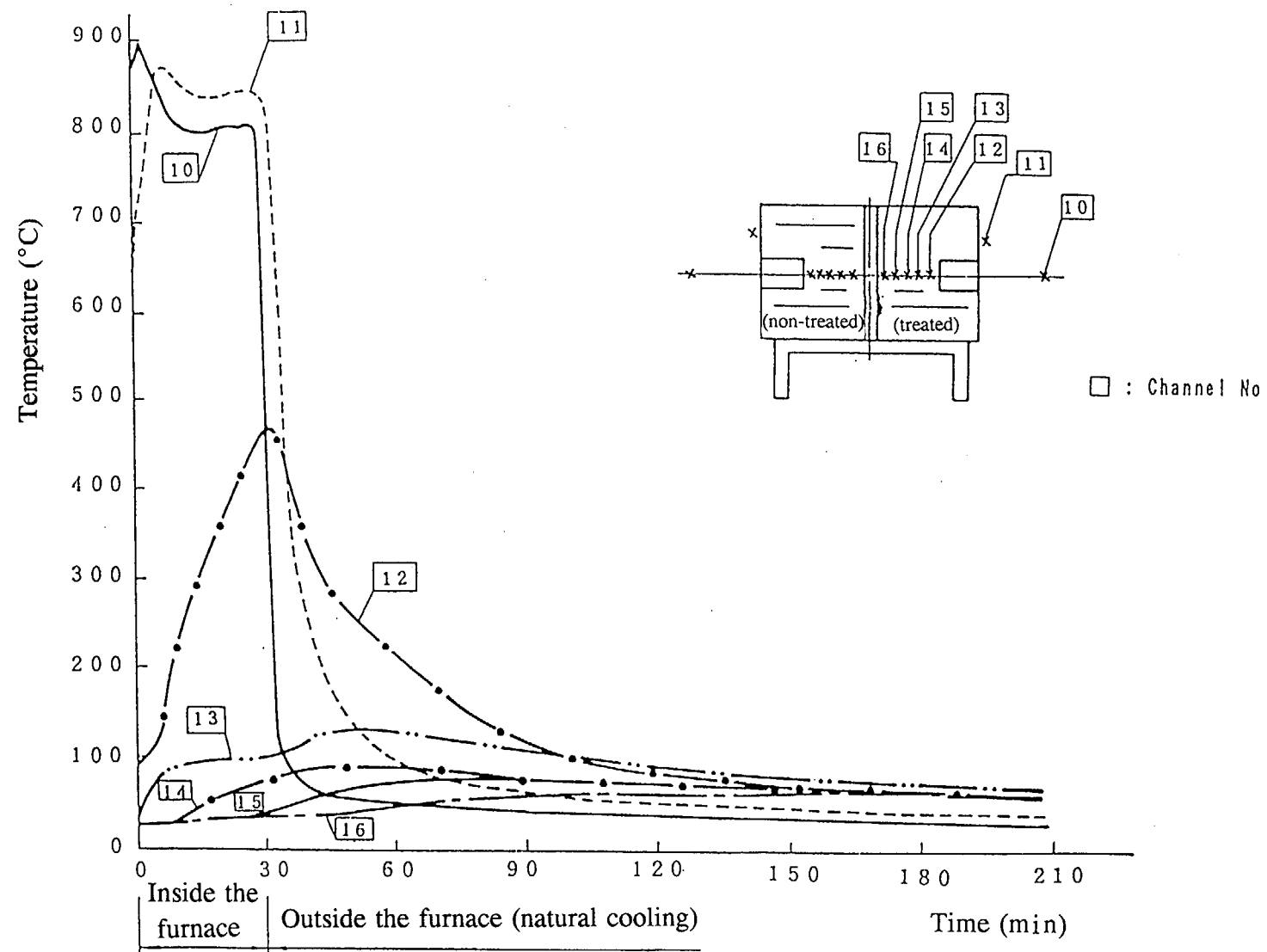


**Fig. (II)-B-App.15 Change in Temperature of Test Model A (treated side)**

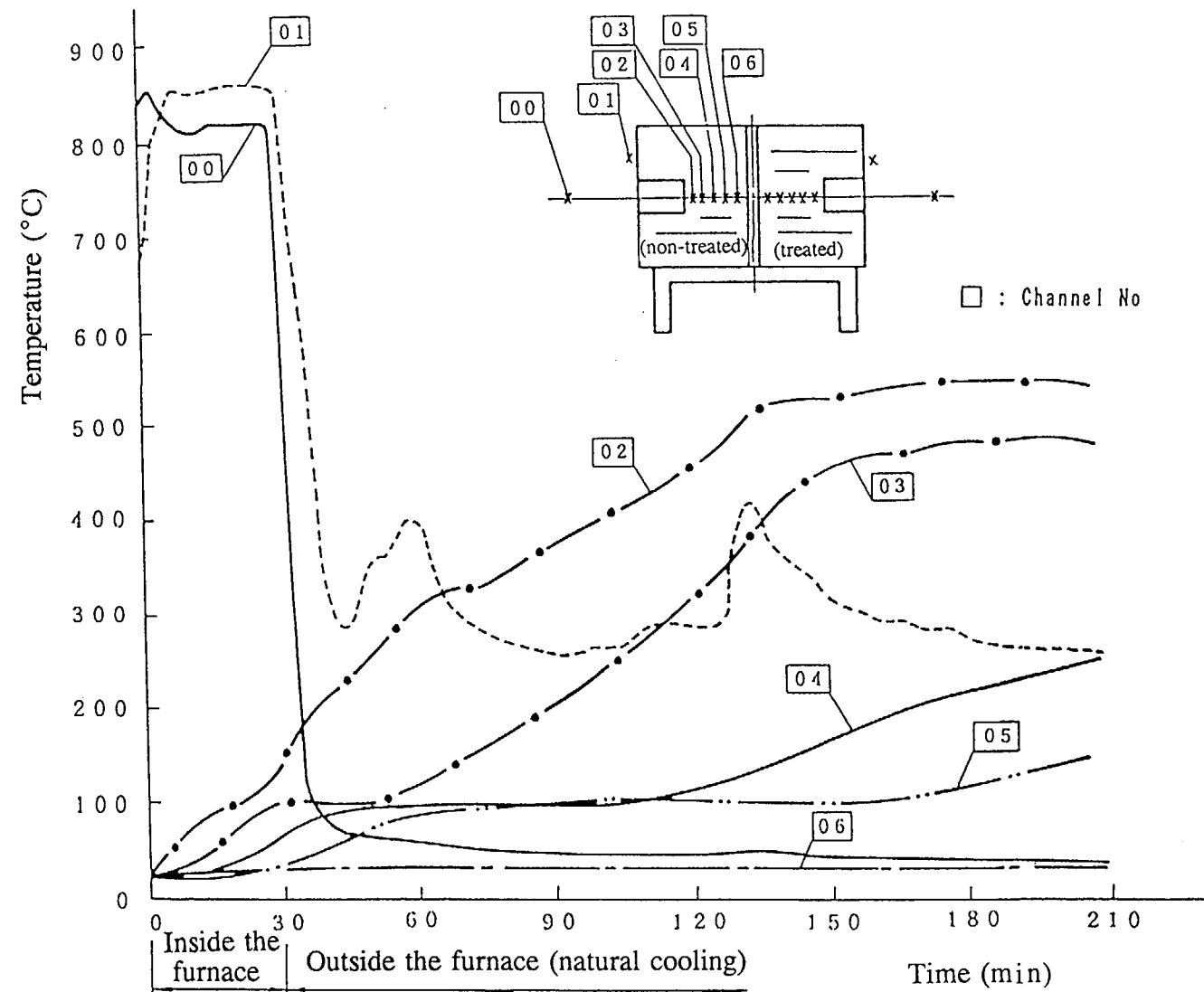


**Fig. (II)-B-App.16 Change in Temperature of Test Model A (non-treated side)**

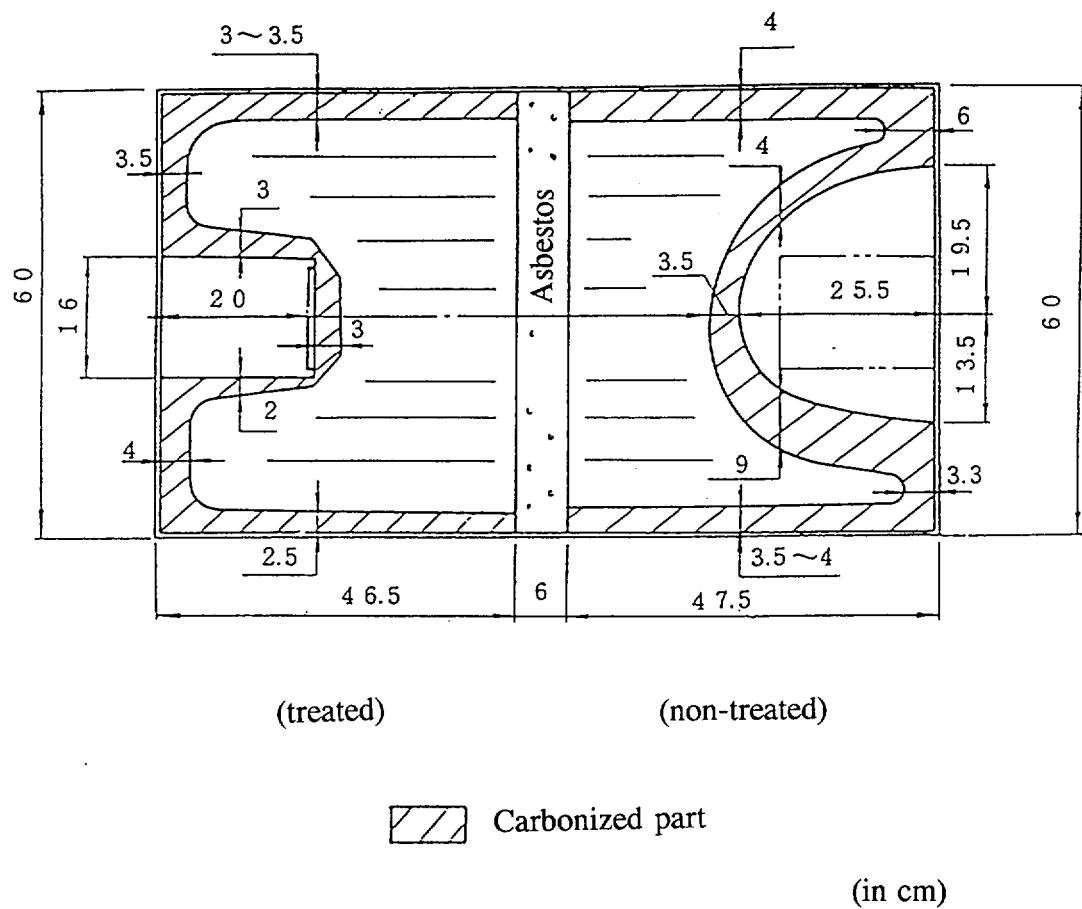


**Fig. (II)-B-App.17 Carbonization of Balsa Wood**

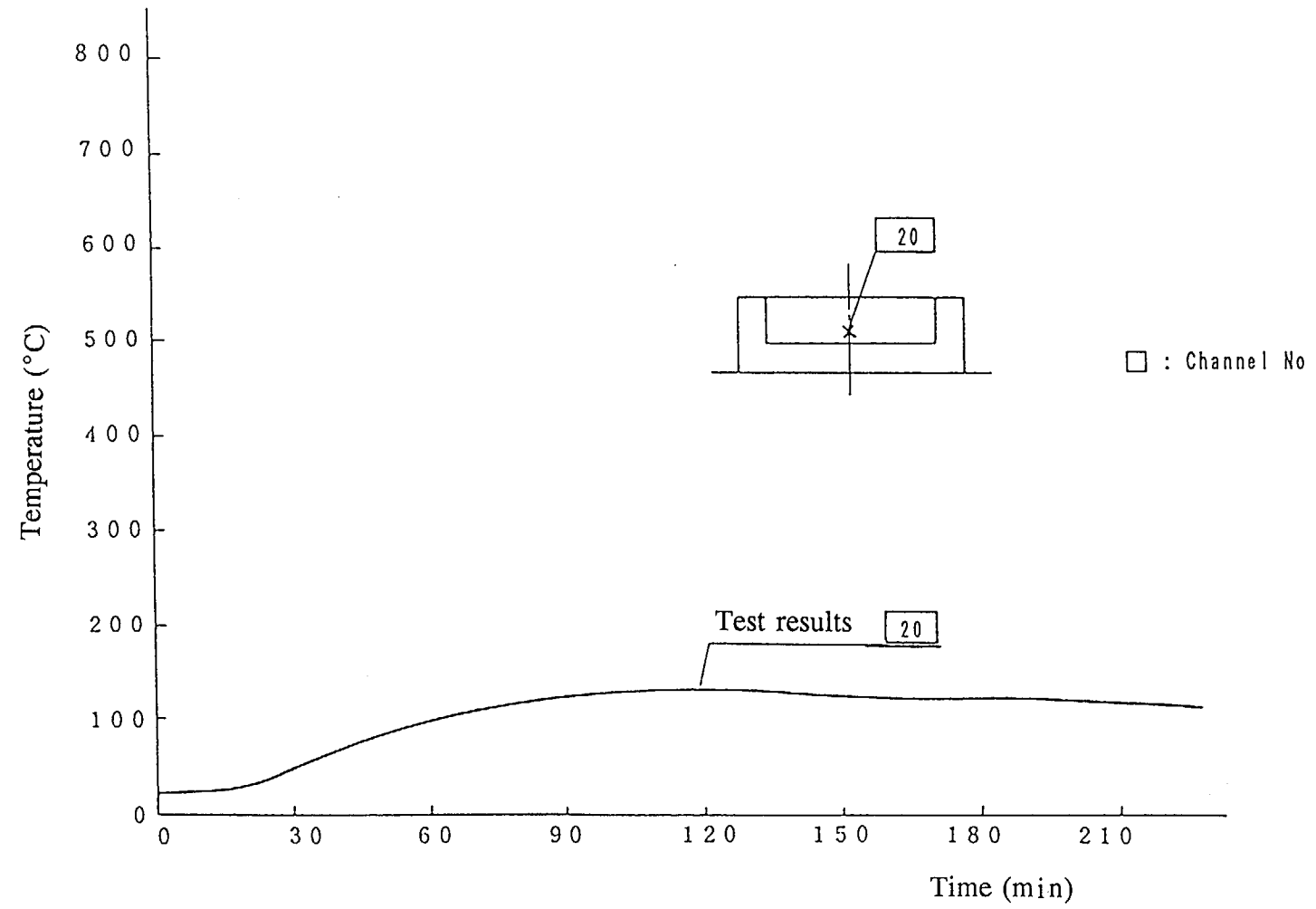
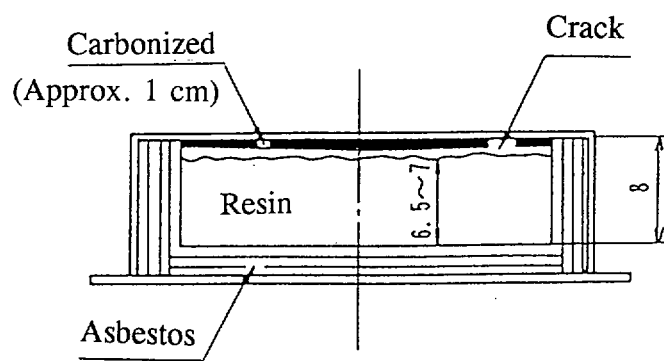


**Fig. (II)-B.App.18 Change in Temperature of Test Model B**





(in cm)

**Fig. (II)-B-App.19 Carbonization of Resin (sectional view)**

## **(II)-C Containment Analysis**

### **C.1 Outline**

The objective of this containment analysis is to make certain that the leak of radioactive material is within the criteria stipulated by law. In the case of Contents I through VIII accommodated in the hermetically sealed container of the package, conformity to this criteria is checked under both normal and accident test conditions. In the case of gaseous contents, adherence is determined using Poiseuille and Knudsen's equation. In the case of plutonium in the form of fine particles, conformity is confirmed by determining the amount of leak of radioactive material using the results of experiments (involving helium gas and plutonium powder) performed at the U.S.-based Battelle Laboratory.

### **C.2 Containment System**

As shown in Fig. (II)-C.1, the containment system of the package consists of the following:

- the inner shell of the outer container
- the shielding plug lid and the rear lid, which make up the rear lid unit
- the rotating plug lid, the penetration hole lid, the front lid, and the front and rear sampling valve lids, which make up the front lid unit

Although the front and rear sampling valves and the orifice plug used to fasten the shaft of the rotating plug provide hermeticity, they are not treated as containment systems.

Furthermore, although the inner container features a hermetically sealed construction in which an O-ring-equipped cap is screwed into either end, it is not treated as a containment system. At the same time, although fuel supporting cans and receiving tubes shown in Fig. (II)-C.2 serve as secondary containment systems because they are hermetically sealed by welding after irradiated fuel elements (Contents I, II, IV, V, VI, VII, and VIII) are placed in them before these are in turn placed in the inner container, they are not treated as containment systems, either.

#### **C.2.1 Containment System**

Here in this section, the inner shell of the outer container, the lids of the front and rear lid units, and the lids of the front and rear sampling valves, which combine to make up the containment system, are discussed. Also discussed here are the fuel supporting cans I and II as well as the receiving tubes I and II, all of which feature gastightness comparable to that of the containment system, but are not rated as containment systems.

As already mentioned, the containment system consists of the outer container's inner shell, the rear lid unit's shielding plug lid and rear lid, the front lid's rotating plug lid, penetration hole lid, front lid, and front and rear sampling valve lids. All of these components are made of stainless steel (SUS304). All of them, except the front and rear lids, use lead or a tungsten alloy to provide an enhanced shielding effect. Structurally, these individual lids are equipped with O-rings and are fastened with bolts made of stainless steel (SUS630) to ensure containment.

As an index of containment performance, the containment system has a helium leakage rate of  $1.0 \times 10^{-5}$  atm • cc/sec. or less. This performance has been verified by leakage testing in the course of manufacture. The constituent components of the containment system and their materials are listed in Table (II)-C.1.

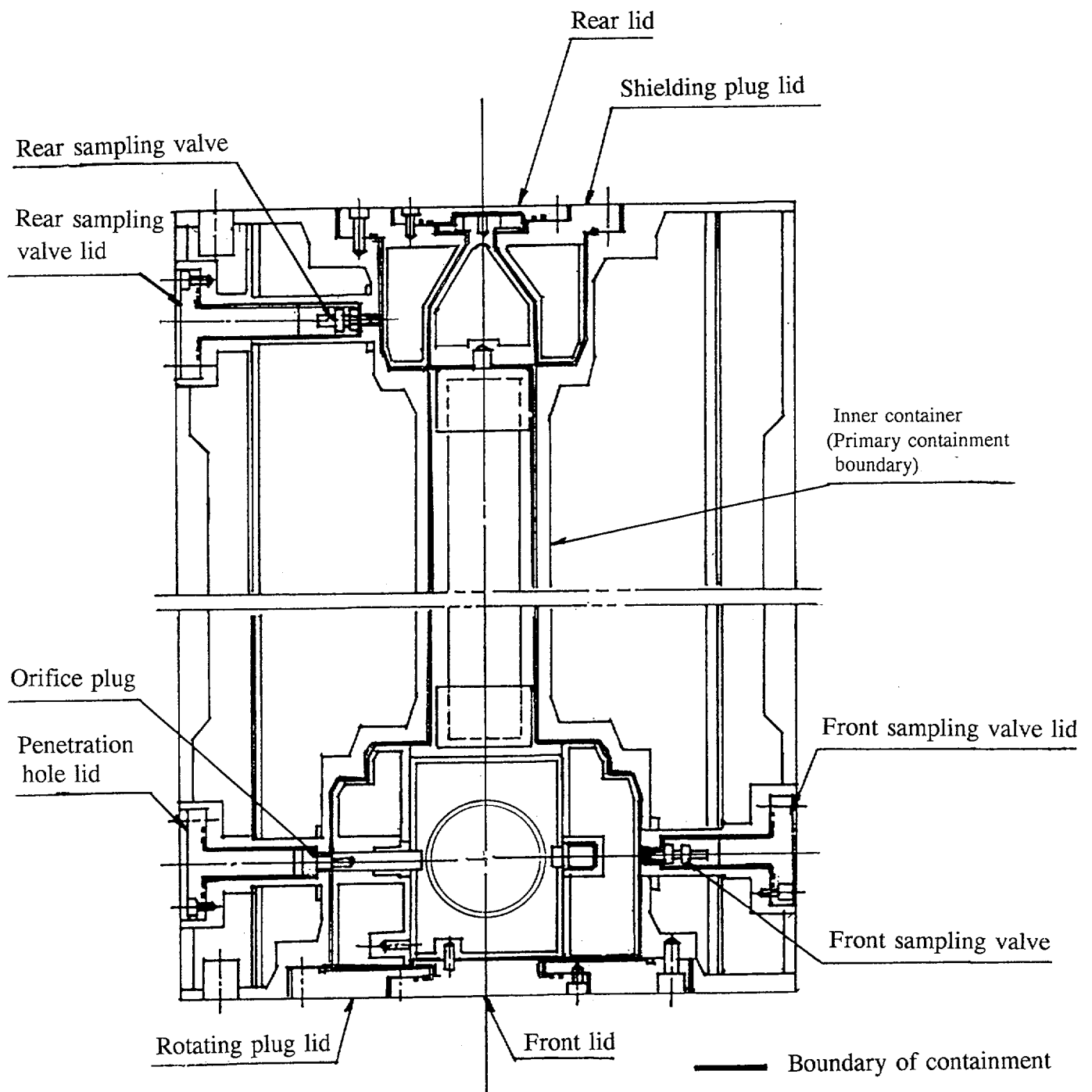


**Fig. (II)-C.1 Containment System and Boundary of Containment**

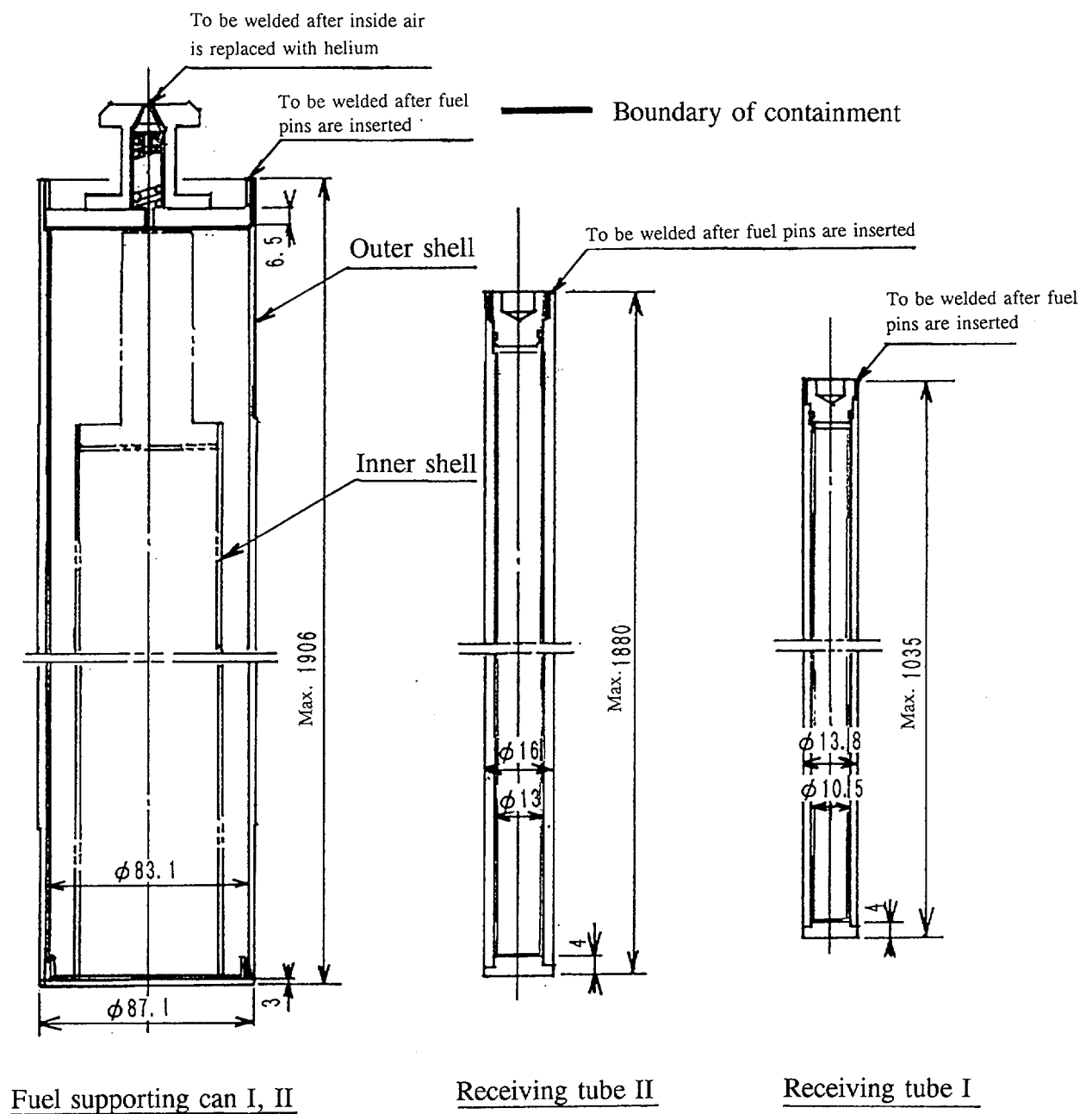


**Fig. (II)-C.2 Fuel Supporting Cans I, II, Receiving Tubes I and II**

**Table (II)-C.1 Constituent Materials of Containment System**

Component	Material
Inner shell of the outer container	Stainless steel (SUS304)
Rear lid	Stainless steel (SUS304)
Shielding plug lid	Stainless steel (SUS304) Lead Tungsten alloy
Front lid	Stainless steel (SUS304)
Rotating plug lid	Stainless steel (SUS304) Lead Gunmetal (BC2)
Front and rear sampling valve lids Penetration hole lid	Stainless steel (SUS304) Lead

All of the lid units of the containment system are covered by the front and rear shock absorbers. These lid units can, therefore, be subject to drop and thermal tests conducted under accident conditions without damage, and their containment can maintain its integrity.

Under normal and accident test conditions, the pressure inside the containment system and the temperature of the O-ring sections increase until they reach the figures given in Table (II)-C.2. The containment system is designed to withstand this maximum internal pressure without damage, and the performance of the the O-rings (made of fluorocarbons) is not adversely affected because their service temperature range extends from -50°C to 200°C. Furthermore, the individual lids are protected by front and rear shock absorbers during transport, and the containment system will not be opened unintentionally.

**Table (II)-C.2 Containment System’s Maximum Pressure and O-ring Sections’ Maximum Temperature**

Test conditions	Maximum pressure (kPa)	Maximum temperature (°C)
Normal test conditions	160	75
Accident test conditions	180	125

Irradiated fuel pins (Contents I, II, IV, V, VI, VII, and VIII) are placed in fuel supporting cans I/II or receiving tubes II/I for transport. Both types of receiving containers are made of stainless steel (SUS304). Fuel supporting cans I and II have a dual-cylinder construction as shown in Fig. (II)-C.2. and the space between the inner cylinder and the outer cylinder is sectioned (into five compartments for fuel supporting can I and six compartments for fuel supporting can II) for accommodating irradiated fuel pins (up to 15 pieces into fuel supporting can I and 6 pieces into fuel supporting can II. On the other hand, receiving tubes I and II, which are cylindrical as shown in the above figure, are designed to hold irradiated fuel pins on an one-on-one basis.

After the fuel pins have been placed in their interiors, fuel supporting cans I and II are welded shut with their lids to ensure containment. The air inside each fuel supporting can is then replaced with helium through a hole bored through the top of the lid. Thereafter, this hole is stopped up by welding. On the other hand, in the case of receiving tubes I and II, the plugs are welded shut after accommodating fuel pins in their interiors to ensure a containment.

As already discussed, since fuel supporting cans I and II, as well as receiving tubes I and II are hermetically welded shut, they serve as secondary containment systems. Their design leakage rate is set at  $1.0 \times 10^{-6}$  atm·cc/sec. or less, and conformity with this rate is verified at the time of shipment.

Table (II)-C.3 shows the pressure and maximum temperature that have been registered by the highest-pressure, highest-temperature fuel supporting can I and receiving tube I in the course of testing performed under normal and accident test conditions.

Fuel supporting can I and the receiving tube I (including fuel supporting can II and the receiving tube II, whose pressure and temperature readings fell short of those values) have been verified as sound and structural evaluations indicate that their containment is not impaired even if they are placed under these temperature and pressure conditions.

**Table (II)-C.3    Maximum Pressure and Temperature Registered in the Worst Case by Fuel Supporting Can I and Receiving Tube I**

Test conditions	Maximum pressure (kPa)		Maximum temperature (°C)*	
	Fuel supporting can I	Receiving tube I	Fuel supporting can I	Receiving tube I
Normal test conditions	307	699	338	305
Accident test conditions	327	748	366	341

\* The maximum temperatures refer to the highest registered temperatures of the gas (helium or air) contained inside.

### C.2.2 Penetration Sections of the Containment System

The penetration sections of the containment system refer to the front and rear sampling valve sections and the penetration hole that provides access to the rotating plug. The sampling valves are designed to be used to check the air inside the containment system for possible contamination by radioactive material and to depressurize the internal pressure so that it matches the atmospheric pressure prior to retrieving the contents.

The sampling valves are made of stainless steel (SUS304) and are each equipped with a gasket made of fluoro rubber, which has a service pressure rated at 4.9 MPa. The sampling valve sections have a gastight construction in which hermetic sealing is achieved by means of a sampling valve lid equipped with double O-ring made of fluoro rubber. Since these sections are covered by the shock absorbers, their containment maintains its integrity, and sustains no damage in the course of the drop tests and the thermal test conducted under accident conditions.

The penetration hole for the rotating plug is designed to permit the insertion of a handle from the outside, so that the rotating plug can be actuated. Its containment is maintained by means of the penetration hole lid for the rotating plug equipped with double O-ring (made of fluoro rubber). Since it is covered by one of the shock absorbers, as in the case of the sampling valve lids, its containment is maintained intact, and sustains no damage in the course of the drop tests and thermal test.

Both the fuel supporting cans and receiving tubes, which are categorized as secondary containment systems, are hermetically sealed by welding at either end. For this reason, they have no penetration hole section.

### C.2.3 Containment System Gaskets and Welded Joints

#### (1) Gaskets (O-rings)

The individual lids of the containment system are equipped with O-ring sealing made of fluoro rubber. The specifications of the O-rings in use are shown in Fig. (II)-C.4. Moreover, since the orifice plug is also equipped with an O-ring to stop up the rotating plug axis hole, this O-ring is also listed in the table.

Since the working temperature of the fluoro rubber ranges from -50°C to 200°C, O-rings made of this material can maintain their intended performance under both normal and accident test conditions.

**Table (II)-C.4 O-ring Specifications for the Lids**

Lid		Dimensions of O-ring	Material
		Cross-sectional × Ring diameter (mm) diameter	
Rear lid	(2)	φ5.7 × φ130	Fluoro rubber
		φ5.7 × φ165	Fluoro rubber
Shielding plug lid	(1)	φ8.4 × φ280	Fluoro rubber
Front lid	(2)	φ5.7 × φ165	Fluoro rubber
		φ5.7 × φ195	Fluoro rubber
Rotating plug lid	(1)	φ8.4 × φ430	Fluoro rubber
Front/rear sampling valve lid	(2)	φ5.7 × φ72	Fluoro rubber
		φ5.7 × φ96	Fluoro rubber
Penetration hole lid	(2)	φ5.7 × φ72	Fluoro rubber
		φ5.7 × φ96	Fluoro rubber
Orifice plug	(1)	φ3.5 × φ38	Fluoro rubber

No gasket is used on the fuel supporting cans, which are categorized as secondary containment systems. On the other hand, each individual receiving tube is furnished with a plug equipped with an O-ring made of fluoro rubber, which is welded down after a fuel pin has been inserted into its interior.

(2) Welded Sections

The containment system is made of stainless steel (SUS304), and its welded sections are checked for integrity. In other words, the rates of leakage through the welded sections are verified to be within their design specifications as they are subjected to a radiographic test or a liquid penetrant inspection in the course of manufacture and a helium leakage test during assembly.

C.2.4 Lids

Since the individual lids of the containment system are made of stainless steel (SUS304) and are equipped with fluoro rubber O-ring sealing, they remain sound when exposed to pressures and temperatures that are prevalent under the normal and accident test conditions, and can therefore maintain their intended containment. Furthermore, the fastening bolts used to tie down each individual lid are tightened to the torque specified in Table (II)-C.5

**Table (II)-C.5 Specified Tightening Torque of Bolts for the Lids**

Lid	Bolt specifications	Torque (N·m)
Shielding plug lid	M20	110
Rear lid	M12	25
Rotating plug lid	M20	110
Front lid	M12	25
Rear sampling valve lid	M12	25
Front sampling valve lid	M12	25
Penetration hole lid	M12	25

The gastight containment sealing of fuel supporting cans and the receiving tubes is secured by means of a lid or a plug which is hermetically welded on these parts.

C.3 Normal Test Conditions

The effect of the normal test conditions on the containment system of the package are summarized below.

(1) Effect of heat

Assuming that the package holds Contents I (low-burnup pins; this case represents the most stringent thermal conditions) which are known to produce 260W of decay heat, the temperature of the O-rings in the individual lids reaches a maximum of 75°C at an ambient temperature of 38°C even when solar heat load is taken into account. Since the service temperature of the O-rings (made of fluoro rubber) is 200°C, the integrity of the containment system can be maintained intact. (See B.4.2.)

Of the secondary containment systems, fuel supporting can I and receiving tube I, which yield the highest temperature readings, measure 300°C and 245°C, respectively. Since,



structurally, they are made of stainless steel (SUS304) and hermetically welded, their containment remains unaffected. (See B.4.2.)

Next, the heating value of the contents is assumed to be 0W at an ambient temperature of -40°C and the solar heat load is not considered. Given this thermal load condition, the individual sections of the package measure -40°C. The containment system as well as the secondary containment systems, namely the fuel supporting cans and the receiving tubes, are made of stainless steel (SUS304), and the O-rings (which have a service temperature range that extends from -50°C to 200°C) are not subject to performance deterioration at -40°C. (See A.4.2.)

Furthermore, the containment system continues to maintain its strength and integrity in the face of an elevation of its internal pressure (up to 160 kPa) due to the heat generated by the decay of its contents.

(2) Mechanical vibrations/impact and compression impact

The package is not subject to resonance due to vibrations created during transport and its soundness remains unimpaired. (See A.4.7.)

Furthermore, when the package is dropped from a height of 60 cm onto a hard surface in a free fall during the free-drop and corner-drop tests, the impact acceleration is mitigated by the front and rear shock absorbers. For this reason, the containment system as well as the fuel supporting cans and the receiving tubes, which are categorized as secondary containment systems, remain structurally sound, and their containment is maintained intact. (See A.5.3.)

When a steel rod weighing 6 kg is dropped from a height of 1 m onto the package in the penetration test, the containment system along with the fuel supporting cans and the receiving tubes, which are categorized as secondary containment systems, can remain unscathed because all the lid sections of the containment systems are protected by shock absorbers. (See A.5.5.)

Moreover, when a load five times the weight of the package is applied to the package over the course of a compression test, the outer shell can bear this load on its own, and the package remains structurally sound. (See A.5.4.)

Based on the above structural evaluation and thermal analysis results, the containment system along with the housed fuel supporting cans and receiving tubes maintain its integrity and their containment is maintained intact when the package is subject to normal test conditions.

### C.3.1 Leakage of Radioactive Material

Contents that are to be loaded into the package include irradiated fuel pins and test pieces derived from structural radioactive materials. Since these contents are to be transported "dry", the release of radioactive gases or solids is possible when it comes to the leak of radioactive material. The containment system of the package is confirmed by making certain that its leakage rate stands at  $1.0 \times 10^{-5}$  atm·cc/sec. or less during leakage testing using helium or halogen gas conducted in the course of manufacture. As mentioned earlier, the containment system maintains its integrity under normal test conditions and this leakage rate is maintained. Further-

more, fuel supporting cans and receiving tubes that have irradiated fuel pins are also proven to be structurally sound, and their containment is maintained.

Although it is assumed that there is no leak of radioactive material from the fuel supporting cans or receiving tubes for the reasons stated above, radioactive-material leakage is evaluated hereafter on the assumption that those containers do not offer a containment capability.

Of Contents I, II, and IV through VIII, Contents VIII that emit fission product gases in the largest amounts are studied to prove that the leak of radioactive material is within the mandated criteria. (See Table (II)-C.8.)

To begin with, the analysis assumes that fission product gases which are evenly distributed in the containment system leak out together with air.

The design leakage rate set for the containment system is  $1.0 \times 10^{-5}$  atm · cc/sec. or less with helium gas, and the relationship between the leakage rate of air and the leakage hole, which the internal pressure and temperature are 160 kPa and 165°C, respectively under normal test conditions, is given by the following equation:

$$Lr = (Fc + Fm) (Pu - Pd) \quad 1)$$

$$Fc = 2.49 \times 10^{-2} \times d_N^4 \frac{1}{(a \cdot \mu)}$$

$$Fm = 3.81 \times 10^3 \times d_N^3 \sqrt{\frac{T}{M} \frac{1}{(a \cdot Pa)}}$$

where			
Pu	:	Upstream pressure	0.101 (MPa)
Pd	:	Downstream pressure	0.0 (MPa)
a	:	Length of leak hole	0.5 (cm)
μ	:	Viscosity of helium	$1.981 \times 10^{-11}$ (MPa · s)
T	:	Gas temperature	293 (K)
M	:	Molecular weight	4
Pa	:	Average pressure	(Pu + Pd)/2.0
Lr	:	Leakage rate	$1.0 \times 10^{-5}$ (atm · cc/sec)

By substituting these values in the above equation, the diameter of the leak hole is calculated as:

$$d_N = 3.5586 \times 10^{-4} \text{ (cm)}$$

Based on this diameter (d<sub>N</sub>), the leakage rate of the medium (air) under the normal test conditions is obtained:

where			
Pu	:	Upstream pressure	0.16 (MPa)
Pd	:	Downstream pressure	0.025 (MPa)

1) ANSI N14.5-1987 American National Standard for radioactive-material Leakage tests on packages for Shipment

a	:	Length of leak hole	0.5	(cm)
$\mu$	:	Viscosity of air	$2.45 \times 10^{-11}$	(MPa · s)
T	:	Air temperature	438	(K)
M	:	Molecular weight	29	
Pa	:	Average pressure	(Pu + Pd)/2.0	

The leakage rate (Lr) is  $L = 6.346 \times 10^{-6}$  (atm · cc/sec).  
The amounts of radioactive gases that escape each hour are obtained by multiplying the concentrations of the various fission product gases in the air by the containment system's leakage rate obtained above. The obtained leakage amounts are compared with the criteria, and the results are provided in Table (II)-C.6.

**Table (II)-C.6 Leak of Radioactive Gases under Normal Test Conditions (Contents VIII)**

Nuclide	Quantity in storage (Bq)	Concentration (Bq/cm <sup>3</sup> )	Leakage radioactivity (Bq/h)	Criteria (Bq/h)	Ratio relative to criteria
H <sup>3</sup>	$3.50 \times 10^{11}$	$1.19 \times 10^7$	$2.71 \times 10^5$	$4.00 \times 10^7$	$6.78 \times 10^{-3}$
Kr <sup>85</sup>	$6.34 \times 10^{12}$	$2.15 \times 10^8$	$4.91 \times 10^6$	$1.00 \times 10^7$	$4.91 \times 10^{-1}$
I <sup>129</sup>	$2.10 \times 10^7$	$7.12 \times 10^2$	$1.63 \times 10^1$	Not specified	0
I <sup>131</sup>	$1.59 \times 10^1$	$5.39 \times 10^{-4}$	$1.23 \times 10^{-5}$	$5.00 \times 10^5$	$2.46 \times 10^{-11}$
Xe <sup>131m</sup>	$7.33 \times 10^3$	$2.49 \times 10^{-1}$	$5.68 \times 10^{-3}$	$4.00 \times 10^7$	$1.42 \times 10^{-10}$

Total: 0.498

Secondly, radioactive solids include actinoids (actinide elements) and fission products. The leak of radioactive solid matter is assessed using the results of experiments conducted by the U.S.-based Battelle Laboratory (to study the correlation between the leakage rate of helium gas and that of plutonium dioxide powder leaking from a small hole bored in the orifice) on the assumption that all of the above-mentioned radioactive solids are replaced with plutonium.<sup>1)</sup>

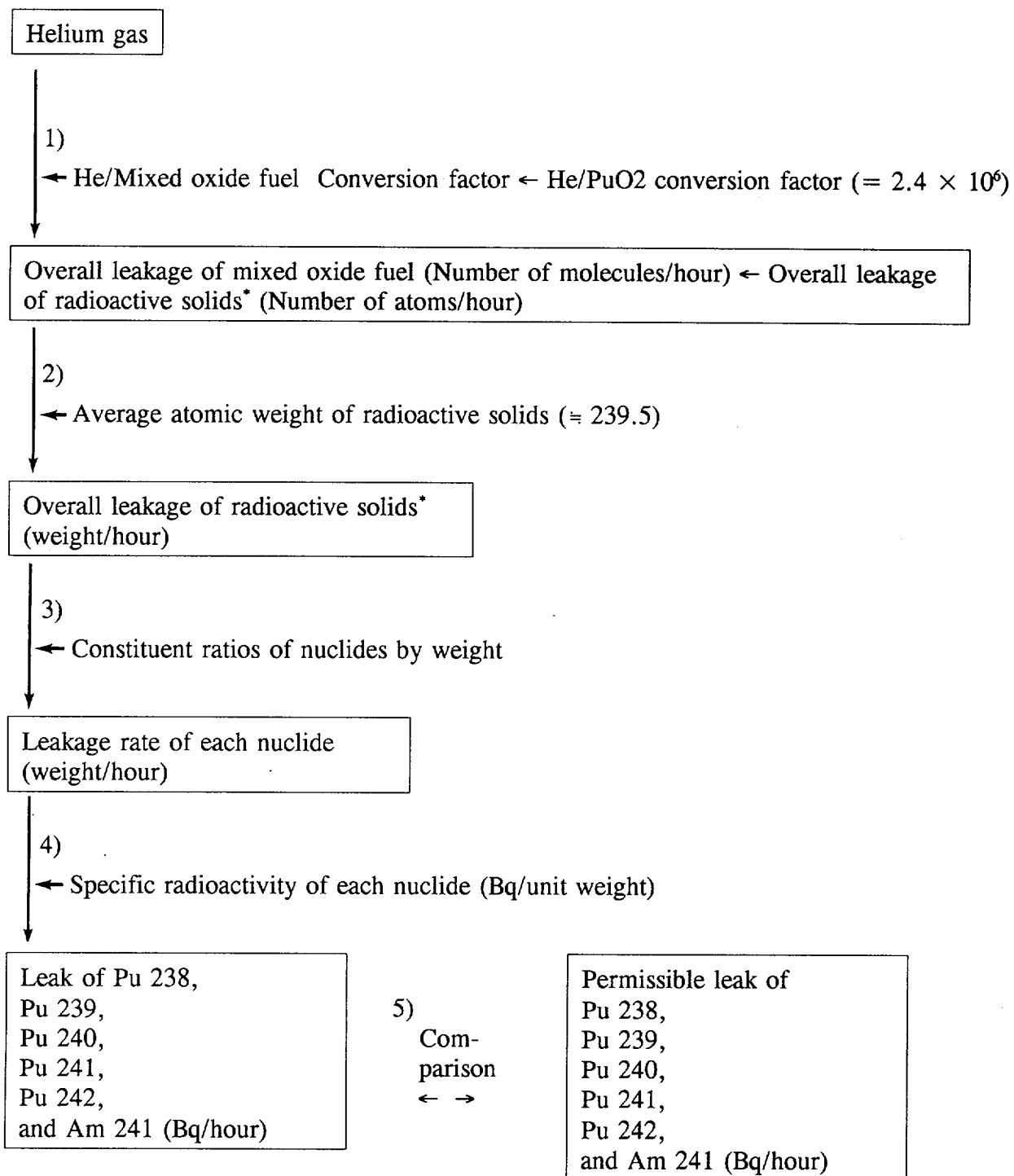
These replacements can be taken as hypotheses that tip the balance in favor of safety for the reasons given below:

- (1) Plutonium represents the second largest constituent component, and is subject to stringent leakage criteria designed to control radioactive material.
- (2) Although plutonium dioxide represents 31% or less in enrichment according to specifications, it was replaced with 100%-enriched plutonium, which is enriched approximately three times as much, for evaluation purposes.

For reference, a containment system measuring  $1.0 \times 10^{-5}$  atm · cc/sec or less in leakage rate and filled with helium gas was used for analysis as was with the gaseous-matter leak analysis. The analysis flow is shown in Fig. (II)-C.3.

---

1) Study of Plutonium Oxide Leak Rates from Shipping Containers, BNWL-2260



1) through 5) are explained in the paragraphs that follow.

\* All radioactive solids are assumed to be plutonium.

**Fig. (II)-C.3 Leakage Analysis Flow**

Step 1)

Calculations shall be based on the assumption that the containment system leaks at a rate of  $1.0 \times 10^{-5}$  atm·cc/sec.

When helium gas escapes at a leakage rate of  $1.0 \times 10^{-5}$  atm·cc/sec, the number of helium atoms that escape per second is:

$$\frac{1.0 \times 10^{-5} \text{ (atm·cc/sec)} \times 6.0 \times 10^{23}}{22.4 \times 10^3 \text{ (atm·cm}^3\text{)}} = 2.68 \times 10^{14} \text{ (pcs/sec)}$$

The leakage rate for mixed oxides is obtained on the basis of the leakage rate of helium and by using "Conversion factor He/Mixed oxides =  $2.4 \times 10^6$ ." In other words, the number of atoms of mixed oxides that leak per second is as follows:

$$\begin{aligned} & \text{Number of escaping helium atoms} \times \frac{1}{\frac{\text{Number of helium atoms}}{\text{Number of mixed oxides}}} \\ &= 2.68 \times 10^{14} \times \frac{1}{2.4 \times 10^6} \\ &= 1.12 \times 10^8 \\ & \text{(pcs/sec)} \end{aligned}$$

Step 2)

The total-weight leakage rate [X] of the radioactive solid matter is obtained by multiplying the total atom count of radioactive solid matter by the average atomic weight of the radioactive material as follows:

$$\begin{aligned} X &= \text{Total atom count of escaping radioactive solid matter} \\ &+ \frac{\text{Average atomic weight of radioactive solid matter}}{\text{Avogadro's number}} \\ &= 1.12 \times 10^8 \times \frac{239.5}{6.0 \times 10^{23}} \\ &= 4.46 \times 10^{-14} \text{ (g/sec)} \\ &= 1.61 \times 10^{-10} \text{ (g/h)} \end{aligned}$$

Step 3)

The weight leakage rate [Xa] of Nuclide a is obtained by multiplying the total-weight leakage rate [X] of the radioactive solid matter by the constituent ratio [xa] of Nuclide a by weight as follows:

$$X_a = X \cdot x_a$$

Step 4)

The specific radioactivity leakage rate [Aa] is obtained by multiplying the weight leakage rate [Xa] by the specific radioactivity [Pa] as follows:

$$A_a = X_a \cdot P_a$$

Step 5)

The radioactivity leakage rates [Aa] of the various nuclides and the permissible leakage rate [Ba =  $A_2 \times 10^{-6}$  Bq/h] are compared. The results of Steps 3) through 5) are shown in Table (II)-C.7.

The table clearly indicates that the sum of the ratios of the leakage rates of radioactive solids escaping from the containment system versus the leakage criteria (Aa/Ba) is 0.012.

From Table (II)-C.7, the ratio between the leakage rate of a combination of gaseous and solid radioactive material and the leakage criteria is given as follows:

$$\text{Ratio of Contents VIII: } 0.498 + 0.012 = 0.51$$

Since the ratio of the leakage rate of Contents VIII, whose fission product gases yield the highest intra-container radioactivity level readings of the various kinds of Contents, versus the leakage criteria stands at 0.51, this ratio satisfies the leakage criteria ( $A_2 \times 10^{-6}$  Bq/h or less) prescribed in the Notification issued by the Science and Technology Agency, designed to control radioactive materials.